RHEOLOGY AND PUMPING OF WAXY CRUDE OILS

AN EXPERIMENTAL STUDY OF THE YIELD STRESSES OF WAXY CRUDE OILS MEASURED USING A RANGE OF RHEOLOGICAL TECHNIQUES

A.M.A. ABDELRAHIM

PhD

UNIVERSITY OF BRADFORD

2011

RHEOLOGY AND PUMPING OF WAXY CRUDE OILS

AN EXPERIMENTAL STUDY OF THE YIELD STRESSES OF WAXY CRUDE OILS MEASURED USING A RANGE OF RHEOLOGICAL TECHNIQUES

A PhD THESIS

SUBMITTED TO THE SCHOOL OF ENGINEERING, DESIGN AND TECHNOLOGY

BY

A.M.A. ABDELRAHIM

PRINCIPAL SUPERVISOR

PROFESSOR HADJ BENKREIRA

UNIVERSITY OF BRADFORD

2011

Abstract

A major problem faced by the petroleum industry is the deposition of wax during the pumping of waxy crude oils. This precipitation occurs at "normal" temperature, typically 20-30^{0}C in Libya. It could occur during the journey from well to terminal through hundreds of miles of pipelines. This kind of transportation is expensive in terms of pumping costs. The pumping has to be continuous; otherwise wax can build up in the pipeline, reducing the pumping or even stopping it. The property that defines this characteristic is the yield stress which depends on wax concentration and cooling rate. The build-up of paraffin and asphaltenes can lead to serious problems in formation, tanks, and pipelines. Blockages can be expensive and time-consuming to deal with; this is precisely the topic of this research.

For this research, model and real waxy crude oils are formulated and their rheology systematically measured under various cooling rates to determine the yield stress. A pipeline loop has been designed to measure the start-up pressure of stagnant oil which has been allowed to precipitate wax. The start-up pressure and the thickness of deposited wax are used in a simple mathematical model to calculate the yield stress. This research thus provides two independent means of predicting the yield stress.

This research studied three different waxy crude oils. An MCR-301 Anton Paar rheometer was used to measure the rheology of the oils, and a pipeline rig was used to obtain the start-up pressure to calculate the yield stress of each type of oil after different stoppage times. Also, the thickness of the precipitated wax is measured to calculate the yield stress precisely.

The data show that the layer thickness has significant effect on the yield stress and start-up pressures and corresponding yield flow stresses have been found to underpin the crystallisation process of the wax and slow cooling rate produce stronger structures requiring higher stresses to fracture and induce flow. Also, longer shutdown times make these structures even stronger and therefore require even larger stresses for flow to commence.

Acknowledgments

I would like to thank the following people for their contributions:

My principal supervisor, Professor Hadj Benkreira for his encouragement, guidance and support in the different stages of my thesis. I am also heartily grateful for his reading and commenting on all my reports and final thesis.

I would like to show my appreciation to my second supervisor Dr. Raj Patel for his support and for his suggestions, and assistance in the experimental stage.

I also appreciate the assistance of Mr. David Steele, the Chief Technician of the Rheology and Coating laboratory and thank him for helping me throughout my project.

I owe a lot of thanks to my Mum "Dahab", my wife, Aisha and daughters, Hajre, Yameen and Umniya for their love and patience.

I also thank my brothers Abd-Rab-Alnabi and Mohammed as well as my sisters Aziza and Sabah

I am thanking a lot my uncle Ehmaida and my anti Kifaya, also my brothers in law Fath-Allah and Mahdi and their sisters

Finally, I appreciate the financial support from the Libyan Educational Program.

Acknowledgments

I would like to thank my wife Aisha Awad for her understanding and love during the past few years. Her support and encouragement was in the end what made this dissertation possible.

Moreover, I would like to express special thanks to her because she helped me to concentrate on completing this dissertation and supported mentally during the course of this work. Without her help and encouragement, this study would not have been completed.

Dedication

The sacrifices, encouragement, and support which I received from my family cannot be compensated by dedication of this piece of work to them. However, I would like to dedicate this thesis to my mother, wife, and children. Thank you very much for your love and support throughout my PhD study.

Table of Contents

List of Figures

List of Tables

CHAPTER 1: INTRODUCTION

This chapter describes the important characteristics of waxy crude oils in relation to the research problem which is the rheology and start-up pressures of these oils. Wax crystal precipitation is shown to be the main cause of pipeline chocking or blockage when the oils have a sufficiently high content of wax. The problem, which is fundamental to the entire world oil industry, is put in the context of the Libyan oil industry which has served as a case study for this research.

1.1 INTRODUCTION

This research is concerned with the rheology and start-up pressures of waxy crude oil in pipelines of various sizes in a range of temperatures and cooling rates. Before introducing the subject area, it is important first to define various terms as used in the oil industry to describe crude oils.

1.1.1 Definition of terms

ASTM: The American Society for Testing and Materials, an international standards organization that develops and publishes voluntary technical standards for a wide range of materials, products, systems, and services.

Pour Point: As defined by ASTM, this is the lowest temperature at which the oil will pour or flow, without disturbance (Hangs, 1963; Boukadi and Amri, 2005).

Cloud Point: As long as the crude oil is at sufficiently high temperature all wax will be dissolved in the oil. Upon cooling, a temperature will be reached- the cloud point-

at which the first paraffin crystals appear. Below this temperature, more and more wax will crystallize with decreasing temperature (Boukadi and Amri, 2005).

API Gravity: American Petroleum Institute Gravity is a measure of how heavy or light the petroleum liquid is compared with water. The crude oils are classified or graded using the API gravity as Table 1.1 shows. The greatest commercial price is for the oils that have API gravity of 40-45 degrees. The values outside this range have a lower commercial price. Above 45 degrees API gravity the molecular chains become short and less valuable to the refining process. The way that the API gravity is calculated with can be found in section 3.1.

Table 1.1 Crude oil classification using API gravity

Crude Oil classification	**API gravity Degrees**
Light	>31.1
Medium	22.3-31.1
Heavy	<22.3

Paraffin content: designates any organic fraction that precipitate to form deposits or agglomerates. The analytic method defines the paraffin content of oil, which is analyzed according to the standard method UOP 46-64. This method involves diluting the crude in a suitable solvent, cooling down to -30 °C, filtering and weighing (Boukadi and Amri, 2005).

1.1.2 Characteristics of Waxy Crude Oils

Crude oil is a naturally occurring petroleum liquid found in rock formations (Bell, 1963) in a number of reservoirs throughout the world. It may contain some waxes (paraffins); in this case, it is called a waxy crude oil. Waxy crude oils are the

most common types of crude oils and are very important from an environment viewpoint since they have low sulphur content (Rashidah, 2005). The percentage of wax in some areas rather than others refers to the nature of the oil and not the structure of the rocks. The quantity of wax in crude oils differs by less than 1% wt to more than 30% wt (Mohamed, 2003).

Wax is a solid or semi-solid material consisting of a mixture of hydrocarbons. Paraffin waxes consist mainly of saturated hydrocarbons. The paraffin waxes in crude oil are valuable sources of refined production ranging from engine oil to jet fuel. However, there are many problems that arise with the waxy crude oil (Becker, 1997). The build up of paraffin and asphaltenes represents the organic equivalent of scale, and their presence in formation, tanks, and pipelines can lead to serious problems over time (Becker, 1997; Benallal et al., 2008). Clearly, in pipelines, if allowed to form in their solid state, they will restrict the available cross sectional area for flow and consequently impede pumping of the oil, sometimes causing complete blockage that can last several months before being removed (Guo and Prud'homme, 2005) with serious economic costs. This is precisely the topic of the research presented in this thesis.

Figure 1.1 illustrates such precipitation blockage in pipelines, aggravated when the waxy crude oil has high viscosity and high pour point (Irani and Zajac, 1982; Guo and Prud'homme, 2005) and the ambient temperature is low, as is the case in Russia's oil fields where the temperature often falls below -20°C (Fusi, 2003). It is important to note however that such extreme temperatures are not always necessary for wax to precipitate. Indeed in the case of the present research with waxy crude oils commonly found in Libya, wax precipitation can occur at 15-30^{O}C, which are "normal" conditions in Libya.

The problem with the wax starts at the well as with ageing and increasingly deeper reservoirs, the concentration of wax increases (Fusi, 2003). As a result, all the equipment that the waxy crude oil comes into contact with e.g transfer lines, treatment vessels and storage tanks are all negatively affected by the presence of paraffin waxes mixed together with emulsions, solids, and corrosion by-products (Becker, 1997). Paraffin wax deposition within the producing reservoir is an extremely difficult problem to resolve once it begins and the technological efforts are in finding remedies to the wax problem as the waxy crude is transported, either by heating prior to admitting it into the pipeline for pumping or injecting solvent to dilute the wax. Clearly both procedures add to the cost of the pumping operation with solvent addition being the least desirable option as the wax are valuable and easy recovery in later stages is wanted. Thus "coping" with shutdown and re-starting pipelines that have waxy crude oils in them is a common occurrence in the oil industry. The key consideration is how quickly can the pipeline be started and clearly rheological information are the prime data to ensure economic re-start.

Figure 1. 1 Typical deposition in oil pipelines

Source: Granherne Pty. Ltd. Internet: http://www.granherne.com (02/02/2010)

1.1.3 Waxy Crude Oils around the World and in Libya

World oil production stood in September 2008 at 84 MBPD (million barrels per day) with 20% of this production estimated to be of the waxy type. Over the years, pumping very large amount of crude in very long pipelines has become common to meet the ever increasing world demand for this key resource. The return on investment of the companies operating these pipelines is crucially dependent on uninterrupted production. As explained earlier, when the temperature drops below the pour point of the oil and the wax precipitates, chocking or blocking of the pipelines will occur leading to stoppage and they need to restart as quickly as possible. This is very costly and in some cases may take a very long time causing serious implications to oil supply. Libya, which forms the case study of this research, holds the largest proven oil reserves in Africa and currently produces 1.7 MBPD, 40% of which is waxy crude (Qabazard, 2008) from various off-shore and on-shore fields as shown in Table 1.2 which lists the various Libyan waxy crudes, their wax content, pour point and other characteristics and gives the dimensions of the pipelines as an indicator to gauge the extent of the pumping operation. Clearly unless there is a smooth pumping of these waxy crudes, the economic consequences for the Libyan oil industry are indeed very serious. The same applies to many other countries including major producers such as the USA, Canada, Russia and the UK northern oil fields where the temperature conditions are extreme and smaller producers (Mcketta, 1993) such as Indonesia (Minas fields in Sumatra) and India (Nahorkatia, Moran and Bombay crudes). Countries such as Venezuela and Mexico, also major producers have significant waxy crude oils productions as have the newer fields of Egypt (Umo-Baraka) and Sudan (El-Gamal and Gad, 1997). The problem

is truly widespread and this makes the subject of this research important and *fundamental* to the oil industry.

It is important to reiterate that temperature drops do not have to be drastic for wax precipitation to occur. The pour point in this respect is a good indicator and it can be seen from Table 1.2 that Libya oils will cause wax precipitation at *normal* temperatures. In Libya, the temperature changes from about 40 °C during the day in summer and autumn to 10 °C during the night. During the winter, the temperature can reach around 0 °C in the day time and drops marginally below zero during the night. The ambient temperature of the area around the Bu-Attifel field is shown in Table 1.3 (Alwaer, 2008) and clearly indicates that Bu-Attifel with a pour point of 40 °C will experience wax precipitation and provisions have to be made to counter-act the problem when it occurs, the cheapest being re-starting the pipeline as quickly as possible and using the lowest energy input. As an indicator of cost, where the pipeline is left un-operational for a substantial period of time (a few days), the work-over process cost is more than US $1M per well for each cleanup, plus the cost of stopping the production for the period of maintenance process.

Table 1. 2 Details of main crude oil pipelines network of Libya

Fields (Crude name)	Export Terminal	distance (miles)	Diameter (inch)	Remarks
Bu-Attifel API = 40.20 degrees. Pour point = 40 °C, Wax content= 37 wt% Sulphur content= very low	103 Field then to Zueitina port	83 132	30 40	Eni oil Co.
Al-Khatip API = 40 degrees. Pour point = 41 °C, Wax content= 25 wt% Sulphur content= very low	Al-khatip Field to UU Field	10	12	Eni. Oil Co.

Remal API =32 degrees. Pour point =42 °C, Wax content= 35 wt% Sulphur content= very low	Remal Field To A100 field	62	16	Eni Oil Co.
Al-Buri API =39 degrees. Pour point =15 °C, Wax content= 13 wt% Sulphur content= very low	Platform Drilling 3 to Solog Tank	3	16	Eni Oil Co.
Sarir API =37.2 degrees. Pour point =30 °C, Wax content= 13 wt% Sulphur content=0.133 wt%	Marsa El Hariga (Tobruk)	319	34	AGOCO
El-Sider API =37 degrees. Pour point =22 °C, Wax content= 8 wt% Sulphur content= very low	El-Sider To Zueitina port	87	30	*
Al-Mabrouk API = 38 degrees. Pour point = °C, Wax content= 15 wt% Sulphur content= very low	*	*	*	Total
Messlah	Ras-Lanuf	298	30	AGOCO
Waha	Es Sider	267	34	Al-Waha
El-Hamada	Zawiya	236	34	
Amal	to Ras-Lanuf,	170	30	Al-Waha
Intisar	Zueitina	132	30	
Nasser (Zelten)	Marsa El Breaga	67	34	

- Unavailable Data

Table 1. 3 Temperature changes of Bu-Attifel area for 2009

Month	*Average Highest ℃*	*Average Lowest ℃*
January	27	2
February	29	3
March	34	6
April	39	11
May	39	11
June	46	17
July	45	21
August	42	22
September	42	17.5
October	37	14
November	37	4
December	25	1

1.2 WAX FORMATION, PUMPING FAILURE & RHEOLOGY

Waxy crude oils consist of wax, a mixture of light and intermediate hydrocarbons (paraffins, aromatic and naphthenic) and a variety of other heavy organic (non-hydrocarbon) compounds. These wax components exist in various states i.e gas, liquid, or solid depending on temperature and pressure. At high temperatures, well above the pour point, a waxy crude oil is in a liquid state with all the particulates fully dissolved in the solvent base of the oil. When the temperature falls below the wax precipitation temperature, the wax will precipitate out of oil solution. Paraffin wax forms as a non-volatile long chain hydrocarbon with a composition of C_nH_{2n+2} where n is 18 or greater (Chin, 2001). On further cooling,

more and more wax crystals form, separate out and interlock into a network structure of plates, needles, or malformed crystals (see Figure 1.2) that entraps liquid oil into its structure, resulting in the gelation of the crude oil (Lie and Jin-jun, 2007).

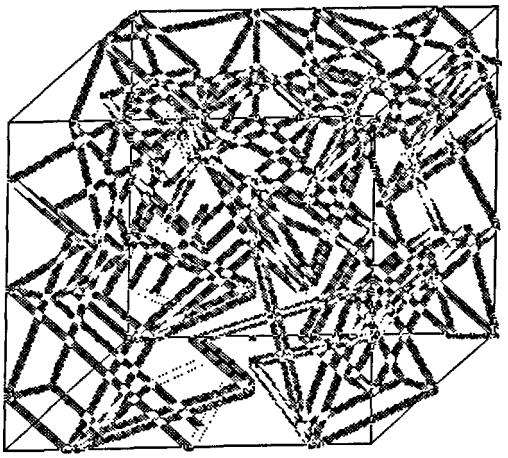

Figure 1. 2 Schematic diagram of the wax crystal network

Source: Granherne Pty. Ltd. Internet: http://www.granherne.com (20/01/2010)

The crystals which form can be of different types depending on the rate of cooling. Large crystal or macrocrystalline waxes will form at slow rate of cooling and these are mixtures consisting chiefly of saturated, normal C18-C30 hydrocarbons and smaller amounts of iso-alkanes and cyclo-alkanes. The molecular weight of the components in macrocrystalline waxes varies between 250 and 450 and their melting point between 40 °C and 60 °C. Their crystals are plate-shaped or needle-shaped (Mozes 1982) & (Chin 2001) as shown in Figure 1-3 and Figure 1-4.

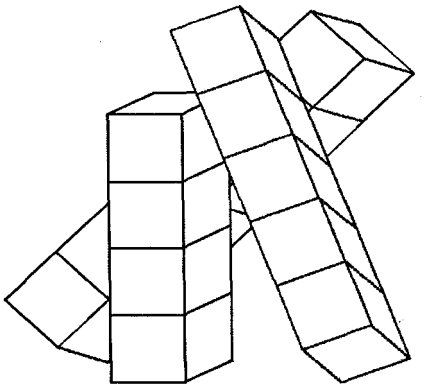

Figure 1. 3 Plate like crystal structure

Source: Granherne Pty. Ltd. Internet: http://www.granherne.com (20/01/2010)

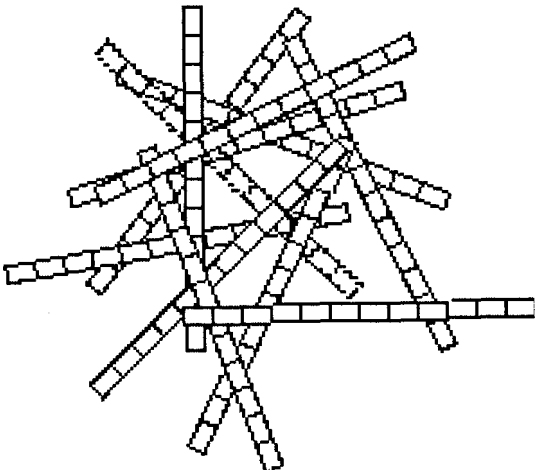

Figure 1.4 Needle like crystal structure

Source: Granherne Pty. Ltd. Internet: http://www.granherne.com (20/01/2010)

When the cooling rates are rapid, smaller crystal structures form. These microcrystalline waxes contain, in addition to normal hydrocarbons, large amounts of iso-alkanes and naphthenes with long alkyl side-chain and their melting point varies between 60 °C and 90 °C (Mozes, 1982).

Clearly, these wax crystals will deposit in pipelines and when the wax content is significant (above 7%), pumping problems will occur, leading at high wax content to chocking and blockage of the pipelines (Mcketta, 1993). There are thus several

stages leading to wax formation and eventual pumping malfunction and these can be summarized as follows (Chin, 2001; Narjes, 2003):

1. When the temperature of waxy crude is decreased below the cloud point, the heavier fractions in wax content appear first.
2. Paraffin will precipitate under slight changes in equilibrium conditions, causing loss of solubility of the wax in crude.
3. Wax nucleation and growth occur along the pipe surface and within the bulk fluid and this will depend crucially on cooling rate.
4. Precipitation within the fluid causes its viscosity to increase and alters the non-Newtonian characteristics of the carrier fluid.
5. Increases in frictional drag causes pumping problems and higher overall pipe pressure.

Stages 4 and 5 bring us to consider the important rheological aspect that develops as wax precipitation occurs, i.e. as the temperature is dropped either because of extreme temperature conditions or more normally because of electrical failure interrupting prior heating of the oil. Note that electrical failure is the prime cause as when failure occurs the pump will stop and the oil now stationary will be prone to cooling. Clearly viscosity is at the heart of pumping and the larger it is the higher will the pressure be. These pressures will be aggravated further as the cross-sectional area for flow reduces because of the deposit around the inside of the pipe. At high temperature, with all the wax fully dissolved, the rheological behaviour of the crude oils will be essentially purely viscous and probably Newtonian as there are no particulates in the fluid. As the temperature is reduced, wax particulates will form and these will cause non-Newtonian behaviour, most probably of a shear

thinning nature. However, if the pipeline is not continuously operated, a whole section of the pipeline will be stagnant and interlocked by the network of wax crystals, giving now a viscoelastic characteristic. To restart the pipeline, this structure will need to be broken, i.e. made to yield and it is this start-up pressure that is fundamental to the re-start problem. This start-up pressure can be measured either using a pilot pipeline system made to mimic the actual stoppage or using careful rheological data to measure how the "solid" waxy crude is made to yield and eventually flow. Careful reproduction of temperatures and cooling rates in both the pipeline rig and the rheological tests need to be achieved in order to obtain data accurate enough to be scaled to the large pipeline dimensions. This is precisely the brief of this research, the aim and objectives of which will be clearly enunciated in the next section.

1.3 AIM, OBJECTIVES & ORGANISATION OF THE THESIS

As explained above, the principal aim of this research is a rheological study of waxy crude oils using Libyan oils as good representative samples of the oil industry. Other oils are also used including model waxy oil made in our laboratory. The study will be essentially experimental but based on the firm theoretical principles of rheology. By rheological study, it is meant here measuring the entire spectrum of the behaviour of waxy crude oils, above and more important near and below the wax precipitation temperature in order to inform the pressure start-up requirement after pumping stoppage. Thus temperature and rate of cooling control are key aspects of the measurements schedule. Having defined the broad aim, we can state the objectives that need to be fulfilled to achieve the aim. These are:

1. Sourcing suitable waxy crude oils and developing model waxy crude oil to be used in the rheological study.
2. Characterising these oils in terms of their basic properties, particularly measuring their pour points, the key indicator of wax precipitation.
3. Performing rheological measurements using state of the art rheological instruments and techniques, including measurements at constant shear rates but more importantly at constant shear stress to measure as precisely as possible the onset of yielding (yield stresses).
4. Performing start-up pressure measurements using a pilot pipeline rig to simulate the actual problem in the field, controlling temperature and rate of cooling at the conditions normally observed in industrial case problems.
5. Using the pressure data obtained from objective 3 to evaluate the yield stress for start-up and compare it with the yield stress measured using rheological instruments. Here the two objectives are linked through the theoretical principles of pumping of non-Newtonian fluids in pipeline systems.
6. Compare the results obtained with actual waxy crude oils with those obtained using model oil developed in our laboratory to assess their potential use for further research.
7. Using the results from all above objectives to evaluate the actual start-up pressures that will be required in the larger industrial pipelines as operated in Libya, the industrial case study of our research.

One other objective not listed above and very important is the carrying out of a literature survey to assess prior knowledge in the research area. This will form Chapter 2 following from this introductory chapter. In Chapter 3, the experimental method is presented and this includes description of the rheological instruments and

the pipeline rig as well as the sourcing and characterisation of the various oil samples used. The important data on rheology, including viscous and viscoelastic properties are presented and discussed in the Results & Discussion chapter. Finally, Chapter 5, will bring the conclusions of this research together as well as making recommendations for future research.

CHAPTER 2: LITERATURE REVIEW

2.1 INTRODUCTION

As stated earlier, waxy oils are very important from an environmental viewpoint since they have low sulphur content (Barry, 1971) and the availability of these oils combined with the need for new sources of petroleum has encouraged production of these crude oils. The problem, however, is that the wax agglomerates increase the apparent viscosity of the waxy oil which increases the energy requirements associated with transportation of the oil. Since the temperature at which wax crystallizes is not particularly low (usually between 10°C and 30°C), all the waxy oils are affected with this problem (Rashidah, 2005). Some waxy oils have a pour point of more than 30°C such as Abu-Attifel waxy crude (Rashidah, 2005). Clearly upon cooling, the problem is aggravated with the wax oil gelling and blocking the pipeline.

It has been stressed in the introductory chapter that rheology is the key for understanding the flow of waxy crude oils and predicting the pressure required to start-up gelled pipelines. Thus, in this chapter, the principles of rheology and research works specifically related to the start up pressure of waxy crude oils are presented. Clearly, the huge economic importance of oil has led to much work on the subject over many years. A lot of the work published is technology related and although it is relevant but not helpful to this research in terms of identifying research gaps. Most of the earlier research was conducted on methods to move the waxy oils above the pour point. A lot of studies have been carried out by the oil industry for solving specific problems arising in the production and storage of waxy oils. In

order to address the important research issues, this literature survey has been divided into the following key sections:

1. Rheology of Waxy Crude Oils
2. Start-up Pressure of Waxy Crude Oils
3. Wax Deposition Survey
4. Determining of the Wax Thickness in Pipelines
5. The Accuracy in Determining the Static Yield Stress

The last two sections, regarding the determination of the wax thickness in the pipeline and the accuracy in the measurement of the static yield stress are the two most important aspects this research will be contributing to. Indeed unless, the thickness of the wax layer deposited on the wall of a pipeline is known, the force balance between the yield stress and pressure is flawed as it requires the "right" cross sectional area as we shall explain later. Also unless the yield stress is measured "precisely" in both the rheological instrument and the pipeline rig, there is no possibility that the measurement will agree and give confidence in utilizing yield stress measured in rheological instruments as truly indicative of start-up pressure. This is broadly the gap identified in the entire literature survey, i.e. the need to narrow the discrepancy in the measured yield stress using rheological instrument and laboratory pipeline rig.

2.2 RHEOLOGY OF WAXY CRUDE OILS

As explained earlier, oil is an important material, the life blood of modern civilization. It is found in many remote places, in the deserts of the Middle East and North Africa, under the cold northern seas around Europe and America, and thus requires pumping many thousands of miles away from the source of production. Clearly this requires a very expensive network of pipelines buried deep under the

seas and in deserts and good uninterrupted pumping is critical. The problem is that naturally because of its make-up (a mixture of light, intermediate and long chain hydrocarbons, paraffins, aromatic and naphthenic), crude oil is prone to gellation, i.e. solidification in the pipeline when the temperature drops below the gel point. Very importantly, this gel point is not very low and can be normal, 20 or 30^{o}C are typical values of many oils. So oil at the source is at the margin of being equivalent to a solid *suspension* (the hydrocarbon molecules when large may be regarded as solid particles contained within a solvent mass) which can turn into solid upon the crystallization of these particles when unexpected cooling occurs. Clearly waxy oils are not a simple suspension but a suspension in which the particles have a potential to crystallize, combine together to form a structure. It is this structural feature that makes waxy oil complex materials rheologically. It is thus helpful to give a brief overview of the rheological behaviour that may be exhibited by the oil throughout its journey from the source to the refinery for example. Such an overview can then lead to the consideration of yield stress and other difficult rheological concepts.

2.2.1 Overview of Rheology & Approaches to Measuring Yield Stress

It is known since Newton's (Newton, 1687) original work that except for pure liquids of low molecular weights and gases, most "fluid" materials are non-Newtonian by definition and that their apparent viscosity, μ_a is function of shear rate, $\dot{\gamma}$ and shearing time, $t_{\dot{\gamma}}$ as well as temperature, T, i.e.:

$$\mu_a = \frac{\tau}{\dot{\gamma}} = f(\dot{\gamma}, t_{\dot{\gamma}}, T) \qquad (2.1)$$

Depending on how the apparent viscosity varies, at given temperature, with the variables, $\dot{\gamma}$ and, $t_{\dot{\gamma}}$, the material can be classified as purely viscous (variation with

shear rate only and no variation with shearing time) or time dependent (variation with shearing time as well as with shear). Clearly, the apparent viscosity may decrease as the shear rate is increased in which case the material is said to be shear thinning or pseudo-plastic (see Figure 2.1).

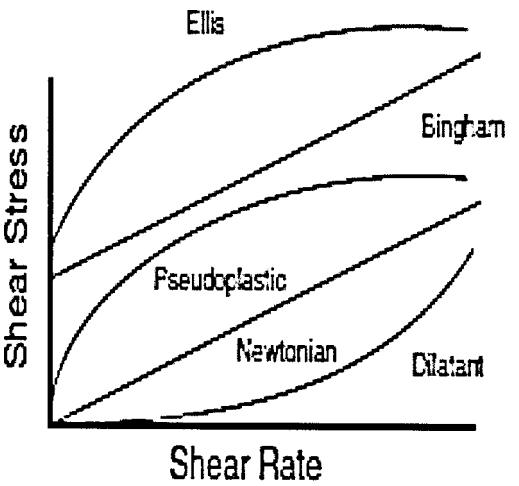

Figure 2-1 Typical shear stress behaviour for most materials

The reverse may also be observed, i.e. the apparent viscosity increasing as the shear rate is increased, in which case the material is said to be shear thickening or dilatant (see Figure 2.1). In general, a material may exhibit any of these features of Newtonian, shear thinning and shear thickening depending on the applied shear rate so over a wide range of shear rate, we may observe all of these features as shown in Figure 2.1. One interesting behaviour, which is particularly relevant to waxy crude oils is that the material may not flow until a certain level of stress is applied to it. This type of behaviour is referred to as Bingham Plastic (after the eminent rheologist E.C. Bingham (Bingham, 1922)) also shown in Figure 2.2.

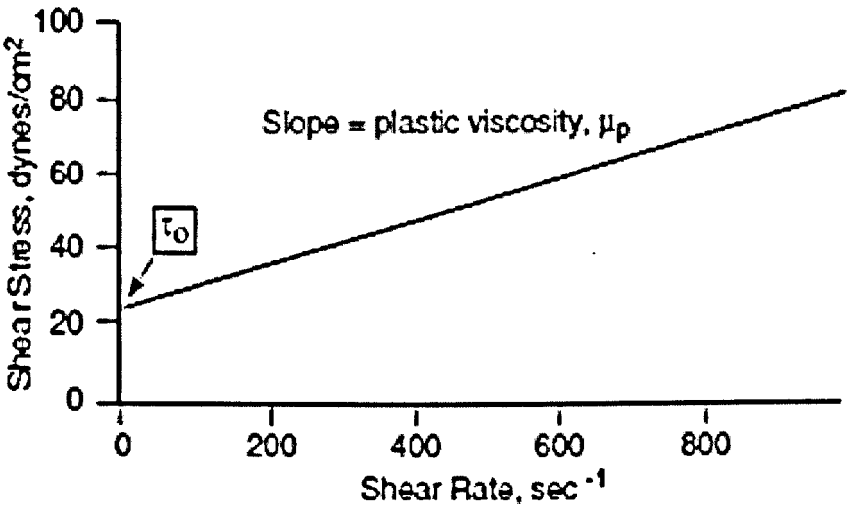

Figure 2-2 Idealized Bingham plastic fluid behaviour

Clearly, the range of behaviours observed can be very complex and most importantly cannot be predicted, it has to be measured. Already, we can suspect that in order to measure the yield stress we shall need an instrument that is capable of applying very small stresses and measuring the smallest movement (shear rate).

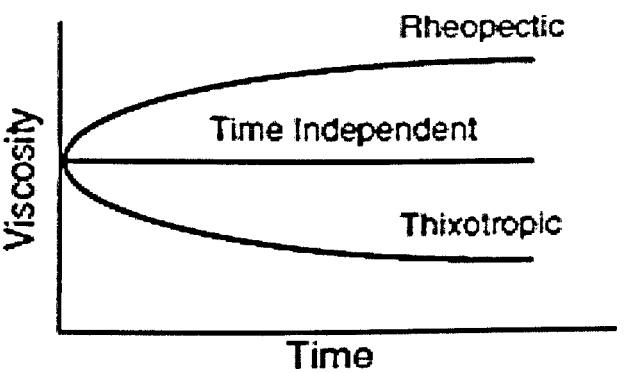

Figure 2-3 Schematic diagram showing the effect of shear time on different materials at a constant shear rate

Equation (2.1) also shows that the time of shear at constant shear can equally be important in reducing viscosity, in which case we refer to the behaviour as being

thixotropic, an important feature of waxy crude oils as reported by (Mezger, 2002; Mezger, 2006; Zhang, 2007; Hou Lei, 2007). This behaviour is easily explained in relation to the breakdown of structure with time given a sufficient applied constant shear rate (see Figure 2-3).We can already suspect that considering that waxy crude oils have a structure, their yield stress itself will be time dependent. This will become clear later in the review.

So far the discussion has been directed at materials that behave like a fluid and show a flow upon the application of a stress. The concept of yield stress is however much better established with reference to solids which upon the application of a stress will deform, usually elastically, following Hookes's law (Hooke, 1678) (another famous "solid" rheologist during the same era as Newton):

$$G = \frac{\tau}{\gamma} = f(\gamma, t_\gamma, T) \qquad (2.2)$$

In the above equation G is the elastic modulus, γ is the strain and t_γ the straining time. Equation 2.2 is very similar to Equation 2.1 with G here having a similarity with μ_a and expressing the resistance to deformation rather than resistance to flow which is what the apparent viscosity expresses. As shown in Figure 2.4, G remains constant as the stress or strain is increased but beyond a critical point, the material no longer deform uniformly but begin to yield before creeping and finally breaking as most solids do. The question is: is it possible that waxy crude oils that are gelled will deform in a similar way?

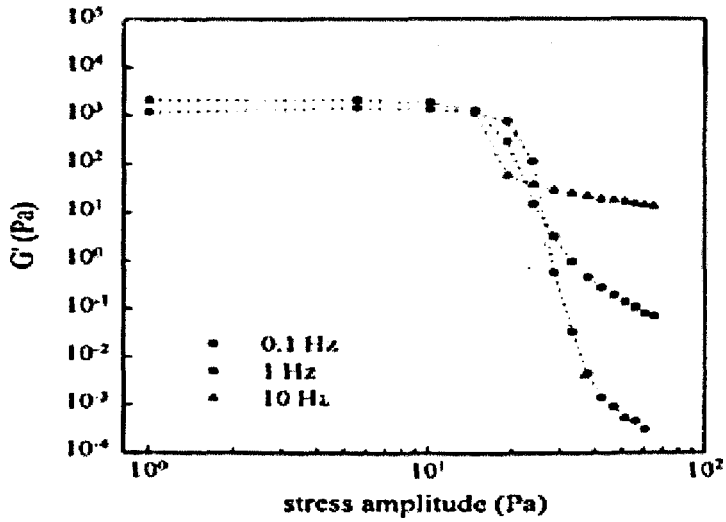

Figure 2-4 Effect of shear rate on viscosity beyond a critical point

Thus considering these simple rheological concepts and a simple definition of what may be defined as a yield stress, we see that it can be approached the "fluid" way or the "solid" way. In reality, materials with a structure such as waxy crude oils (or food-stuff, cosmetics, paints, polymer melts, blood, synovial fluids, etc.) behave neither as liquid nor as solid, they show mixed solid-liquid behaviour and are defined as viscoelastic. Such materials will not only flow like a liquid but also deform at the same time like a solid. A simple model of this behaviour is to attribute an elastic modulus to the material as well as a viscosity. Such a model (Maxwell model is one example (Maxwell 1853)) can be represented by a purely viscous damper and a purely elastic spring connected in series. In this configuration, if the applied axial stress is τ, we can decompose the total strain γ_T into a strain in the damper γ_D and a strain in the spring γ_S or:

$$\gamma_T = \gamma_D + \gamma_S \qquad (2.3)$$

To track how the strain varies in time, we can take the derivative of this equation and obtain:

$$\dot{\gamma}_T = \dot{\gamma}_D + \dot{\gamma}_S = \frac{\tau}{\mu_a} + \frac{\dot{\tau}}{G} \qquad (2.4)$$

In this equation, the "dot" represents a derivative with respect to time, μ_a is the viscosity of the fluid in the damper and G is the elastic modulus of the spring, i.e. the liquid and solid parts of the material are now both represented in the constitutive equation. We now have a 3rd track on how to measure yield stress by considering the material as being viscoelastic and devising tests that suitably "bring out" both the elastic and fluid nature of the waxy crude oil.

2.2.2 Techniques for Measuring the Yield Stress of Waxy Crude oils

As explained above, a variety of techniques are possible to measure the yield stress of materials but an assessment of the techniques is necessary to ensure that the measurement obtained is indeed valid and represents the yielding behaviour of the material considered. Oil being an important material, interest in its flow behaviour goes back a long time, since large scale exploitation began in the early 1900. At the outset, it was found that waxy crude oils presented unusual rheological characteristics. For example Beale in 1938 showed that waxy oils do not fit the usual rheological models, for example the Bingham model and their behaviour are influenced by thermal history (Beale, 1938). Much research followed from this work using the rheological instrument available at the time, Gill and Russell (1954) using a small scale pipeline (capillary viscometer) for example and Savins (1963) using the Ferranti cone and plate viscometer and Ackroyd (1960) extending the work to cover the flow properties of waxes, asphaltenes and resin compounds (Ackroyd, 1960; Savins, 1963; Gill and Russell, 1954). All these studies reveal the highly non-Newtonian character of waxy crude oils, including a strong time dependency as found by Billington in 1960 who hypothesised that the reduction of the viscosity

with time was caused by a breakdown in the Bingham yield value (Billington, 1960). The results were important in that they established the importance of the yield value of waxy oils and showed how shearing at constant time could effectively destroy the yield value. Gill and Russell (1954) work is important in that it was the first to cast doubt on the suitability of the pipeline instrument (capillary rheometer) to produce accurate data (Gill and Russell, 1954). They found with their 1mm diameter pipe start-up pressures (i.e. inferred yield stress as from Equation (2.1) above) that strongly dependent on the length to diameter (L/D) ratio when this ratio was below 200. They also observed that changing the pipe material from glass to stainless steel gave vastly different results. Many other studies considered both the yield stress and time effects and measured them to the accuracy of the instruments available at that time (Barry, 1971; Perkins and Turner, 1971; Somper and Davenport, 1971; Govier and Fogarasi, 1972). Sifferman in 1979 attempted to propose a standard procedure to measure the yield value (Sifferman, 1979). He considered three waxy oils from different parts of the world (USA, Indonesia and Libya) and investigated how the yield values varied when adding flow improvers and emulsifiers. A Brookfield concentric cylinder viscometer and a laboratory pipeline rig were used in his study to compare results. The data obtained from this study showed that the measured yield stresses depended on the measuring techniques. Somper and Davenport (1971) studies with Libyan and Nigerian oils revealed further complications- that repeatable results could not be obtained even with the same apparatus (Somper and Davenport, 1971). Clearly a systematic assessment of the rheological techniques to measure the yield stress of waxy crude oils became necessary as it provided not only an interesting research challenge (see the debate about the existence of yield stress in Barnes and Walters, 1985) but also a real practical need to solve the industrial

problem of re-starting gelled pipelines as quickly and economically as possible (Barnes and Walters, 1985).

Such an assessment has been made by the eminent rheologist Boger and his co-workers at the University of Melbourne, Australia in the early 1990. In their seminal paper, Wardhaugh and Boger , reviewed all the literature prior to 1990 and found that the capillary viscometer or pilot scale pipelines (which are effectively also capillary viscometer but with very long and much larger diameter tube, coil tubes have also been used), although the obvious choice because they mimic flow in pipe, do not give repeatable results on the measured yield stress (Wardhaugh and Boger, 1990). Note that from simple laminar pipe flow theory, the yield stress can be obtained from force balance:

$$p(\pi R^2) - (p - dp)(\pi R^2) = \tau_W (2\pi RL) = \tau_Y (2\pi RL)$$

$$\tau_Y = \frac{dp}{2L} R = \frac{dp}{4L} D \qquad (2.5)$$

Clearly, as the waxy crude oil gels in the pipe, a layer of wax will deposit on the wall of the pipe, the force balance above is flawed and should be revised to take this into account by using the effective diameter, D_e =D-2 x (wax layer thickness on wall):

$$\tau_Y = \frac{dp}{4L} D_e \qquad (2.6)$$

Therefore unless the wax layer thickness is precisely measured, the error in the evaluation of the yield stress will be significant and directly proportional to the error in evaluating D_e, i.e. in evaluating the wax thickness. Secondly, the force balance as written above assumes that the pressure drop is linear whereas in practice data collected (Gill and Russell, 1954; Davenport and Russell, 1960; Smith and Ramsden,

1978) show that pipeline presents a very high concentration of pressure at the upstream end of the pipe which is not picked up at the end of a pipeline for 1 hour (see Smith and Ramsden, 1978), i.e. compressibility of the oil plays a major part in determining yield stress (see further data from Perkins and Turner, 1971 and Ronningsen, 1990). Finally, in pipeline type apparatus, it is conventional to make an assessment of when flow starts (i.e. once the yield stress is just overcome) by observing when flow reaches an arbitrary small steady level from no flow. The complex nature of the gelled waxy crude oil can cause wax oil free oil to leak through the bulk structure prior to bulk yielding and this is another potential error in the measuring technique.

Clearly, capillary viscometers, particularly pipeline type devices have a potential as useful devices to measure yield stress but only if due consideration is made (i) about the wax layer thickness that deposits on the wall, (ii) the method of gauging when flow commences and (iii) accounting for compressibility and shrinkage of the oil when it gels. The present research as we shall see considers the key issue that concerning the wax layer thickness.

Following from their assessment of the capillary viscometer, Wardhaugh and Boger in 1990 went to review yield stress measurements obtained with rotational viscometers. These are standard rheological instruments (concentric cylinders, cone and plate, plate and plate) in which the sample can be suitably conditioned (sheared first to remove its memory and cooled down at a prescribed cooling rate to a test temperature) and then subjected to either a shear stress, applied gradually from the lowest permissible level as dictated by the instrument drive, until flow is observed through a measurable shear rate or a fixed shear rate leading to a measurable shear stress to detect the yield point. Up to 1990, such devices suffered from the lack of

accuracy in the lower scales of stresses and shear rates and clearly were not suited for the measurement of yield stress often obtained by extrapolation of data obtained in the higher range. Clearly although convenient, the data obtained by linear extrapolation are not necessarily representative data.

Having established that up to 1990 no repeatable data on yield stresses had been obtained using capillary or rotational viscometer, Wardhaugh and Boger undertook a major programme of work to measure yield stress of waxy crude oils assessing four experimental techniques (Wardhaugh and Boger, 1990):

- The vane technique,
- The cone and plate viscometer at constant shear rate.
- Oscillatory testing using the R19 Weissenber rheometer fitted with cone and plate geometry and
- Constant applied shear stress with a Bohlin CS rheometer fitted with a cone and plate geometry.

All these devices are rotational viscometers but their principle of measurement differs.

The vane technique is essentially a stirring device (see Figure 2-5), typically a four blade vane inserted into a sample of the oil contained in a cylindrical vessel. In order to prevent wall slip, baffles are fitted at the cylinder wall. Further details on the vane technique can be found also in Nguyen (1983), Nguyen and Boger (1983), Wardhaugh (1990).The yield stress is measured by applying a constant rate of increase in the applied torque (stress loading rate) until a creeping motion is observed as indicated by the slow movement of the vane.

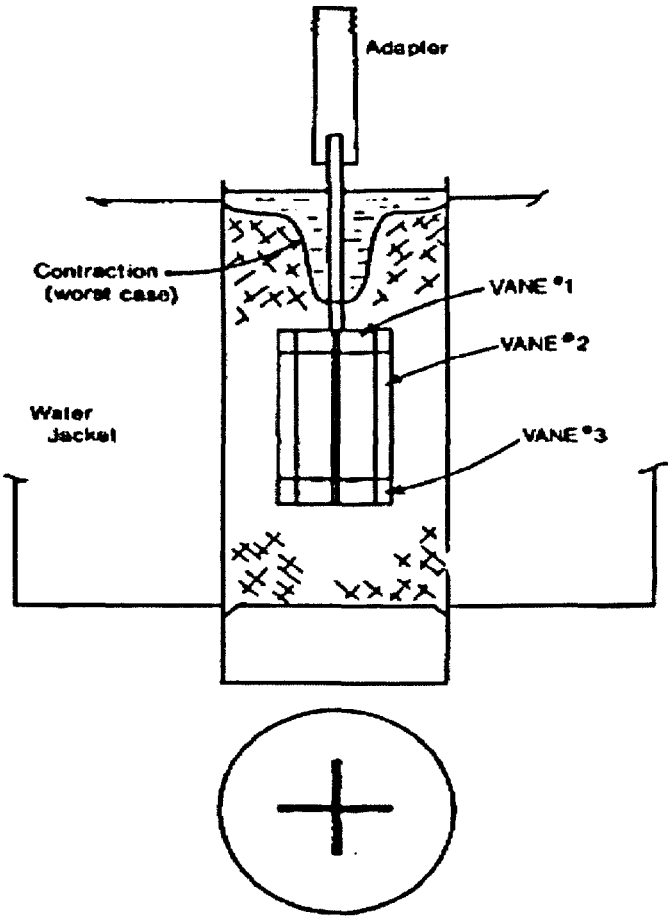

Figure 2-5 Diagram of three vanes used in the experimental work showing relative dimensions and position in the wax sample. [Horizontal dashes-original sample volume at start 50 °C; cross hatching – final shape of the gelled sample showing the worst case of contraction] (Wardhaugh and Boger, 1990)

A typical data trace is shown in Figure 2-6. Yielding is deemed to occur when, beyond a critical point, neither the rate of increase of the torque nor the movement of the vane is constant or gives repeatable values. As Figure 2-6 shows, the observed behaviour is that of a yielding of a solid, with the initial deformation being similar to an elastic solid followed by creep and fracture, after which the gelled oil begins to flow as a liquid.

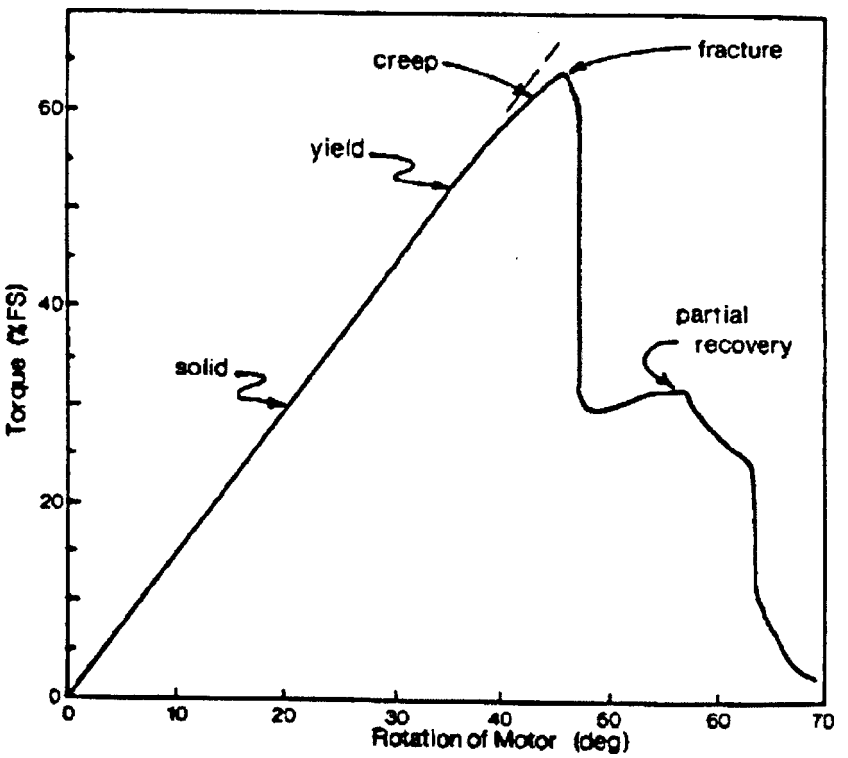

Figure 2-6 Typical response of the measurement of yield point using the vane technique. (Jackson-Hutton crude oil at 10 °C sample cooled from 50 °C) (Wardhaugh and Boger, 1990)

The true yield point is thus at the limit between the end of the elastic response and the beginning of creep. Clearly this yield point will depend on the stress loading rate, i.e. the rate at which the torque is increased and this is shown in Figure 2-7; so it is not uniquely defined. However we can define the true yield stress as being the value obtained which is independent of stress loading rate. In other words to obtain this true yield stress we repeat the experiments, decreasing the stress loading rate until we observe no change in the measured yield stress. In order to carry out such measurements, the torque accuracy has to be fine indeed and this limits the accuracy of the vane technique. Nevertheless, this technique shows that the yielding of waxy crude oils is the same as the mechanisms of the fracture of

solids showing a transition from ductile to brittle fracture as the strain rate is increased.

So gelled waxy crude oils behave similarly to metals, plastics and building materials and cannot be described by the rheological models used to describe non-Newtonian fluids because of the complex nature of their yield stress.

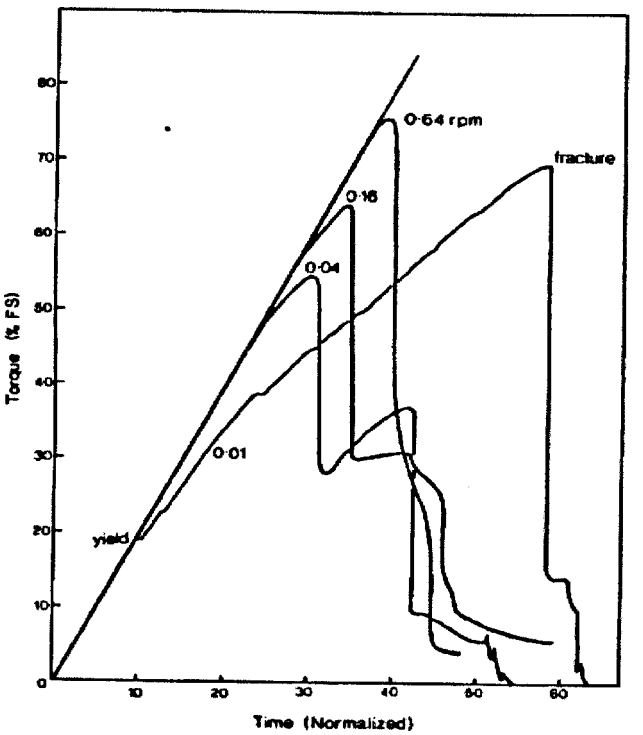

Figure 2.7 Effect of the rotation rate (nominal values) on the torque response using the vane technique (Jackson-Hutton crude oil at 10 °C; 100% FS= 0.50 Nm) (Wardhaugh and Boger, 1990)

Having established the power of the vane technique in describing the mechanism of yielding of waxy crude oils, Wardhaugh and Boger then considered the more standard rheological instrument, the cone and plate viscometer operating at constant rotation (Wardhaugh and Boger 1990). They found the yielding response to

be similar in shape (see Figure 2-7) to that of the vane technique and this suggests that the elastic response, creep and fracture are real phenomena of the yielding behaviour of gelled waxy crude oil.

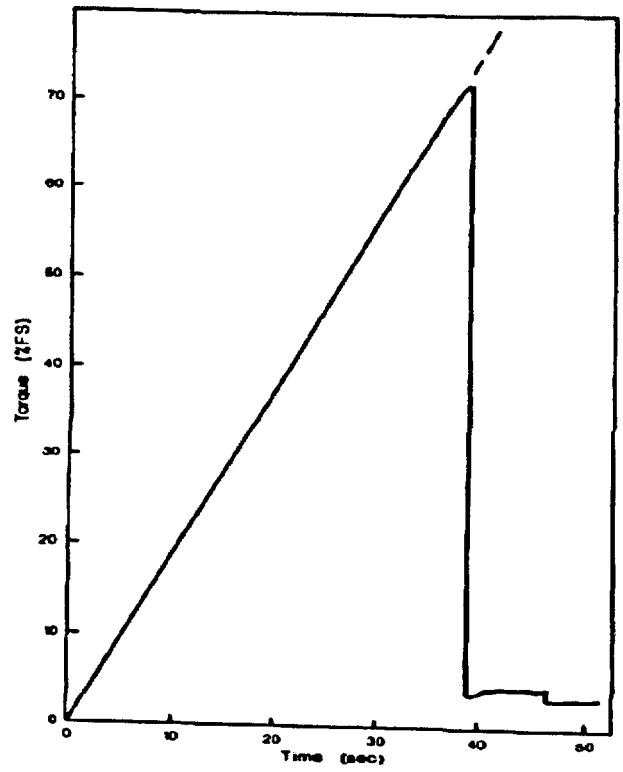

Figure 2-7 Typical yielding response for the cone and plate viscometer (constant rotation). (rpm equivalent to 0.015 ; Jackson- Hutton crude oil at 10 °C, conditions as for run 2- Table II; 100 % FS = 3.34 Nm) (Wardhaugh and Boger, 1990)

The degree of creep observed with the cone and plate was however less pronounced and this may be due to the higher rate of stress loading or the more uneven distribution of the stress over the plate surface. Clearly this points to the need to use the cone and plate viscometer with due care with regard to stress loading and the nature of the plate surface (roughened vs. polished). Further discussion on these aspects with waxy oils can be found in Atkins and Mai (1985), Petrellis and Flumerfelt (1973) and Ronningsen (1990 & 1991).

Following from the cone and plate, Wardhaugh and Boger examined yielding when a small amplitude sinusoidal oscillation is applied using the R19 Weissenberg rheogoniometer (Wardhaugh and Boger, 1990). Clearly with this system it is necessary to select a torsion head and an amplitude input that provides sufficient stress in the sample for yielding to occur. When a very low level of induced shear stress is applied, it was observed that the sample was completely in phase with the applied motion, regardless of the amplitude and frequency. This behaviour indicates that at these low stresses, the gelled waxy crude oil behaves as a Hookean solid with a constant storage modulus, G'. Note that for a viscoelastic fluid, the storage modulus has a sharp positive slope being a strong function of frequency and for inelastic fluids, G' would be expected to be zero. Clearly, gelled waxy crude oils possess a true yield stress (see debate about the existence of yield stress in Barnes and Walters, 1985). Now as the applied shear stress is increased, the response ceases to be sinusoidal and changes as the yielding process proceeded (see Fig 2-8).

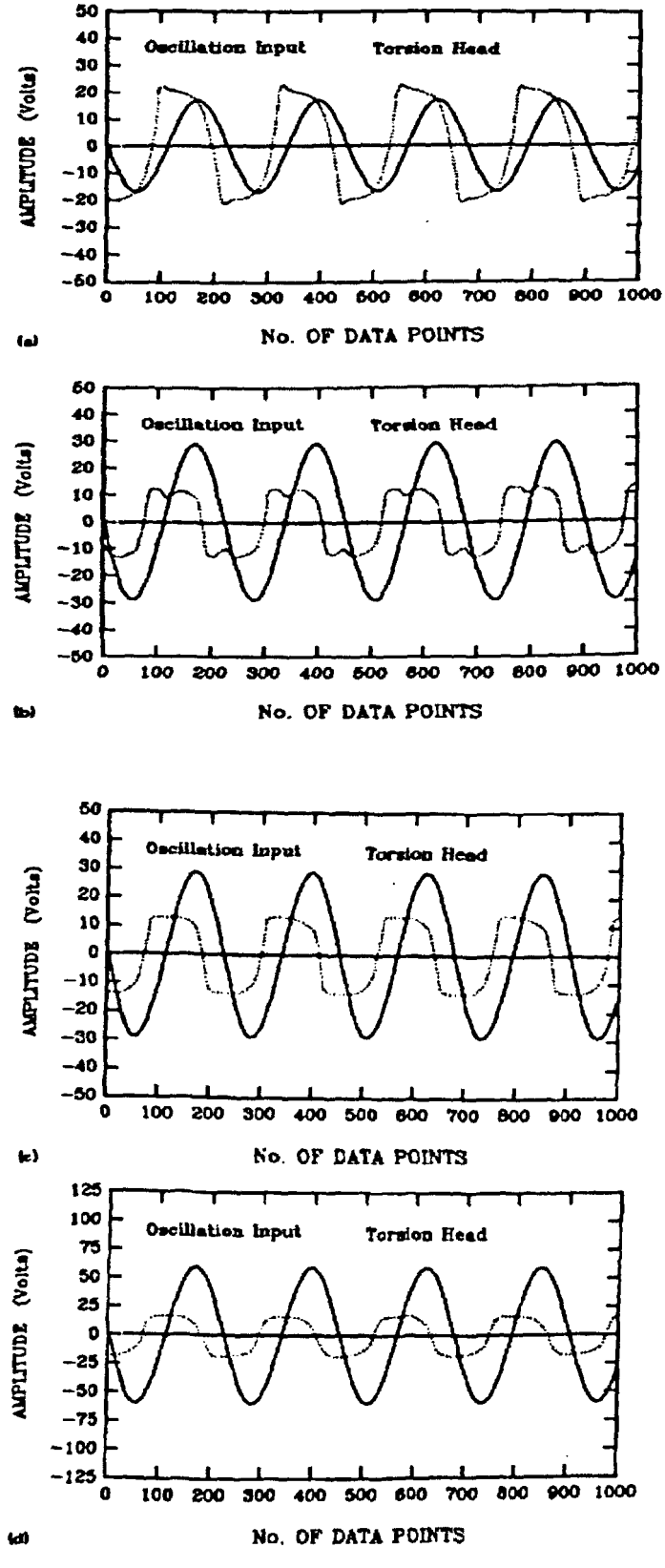

Figure 2-8 Nonlinear response of Jackson- Hutton crude oil at 10 °C at high levels of induced stress. [Max. applied stress = (a) 3712 Pa, (b) and (c) 5492 Pa, (d) 11279Pa; frequency (all runs) = 0.3155 cps.] (Wardhaugh and Boger, 1990)

From these traces, it is clear that as the oscillations continued and/or the amplitude increased, the phase shift was approaching 90^0 indicating that the shear is destroying the elastic nature of the material and transforming the gelled oil into an inelastic fluid with little or no yield stress. Interestingly, Wardhaugh and Boger observed that this breakdown occurs at a level of shear stress at which the vane technique shows a creep behaviour. So the fact that it appears with the vane technique that the same sample exhibits an elastic response at higher stress points to instrument artefacts, i.e. these yield stress are real, reproduced in both instruments but their value appear to depend on the instrument used to measure them (Wardhaugh and Boger, 1990).

The final assessment by Wardhaugh and Boger was made using constant stress rheometry with a Bohlin CS rheometer fitted with a cone and plate geometry. They observed over a period of 5 min that no movement occurred when a low shear stress was applied (1 Pa) to a sample of Jackson-Hutton crude oil at 21^0C. This confirms that the gelled oil was behaving as a Hookean solid and did not simply possess a very high zero shear viscosity. When they increased the stress to 10 Pa they observed what they describe as stick-slip, a period of movement followed by a period of no movement. When the stress was increased further to 20 Pa, the stick-slip phenomenon was observed initially however after 20 s, a definite movement was observed and continued to increase with time up to the end of the experiment which lasted 20 minutes. This behaviour was seen for constant shear stress up to and including 120 Pa. On removing the stress, no change was detected. With the next increment in applied shear stress (240Pa), the creep behaviour continued for a period of 28 mins. Interestingly, Wardhaugh and Boger observed that the commencement of creep seen in the constant stress rheometer coincides closely with the

commencement of creep seen in the vane technique (Wardhaugh and Boger, 1990). The yield stress however (which would correspond to the commencement of stick-slip) occurred at lower levels.

The conclusions that can be drawn for this study are as follows:

- The behaviour of gelled waxy crude oil is not like that of conventional yield stress materials (suspensions for example) for which it is enough to know the yield stress which a single value.
- Gelled waxy crude oils yielding behaviour has three distinct characteristics: an elastic (Hookean) response, a slow deformation (creep) leading to fracture-like behaviour resembling the fracture of solids.
- The vane technique although able to reproduce the yielding feature cannot be used without critical evaluation of the results which are geometry and measurement procedure dependent.
- Oscillatory testing and constant stress techniques measurement have not provided a full picture of the creep region and require further study. This is because of the instrument stress levels that can be applied accurately and the distribution of the stress on the plate.
- The capillary viscometer is the least suitable to measure yielding because of the wax deposition, compressibility and shrinking effects. It is however the most attractive potentially as it mimics the real pipeline situation, so any improvement of the technique will be very welcome by industry.
- It is clear that the rheological techniques are concerned with probing very carefully the very low creeping flow associated with yield stress. These are however of no interest to industrialists seeking technical knowledge to start their gelled pipelines. What is of interest is the fracture stress, that

stress beyond the yield point and creep region which allows full flow to proceed.

More recent studies all support these conclusions (see Venkatesan et al., 2002; Silva and Coutinho, 2004; Mohamed and Hadj, 2006; Ding et al., 2007; Lee et al, 2007; Lee et al, 2008; Ekweribe et al, 2008; Amhamed, 2009). Amhamed (2009) work was particularly important as it was carried with a pipeline type rheometer with comparison made with a modern rheometer (Anton Paar) at constant stress and oscillatory tests. The discrepancy between the data obtained by Amhamed (2009) using the pipeline instrument and the constant stress and oscillatory tests confirm the need to re-examine the pipeline instrument and account for wax deposition in the calculation of the yield stress.

The directions of the present work were made on the basis of these conclusions. In particular, the pipeline instrument is highly desirable if the main problem of wax deposition can be taken into consideration. Clearly however if the pipeline approach is to be followed the data obtained from such a device have to be assessed against conventional rheological instruments particularly the oscillation and constant stress types.

It is thus proposed in this research to develop the pipeline device and assess the data against oscillation and constant stress data.

2.2.3 Techniques for Measuring the Gel Point

In the above review and the introduction preceding, the term gel or gellation was often used meaning the temperature at which the wax crystallized to form a structure. Clearly it is an important property that needs to be measured to define a particular waxy crude oil. In industry, this temperature is approximated to the pour point: the

temperature at which a certain minimum amount of the oil can be poured from a standard container. Clearly as Gill and Russel (1954) already explained in 1954, this is a gross approximation as if the oil gels no flow is possible (Gill and Russel, 1954). From the discussion on the nature of waxy crude oils, this property should thus be defined rheologically as the transition from solid to liquid behaviour. It is thus closely linked to the measurement of the yield stress as explained above. Kane et al. in 2004 showed that the gel point could be uniquely defined from rheological tests that located the temperature at which the measured storge modulu (G') and loss modulu (G'') cross over, which corresponds to the transition from solid to liquid behaviour or from deformation to flow (Kane et al., 2004). As explained by Silva and Countinho (2004), the gel point of a waxy crude oil does not depend on the wax content only but on other components present in the oil that can affect the wax crystallisation, asphaltenes for example (Countinho, 2004). Also Guo et al. in 2006 explained from their study that the *strength* of gels formed by crystallizing long-chain paraffins from solution increase with increasing cooling rate for C_{36} and C_{32} waxes, but decrease for C_{28} (Guo et al., 2006). Clearly the type of wax material of the oil is also important and will define the gel point.

In this research, a similar approach to the measurement of the gel point will be used.

2.3 WAX DEPOSITION IN PIPES & TECHNIQUES FOR MEASURING IT

Clearly from the above discussion, the wax which deposits on the wall of the pipe is a key determinant in improving the estimate of the yield stress using a pipeline type rheometer and Equation (2.6). We review below the related work in order to help

chose or develop a technique to measure the wax thickness that deposit in the pipeline instrument, the intended rheological tool of the present research.

2.3.1 Introduction

As explained earlier, crude oil is a complex mixture containing aromatics, paraffins, naphthenes, asphaltenes and resins but it is the long-chain paraffins (*n*-alkanes) which have a tendency to deposit on the cold walls of pipes and other process equipment surfaces (heat exchangers, tanks, separators, distillation columns, etc.). The phenomenon of wax precipitation is induced because of solubility limits. At reservoir temperatures (in the range of 70-150 °C) and pressures (in the range of 8000-15000 psi), paraffins remain dissolved in the crude oil and the system behaves as a Newtonian liquid.

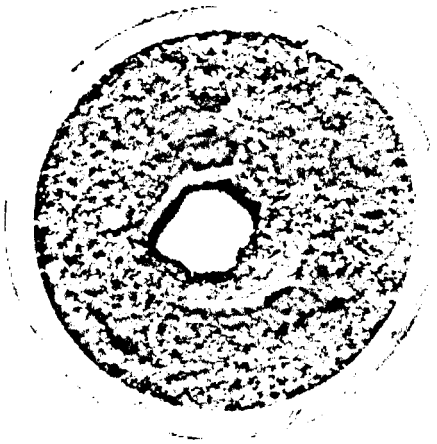

Figure 2-9 Deposition of wax in oil pipelines

Source: http://tigger.uic.edu/~mansoori/Wax.and.Waxy.Crude_html (09/08/2010)

As the crude oil leaves the reservoir and flows through pipelines, its temperature drops due to the cold environments of the ground or the ocean floor

(usually less than 4 °C). The solubility of the paraffins in the crude oil decreases severely with decreasing temperature, hence they precipitate out, crystallize and deposit on the cold pipe walls, thereby restricting flow. Figure 2-9 shows the cross-sectional view of a cut-away segment of a pipeline affected by wax deposition. As it can be observed, the area available for the crude oil flow has been significantly reduced. Under this state of affairs, the part of the pipeline that is plugged would have to be cut out and replaced, resulting in significant operational costs. According to the US Department of energy, remediation of pipeline blockages in water depths of about 400 meters can cost $1 million/mile (Venkatesan, 2002). In one instance, Lasmo Oil Company which is one of the UK oil companies had to abandon an off-shore oil platform due to recurring paraffin plugging problems at a cost of over 100 million dollars. Overall, the paraffin deposition problem is a billion dollar problem in the oil industry (Venkatesan, 2005). Singh (2000) termed the phenomenon of gel deposit of increasing solid wax content with time as aging, leading to the gel hardening with time. Venkatesan (2005) observed that the properties of the gel deposit, such as the gelation temperature and the solid wax content, are, as might be expected, strong functions not only of the waxy oil composition but also of the shear and thermal histories under which the deposit is formed. Thus, in order to achieve efficient remediation of the problem (choosing the appropriate deposit removal technique and the appropriate way to administer the chosen technique), it is important to investigate the wax precipitation process and the nature of the wax precipitates (Venkatesan, 2005). Two important techniques for removing wax deposits are mechanical pigging and melting the deposit using heat produced by a chemical reaction. Pigging is the standard industrial process of using a 'scraper' device to remove the wax deposits from the pipe walls. If the gel deposit is too hard,

then such mechanical methods of remediation would prove to be difficult, as exemplified by instances when the pig has been stuck in the pipeline during the cleaning process. When the deposit is hard, thermal methods of remediation maybe used either to dissolve the wax deposit completely, or to soften the deposit for subsequent pigging.

Figure 2-10 shows the gel deposition process on a cold surface. Majeed (1990) reported that many theories, including molecular diffusion, Brownian diffusion, shear dispersion and gravity settling, have been proposed to explain the precipitation process of the paraffin culminating in several mathematical models (see Bern, 1980; Haq, 1981; Majeed, 1990; Brown, 1993, Svendsen, 1993 and Singh, 2000). Amongst these researchers, Singh (2000) for example explains that an external convective mass flux of wax molecules from the bulk oil flow towards the cold wall and an internal diffusive flux within the gel layer are responsible for the growth and aging of the gel deposits (Singh, 2000).

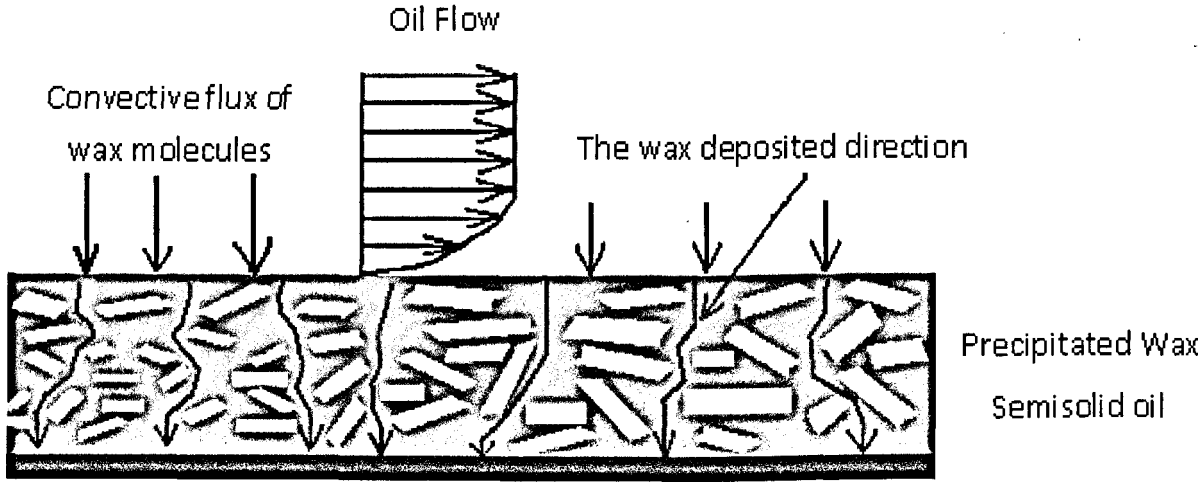

Figure 2-10 Schematic diagram showing the wax precipitation process

Haq (1981) investigated the parameters controlling the deposition of paraffin wax from its solutions in kerosene onto a pipe surface. As expected, their data showed that the paraffin wax deposition increased with increasing time and wax concentration, but decreased with increasing flow rates and temperature difference between the bulk solution and the cold surface of the pipeline. There appeared a critical deposit thickness at which deposit breaks up giving rise to the fluctuating flow conditions (Haq, 1981).

2.3.2 Determination of the Wax Thickness deposited in pipelines

Four methods have been used by previous investigators for measuring or interpreting wax thickness during single-phase flow in pipes, namely spool piece, pigging, pressure drop and heat transfer methods. The first two methods can be categorized as direct methods whereas the last two as indirect methods. There are other methods but less generally used which include the liquid displacement (Chen, 1997) and the ultrasonic methods (Andersen, 1997; Brian, 2007). The liquid

displacement method uses a complex combination of low and high pressure being applied through the flowing system from which the wax thickness is inferred. The ultrasonic method is based on a standard pulse-echo technique, where thickness is estimated from the time-of-flight of echoes from the steel/wax- (inner pipe wall) and wax/gas interface, respectively.

***Spool Piece Method*:** Clearly, this method is direct and simple. It also allows visual examination of the wax deposits and sampling wax deposits for desired compositional analysis. In this method, a take-out section with deposited wax film is dismantled from the testing pipe after being drained. Then, the wax thickness is determined by measuring the weight or volume of wax deposits removed from the take-out section or weighing the take-out section. Because of the advantages of this method it is still widely used in experimental studies of wax deposition in low pressure, single-phase flow. However, this method is time consuming. Each time a measurement of wax thickness is performed, the testing pipe must be bypassed or the entire test system must be completely shutdown in order to remove the take-out section. This may not give acceptable wax deposition data in high pressure, single-phase and multi-phase systems since the testing pipes must be depressurized and the phase equilibrium is consequently changed.

***The Pigging Method*:** In this method, the wax thickness data are obtained by passing spheres through a pipeline and measuring the wax volume removed. This method has found wide application in removing liquid accumulation in natural gas pipelines. Its advantages and disadvantages are similar to those of spool piece method; however, it is used more in field studies than laboratory studies.

Pressure Drop Method: This method is based on the concept that wax deposition in a pipe section reduces the hydraulic diameter of the flowing fluid inside the pipe, resulting in an increase in frictional pressure drop over the pipe section. The frictional pressure drop across a section of pipe with wax deposited inside can be calculated using the following well-known equation (Abdel-Wali, 1997):

$$\Delta P_f = 4f\frac{L}{d}\frac{\rho}{2}\left(\frac{4Q}{\pi d^2}\right)^2 \qquad (2.6)$$

ΔP_f : is the pressure drop.

f : is the Fanning friction factor.

L : is the length of the pipe.

d : is the hydraulic diameter.

ρ : is the fluid density.

Q : is the volumetric flow rate.

A waxy crude oil often behaves as a non-Newtonian fluid when temperature becomes lower than the cloud point and wax crystals are present in the crude oil. However, when the wax content is low, e.g. less than 5% by weight, this non-Newtonian behaviour is not appreciable and the crude oil can be treated as Newtonian fluid (Abdel-Wali, 1997).

The friction factor in equation [2.6] can be estimated from (Abdel-Wali, 1997):

$$f = cN_{\mathrm{Re}}{}^{-n} \qquad N_{\mathrm{Re}} = \frac{4\rho Q}{\pi\mu d} \qquad (2.7)$$

μ : is the apparent viscosity of the crude oil. N_{Re} : is Reynolds Number

Laminar flow exists when $N_{Re} < 2000$ where c =16 and n =1. However, for the turbulent flow c = 0.046, and n = 0.2 (Chen, 1997). This method is too simplistic as it regards the wax layer as simply reducing the flow cross sectional area and not interfering with flow, i.e. diminishing in size with increasing flow when it could do. It is probably more appropriate with wax that has aged in a pipeline and becomes hard.

Heat Transfer Method: In any flowing fluid pipe system, the total resistance to heat transfer from the flowing fluid to the environment is comprised of the resistances due to convective heat transfer from the flowing fluid at the pipe wall, heat conduction through the pipe wall and any insulation or other coatings, and an appropriate heat transfer process to environment (e.g. convective heat transfer if the pipe is exposed to water, air or other cooling fluids). With a waxy crude oil flowing in a pipe, after a layer of wax deposit is formed on the pipe wall, convective heat transfer with paraffin solidification will take place on the interface between the flowing fluid and the deposited wax layer. A thermal resistance term due to heat conduction through the wax layer is added to the total resistance to heat transfer from the flowing fluid to the environment. This added thermal resistance is approximately in direct proportion to the thickness of the wax layer on the pipe wall. Hence, the wax thickness can be determined from measurements of relevant thermal parameters by solving the relevant heat transfer equation which in this case is (Abdel-Wali, 1997):

$$\frac{T_f - T_o}{q_o} = \frac{1}{h_w}\frac{r_o}{r_i - \delta_w} + \frac{r_o}{k_w}\ln\frac{r_i}{r_i - \delta_w} + \frac{r_o}{k_p}\ln\frac{r_o}{r_i} \qquad (2.8)$$

T_f : bulk fluid temperature in the pipe.

q_o : heat flux through the outside pipe wall.

r_o & r_i : outside and the inside diameters of the pipe respectively.

h_w : film heat transfer coefficient from the flowing fluid to the wax. h_w can be estimated using an appropriate correlation or model.

k_p & k_w: thermal conductivities of the pipe wall and deposited wax respectively. k_w can be assumed equal to the thermal conductivity of waxy crude oil, since wax thermal conductivity is very close to that of waxy crude oil and significant amount of oil is usually trapped in the wax deposits (Brown, 1993).

δ_w: thickness of the wax layer.

Thus, the wax thickness can be calculated from equation (2.8) when the bulk oil temperature T_f, the outside pipe wall temperature T_o, and the heat flux through the outside pipe wall q_o are measured. q_o can also be obtained from a heat balance. The heat lost from the fluids over a length of pipe must equal the heat transfer to the surroundings (Brown, 1993).

Thus,

$$C_p \rho Q \Delta T_f = 2\pi r_o L q_o \qquad (2.9)$$

ΔT_f is the oil temperature drop over the wax measurement pipe section and C_p is the specific heat of the waxy oil. If there is no provision to measure the outside pipe

wall temperature T_o, but the environment temperature T_e is available, the wax thickness can be calculated from the following heat transfer equation (Brown, 1993):

$$\frac{T_f - T_e}{q_o} = \frac{1}{h_w}\frac{r_o}{r_i - \delta_w} + \frac{r_o}{k_w}\ln\frac{r_i}{r_i - \delta_w} + \frac{r_o}{k_p}\ln\frac{r_o}{r_i} + \frac{1}{h_o} \qquad [2.10]$$

h_o is the film heat transfer coefficient from the outside pipe wall to the environment.

2.4 MODELLING OF START-UP PRESSURES OF GELLED PIPELINES

Apart from the simple force balance expressed by Equation (2.1), no mention has been made in this literature survey on modelling work. Clearly this is very important and an overview of the research efforts in this direction is now given. However it must be stated at the outset that however sophisticated a model is, unless the flow-deformation behaviour of the waxy crude oil is well represented by data, the model outcome and results cannot be trusted. This explains in a way the direction of this work, which is to help develop constitutive flow-deformation equation from data that represent well the rheological behaviour, particularly the yield stress region and how it varies with cooling rates, applied stress and time.

The force balance equation 2.1 is naturally a simple model but as explained it cannot predict accurately the start up pressure because a linear pressure drop is assumed and incompressible flow. When the wax gels, a structure is formed and this structure shrinks depending on the cooling rate and creates a porosity, i.e. the material is compressible (see Verschuur et al., 1971; Wardhaugh and Boger, 1991). Due considerations must be made to account for a yielding model that is representative of the real situation (see discussion above) and also of compressible

effects. One key development in the modelling attempts has been made by Chang et al. (1999) (working with Boger) who used a three yield stress constitutive equation with an elastic- limit yield stress, a static yield stress and a dynamic yield stress (see Figure 2-11 defining these 3 terms) but did not consider compressibility effects. Recently a series of models have followed using the original 3 yield stress constitutive equation proposed by Chang et al. (1999) but taking into account compressibility effects (Chang et al., 1999). These models are by Davidson et al. (2004), Vinay et al. (2006) and Davidson et al. (2007) and are numerically based and they all model the gelled oil in the pipe as multiple gas separated plugs (see Figure 2-11) to account for the effect of shrinkage during shutdown prior to restart (Vinay et al., 2006; Davidson et al., 2007).

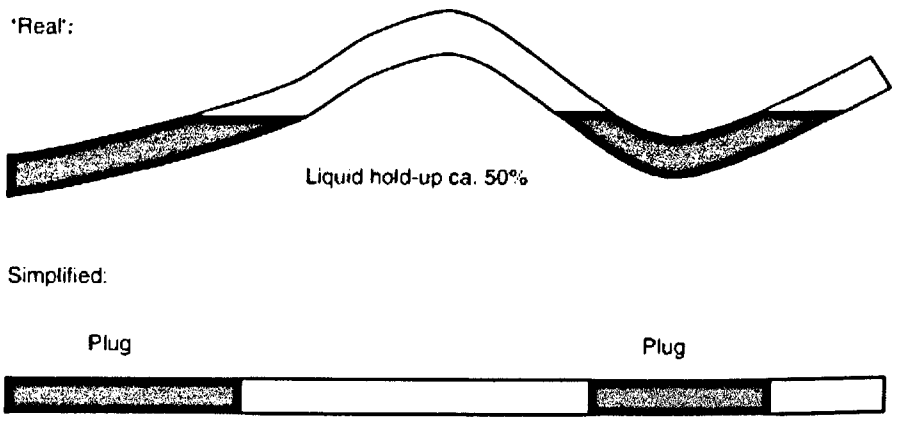

Figure 2-11 Schematic of simplified pipeline with gas-separated gelled oil plugs

In these models, in addition to the 3 stress constitutive equations of the gelled oil, the gas plugs are given a constant compressibility coefficient and the flow in the pipeline is restarted by pumping in an incoming fluid (ICF) to displace the gelled oil

which becomes the outgoing fluid (OGF). The ICF may be water or an oil of the same properties as those of the gelled oil before shutdown so it is given a simple rheological model (Bingham or Newtonian). Also, the interface between the ICF and OGF are assumed to be flat. Clearly without continuing with the details of these models, they are very broad approximation of the real scenario particularly in relation to representing compressible effect by a series of gas plugs. This explains why it is desirable to revisit the capillary viscometer (pipeline rheometer) and use it as the closest means of predicting the start-up pressure but improving on the technique by accounting for wax deposition and compressibility effects. This explains the direction taken by the present research.

2.5 CONCLUSIONS

From the review of literature on the start up pressure of waxy crude oils, it can be concluded that the key element is a proper evaluation of the rheology of the waxy crude oils upon a set cooling rate which brings the oils below or near its gel point. All efforts in measuring this rheology have shown that waxy crude oils are materials that resemble solids near the gel point with three distinct characteristics: an elastic (Hookean) response, a slow deformation (creep) leading to fracture-like behaviour. None of the rheological techniques, vane, rotational, oscillatory and capillary, lead to consistent data. Seemingly the data are instrument dependent and are not reproduced from one technique to another. In particular, it was found that the capillary type technique which in principle is the most attractive as it mimics flow in pipes does not give reliable data because the wax deposited is not taken into consideration in the force balance controlling flow. Also the capillary method considers the oil to be incompressible when in actual behaviour it is not. The literature review also showed that most of the recent rheological work has been

concerned with probing very carefully the very low creeping flow associated with yield stress. These are however of no interest to industrialist seeking technical knowledge to start their gelled pipelines. What is of interest is the fracture stress, that stress beyond the yield point and creep region which allows full flow to proceed. Therefore the pipeline instrument is highly desirable if the main problem of wax deposition can be taken into consideration. This will be one objective of the present research to measure the wax layer. Clearly however if the pipeline approach is to be followed the data obtained from such a device have to be assessed against conventional rheological instruments particularly the oscillation and constant stress types which from previous work have shown to reproduce the solid like behaviour. This will be a second objective to assess the pipeline rheological data against oscillation and constant stress data obtained with the new advanced Anton-Paar instrument which is capable of operating at much wide range of conditions (cooling rate, stress ramp rate and lowest level of stresses and shear). The third objective is more industrially targetted as the experiments will be carried out on typical industrial waxy crude oils as found in the field: Libya Remal waxy crude oil, British Petroleum Azerbaijani waxy crude oil and a mixture of both at 50-50% as a model industrial waxy crude. It is important to note that the start-up pressure in themselves, obtained from the rig of this research, are valuable information that can help industry with operating larger pipelines.

CHAPTER 3: EXPERIMENTAL METHOD

This chapter describes the various equipments and techniques used to perform the characterisation of the waxy oils, measure their rheological properties in standard but advanced instruments and measure the start-up pressure in a pilot line designed specifically for this type of research. In this chapter no data on the waxy crude oils studied are presented. However as the rheology of waxy crude oils is a complex issue, in describing the various techniques to be used, we shall present some illustrative examples of the expected behaviour that can be obtained with each of the techniques. These discussions will be helpful and are indeed the necessary background required to undertake this research and the difficult task of tracking the yielding process of the waxy crude oils and measuring the corresponding yield stress(es).

3.1 GENERAL PHYSICAL CHARACTERISATION OF THE OILS

Three waxy crude oils have been used in these experiments: one provided by BP (British Petroleum) and originating from the Azeri Well BooZ 2 in Azerbaijan, one by ENI[1] Oil Company of Libya and originating from their Remal well and the third one is a *model* oil referred to as MIX, produced in our laboratory by mixing equal volumes (500ml) of the BP oil with the Remal oil. The original oil samples were previously heated at (70-80^{0}C) and stirred in agitator at 80rpm for 1 hour and the mix kept under similar conditions of temperature and agitation before storing in a sealed jar ready for further testing (rheological) or processing (pumping)

These oils were characterised by measuring the following properties:

[1] ENI stands for Ente Nazionale Idrocarburi, the original Italian name of the company

Pour Point: This was determined according to standard methods (Mcketta, 1993) which consist of detecting the temperature at which no flow is observed. This imperfect method was performed as follows:

- Heat oil sample 30^0C above the quoted pour point, pour it in a beaker of reasonable surface area and place it in refrigerator or crushed ice.
- Inspect the sample at 5 minute intervals by tilting it horizontally, observing movement of the surface.
- The pour point is deemed to have been reached when upon tilting the beaker, the oil surface does not sag for 5 seconds. The standard is for the pour point to be 3 °C higher than this "critical" temperature.

As stated above, this method is imperfect and represents only a rough guide to situate the waxy crude oil in the rheometric experiments planned. We shall see that the rheological data using oscillatory tests (see below) enables a more accurate detection of the gel point or the temperature at which wax first appears.

API Gravity: The American Petroleum Institute gravity is another measure of specific gravity designed specifically to compare the relative densities of petroleum liquids at 15.5^0C designated as *light* when the API is greater than 10 and heavy when it is less than 10. The instrument that is used for such measurement is a hydrometer, graduated in degrees in a scale such that most values would fall between 10 and 70 API gravity degrees. It is important to note that the degree API is not a unit but simply a denomination. This characteristic is of course related to normal specific gravity (SG) which can be measured in the usual manner (Becker,1997):

- Cool a sample of waxy crude oil to 15.5 °C.
- Place approximately 500 ml of the waxy oil in a graduated cylinder.

- Weigh the amount of 500 ml of the sample.
- The density of the sample can be measured by dividing the weight of the sample over the volume of it.
- The specific gravity can be measured by dividing the density of the sample over the density of water.

The API and S Gravity are related as follows:

$$API = \frac{141.5}{SG} - 131.5 \qquad (3.1)$$

It is important to put in perspective the API gravity and crude oil classification:

- Light crude oil is defined as having an API gravity higher than 31.1 °API. (less than 870 kg/m^3)
- Medium oil is defined as having an API gravity between 22.3 °API and 31.1 °API. (870 to 920 kg/m^3)
- Heavy oil is defined as having an API gravity below 22.3 °API (920 to 1000 kg/m^3)
- Extra heavy oil is defined with API gravity below 10.0 °API (greater than 1000 kg/m^3)

Also, it is important to note that the API gravity does not give an indication of the wax content and that waxy crude oils are not for example "heavy" or "extra heavy". Table 3.1 which lists the API gravity of the waxy crude oils considered in the study shows this clearly.

Wax Content: This was determined following standard procedures (Mcketta, 1993; Narjes, 2003) which consists of the following steps:

- Use acetone and a flask with a funnel, both chilled at 0 °C.
- Place in a beaker acetone and dry ice.

- Mix in the flask 4g oil with 40 ml of dichloromethane solvent (DCM).
- Keep the flask agitated and placed inside a water bath to allow the formation of wax for approximately two hours.
- Filter the mixture using filter paper-funnel connected to a vacuum pump.
- Wash with DCM to make sure all the oil is removed.
- At the end, the wax should be washed with hot petroleum ether (PE) to dissolve all the wax and it should then be evaporated until dry to calculate the %wt of wax.

The pour points, API gravity and wax content of the three oils studied in this programme are presented in Table 3.1. This data show that the wax contents are in a good range for experimental studies, 15, 25 and 35% as are the corresponding pour points 20, 37 and 42^{0}C. It is interesting at the outset to remark that these pour points are high but not abnormal and stress the observation that gelling of waxy crude oils occurs commonly at normal temperatures and not below zero as it may be presumed.

Table 3-1 Physical characteristics of the three waxy crude oils used in this study

Character	**Method**	**BP Sample**	**Mix Sample**	**Remal Sample**
SG@60°F	Measured in the Lab	0.8795	0.8766	0.8770
API@60°F	Measured in the Lab	29	30	30
Pour Point °C	IP 15/D97 (measured in the Lab)	20	37	42
Wax Content (wt %)	UOP 46/64	15	25	35

3.1 SAMPLES PREPARATION

As the rheological properties are the key to this research, it was necessary to organize the samples in a systematic manner so that no previous rheological history could affect the measurements planned and also to facilitate repeat comparative testing. To that effect, all the oil samples were preheated to remove the memory effects of thermal and shear history on waxy structure. The preheating was carried out "slowly" in a water bath, bringing the temperature from room temperature to 80^0C, gradually over a period of 2 hours, whilst also stirring at 80 rpm using an anchor agitator (see Figure 3.1). Once the 80^0C temperature was reached, stirring at 80 rpm and at this temperature was maintained for 2 hours, before storing the samples in sealed jars for 48 hours ready for rheological testing thereafter.

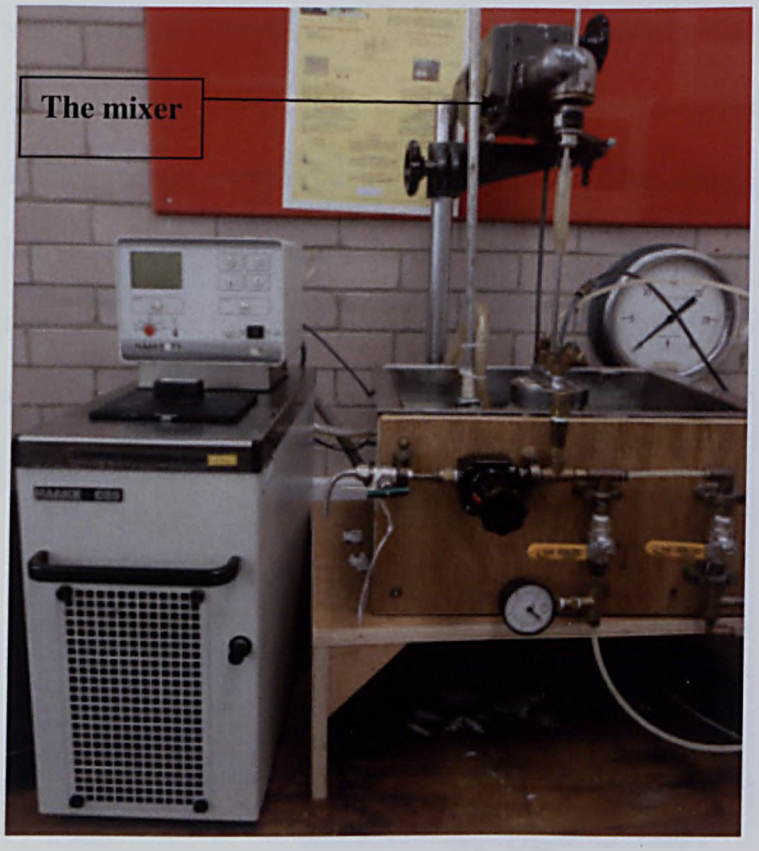

Figure 3-1 Photograph of the mixer used in this study

Note that this 80^0C temperature is well above the pour point temperature of the samples indicated in Table 3.1 (20, 42 and 37^0C respectively for BP, Remal and Mix). Such a method of preparation is widely used for rheological testing of waxy crude oil (Lie and Jin, 2007).

3.2 RHEOLOGICAL METHODS OF MEASUREMENT

As stated at the outset, this programme of research is concerned essentially in the measurement of the yield stress as it is this equivalent pressure that must be overcome when starting a pipeline that has had the oil it transports allowed to precipitate its wax and gel into a semi-solid plug. Performing rheological testing in the appropriate mode of operation is necessary if an accurate determination of the yield stress is desired. This requires rheological equipment that can be operated in controlled stress, oscillatory or creep modes, the three techniques most appropriate to measure yield stresses and the yielding process of gels and materials that contain solidifying particles such as waxy crude oils. We are fortunate that the laboratories at Bradford University are equipped with the latest such equipment, the Physica MRC 501 Anton Paar (see Figure 3.2), which can operate both at constant shear stress and constant shear rate and under rotational and oscillatory modes.

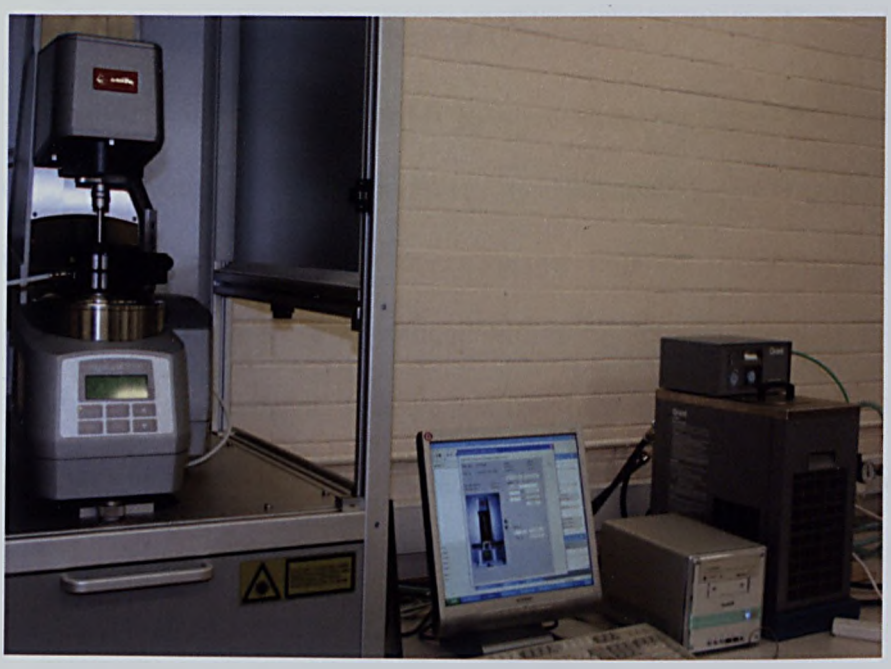

Figure 3-2 The Physica MCR 501 Anton Paar Rheometer

Whereas the constant shear rate mode can give information about the behaviour during large deformation such as pumping, stirring the constant shear stress mode can be used in a ramp up-down mode to track the onset of yielding. The oscillatory tests exploit the concept of viscoelasticity in material deformation which is measured by subjecting the sample to an oscillatory deformation and measuring its response in time which in the presence of a solid component of flow will show a phase shift. Also, instead of ramping up and down, it is possible to carry out similar controlled stress experiments by imposing different constant stresses for a creep time over a period of time and then removing the stress abruptly while recording the resulting strain recovery over time. These three techniques allows not only to determine the yielding process and relevant yield stresses but also enable to analyze the structure of the material at rest and give information about storage stability, elasticity over long time scales.

3.2.1 Generalities & Rotational Mode of Operation

A schematic of the Rheometer MCR-501 is shown in Figure 3.2. As with all viscometer, the device essentially measures the resistance to an imposed flow by measuring a torque (constant shear operation) or imposes a force. In this new rheometer design, an air bearing is provided with technology for digitally controlling the shear stress in a range 10^{-7} to 3000 Pa and the shear rate in a range 10^{-6} to $3000s^{-1}$. The accuracy in the scale is thus very good, enabling to detect very small yield stress values. Also important with this instrument which is fitted with a Peltier device, is the ability to control very accurately temperature to within ±0.5°C and program cooling rate from very low values of 0.1°C/minute to higher rates of 5°C/minute, in very small steps if so desired. These features are most suited for this research as we seek to mimic temperatures and cooling conditions in the ground which can vary depending on climatic conditions. Earlier research as reported in the literature survey were limited by the available rheometer technology so this research offers a step-up in accuracy of the yield stress that can be measured in a very wide range of cooling rates from a set temperature.

The Rheometer MCR-501 can accommodate two measuring systems, the cone and plate and the plate and plate systems and operate in the rotational or oscillatory modes. Both systems are described below such flow situations in both the cone and plate and the plate and plate systems.

Cone-and-Plate System: Figure 3-3 shows the geometry of the system which consists of a circular cone and a plate holding in between them the sample to be tested. The dimensions of the conical area of the flow field are defined by the cone radius R and the cone angle α which according to the International Organisation of Standards ISO

should not be greater than 1° if constant shear rate is to prevail. Under such conditions, the shear stress τ, shear rate γ and their ratio the apparent viscosity η are related to the measured torque M and cone rotational speed N by (Mezger, 2006):

$$\tau = (3M)/(2\pi.R^3) \tag{3.2}$$

$$\dot{\gamma} = 2\pi N / \tan\alpha \tag{3.3}$$

$$\eta = \tau/\dot{\gamma} = (3 * M * \tan\alpha)/(2\pi * R^3 * N) \tag{3.4}$$

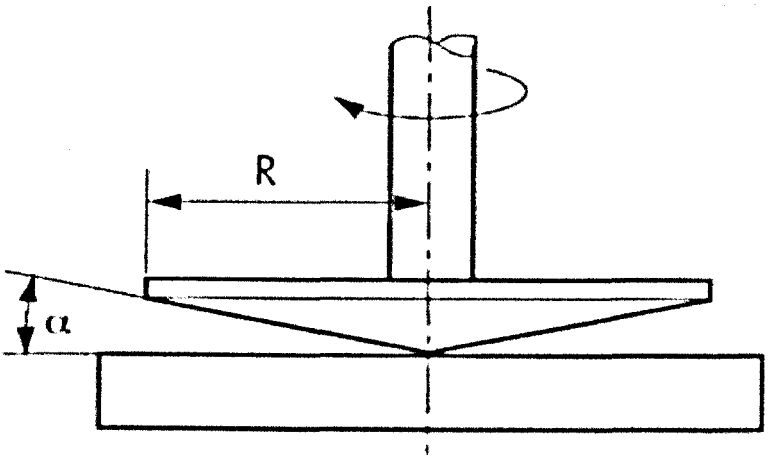

Figure 3-3 Cone-and-plate measuring system CP-MS (Mezger, 2006)

Parallel-plate System: Figure 3.4 shows the geometry of the system which consists of two parallel plates separated by a gap where the fluid to be measured is sheared.

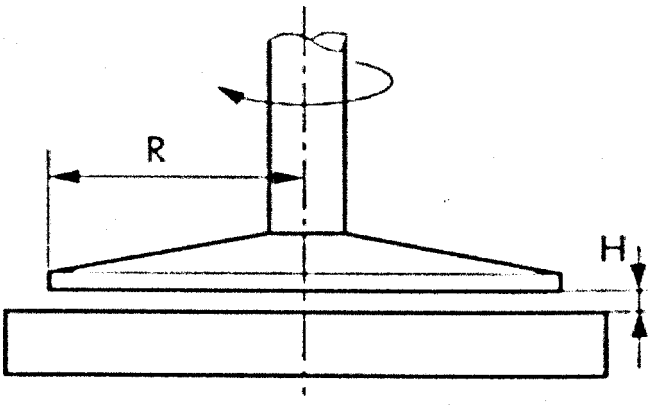

Figure 3-4 Plate-and-plate measuring system CP-MS (Mezger, 2006)

In order to ensure 1D viscometric shear flow, this gap H has to be very small in comparison the plate radius, R. Under such conditions, the shear stress τ, the shear rate $\dot{\gamma}$ and their ratio the apparent viscosity, η are related to the measured torque M and plate rotational speed N by the shear stress τ, shear rate $\dot{\gamma}$ and their ratio the apparent viscosity η are related to the measured torque M and plate rotational speed N by (Mezger, 2006):

$$\tau = (2M)/(\pi.R^3) \tag{3.5}$$

$$\dot{\gamma} = (2*\pi*N)/H \tag{3.6}$$

$$\eta = \tau/\dot{\gamma} = (M*H)/(\pi^2*R^3*N) \tag{3.7}$$

There are advantages and disadvantages of using either system but the essential difference is that with the parallel plate system, the shear rate is not the same over the diameter of the plate.

The rotational tests can be carried out either with controlled shear rate (CSR) or controlled shear stress (CSS). Clearly CSS experiments are necessary to determine the yield stress although in principle CSR experiments are also able to but the difficulty in getting a very low shear rate limits the accuracy in determining the yield stress using CSR experiments. In this research, both CSS and CSR experiments were carried out in order to obtain the yield stress but also viscosity data beyond the yield point. The viscosity data are of course important in assessing the pipeline performance during normal conditions. Note that before the start of the rheological experiments, the rheometer was calibrated using standard oil provided by the manufacturer (Oil 2700-VO7). The results of the calibration are shown in Table 3-2 and show that the error in the measurements of viscosities is less than 1%.

Table 3-2 Calibration results of the Physica MCR 501 Rheometer

Temperature, °C	**Specified Viscosity mPa.s**	**Measured Viscosity mPa.s**	**% Error**
20	35.35	35.08	0.76
25	27.72	27.49	0.83
40	14.74	14.65	0.61

3.2.2 Yield Stress Measurements using Control Stress Ramp Mode

Having defined the operating equations of shear stress and shear rate in the steady rotational mode, we now describe how the rheometer can be adapted in this mode to measure yield stress using controlled stress experiments. Clearly, as we are seeking to detect the stress at which flow, i.e. yielding occurs, the device must be operated by

ramping the stress up, gradually (linearly) from a very low value or zero to a value higher than the yield stress then decreasing back the stress to zero and measuring the corresponding shearing rate. This essentially a "hysteresis" technique and usually the ramping up is carried out more slowly (typically 5 minutes) than the ramping down (1 minute). Also no data can be recorded in the up curve before the shear rate reaches the resolution limit of the rheometer. This is the most serious limitation of this technique which by definition cannot give the *elastic limit yield stress* unless the rheometer is designed to measure very small shear rates.

In this research we use such technique to assess the extent of the rheometer to measure the very low level of shear rate if required and also to compare the data obtained with this method with other methods presented below.

Figure 3-5 presents some data to illustrate the technique and the interpretation of the results. It is important to note the need to use both linear and log scale to enlarge the scale and enable the identification of the yielding region A-B-C which is composed, if the rheometer is capable of measuring very low shear rates, of a creep region A-B and a fracture region B-C. In this illustration, point B is identified as the starting of the fracture. The region A-B is the most difficult to track because the shear rate there will be very small. Beyond C and into the region C-D we are entering viscous flow, shear thinning in nature because of the breakage of the wax crystals (Chang, 1998). The *dynamic yield stress* must thus be determined from the up curve by extrapolating tangentially from D as shown in the illustration. This dynamic yield stress is thus a fictitious property but useful as a rheological parameter (Chang, 1998).

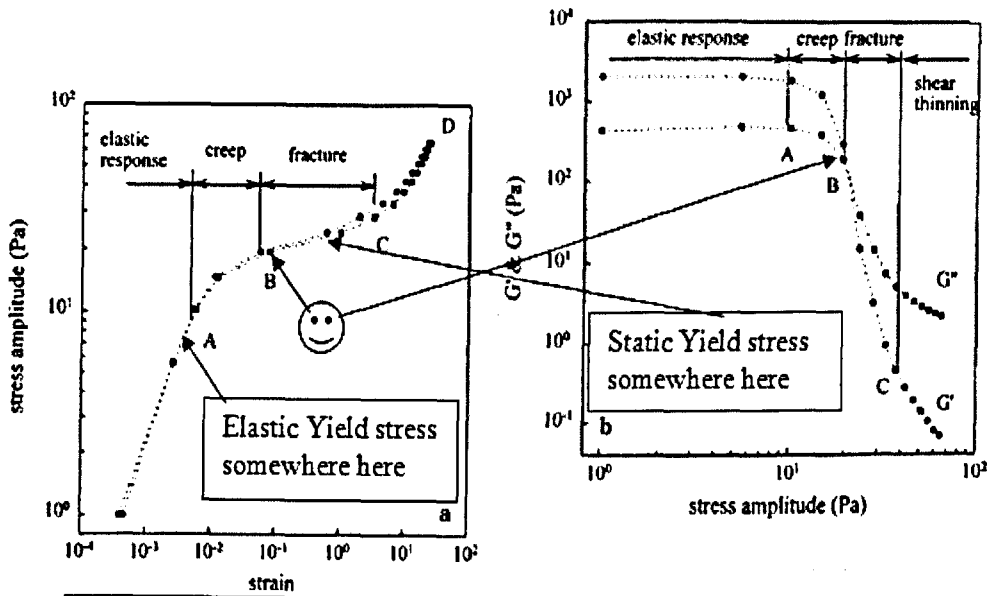

Stress amplitude increased linearly from 0 to 65 Pa. Frequency kept constant at 1 Hz

Figure 3-5 Results from oscillatory test: (a) stress vs strain relationship during the yielding process (DH19, 20 C, 1 Hz); (b) G' and G" during yielding (DH19, 20 C, 1 Hz) (Chang, 1998)

One important note here is the values as measured in the region A-B-C-D will be all time dependent, so it is important to carry out ramping up and down experiment at different rate to capture the effect of shearing time on yielding. This is very important in practice as it may be that time of shear can be more than compensate for stress, i.e. when starting a gelled pipeline, it may be that much lower stresses (pressures) are required but for a comparatively longer time, but not excessively long to justify not going for very high stresses that require very short time to start up the pipeline. Figure 3-6 shows illustrative data to quantify the time effect. It also explains a tentative link between the elastic limit yield stress and the dynamic yield stress, the two being the same if the controlled stress tests are performed at an infinitely low stress loading rate (Chang, 1998).

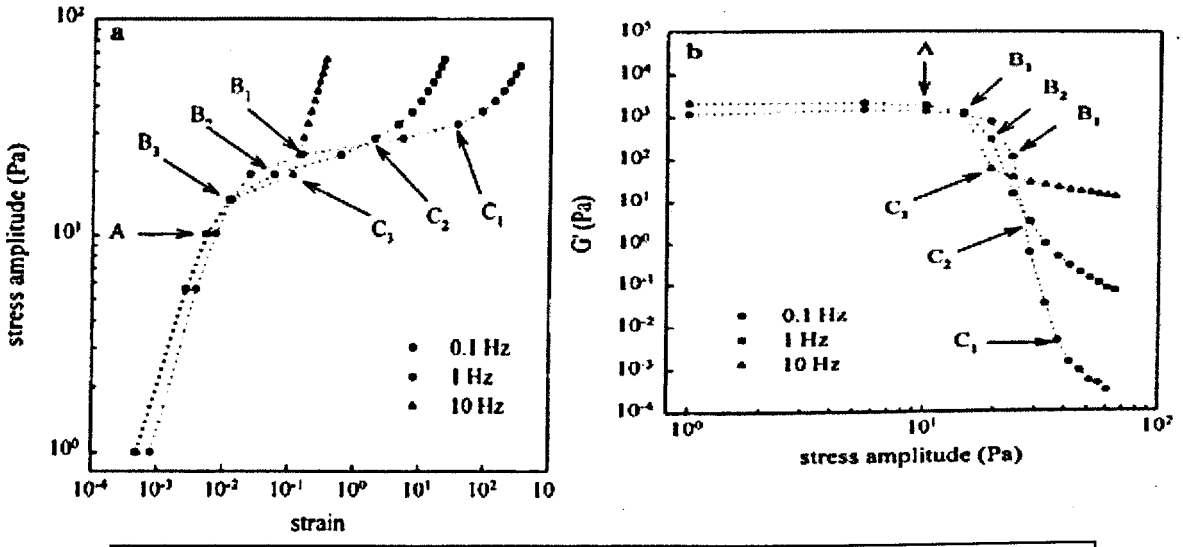

Stress amplitude increased linearly from 0 to 65 Pa. Frequency kept constant at 0.1, 1 and 10 Hz respectively to assess time dependency

Figure 3-6 Results from oscillatory test: (a) effect of frequency on stress vs strain relationship during and after yielding (DH19, 20 VC): (b) effect of frequency on G' and G" during and after yielding (DH19, 20 C) (Chang, 1998).

3.2.3 Yield Stress Measurements using Oscillatory Mode of Operation

Theoretical Background: Also referred to as dynamic mechanical analysis (DMA), this mode of operation was also used to measure the rheology of the waxy crude oils at temperatures below the pour point in order to determine yielding properties.

The principle is explained with reference to Figure 3-7 which shows oscillatory motion induced mechanically in a plate and plate system by a drive wheel-rod arrangement leading to the upper plate moving back and front under a shear force ±F. The resulting deflecting path and angle are ±s and ±φ respectively.

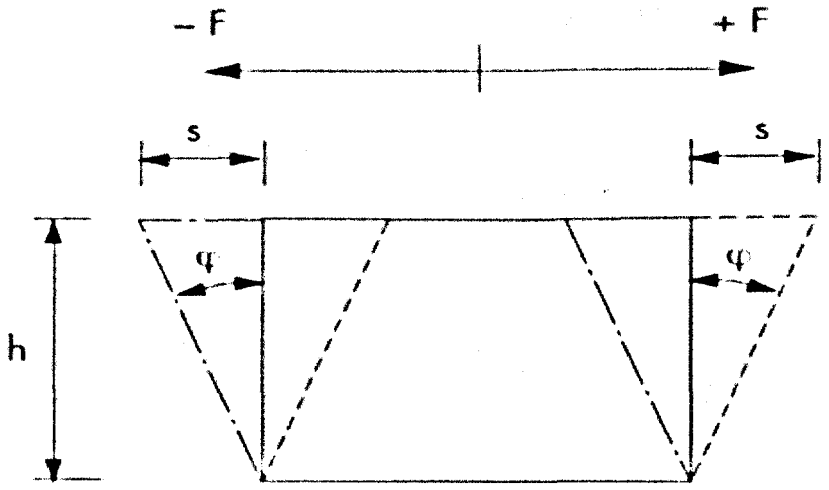

Figure 3-7 Oscillatory motion of plate and plate system: shear force ±F, deflection path ±s, and deflection angle ±φ in the shear gap h (Mezger, 2006)

If A is the plate area and h, the gap between the plates, then the shear stress and shear strain are, respectively (Mezger, 2006):

$$\pm\tau = \pm F/A \qquad \pm\dot{\gamma} = \pm s/h = \pm \tan\varphi \qquad (3.8)$$

Figure 3-8 shows the position or time-dependent function of τ(t), $\gamma(t)$ and $\dot{\gamma}(t)$ for an ideal-elastic behaviour. At angle positions of 0° and 180° during continuing rotation, the upper plate is in the zero position and therefore, □=0 and τ=0 but the shear rate is at its maximum because the velocity is at its maximum.

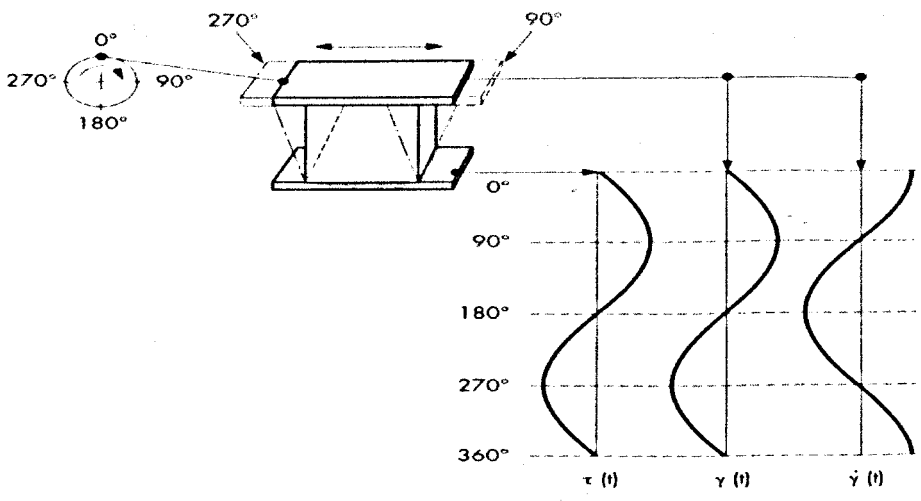

Figure 3-8 Sine and cosine curves of the time-dependent function of τ(t), and for ideal-elastic behaviour (Mezger, 2006)

At angle position 90°, the upper plate exhibits maximum deflection to the right, and at 270° the maximum deflection occurs to the left. Following Hooke's law describing an ideal elastic deformation, we can write:

$$\tau(t) = G^*.\gamma(t) \qquad (3.9)$$

where G^* is the complex shear modulus. Similarly, for an ideal-viscous behaviour, Newton's law applies and we can write:

$$\tau(t) = \eta^*.\dot{\gamma}(t) \qquad (3.10)$$

where η^* is the complex viscosity.

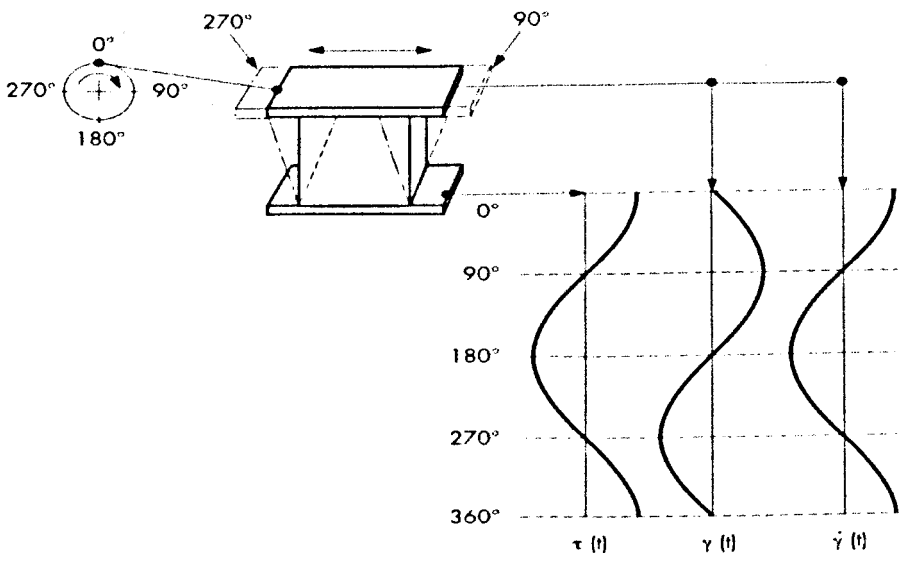

Figure 3-9 Sine and cosine curves of the time-dependent function of τ(t), and for ideal-viscous behaviour (Mezger, 2006)

In the real case of viscoelastic behaviour as shown in Figure 3-9, the applied oscillatory (sine wave) shear strain and shear stress are in the form:

$$\gamma(t) = \gamma_0 . \sin \omega t \qquad \tau(t) = \tau_0 . \sin \omega t \qquad (3.11)$$

where ω is the pulsation or frequency and γ_o the amplitude. The resulting shear stress and strain will show a phase shift angle δ between 0° and 90°:

$$\tau(t) = \tau_0 . \sin(\omega t + \delta) \qquad \gamma(t) = \gamma_0 . \sin(\omega t + \delta) \qquad (3.12)$$

Using equations (3.11) and (3.12), it is clear that the complex modulus G* is defined as:

$$G^* = \tau_{o} / \gamma_o \qquad [3.13]$$

This complex modulus is made up of two components, the storage and loss moduli, G' and G''defined from vectorial decomposition as:

$$G'(\omega)= G^*(\omega)\cos(\delta) \quad \& \quad G''(\omega)=G^*(\omega)\sin(\delta) \tag{3.14}$$

$$\left|G^*\right| = \sqrt{(G')^2 + (G'')^2} \tag{3.15}$$

G' is a measure of the energy stored during the vibration procedure. If $G'= 0$, the sample is a purely viscous fluid. G'' measures the energy dissipated. If $G''= 0$, the sample is a Hookean solid. A damping factor may also be defined from the vector decomposition linking the phase angle to these moduli:

$$\tan\delta = G''/G' \tag{3.16}$$

It is important to note that by definition, G', G" and Tan δ are all frequency dependent. Table 3-3 shows values of G', G'' and δ for typical gel materials like waxy oils at temperature below the pour point (Mezger, 2006).

Table 3-3 Values of G', G'' and δ for different materials (Mezger, 2006)

The behaviour of				
Idealviscous flow	**Viscoelastic liquid**	**50/50 viscous and elastic**	**Viscoelastic gel or solid**	**Idealelastic deformation**
$\delta = 90°$	$90° > \delta > 45°$	$\delta = 45°$	$45° > \delta > 0°$	$\delta = 0°$
$\tan\delta \rightarrow \infty$	$\tan\delta > 1$	$\tan\delta = 1$	$\tan\delta < 1$	$\tan\delta \rightarrow 0$
$G' \rightarrow 0$	$G'' > G'$	$G' = G''$	$G' > G''$	$G'' \rightarrow 0$

In the same way as the complex modulus was defined, a complex viscosity η* can also be defined and decomposed in a vector form into component η' and η'' leading to the following expressions:

$$\eta' = G''/\omega = (\tau.\sin\delta)/(\gamma.\omega) \quad \& \quad \eta'' = G'/\omega = (\tau.\cos\delta)/(\gamma.\omega) \qquad (3.17)$$

$$|\eta^*| = \sqrt{(\eta')^2 + (\eta'')^2} \qquad \tan\delta = \eta'/\eta'' \qquad (3.18)$$

Application to Measuring Yield Stress: Clearly when measuring the properties of the waxy crude oils below the pour point the interest is in measuring all these quantities, G', G'' and δ and determine from them the yield process hopefully some critical values equivalent to a yield stress. We have already defined these quantities as being frequency dependent so tests at different frequencies will be required. The amplitude of these frequencies is clearly the parameter that will dictate the extent of flow and as we are seeking to determine yielding, i.e. the critical region where flow begins, it is important to operate in the region where the oil sample remains solid, i.e. deforms elastically and "push" it just until it breaks and begins to show viscous flow. This translated in rheometric terms means to operate the oscillatory test in the Linear Viscoelastic Region (LVR) first then following this in the non linear region. Thus in this study, measurements were done at a fixed low frequency (~1 Hz) whilst increasing slowly the amplitude of the oscillation and measuring the strain response in both linear and nonlinear regions, from which the storage modulus (*G'*) and the loss modulus (*G''*) during the entire yielding process can be determined. Figures 3-5 and 3-6 illustrate the type of data searched and their interpretation in relation to evaluating yielding and yield stresses (there is more than one critical value). We note from this illustrative example the following:

- The initial linear stress-strain relationship before point A indicates elastic behaviour with approximately constant *G'* and *G''* and reflects the fact that the waxy network in the oil is not destroyed when the stress amplitude is below a

certain low critical value (to be determined as part of the rheological investigation).

- When the stress amplitude increases above the critical value, G' and G'' decrease gradually with increasing amplitude, indicating a creep response in which both elastic and plastic strains are involved. The elastic-limit yield stress may be determined to be at the boundary point near A where the linear elastic region gives way to the non linear creep region. .
- An oscillatory stress with amplitude higher than the elastic limit yield stress will cause creep, which will partially damage the waxy structure, if the stress is not sufficiently high to produce fracture.
- After point B, a sudden increase of the strain occurs together with sharp drops of G' and G'', indicating the fracture process of the waxy network. Another important change around B is that G' becomes lower than G'' after B, which also indicates a change of the oil sample from solid-like to liquid-like. Point B may be identified as the starting point of the fracture and defines the static yield stress. It is also the gel point as it will be explained in the Result section, Chapter 4.
- Oscillation beyond point B (in Figure 3-5), i.e. with stress amplitude higher than the static yield stress will destroy the waxy structure completely. The oil after the destruction displays a typical viscous behaviour, with very high strain responses and G' much lower than G'', as displayed by the final range of the curve after point C.

Again and as in the case of the controlled stress tests, time effects must be fully evaluated as they will affect these yield stresses. In this oscillatory type of deformation, time effects are imbedded in the frequency and must be measured by

carrying out tests at different frequencies. Only then and on the basis of experimental evidence, can the elastic-limit yield stress be determined as frequency independent.

3.2.4 Measurement Procedure & Range of Conditions

Having explained the sample preparation to erase all memory effects (see Section 3.2) and described the measurements techniques, it is important to explain that the purpose of the rheological experiments was to measure the yield stresses of these waxy oils under conditions similar to the ground, i.e. duplicating scenarios of cooling rates down to a set temperature. The same protocol is also to be applied to the pipeline rig described below to measure start-up pressure from which we can infer (calculate using a simple model) the yield stress. So the purpose of the rheological experiments is to assess if the yield stress measured in the rheometer "resemble" those measured in the pipeline rig. Strictly, they should but as we shall explain, the calculation of the yield stress from the start-up pressure using models is subject to many assumptions so the "target" is to assess how close the yield stress measured in the rheometer are to those inferred from the start-up pressure data.

In terms of procedure, the steps taken to mimic cooling in the ground were as follows:

1. Retrieve no-memory sample from the stock as prepared and described in Section 3.2 and place in a 0.5 litre beaker.
2. Heat-up in a water bath gradually (0.5^0C/minute) from room temperature to 80^0C, inserting the agitator when the waxy crude oil has melted completely (10^0C above the measured point, as shown in Table 3.1).

3. Keep the oil agitated at 80^0C at 80 rpm using an anchor type agitator (see Figure 3-10) for 30 minutes.

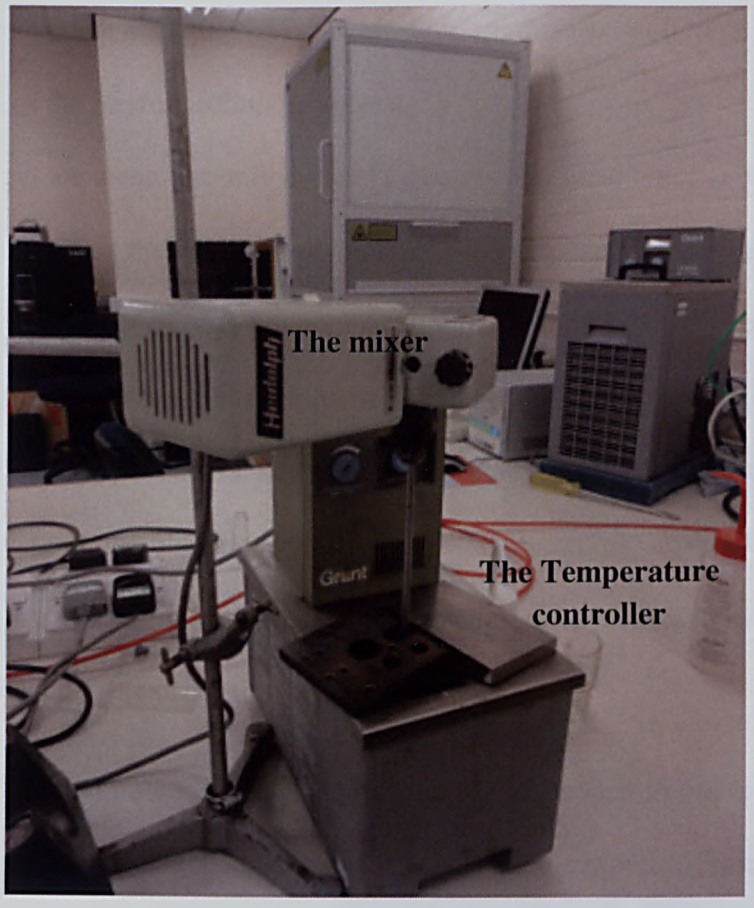

Figure 3-10 Agitator, temperature controller and water bath used for conditioning the oil sample

4. Using a pipette or a spatula, withdraw the required quantity (a few cc 0.70 ml) from the beaker and place on the plate of the rheometer whose temperature had been set to 80^0C, at least 30 minutes before the start of the experiment.
5. Start measurement programme down to the set temperature and measure rheology. This step is carried out automatically in the Physica MRC 501 Anton Paar and requires the input of the desired temperature, cooling rate and the measuring mode (creep, ramp or oscillatory mode). In all cases, there is a

time delay (automatically accounted for in the programme and set here as 5-15 minutes depending on the mode) for the sample to settle on the plate at the set initial temperature, here 80^0C. Also, the data are recorded in the pc connected to the rheometer and processed with the appropriate software. Further discussion in the Result section, chapter 4.

6. By rheology, we mean not only the yield stresses and yield process but also the gel point as well as the variation of apparent viscosity with shear rate, shearing time for a wide range of temperatures and cooling rates (0.16 - 5 ^{0}C/min).

The range of conditions investigated in this programme was designed to cover scenarios that could happen in practice in the field but extended beyond to develop an understanding of the rheology. Thus the temperatures covered included temperatures well below the pour points and the cooling rates includes low and large extremes that were possible using the rheometer Peltier.

It is important to note that the scenarios that could happen in practice include the real situation where once gelled the oil is left static in the pipeline for a period of time before the pipeline is started. Therefore such eventuality which was the most important one in practice needed also covering in the scheduled of the rheological experiments. So typically, in a yield stress measurement for this situation, after being cooled to the desired temperature, the sample is left at this temperature on the rheometer plate for 1 hour, 8 hours or days to mimic stoppage and restart in the field.

3.3 THE PIPELINE RIG

3.3.1 Background & Theoretical Considerations

The aim of this research as stated in the introductory chapter was to develop a technique to estimate the yield stresses of the waxy crude oils as accurately as it is

possible using state of the art rheological instruments. Such an instrument was presented and described above. Now to verify that the yield stresses so obtained are reproduced in practice, a pilot pipeline rig is required. This section describes such a rig is used in this programme to measure start-up pressures from which the yield stress can be inferred from a simple flow model summarized by the well known force balance between pressure drop ΔP and the wall shear stress, τ_w in a pipeline (see Figure 3-11 explaining this force balance) of length L and internal diameter D:

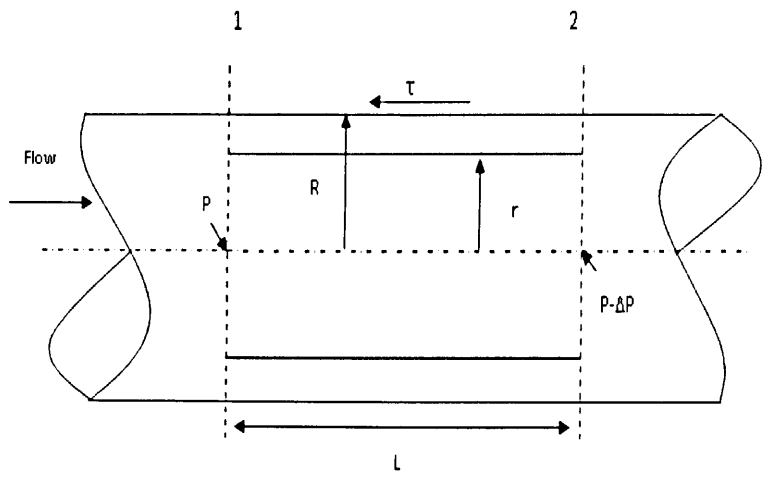

Figure 3-11 Force Balance on a section of fluid in a pipe

$$P\pi r^2 - (P - \Delta P)\pi r^2 - 2\pi rL\ \tau = 0$$

$$\Delta P\ \pi r^2 = 2\pi rL\ \tau$$

$$\tau = \frac{\Delta P}{2L} r$$

The last Equation can be extended across the whole radius of the pipe

$$\tau = \tau_R = \frac{\Delta P.R}{2L}$$

This can be written as

$$\frac{\Delta P}{L} = \frac{4\tau}{D}$$

$$\tau_w = \Delta P\left(\frac{D}{4L}\right) \qquad (3.19)$$

Equation (3.19) is the extent of the model which can be improved upon if the actual diameter for flow is measured taking into consideration wax that has gelled and settled on the wall of the pipeline. This is the limiting issue with regard to the accurate estimation of the yield stress. Thus if the wax layer, h_w that deposits during gelling is measured, then an improved estimate of the yield stress can be obtained as:

$$\tau_w = \Delta P\left(\frac{D-2h_w}{4L}\right) \qquad (3.20)$$

Taking the model further, we can write that this thickness of wax deposited will be function of wax content, Cw of the oil in the pipeline and the holding time, th or the time the oil remains stagnant in the pipeline from when it has dropped to its gel point, the temperature at which wax first precipitates. This can be expressed by the following general relationship:

$$h_w = f(C_w, t_h) \qquad (3.21)$$

In principle a series of experiments can be carried for each oil to evaluate how h_w varies with parameters C_w and t_h. This exactly what was carried out in these experiments in addition to measuring the yield stress in the pipeline at start-up under controlled cooling conditions, hold up times and temperatures.

3.4 Start-up Pressure and Yield Point of Waxy Crude Oil

Gill and Russell, 1954 studied the first laboratory measurements of the yield point of waxy oils by testing them in 1mm diameter U-tube capillaries. The results were found to be strongly dependent on the Length to Diameter (L/D) ratio when this ratio was below 200. Changing the material from glass to stainless steel gave vastly different results.

Start-up pressure is the main problem of pumping the waxy crude oil once the pipeline has been blocked. For start-up, a minimum pressure drop is required before the oil will yield and the flow starts. The starting pressure is thus very important factor in pipeline design to operate safely and economically. This pressure can be calculated from rheological data and indeed this is an important aspect of this study. Also, it can be measured in a laboratory pipeline rig and this is covered later in this report. Several researchers discuss the handling of waxy oils in pipelines designed using rheological data (Herring 1974; Smith 1979a; Smith 1979b; El-Eman, Bayoumi et al. 1993). The capillary viscometer is the natural instrument to use because of the geometric similarity of the full-scale pipeline. The difficulty in measuring yield stress using the capillary viscometer is that the value cannot be obtained precisely. The start-up pressure is obtained first and the yield stress is then inferred (Smith 1979a; Smith 1979b; Wardhaugh 1990).

In conclusion, up until 1980 these researchers measured the yield stress albeit badly because of the instrument which operated only at constant shear rate rather than constant shear stress. Many instruments with better operating capabilities have been developed in the last two decades. Chang et al, 1998 used one of these and examined the yielding process under stress, a creep-recovery, and oscillatory tests. The results

showed that the yielding point of the waxy oils occurs by an initial elastic response, followed by viscoelastic creep and a final fracture. Also they concluded that elastic-limit yield stress, which is the minimum limit of the pump pressure required to initiate flow in a pipeline, is independent of the time scale.

The time scale of the measurement in the controlled stress test is expressed in term of the stress loading rate. Clearly, the measured static yield stress from the rheometer can only be applied to the design with the information of the time scale of the measurement.

As in any pipe flow, the flow regime must also play a part. Ideally turbulent conditions are desirable but these may not be achievable in practice. The comparison between turbulent flow data in a real production pipeline with two model pipelines, one with a turbulent flow whiles the other with laminar flow, was investigated by Barry in 1971. He compared from 16 inch pipeline carrying North African crude with two model pipelines, one with laminar flow (6 mm) and the other turbulent flow (50.8 mm). He found that at high shear rates (above $200s^{-1}$), the model pipelines displayed a Bingham behavior. Low shear rates obtained from a concentric cylinder viscometer showed the oil hardly followed the Casson model. The restartability and flow behaviour of Bombay high crude oil under different conditions was discussed by Khan et al in 1990. They used a laboratory model pipeline rig of 6 mm ID over 16 m long. It is observed that the restart pressure increases with decreasing the cooling rate, test temperature and hold up time. The same condition was studied by F. Mohamed at the University of Bradford in 2003.

During a temporary shutdown in oil production, due to emergency reasons or otherwise, the waxy crude oil is cooled in the pipelines under quiescent (no flow)

conditions. Under such circumstances, the stagnant oil can form a candle of wax-oil gel that blocks the entire pipeline on the very cold floor. In order to restart flow, the gel has to be broken down. This breakage can be achieved by applying pressure on the gel until breakdown occurs. In order to predict the breakdown pressure required to restart flow in a safe manner, it is again necessary to estimate the gel strength. The gel strength is measured in terms of the yield stress of the gel. Breakdown of the wax-oil gel occurs if the shear stress exerted on the gel due to the applied pressure exceeds the yield stress of the gel (Venkatesan, 2005).

Clearly the static yield stress for the waxy crude oils is the most useful information and it is not easy to measure in practice. The dynamic yield stress can be determined from rheological data at the lowest possible shear rate or stress. Here the rheometer enabled us to get this point (F. Mohamed, 2003). However, the static yield stress is determined as the shear stress at the wall of the pipe τ_w when flow of crude oil starts under increasing inlet pressure. The yield stress of the crude oil along the length of the pipeline is a function of the ambient temperature and the shear rate history.

3.4.1 Description of the Pipeline Rig

Figure 3-12 shows the design of the pipeline rig that was used in this research. In essence it is a very simple set-up, a pipeline, 10 m long with a 13.5 mm internal diameter, fed from one end, isolated by two valves, and open to atmosphere via a graduated up right transparent pipe section

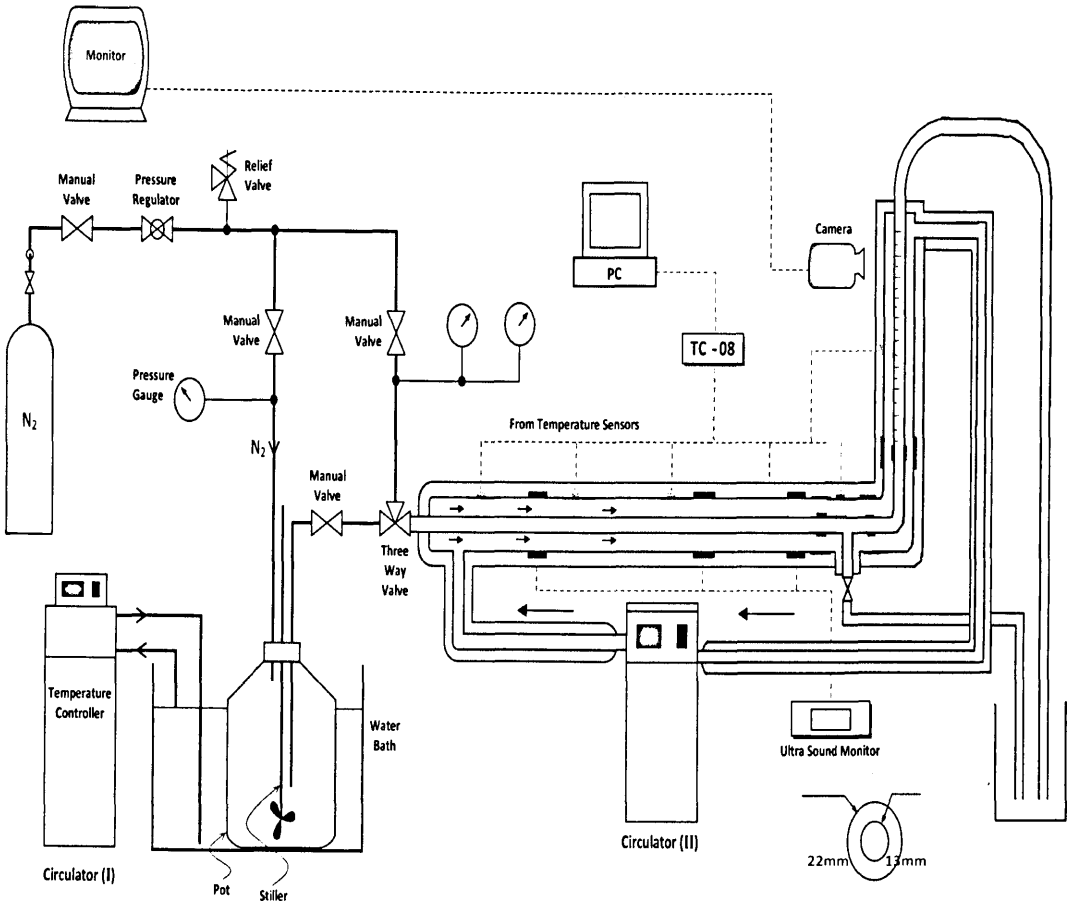

Figure 3-12 The pipeline rig used to determine the static yield stress

However, unlike previous rigs used, this pipeline is of the concentric type, allowing recirculation around the wall and length of the pipe thus very good control of temperature enhanced by the copper conductivity of the pipe material. The fluid in the cooling/heating jacket is connected to a temperature controller that is capable of setting a wide range of heating and cooling rates (from 0.16 to 5 ^{0}C/minute). Also the feed section is connected to a 2L pot which holds the sample of waxy crude to be processed in the pipeline.

The pot is aluminium (good for heat transfer) made and held in a water bath connected to a temperature controller, capable of setting a wide range of heating and cooling rates. An agitator is also embedded in the pot to allow for good mixing of the oil and the setting of a uniform temperature. In order to push the oil from the pot into the pipeline section, nitrogen gas provided from a cylinder is used. The setting of the temperature and the admission of the oil into the pipeline is carried out as follows.

- About 2-litre of waxy crude oil is poured into the pot.
- The oil is heated to a specific temperature and agitated at 80 rpm for 30 minutes.
- The oil is cooled to the desired temperature at the desired cooling rate.
- The oil is allowed to rest in the pot at this temperature for 15 minutes to ensure full equilibrium
- The oil is pushed from the pot into the pipeline section by opening the manual valve and the three way valve. Pumping is achieved by opening the valve of the nitrogen inlet line.
- The oil in pipe is then cooled to the desired test temperature at a desired test cooling rate.
- The oil is held for a given time (1hour or more) to simulate shutdown by closing the valves isolating the pipeline.
- After the desired hold-up time has been reached, the nitrogen gas valve is open and pressure is increased in steps of 0.5 psi until continuous movement of the oil is observed in the graduated upright transparent pipe section. Oil movement or flow is defined when 2-3 ml of oil flows out in

10-15 minutes. This pressure is referred to as the start-up pressure and is used to determine the yield stress.

Details of the heating and cooling conditions tested with the three waxy crude oils sample are shown in Table 3-4.

Table 3-4 Heating and cooling conditions for the waxy oils used in this study

Crude Oil Sample	**Azeri Well BooZ2 oil of BP**	**Mix**	**Remal**
Dynamic Cooling			
Initial Temperature, °C	40	65	70
Final Temperature, °C	30	40	50
The cooling rate is controlled °C /min	0.16, 0.25	0.16, 0.25	0.16, 0.25
Static Cooling			
Initial Temperature, °C	30	40	50
Final Temperature, °C	13, 18	30, 35	35, 40
The used cooling rate are (°C /min)	0.16, 0.25, 0.5, 1, 2 and 5	0.16, 0.25, 0.5, 1, 2 and 5	0.16, 0.25, 0.5, 1, 2 and 5

3.4.2 Measurement of wax layer, h_w deposited on the wall pipe

After much trials, it was found that the simple method of holding oil in a section of copper tubing produce meaningful data on the wax layer, h_w deposited on the wall pipe. Thus small pipe sections were cut (175mm long x 13.5mm ID), filled with the waxy oil under investigation, sealed at both ends and then placed in a water bath where the cooling rate and temperature were precisely controlled (see Figure 3-13). After the set holding time has elapsed, the plugs were removed, the oil allowed to drain out of the pipe and the wax remaining on the wall measured by weight difference prior after draining. The oil that was drained out by gravity out of the tubes was allowed to flow either in a balloon attached to the pipe or directly into a beaker positioned on a weighting scale (see Figure 3-14 and Figure 3-16 and Figure 3-17). In the balloon method, the drained fluid was weighed altogether after waiting 5-10 minutes for the oil to drain out of the tube. In the beaker method, weighing was continuously monitored until no change in the scale was observed.

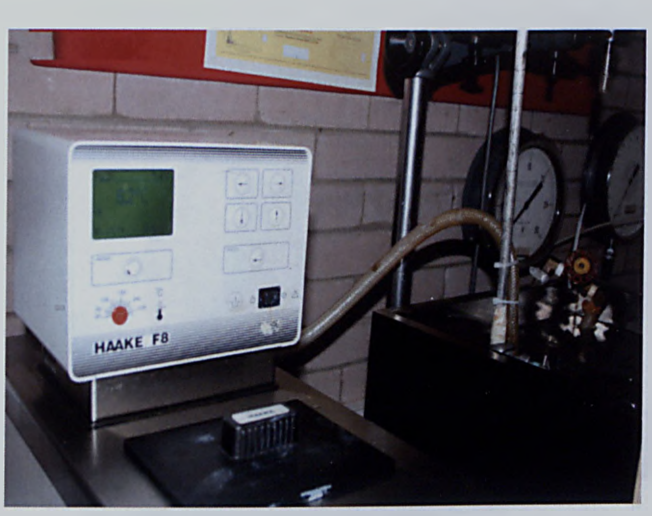

Figure 3-13 Temperature controller and water bath used for conditioning the small pipe sections

Seven pipe sections were used for each experiments and the average value gave an indication of the feasibility and accuracy of the technique. Figure 3-15 shows evidence of the wax deposition on the tube wall and Table 3-5 shows the data and the accuracy in the measurement method.

Figure 3-14 Sealed pipes before dipping them in the controlled temperature bath

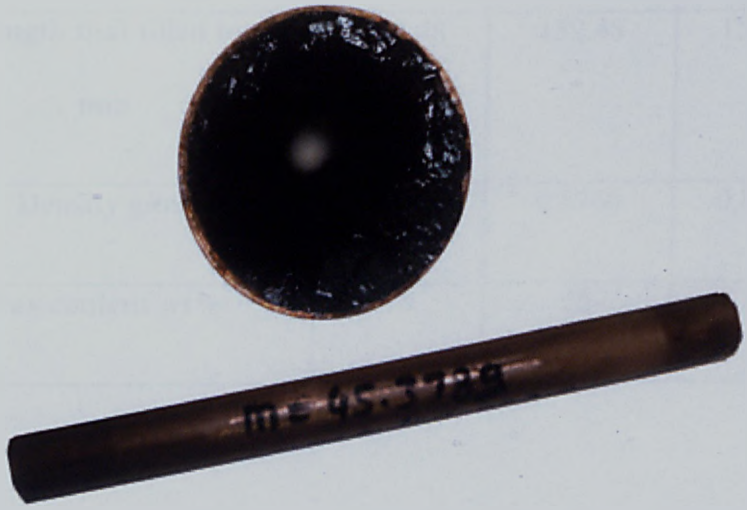

Figure 3-15 Deposited wax on the wall of the pipes

These measurements gave an estimate of both the actual flow diameter, D_W and the wax layer thickness, h_w, assuming of course that the wax deposits uniformly around the wall of the pipe which strictly is not true as the influence of gravity was not tested in these experiments.

$$D_w = \sqrt{\frac{4m_{removed-oil}}{\pi L_{occupied-by-oil}\rho_{waxy-oil}}} \qquad (3.22)$$

Table 3-5 Wax deposition data for the three oils studied and the dimensions of the used pipes

	BP	**Mix**	**Remal**
Weight g of the used pipe	47.108	45.29	45.38
Weight g of the used sample	19.524	19.46	19.47
Pipe Length mm	175	174.8	174.9
Pipe Wall Thickness mm	1.5	1.5	1.5
The length that filled by oil mm	152.48	152.48	152.48
Density g/ml	0.8795	0.8766	0.8770
Wax content wt%	15	25	35

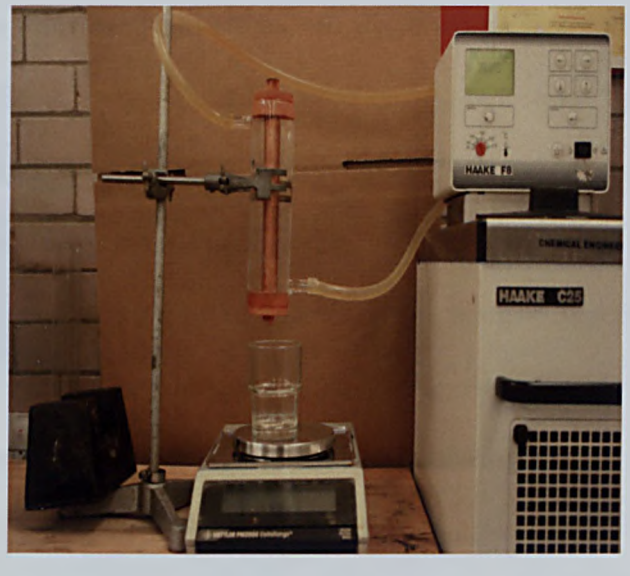

Figure 3-16 Apparatus used to measure the mass of fluid oil (at time t_0)

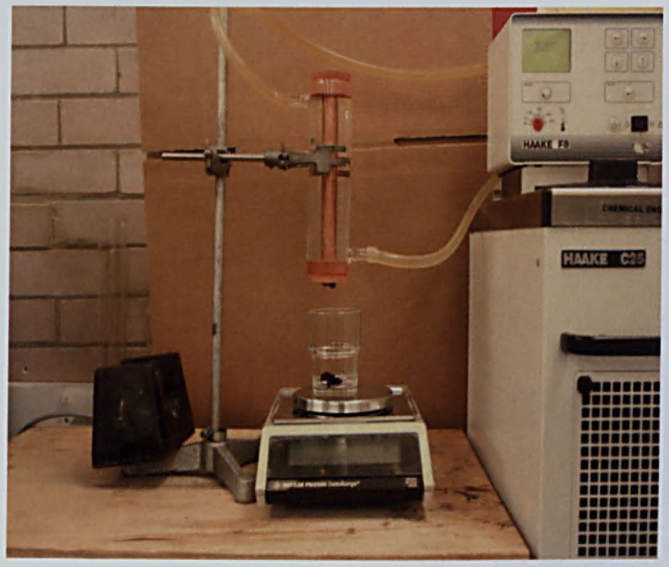

Figure 3-17 Measurement of mass of fluid oil after time t_t

3.5 CONCLUSIONS

This chapter described the experimental equipment and methods used to track the yielding process of waxy crude oils and measure engineering quantities such as yield stresses that can help predict the start-up pressure necessary to start a gelled pipeline. Unlike previous studies, the pilot line used here to measure the start-up

pressure and then infer the yield stress was designed so that cooling was set-up as quickly as possible using a concentric pipe design and very "quick" temperature heaters/coolers capable of generating very low as well as very large cooling rates, from 0.16 to 5^0C/minute, more than covering the range that may be encountered in practice. Also in measuring the yield stress in the start-up pipeline rig, provisions were made to correct for the actual flow diameter by performing separate experiments to measure the wax layer that deposits during gelling and holding of the gel in the pipeline. This correction will hopefully narrow the gap between the yield stress measured in the rheometer and that measured from the pipeline experiments.

CHAPTER 4: RESULTS & DISCUSSION

4.1 INTRODUCTION

In this chapter, data on the rheology and start-up pressure of the three waxy crude oils used in this study are presented. These were Azeri BooZ2 from BP, Remal from Eni Oil Company of Libya, and a 50-50% mix of the two. For simplicity these are labelled BP, Remal and Mix oils. Recall that these oils have different wax contents, 15, 35 and 25 % respectively, thus covering a wide range, representative of the wax oils available throughout the world. The rheological tests, are essentially shear flows (this is because the flow problem studied is one of shear) in rotational and oscillatory flows and the start-up pressure were performed on a small scale pipeline rig suitably designed and instrumented to mimic operation in the field but over a wider range of cooling conditions and shutdown times to test a wider range of field scenarios. This is a particular merit of this study as it aims to guide industrial start-up which is very costly if not carried out intelligently. On an academic perspective, the small scale pipeline rig is effectively a capillary shear viscometer so essentially a complete range of rheological shear techniques were used (rotational, oscillatory and capillary). The results are thus presented in the order the research was carried out to provide both a practical guide to waxy crude oil pipeline re-start and an academic exercise to define and measure yield stress using a variety of method. Thus, the results are structured in the following sections supplemented with comparison and discussion, i.e.:

1. *Shear Data in Oscillatory Flows*: These were used to measure the gel point, the important property that defines the critical point at which the wax

precipitates and forms a solid structure. It is a property that is required at the outset of the work.

2. *Shear Data in Capillary Flows*: These were to measure start-up pressure and yield stress in a pilot pipeline rig which both mimics industrial operation and provides a well define rheological flow. The data here are substantial and examine all the possible pipeline scenarios on various cooling rates and shutdown times. Crucially, we examine the start-up behaviour when the oil reaches the gel points.
3. *Shear Data in Oscillatory Flows to measure yield stress*
4. *Shear Data in Rotational Flows under a Range of Stress to measure yield stress*
5. *Comparison of Data from the four tests*

4.2 RHEOLOGY IN OSCILLATORY FLOWS & GEL POINT

4.2.1 Introduction & Importance of the LVE region

As explained earlier, oscillatory shear flows are used widely in the characterization of viscoelastic materials. In this study, the strain $\gamma(t)$ were varied sinusoidally in time, the most commonly used oscillation, and the resulting stress $\tau(t)$ measured. Because of the viscoelastic nature of waxy crude oils, the stress will have a phase lag, δ. The pertinent equations are:

$$\gamma(t) = \gamma_0 . \sin(\omega . t) \qquad [4\text{-}1]$$

$$\tau(t) = \tau_0 . \sin(\omega . t - \delta) \qquad [4\text{-}2]$$

One specific characteristic of the measurements carried out here is that they were carried out at low amplitudes of strain (γ_0) in order not to disturb the structure too

drastically and obtain a gradual linear response in the form of data on the shear storage (G′) and loss (G″) moduli which make up the stress into a viscous and an elastic component following:

$$\tau_0 = G' \sin(\omega t) + G'' \cos(\omega t) \quad [4\text{-}3]$$

The shear storage and loss moduli are calculated as follows. First the complex shear modulus, G* is defined as the ratio of τ_o and γ_o or:

$$\text{abs}\{G^*(\omega)\} = \tau_o / \gamma_o \quad [4\text{-}4]$$

G'and G'' are then derived from the phase angle and complex modulus:

$$G'(\omega) = G^*(\omega) \cos(\delta) \quad [4\text{-}5]$$

$$G''(\omega) = G^*(\omega) \sin(\delta) \quad [4\text{-}6]$$

A further property, the damping factor can be obtained from the ratio of G" to G':

$$\text{Tan}\,\delta = G''/G' \quad [4\text{-}6]$$

Note that as *G'* is a measure of the energy stored during the vibration procedure, *G'*= 0 signifies the sample is a purely viscous fluid and as *G''* measures the energy dissipated, *G''*= 0 implies the sample is a Hookean fluid. By definition, G', G" and Tanδ are frequency dependent.

As expected with gel-like structures, *G'* here will be larger than *G''* and both will almost be constant with respect to frequency. The cross-over point of G' and G" will define uniquely, the gel point. Although these facts are well established for these tests, there is a need to measure the range of strain amplitude that will keep G'

and G" constant, i.e. determine the linear viscoelastic region (LVR). This is very important in the context of determining how the waxy oil yields from an elastic state into a viscous state. Unless the deformation is carried from the elastic state gradually until the viscous state is reached then the data will be flawed. The first data are thus measurement of G' and G" at various strain amplitude and these data, referred to as amplitude sweep tests, are shown in Figure 4.1.

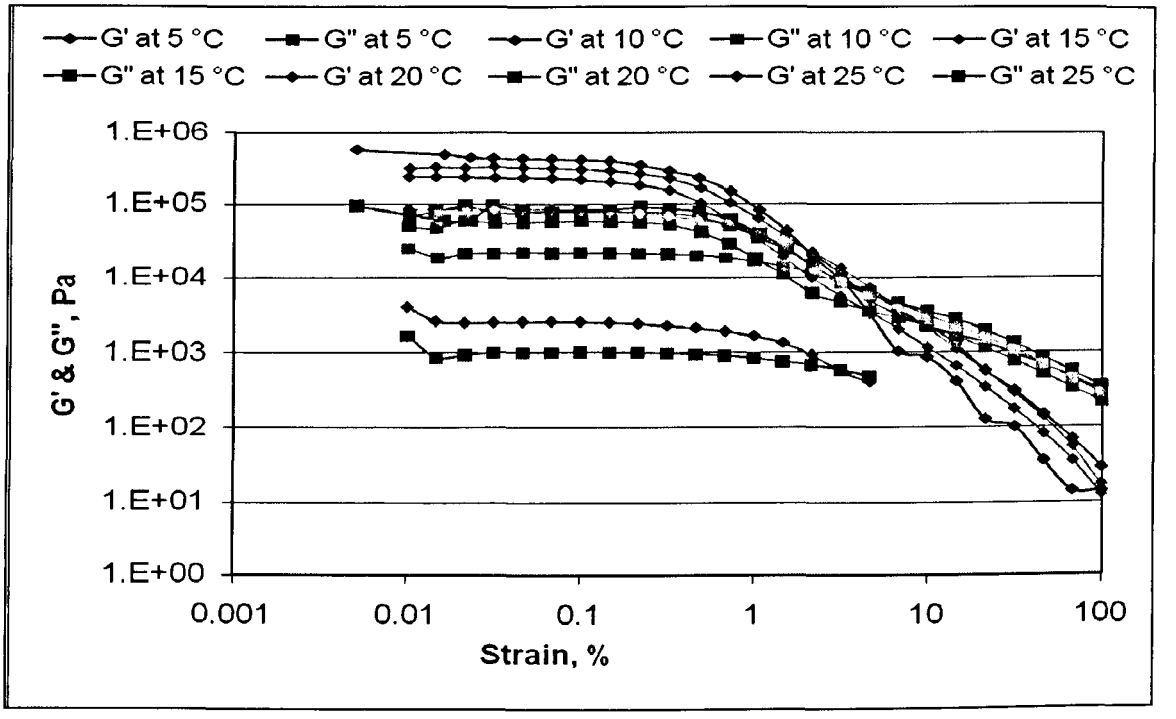

Figure 4-1 Amplitude sweep test for determining the LVR (BP oil sample)

There is also an element of supposition at the outset of the experiments which must be carried out using oils that are firmly into the solid state. The pour point is a good indicator and to be on the "safe" side, the measurements to determine the gel point are carried from temperature well below the pour point. For example, the tests on the BP oils were performed at temperatures of 5, 10, 15, 20 and 25°C to approach the viscous state. As explained in the experimental method, the samples

are first conditioned to remove all their shear and thermal memory and processed from a reference totally fluid state (70 °C for Remal sample, 65 °C for BP sample and 70 °C for Mix sample) down to a set temperature at a chosen cooling rate (from a slow cooling rate of 0.125°C/minute to a fast cooling rate 5°C/minutes with a range in between at 0.25, 0.5 °C/minute, 1 and 2 °C/minute). The data are presented in Table 4.1 for the three oils.

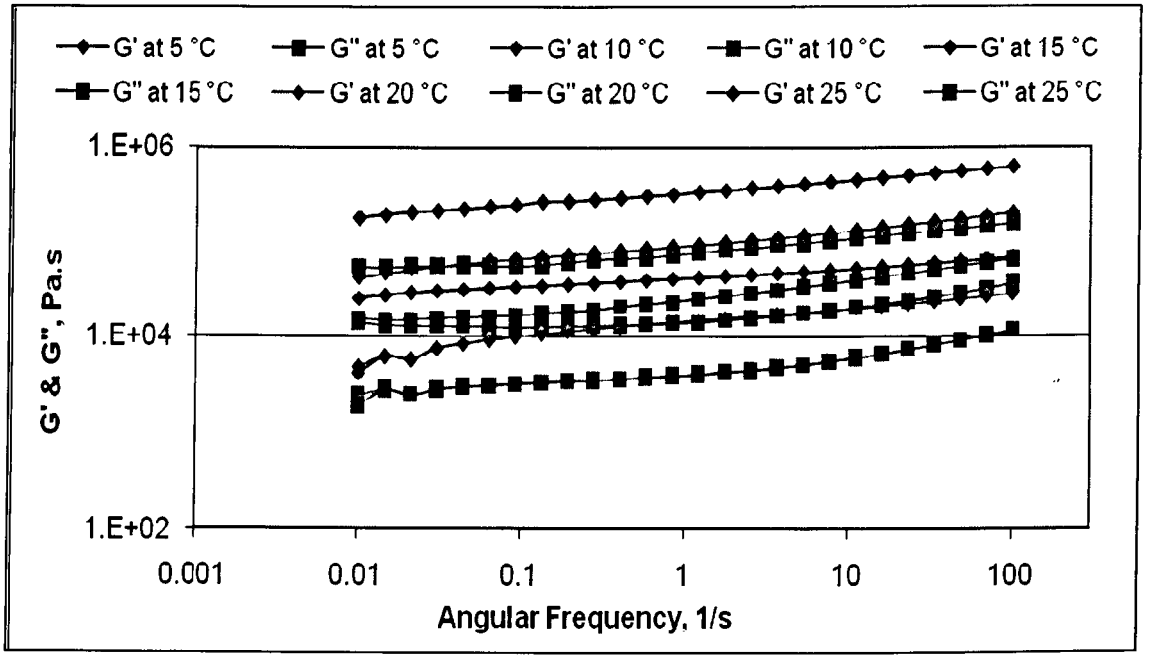

Figure 4-2 Frequency sweep for LVR (BP oil sample)

The data in Figure 4.1, which are those of the BP sample taken here as a basis of discussion, carried out over a range of strain 0.01 to 100% reveal that in all cases, the LVR region for the BP samples occurs over the range 0.01-0.5%. It can be seen that beyond a strain value of 1%, already the structure is beginning to break down leading eventually to a cross over between G' and G" which defines uniquely the gel point.

Having highlighted the importance of the amplitude sweep tests, we now must consider the effect of frequency on amplitude. Naturally, we would expect the yielding to be more sensitive to strain amplitude but it may be that even with a low amplitude a higher frequency of the oscillations could disturb the structure sooner than a lower frequency. In other words, we are bringing the time effect for a given amplitude and this needs to be measured accurately, hence the need of carrying out frequency sweep tests in the LVR level of strain. Figure 4.2 gives precisely these data and show how, for a given temperature, G' varies with frequency. As shown in Figure 4.1 for the BP sample (representative of the data with the other two oils), although the changes are very small, they must be important if an accurate description of yielding is required. Note that for a purely Hookean solid behaviour, G' variation with frequency at low amplitude and low frequency should be flat. The fact that a small variation is observed indicates viscoelastic behaviour even at the smallest amplitude and frequency range. To simplify the analysis whilst still keeping a good level of accuracy, the data in Figure 4.2 shows that a frequency of less than 1 Hz would yield data that will be essentially independent of frequency, so an accurate detection of the elastic yield stress may be obtained in the LVE region at a frequency less than 1 Hz, i.e. from oscillatory tests at amplitude less than 0.5% and frequency less than 1 Hz.

Note a good measure of the experimental effort in obtaining this data can be made in relation to the frequency sweep tests. The measurements at low frequencies take a long time to perform as it is necessary to subject the sample to several cycles of oscillations for a valid measurement to be obtained. For example, for a frequency of 0.01 Hz, one cycle will take 100s; thus a single measurement will take several

100s to complete, so that each of the frequency sweep tests carried out took nearly an hour to complete.

4.2.2 Gel Point Data & Comparison between Oils

Having explained broadly the information obtained from the data, they are now discussed specifically in relation to the gel point for each of the three oils, how it varies with cooling rate and a comparison made between them. Figure 4-3 to Figure 4-8 as explained earlier are the basis from which the gel point data are obtained. Broadly, the values are 20, 50 and 37°C for BP, Remal and the Mix oil respectively. The exact values will vary depending on the cooling rate which controls the onset of crystal formation. As expected, larger cooling rates will induce a lower crystallisation temperature with the formation of numerous and smaller crystals giving more rigid structure than the larger and less numerous crystals at low cooling rates. The effect however is marginal as indicated in Table 4-1.

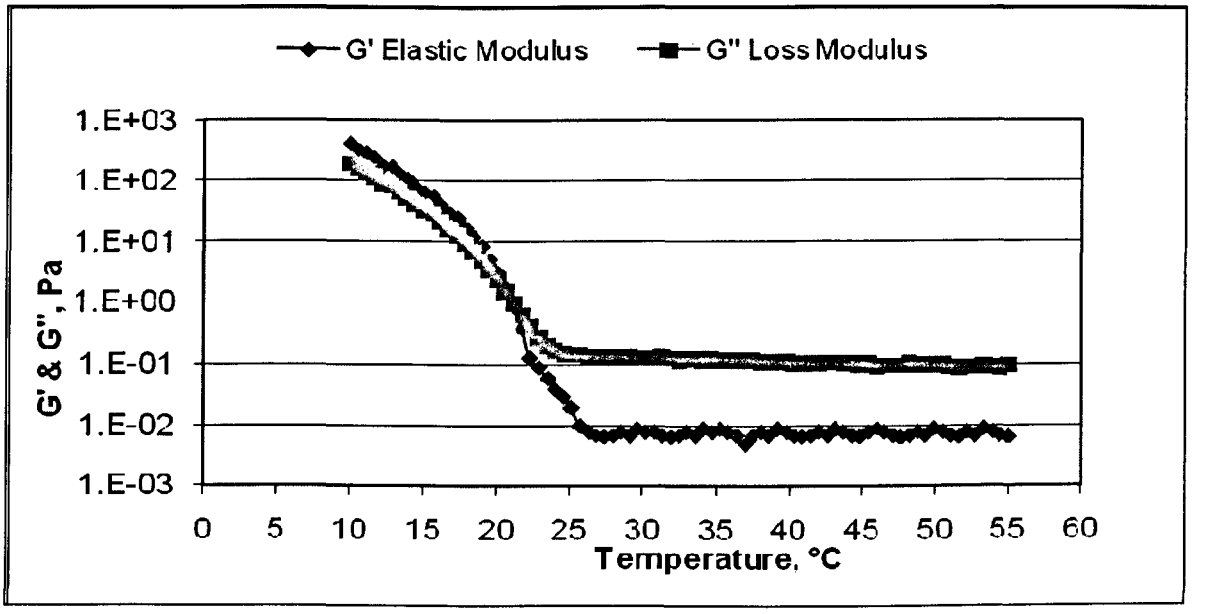

Figure 4-3 Temperature vs. G' and G'' for the BP sample at cooling rate of 0.125 °C/min

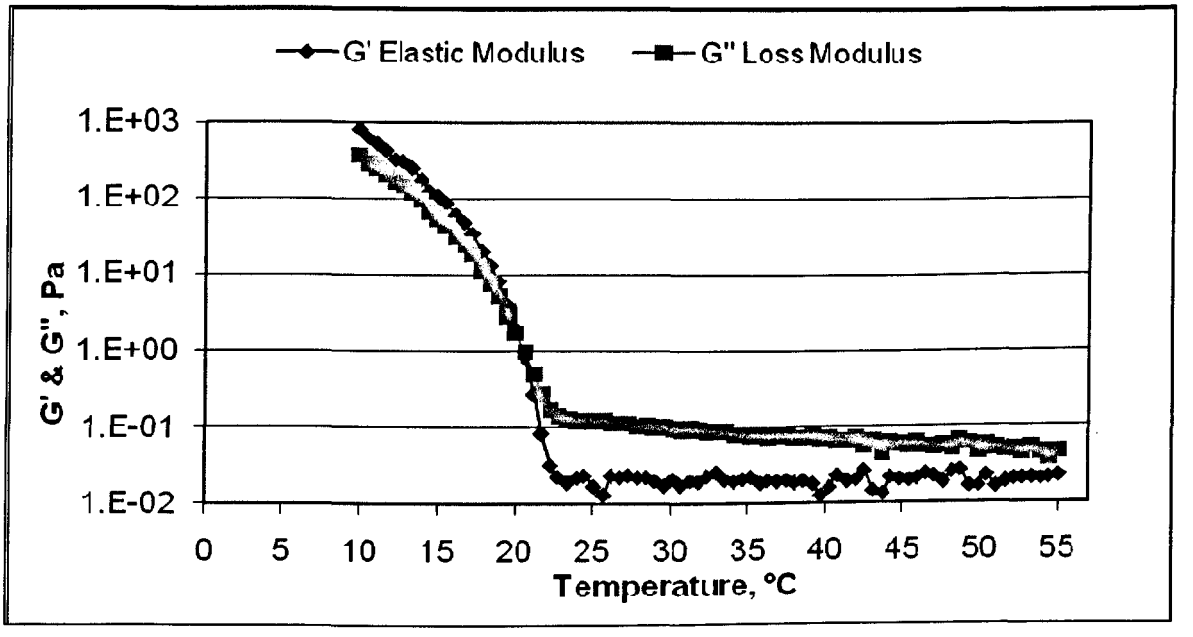

Figure 4-4 Temperature vs. G' and G'' for the BP sample at cooling rate of 0.25 °C/min

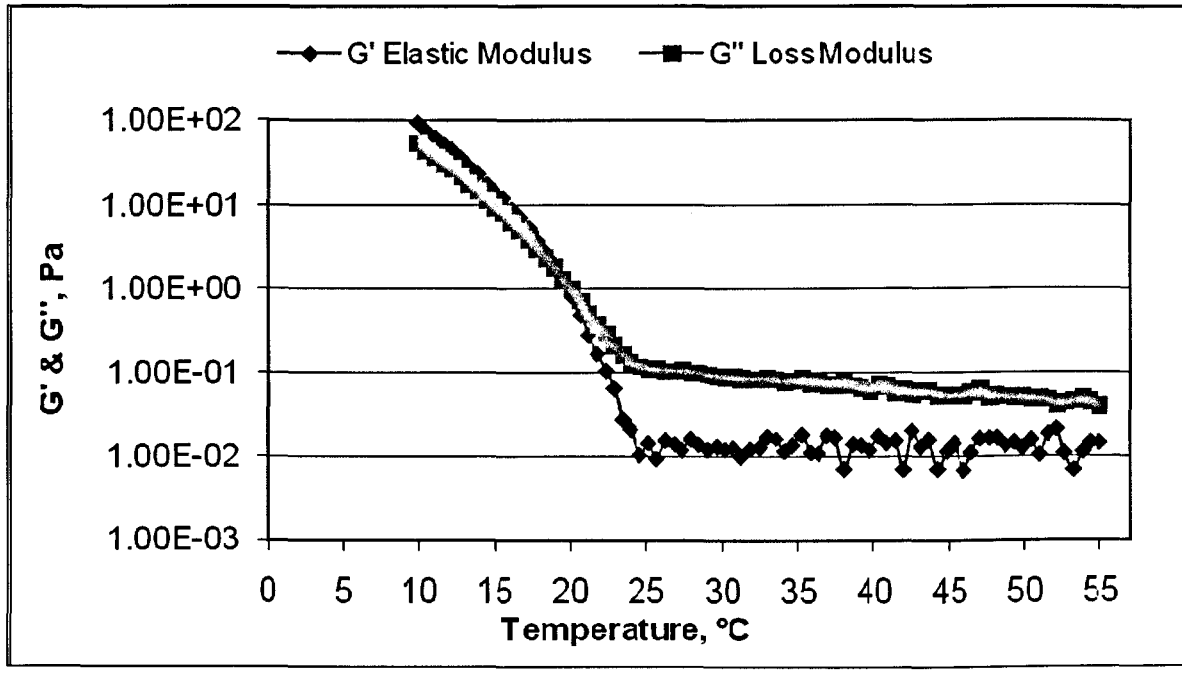

Figure 4-5 Temperature vs. $G^{'}$ and $G^{''}$ for the BP sample at cooling rate of 0.5 °C/min

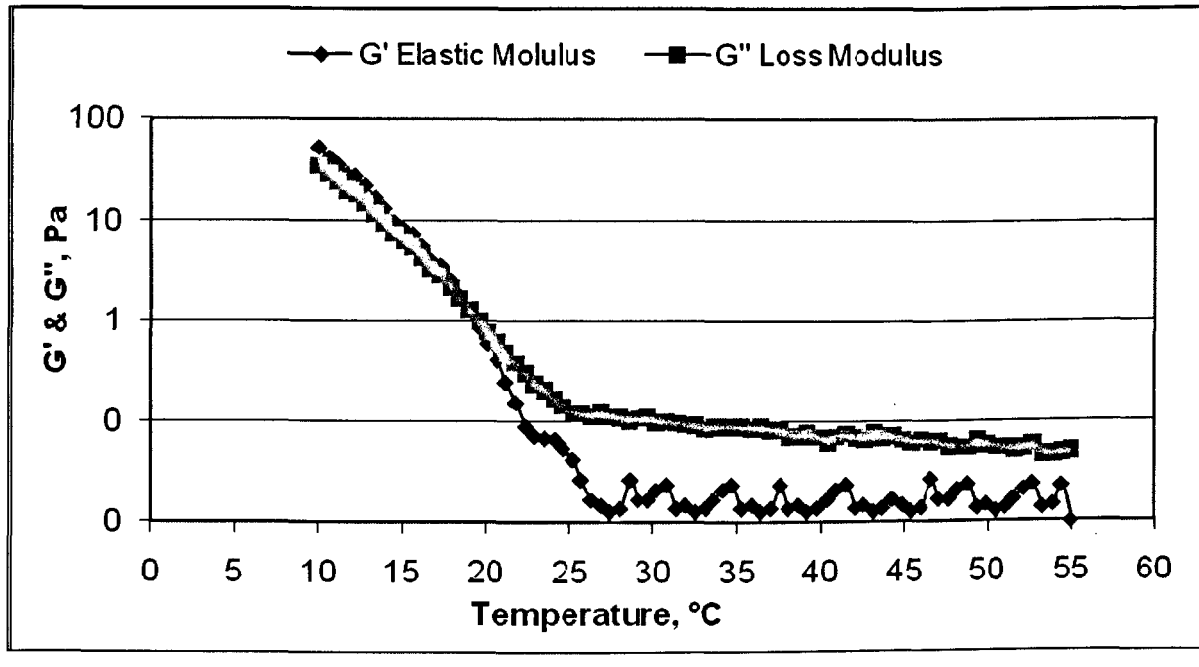

Figure 4-6 Temperature vs. $G^{'}$ and $G^{''}$ for the BP sample at cooling rate of 1 °C/min

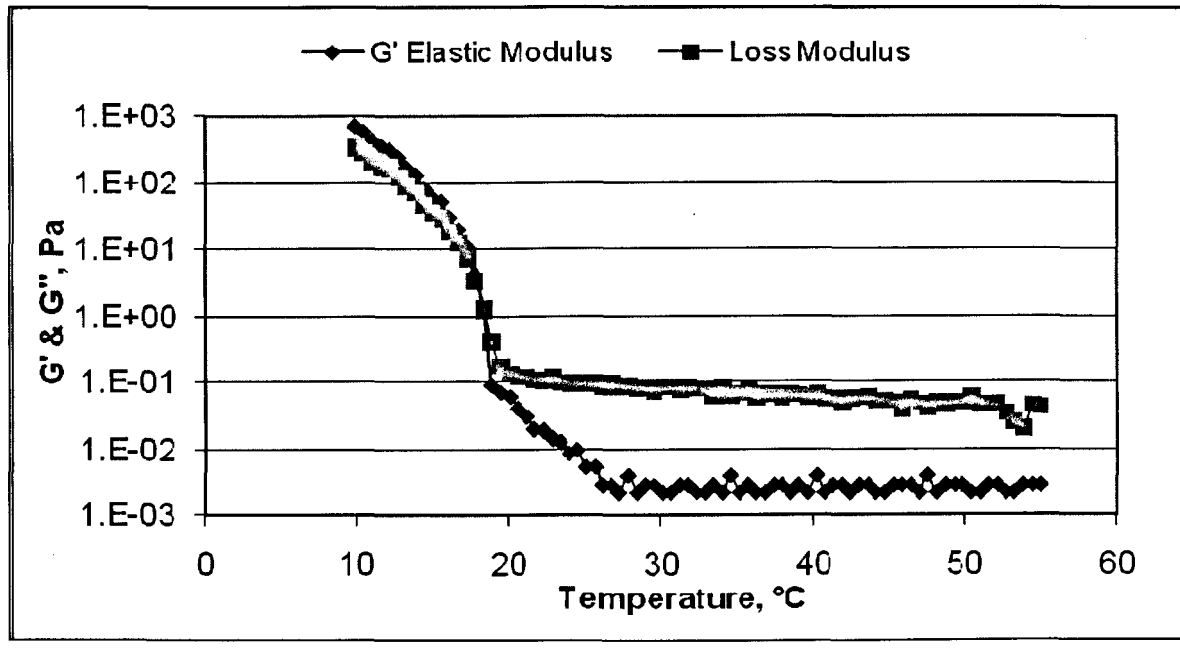

Figure 4-7 Temperature vs. $G^{'}$ and $G^{''}$ for the BP sample at cooling rate of 2 °C/min

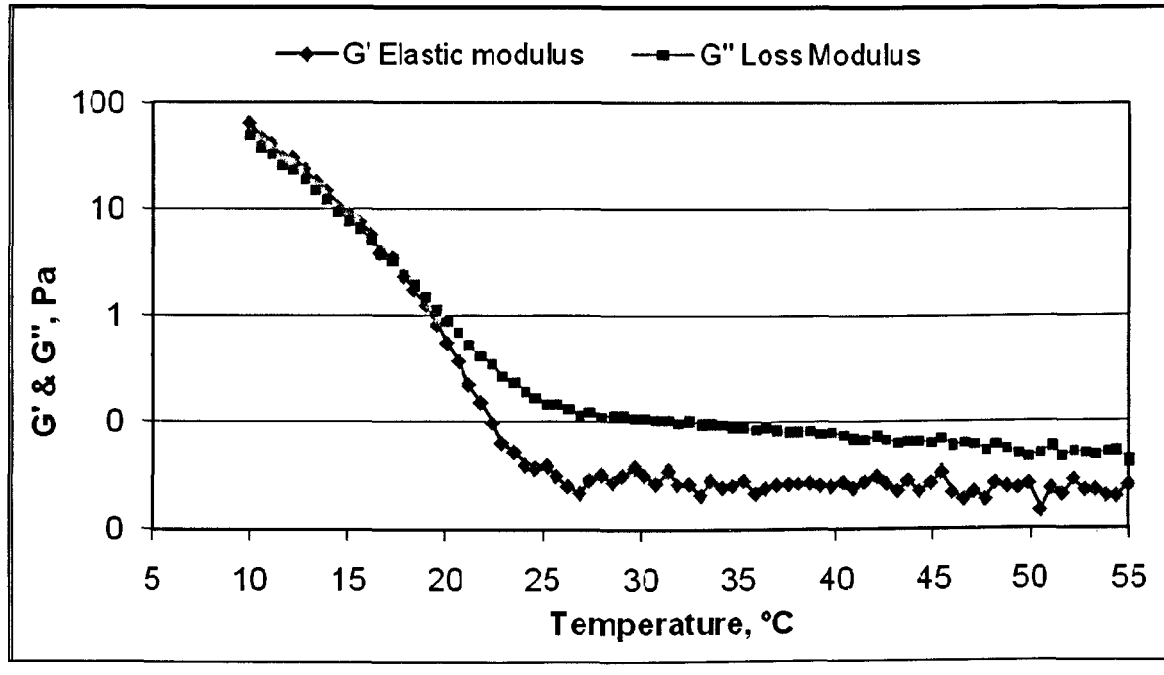

Figure 4-8 Temperature vs. $G^{'}$ and $G^{''}$ for the BP sample at cooling rate of 5 °C/min

The reset of the graphs for Mix sample and Remal sample are placed in the Appendix A1

Table 4-1 Comparison of the gelation point temperature of the three samples at different cooling rates

Cooling Rate °C/min	Gelation Point Temperature, °C Remal Sample	Gelation Point Temperature, °C Mix Sample	Gelation Point Temperature, °C BP Sample
0.125	52.4	39.3	21.2
0.25	52	38.4	20.3
0.5	51	37.9	19.5
1	50	37	19
2	49	36.3	18.2
5	48.5	35.7	17.8

For example, BP oil gellation temperature varies from being 21.2^{0}C at a cooling rate of 0.125^{0}C/min to a value of 17.8^{0}C at the larger cooling rate of 5^{0}C/min. What is striking is the difference in the gellation temperature between the 3 oils, being a very high temperature for the Libyan Remal oil (~50^{0}C) compared with the ~20^{0}C for the BP oil and ~37^{0}C for the mix oil. The implication for the actual transport of these three oils is clear. They will all need to be heated if smooth pumping is required. For the Libyan oil, the heat demands will be very large indeed with clear high cost implication.

Another observation when comparing these oils is the different rate of increase with temperature of the shear modulus of the three oils suggesting different crystallisation kinetics.

4.3 SHEAR DATA IN CAPILLARY FLOWS

4.3.1 Introduction

As explained in the introductory chapter, this research seeks to guide the industrial re-start of pipelines that block as a result of the precipitation of the wax. This is a critical exercise in the operation of pipelines and if it is not carried out intelligently can lead to a very expensive clearing of blocked pipelines. Duplicating the conditions in the laboratory is thus necessary to study the problem and the variables that affect it which are cooling rates and shutdown time. In a typical industrial scenario, a pipeline is shut down as a result of a pumping failure due to electrical malfunctioning or maintenance work. Whilst shut, the pipeline cools down and the oil temperature can reach the gel point and goes below it. In the previous section, oscillatory shear data were used to define and measure this temperature (see Table 4-1) which was found to depend on the nature of the oil (wax content) and the cooling rate and the shutdown time. At and below the gel point, the wax in the oil will precipitate and gradually build up a layer of wax on the wall of the pipe which grows in time. The key information to restart the pipe is to know the minimum pressure required to overcome the structure and induce flow. This is precisely the data that are given in this section and which are used to define the yield stress. Although the pipeline rig will give definitive data on the start-up pressure, it is difficult to infer from this data the yield stress which is a fundamental property. If it were then in principle, yield stress data are sufficient to predict start-up pressure. Thus the quest in academic research to try to measure yield stress as accurate as possible and develop involved pipe flow model that uses the yield stress to predict start-up pressure. The problem with pipe flow is by definition start-up is when there is flow therefore at best the pipeline rig can only measure the end of the yielding

process leading to flow not the true yield stress which is the limit between elastic deformation and creep. So in what follows, it must be understood that the yield stress referred to in pipeline flow is the yield *flow* stress (the flow stress is the stress that is measured by the pipe rig). It is of course very important in practice because it is the actual stress that must be overcome before flow commences.

From a simple model, the yield flow stress and start-up pressure should relate from the force balance of shear stress at the wall with the pressure force applied, i.e. equation 3-19 and equation 3-20 presented in the Literature Survey chapter.

$$\tau_{Y,D} = \frac{dp}{2L}R = \frac{dp}{4L}D \qquad [4\text{-}7]$$

An improved model is one that takes into consideration the development of the wax into a layer on the wall of the pipe, i.e. using the effective diameter, D_e =D-2 x (wax layer thickness on wall):

$$\tau_{Y,D_e} = \frac{dp}{4L}D_e \qquad [4\text{-}8]$$

This requires measurement of the wax layer thickness which is precisely what was carried in this research and for the first time to evaluate yield stress. Note that although this will provide a major correction to Equation 3-19, it does not "guarantee" that the yield flow stress so measured is the "real" yield flow stress because of the other variables ignored in the model, particularly the compressibility of the wax crude oil upon gelling which renders the pressure drop actually non-linear. Nevertheless, the correction using the wax layer will provide novel data that will improve the fit between the real yield stress and the one that can be measured using a laboratory pipeline system. Also, the data that will be obtained can be used

to estimate the pressure start-up required in large pipelines or tested against start-up pressure known in industry to validate the method.

It is helpful before presenting and discussing the data obtained to describe the shutdown scenarios that may occur in industrial practice. This will put in perspective the reasons behind the choice of the various operating variables that may affect shutdown and restart, including cooling rates, temperatures and shutdown times.

4.3.2 Industrial Pipelines Shut Down Scenarios

The information described below was obtained from a visit to the Libyan oil fields which use kerosene or hot water to restart pipeline that have been shut-down for more than six hours. The replacement process as it is called is used for safety reasons to secure the safety of the waxy oil transportation pipelines so that after filling them with the kerosene or the hot water, they will not be subjected to risks of explosion due to the high pressure created by the pumps to overcome the yield stress point to prevent hardening of the oil. The replacement process is clearly very costly as it requires each pipeline to be filled with kerosene, not usable after the pipeline is started because of the changes in oil specifications not being acceptable at the export port.

As for the cooling rates, temperatures at night can drop abruptly in the Sahara desert so provisions were taken in the pilot line to cover a wide range of cooling rates, from a very low of 0.16 ^{0}C/minute to a very high 2 ^{0}C/minute with a range of values in between of 0.25, 0.5 and 1^{0}C/minute to provide a complete picture on this important variable.

4.3.3 Start-up Pressures & Yield Stress Data at Full Diameter

The data are presented in Tables 4-2 and 4-3 and Figures 4-9 to 4-12 for a range of shutdown times and cooling rates from the conditioning temperatures (70, 65 and 60 ^{0}C for Remal, BP and Mix oils respectively) down to a set temperature below the gel point or near it. The experimental effort in this work was substantial as each experiment required (i) careful conditioning in the holding pot (ii) pumping into the pipeline, (iii) isolating the pipeline so that the oil remains stagnant, (iv) cooling of the oil at the required rate down to the set temperature, (v) holding the temperature constant thereafter and (vi) restarting the pipeline by applying a pressure gradually from a very low level until flow is deemed to have started as explained in the Experimental Method Chapter.

The data are now discussed in turn, for each of the three oils. Recall from equations 4-7 and 4-8 that $\tau_{Y,D}$ is the yield stress calculated from the full diameter of the pipe not the effective diameter of the pipe (full diameter minus twice the wax thickness). The start-up pressure Δp, is the actual pressure to cause flow.

Table 4-2 Yield stress data of BP oil sample at 13 °C under different cooling rates and kept for different shutdown times with using the whole pipeline internal diameter

Shutdown Time, hr	0.16 °C/min		0.25 °C/min		0.5 °C/min		1 °C/min		2 °C/min	
	ΔP Pa	τ Pa	ΔP Pa	τ Pa	ΔP psi	τ Pa	ΔP Pa	τ Pa	ΔP Pa	τ Pa
0.5	31026.4	11.03	24131.7	8.58	20684.3	7.36	17236.9	6.13	15513.2	5.52
1	34473.8	12.26	24131.7	8.58	24131.7	8.58	17236.9	6.13	15513.2	5.52
2	41368.6	14.71	27579	9.81	24131.7	8.58	20684.3	7.36	17236.9	6.5
3	44815.9	15.94	30336.9	11.03	27579	9.81	20684.3	7.36	20684.3	7.36
4	51710.7	18.39	34473.8	12.26	27579	9.81	24131.7	8.58	20684.3	7.36
5	55158.1	19.61	37921.2	13.48	34473.8	12.26	27579	9.81	24131.7	8.58
6	55158.1	19.61	41368.6	14.71	34473.8	12.26	31026.4	11.03	24131.7	8.58
7	55158.1	19.61	41368.6	14.71	37921.2	13.48	31026.4	11.03	27579	9.81

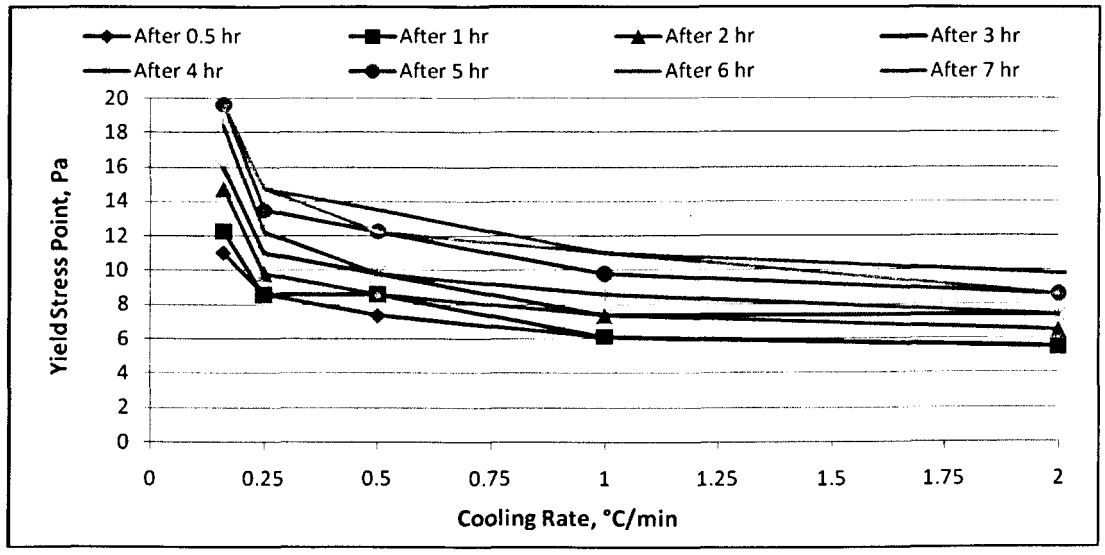

Figure 4-9 Effect of cooling rate on the yield stress value for the BP sample which cooled from 60 °C to 13 °C

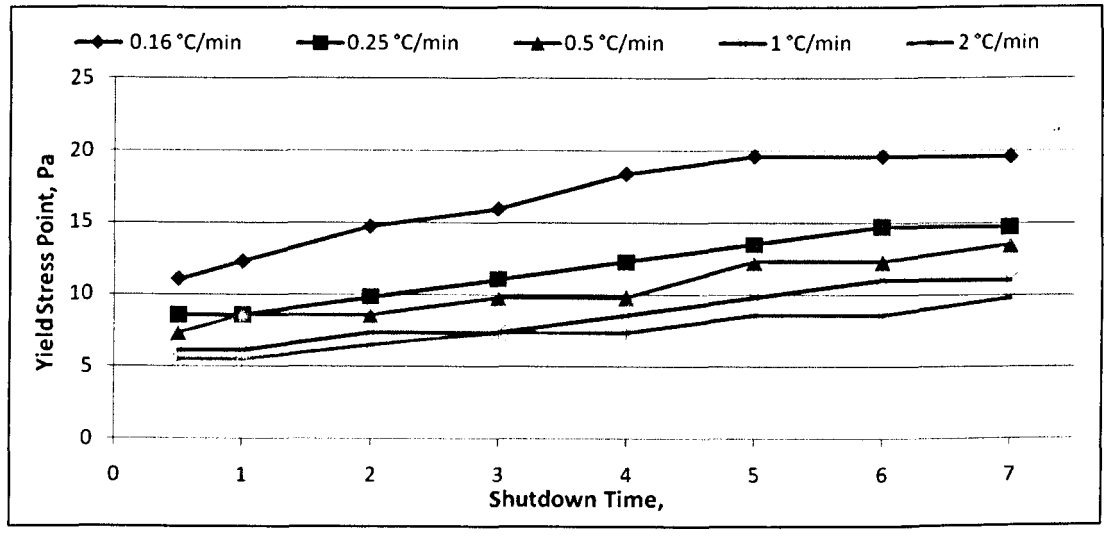

Figure 4-10 Effect of shutdown time on the yield stress value for the BP sample which cooled from 60 °C to 13 °C

Table 4-3 Yield stress data of the BP oil sample at 18 °C under different cooling rates which kept for different shutdown times with using the whole pipeline internal diameter

Shutdown Time, hr	0.16 °C/min		0.25 °C/min		0.5 °C/min		1 °C/min		2 °C/min	
	ΔP Pa	τ Pa	ΔP Pa	τ Pa	ΔP Pa	τ Pa	ΔP Pa	τ Pa	ΔP Pa	τ Pa
0.5	24131.7	8.58	20684.3	7.36	17236.9	5.52	15513.2	5.52	13789.5	4.9
1	25855.4	9.19	22408	7.97	18960.6	6.74	15513.2	5.52	13789.5	4.9
2	27579	9.81	25855.4	9.19	20684.3	7.36	17236.9	6.13	17236.9	6.13
3	29302.7	10.42	29302.7	10.42	22408	7.97	18960.6	6.74	17236.9	6.13
4	31026.4	11.03	31026.4	11.03	22408	7.97	20684.3	7.36	18960.6	6.74
5	32750.1	11.65	32750.1	11.65	24131.7	8.58	22408	7.97	18960.6	6.74
6	34473.8	12.26	34473.8	12.26	24131.7	8.58	24131.7	8.58	20684.3	7.36
7	34473.8	12.26	34473.8	12.26	25855.4	9.19	24131.7	8.58	20684.3	7.36

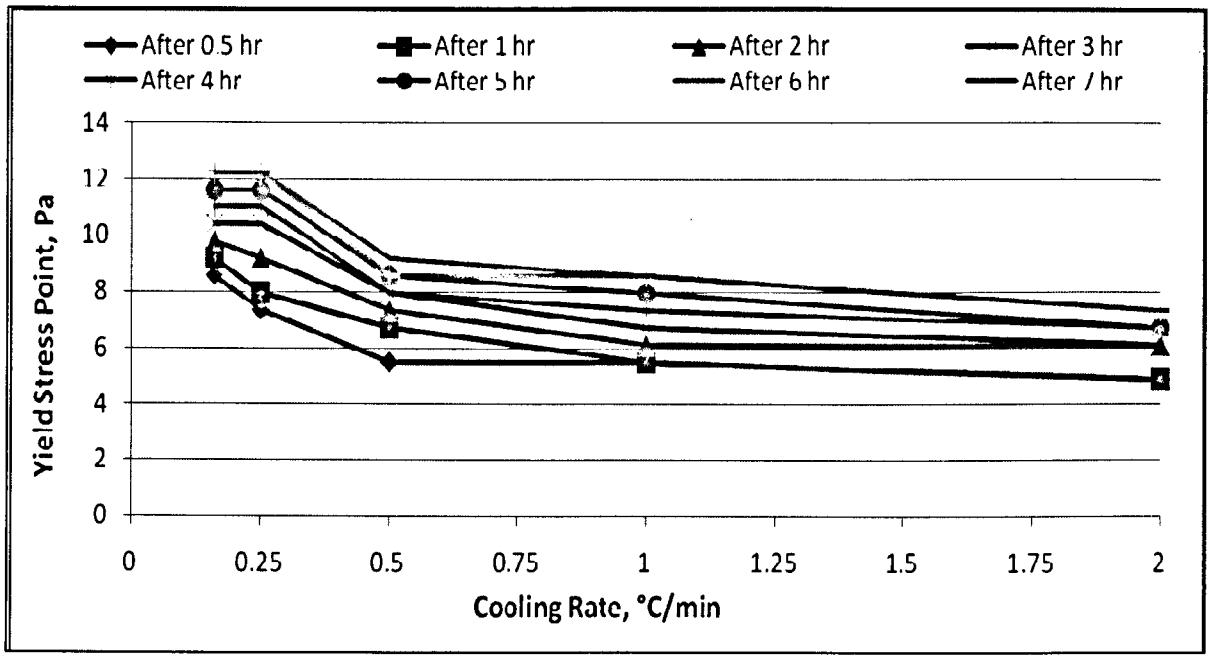

Figure 4-11 Effect of cooling rate on the yield stress value for the BP sample which cooled from 60 °C to 18 °C

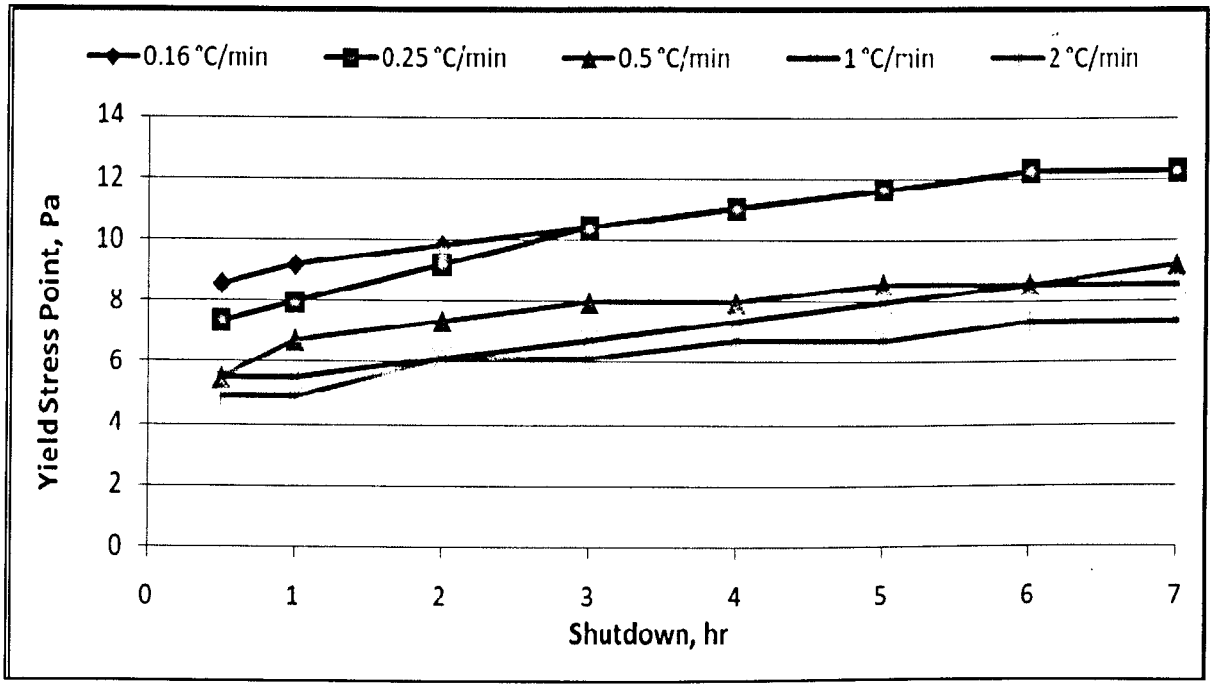

Figure 4-12 Effect of shutdown time on the yield stress value for the BP sample which cooled from 60 °C to 18 °C

The data are presented in Table 4-2 and Table 4-3 and Figure 4-9, Figure 4-10, Figure 4-11 and Figure 4-12 at two temperatures near but below the gel point, 13 and 18 ^{0}C, respectively. Remember that the gel point of this oil is, depending on the cooling rate, between 18 and 21 ^{0}C (see Table 4-1 above). Taking the data at a fixed operating temperature, for example 13 ^{0}C, the first observation is the increase of the start up pressure and the yield flow stress $\tau_{Y,D}$ as the shutdown time is increased and the cooling rate is decreased. Variations by a factor of up to about 2 are observed in the two variable directions. For example for a cooling rate of 0.5 ^{0}C, the start-up pressures and yield flow stresses increase by a factor of about 2 when the shutdown time is increase from 0.5 hour to 6 hours. For the same shutdown time of 0.5 hour for example, the start-up pressures and yield stresses increase by a factor of 2 when the cooling rate is decreased from the very high 2 ^{0}C to the very low 0.16 ^{0}C. The important information here is that the variations are important and cannot be lumped in a single approximately constant value. The variations clearly reflect the kinetics of the crystallisation of the wax that are occurring. The slower the cooler rate, the larger the crystal sizes and the stronger the structures; also the longer the shutdown times, the stronger these structures will get. When the data are scrutinised further as in Figure 4-10, it can be seen that the stresses increase largest when the cooling rates are the lowest as shown in the changes between 0.25 and 0.16 ^{0}C. With shutdown times, it appears that beyond the 6 hours tested, there is a flattening of the yield stress, more so at the lowest cooling rates, suggesting that the crystals are well established but a significant time (hours) is necessary before they do so.

As far as the effect of temperatures, we observe that the data at 18 ^{0}C have lower start-up pressures and yield values compared to 13 ^{0}C, the difference between the values increasing as the shutdown time is increased and the cooling time is

decreased. This is expected because 18 ^{0}C is closer to the gel point than 13 ^{0}C, causing the strength of the crystal structure to be relatively weaker.

Table 4-4 Yield stress data of the Remal oil sample at 35 °C under different cooling rates which kept for different shutdown times with using the whole pipeline internal diameter

Shutdown Time, hr	0.16 °C/min		0.25 °C/min		0.5 °C/min		1 °C/min		2 °C/min	
	ΔP Pa	τ Pa	ΔP Pa	τ Pa	ΔP Pa	τ Pa	ΔP Pa	τ Pa	ΔP Pa	τ Pa
0.5	234422	83.36	224080	79.68	206843	73.55	193053	68.65	186159	66.2
1	244764	87.04	230974	82.13	210290	74.78	198224	70.49	191330	68.04
2	251659	89.49	234422	83.36	213738	76.01	203395	72.33	196501	69.87
3	265448	94.4	241317	85.81	220632	78.56	210290	74.78	203395	72.33
4	272343	96.84	251659	89.49	224080	79.68	217185	77.23	206843	73.55
5	275790	98.07	258554	90.71	227527	80.91	224080	79.68	210290	74.78
6	286133	100.75	262001	93.17	234422	83.36	227527	80.91	213738	76.01
7	293027	102.2	262001	93.17	234422	83.36	227527	80.91	213738	76.01

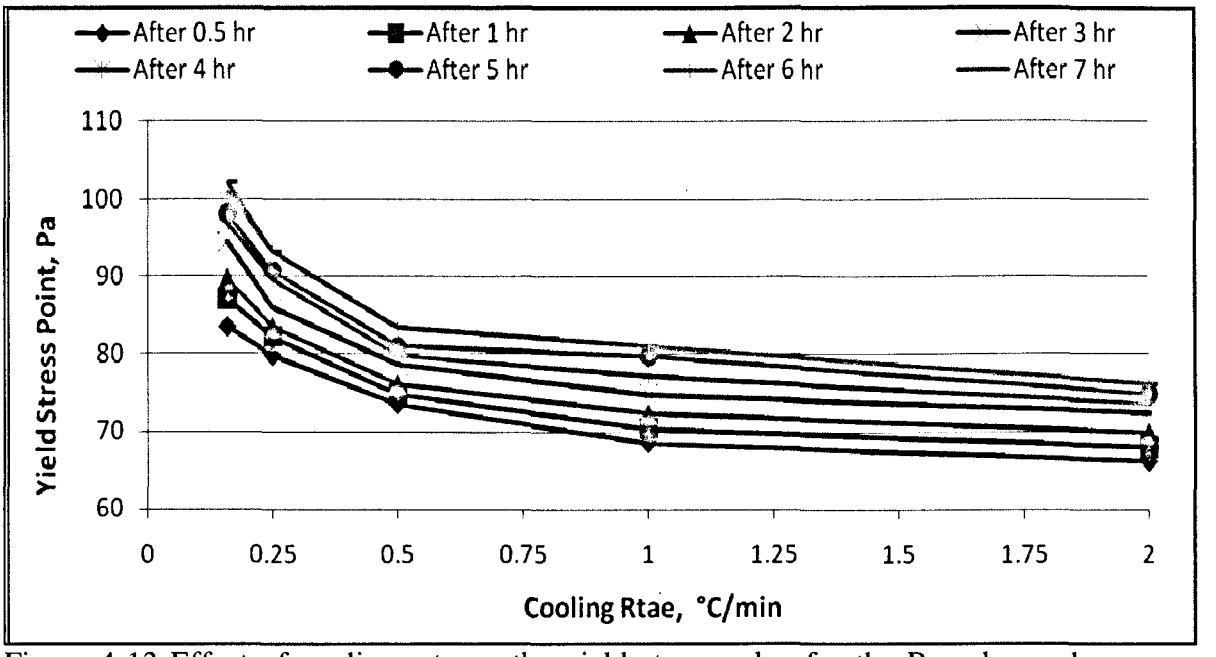

Figure 4-13 Effect of cooling rate on the yield stress value for the Remal sample which cooled from 75 °C to 35 °C

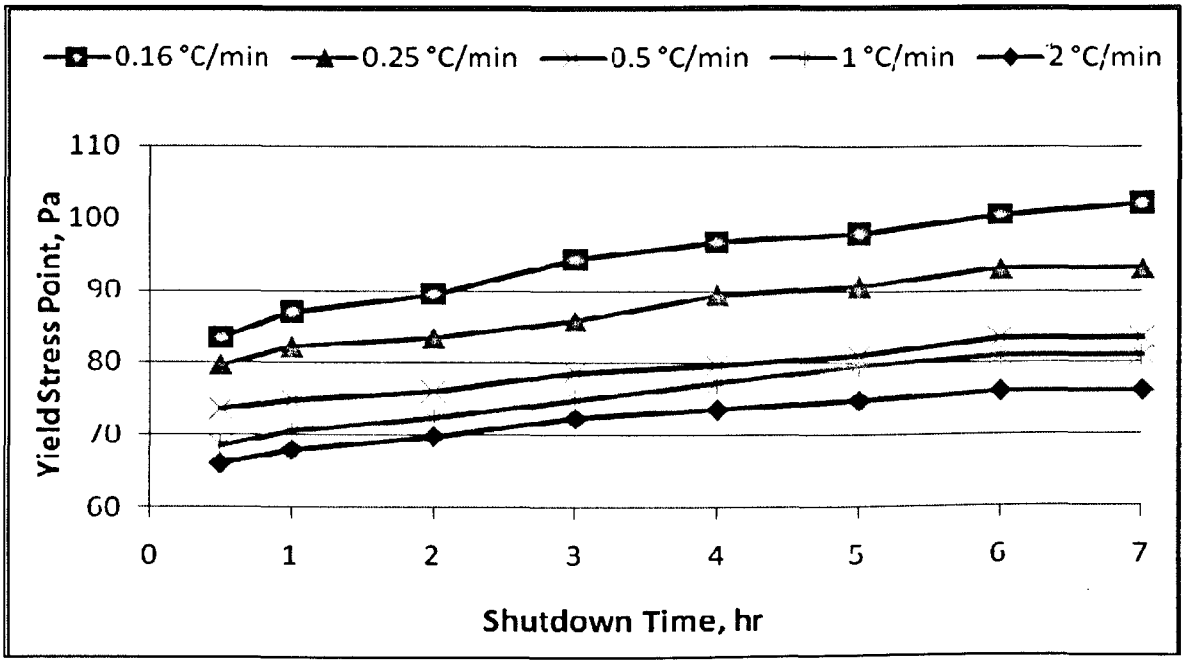

Figure 4-14 Effect of shutdown time on the yield stress value for the Remal sample which cooled from 75 °C to 35 °C

Table 4-5 Yield stress data of the Remal oil sample at 40 °C under different cooling rates which kept for different shutdown times with using the whole pipeline internal diameter

Shutdown Time, hr	0.16 °C/min		0.25 °C/min		0.5 °C/min		1 °C/min		2 °C/min	
	ΔP Pa	τ Pa	ΔP Pa	τ Pa	ΔP Pa	τ Pa	ΔP Pa	τ Pa	ΔP Pa	τ Pa
0.5	206843	73.55	196501	69.87	189606	67.42	179264	63.75	170645	58.84
1	210290	74.78	198224	70.49	191330	68.42	182711	65.97	175816	62.52
2	217185	77.23	203395	72.33	198224	70.49	187882	66.81	182711	64.97
3	220632	78.46	206843	73.55	203395	72.33	193053	68.65	187882	66.81
4	230974	79.68	213738	76	210290	74.78	203395	72.33	198224	69.26
5	237869	84.59	217185	77.23	217185	77.23	206843	73.55	205119	72.94
6	241317	85.81	224080	79.68	217185	77.23	213738	76	210290	74.78
7	241317	85.81	224080	79.68	220632	78.46	213738	76	210290	74.78

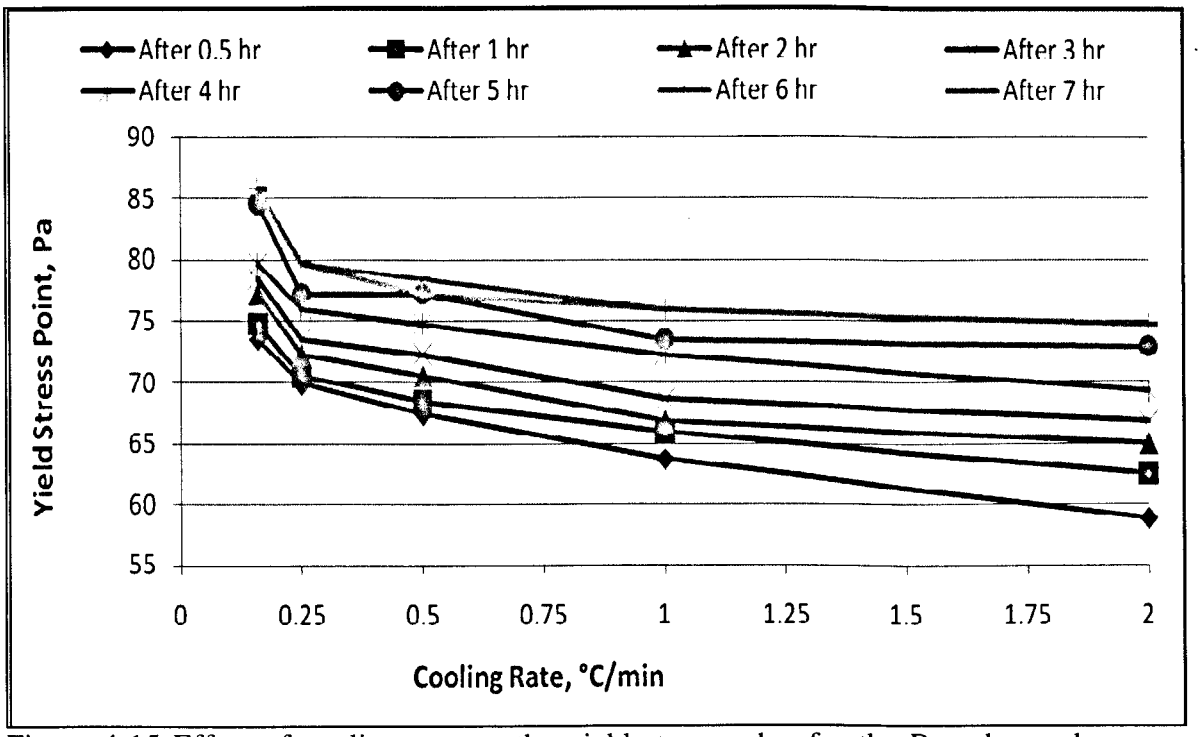

Figure 4-15 Effect of cooling rate on the yield stress value for the Remal sample which cooled from 75 °C to 35 °C

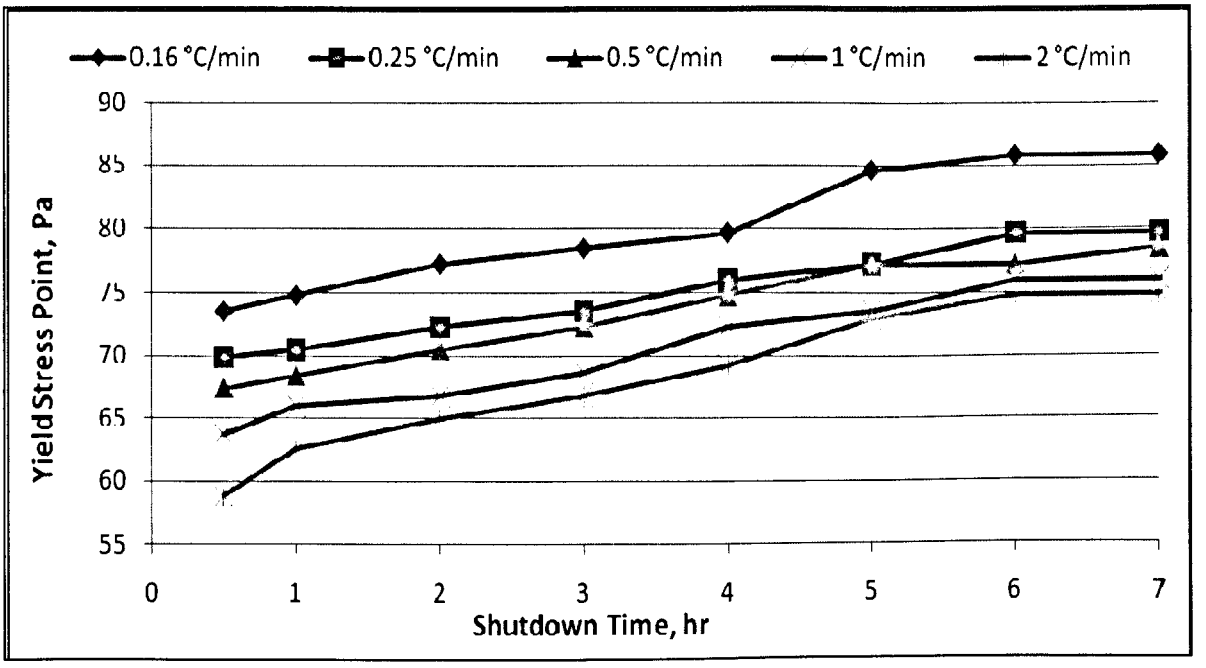

Figure 4-16 Effect of shutdown time on the yield stress value for the Remal sample which cooled from 75 °C to 40 °C

The start-up pressures and yield stress variations with shutdown time, cooling rates and operating temperature behave in a similar manner as those of the BP oil, except that the actual values are comparatively much larger (see Table 4-4 and Table 4-5 and Figure 4-13, Figure 4-14, Figure 4-15 and Figure 4-16). At a temperature of 40 ^{0}C some 12 ^{0}C below the oil gel point, Remal cooled at the lowest cooling rate of 0.16 ^{0}C/min and with a shutdown time of 0.5 hr requires a start-up pressure of 30 psi compared with BP oil 4.5 psi at 13 ^{0}C. Clearly Remal oil, because of its higher wax content 35% compared to 15% for the BP oil, is a more difficult oil to pump and the penalties for start-up are very severe with the start-up pressures increasing even higher to 35 psi when the shutdown time increases to 6 hours.

Table 4-6 Yield stress data of the Mix oil sample at 30 °C under different cooling rates which kept for different shutdown times with using the whole pipeline internal diameter

Shutdown Time, hr	0.16 °C/min		0.25 °C/min		0.5 °C/min		1 °C/min		2 °C/min	
	ΔP Pa	τ Pa	ΔP Pa	τ Pa	ΔP Pa	τ Pa	ΔP Pa	τ Pa	ΔP Pa	τ Pa
0.5	89631.9	31.87	87908.2	31.26	86184.5	30.65	84460.8	30.03	82737.1	29.42
1	93079.3	33.71	87908.2	31.26	87908.2	31.26	86184.5	30.65	84460.8	30.03
2	98250.3	34.94	89631.9	31.87	89631.9	31.87	87908.2	31.26	86184.5	30.65
3	106869	38	91355.6	32.49	91355.6	32.49	89631.9	31.87	87908.2	31.26
4	115487	41.07	93079.3	33.1	93079.3	33.1	91355.6	32.49	91355.6	32.49
5	125829	44.74	101698	36.16	96526.6	34.32	94803	33.71	93079.3	33.1
6	131000	46.58	105145	37.39	98250.3	34.94	94803	33.71	93079.3	33.1
7	131000	46.58	105145	37.39	98250.3	34.94	94803	33.71	93079.3	33.1

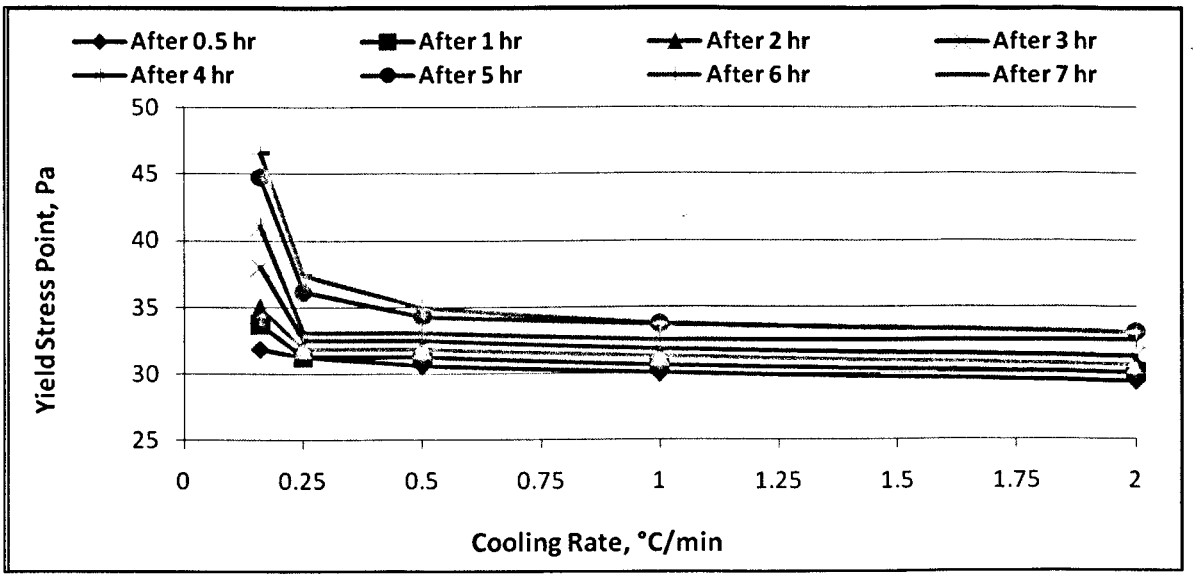

Figure 4-17 Effect of cooling rate on the yield stress value for the Mix sample which cooled from 75 °C to 30 °C

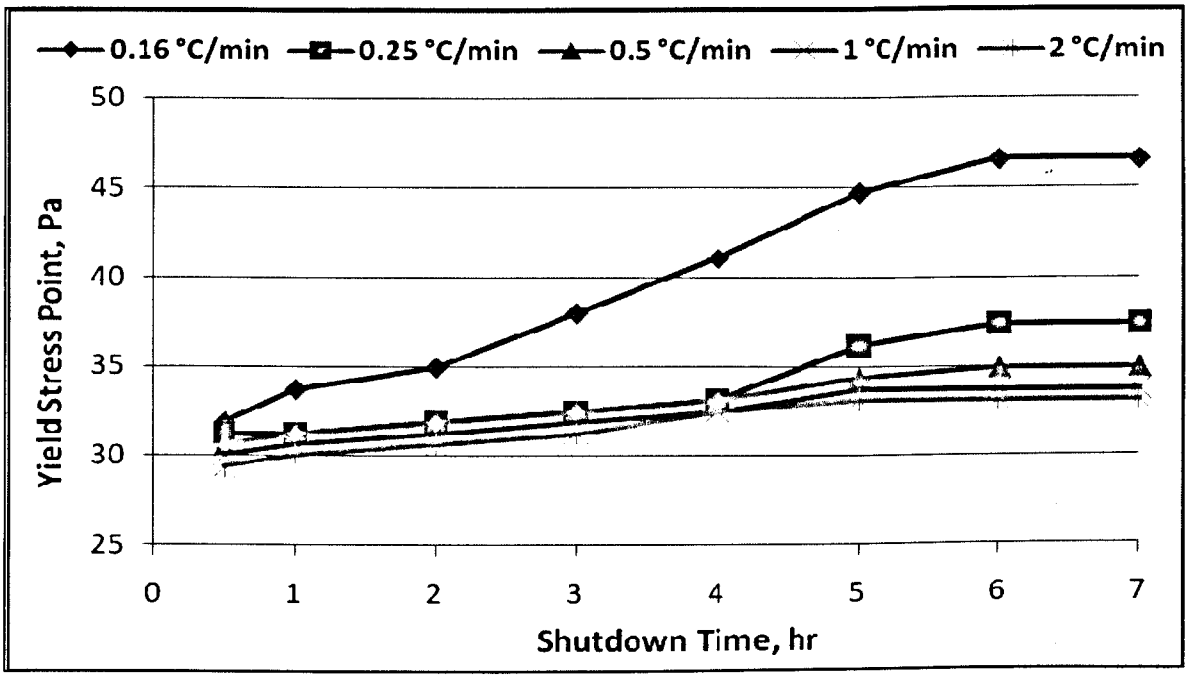

Figure 4-18 Effect of shutdown time on the yield stress value for the Mix sample which cooled from 75 °C to 30 °C

Table 4-7 Yield stress data of the Mix oil sample at 35 °C under different cooling rates which kept for different shutdown times with using the whole pipeline internal diameter

Shutdown Time, hr	0.16 °C/min		0.25 °C/min		0.5 °C/min		1 °C/min		2 °C/min	
	ΔP Pa	τ Pa	ΔP Pa	τ Pa	ΔP Pa	τ Pa	ΔP Pa	τ Pa	ΔP Pa	τ Pa
0.5	62052.8	22.07	60329.2	21.45	58605.5	20.84	55158.1	19.61	53434.4	19
1	63776.5	22.68	62052.8	22.07	60329.2	21.45	56881.8	20.23	55158.1	19.61
2	65500.2	23.29	63776.5	22.68	63776.5	22.68	58605.5	20.84	56881.8	20.23
3	68947.6	24.52	65500.2	23.29	65500.2	23.29	60329.2	21.45	60329.2	21.45
4	72395	25.74	68947.6	24.52	67223.9	23.9	62052.8	22.07	62052.8	22.09
5	75842.4	26.99	72395	25.74	70671.3	25.13	65500.2	23.29	63776.5	22.68
6	79289.7	28.2	72395	25.74	72395	25.74	67223.9	23.9	65500.2	23.29
7	79289.7	28.2	74118.7	26.36	72395	25.74	67223.9	23.9	65500.2	23.29

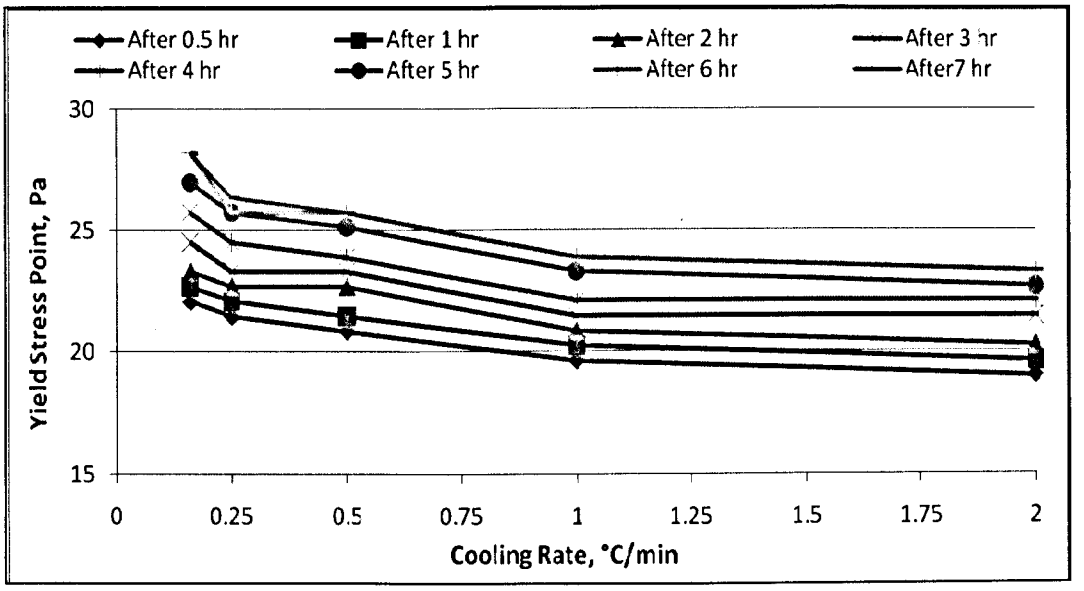

Figure 4-19 Effect of cooling rate on the yield stress value for the Mix sample which cooled from 75 °C to 35 °C

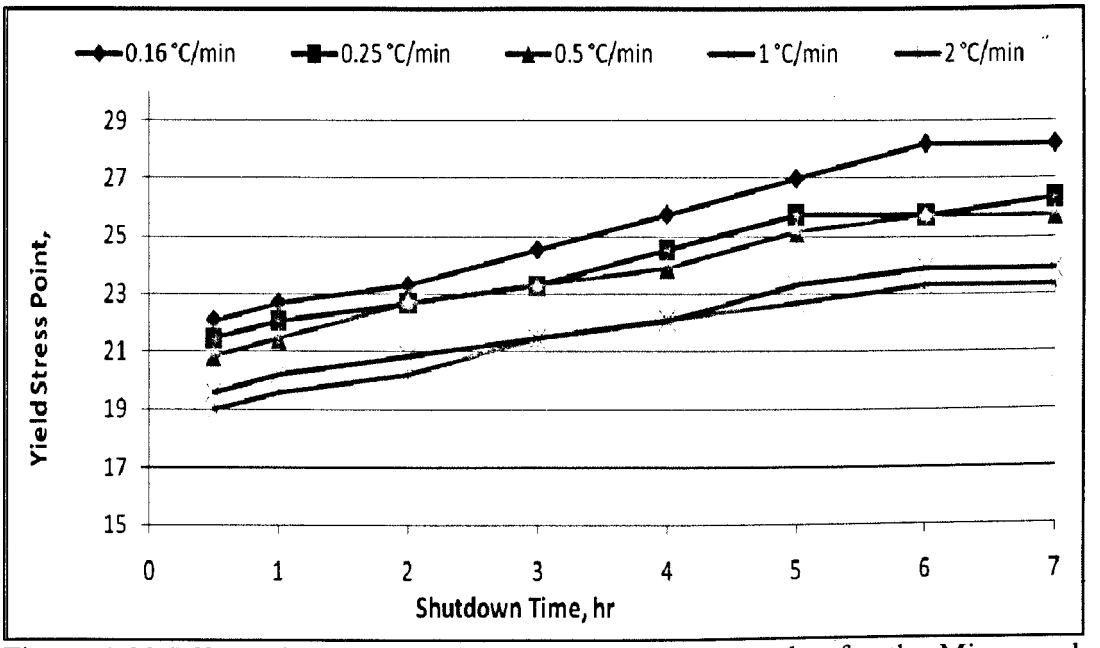

Figure 4-20 Effect of shutdown time on the yield stress value for the Mix sample which cooled from 75 °C to 35 °C

With a gel point of 36 to 39 ^{0}C, depending on cooling rate and a wax content of 25 %, in between that of the BP oil (15%) and the Remal oil (35%), the expectation is that the start-up pressure near the gel point will be in between those of the BP and Remal oils. This is indeed the case as shown in Table 4-6 and Table 4-7 and Figure 4-17, Figure 4-18, Figure 4-19 and Figure 4-20 which gives a value of 9 psi for the start up pressure at 35 ^{0}C for a shut down time of 0.5 hour and a cooling rate 0.16 ^{0}C/min, increasing to 11.5 psi for a shut down time of 6 hours. At 30 ^{0}C, for the same cooling rate of 0.16 ^{0}C/min, the start-up pressure increases to 13 and 19 psi after 0.5 and 6 hours respectively.

4.3.4 Start-up Pressures & Yield Flow Stress Data at Effective Flow Diameter

As explained earlier, there is a need to take into account the wax layer that deposit on the wall during the precipitation of the wax near and below the gel point when the shutdown time increases. Therefore in this section we present such data to improve on the estimate of the yield flow stress. First however, the wax layer needs to be measured in order to determine the effective diameter which is simply the full diameter minus twice this layer thickness. The procedure was as described in the Experimental Method Chapter. Essentially, short sections of pipes were filled with oil, previously conditioned, and subjected to a controlled cooling from a high temperature of 70 or 65 ^{0}C depending on the oil, down to the test temperature. Once the test temperature was reached, these filled short pipe sections were left at the test temperature for a period of time corresponding to the shutdown time imposed in the pilot pipeline, that is 1, 2, 3, 4, 5, 6 and 7 hours. Effectively, the same conditions that prevailed in the pilot pipeline were imposed on these small pipe sections. At the end of this treatment, the pipe sections were allowed to drain oil out to leave only the wax on the wall. To ensure complete drainage, the weight of these pipe sections was

monitored in time until no changes were observed. For each samples, 7 runs were carried out to reduce the experimental error and an average taken. Figures 4-21 and Figure 4-22 show a typical profile of the mass of oil draining out in time with each of the three samples.

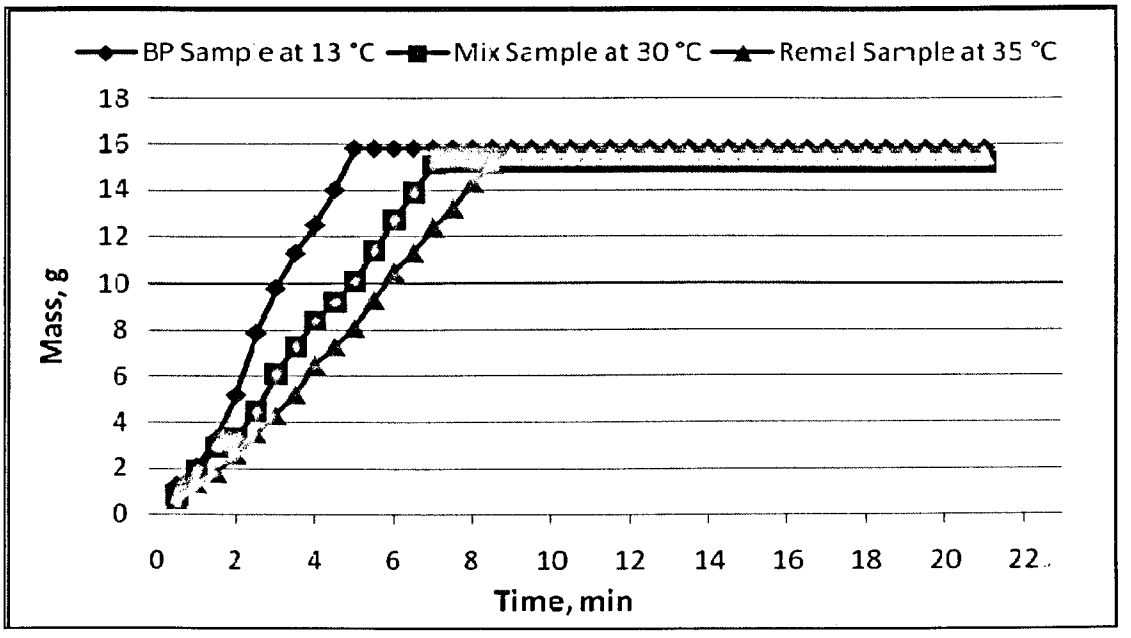

Figure 4-21 Mass of oil removed from the pipe section after a cooling period of one hour

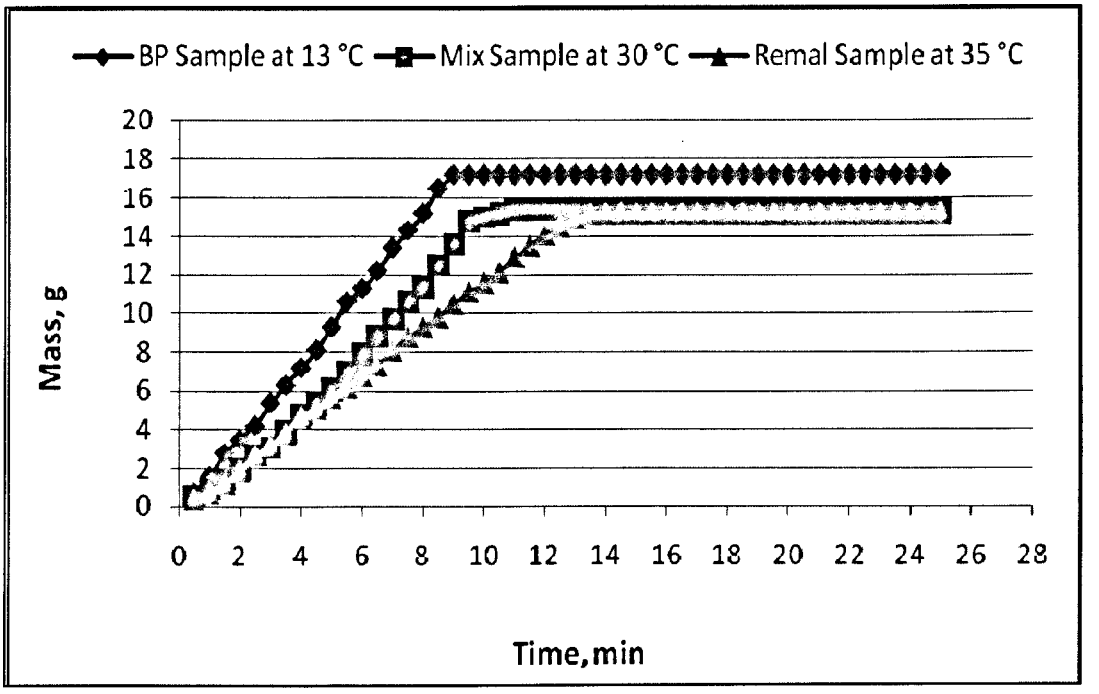

Figure 4-22 Mass of oil removed from the pipe section after a cooling period of seven hour

A leveling of the mass is clearly seen after a few minutes drainage. Once this data were obtained it was a simple matter to calculate the wax layer thickness hence the effective diameter of the pipe.

Table 4-8 Flow diameter determination experiment (Run 1): results for the BP oil sample at 13 °C

Time	T	Pipe mass	Pipe+oil+2 plugs+Balloon	Pipe+wax layer	Layer mass	Removed oil	flow diameter	Wax layer thickness
hr	°C	g	mass, g	mass, g	g	mass, g	mm	(2*hw), mm
1	13	47.108	81.736	49.488	2.38	17.144	12.64903721	0.850962786
2	13	47.108	81.736	49.718	2.61	16.914	12.56390241	0.936097589
3	13	47.108	81.736	49.858	2.75	16.774	12.51179761	0.988202391
4	13	47.108	81.736	50.058	2.95	16.574	12.43698351	1.063016489
5	13	47.108	81.736	50.338	3.23	16.294	12.33148126	1.16851874
6	13	47.108	81.736	50.488	3.38	16.144	12.27458918	1.225410816
7	13	47.108	81.736	50.718	3.61	15.914	12.18683884	1.313161157

Table 4-9 Flow diameter determination experiment (Run 1): results for the Mix oil sample at 30 °C

Time	T	Pipe Mass	Pipe+Oil+2 Plugs+Balloon	Pipe+Wax Layer	Wax Layer	Removed Oil	Flow Diameter	Wax Layer Thickness
hr	°C	g	Mass, g	Mass, g	Mass, g	Mass, g	mm	(2*hw), mm
1	30	45.29	79.854	47.893	2.603	16.857	12.56344444	0.936555562
2	30	45.29	79.854	48.114	2.824	16.636	12.48081759	1.019182412
3	30	45.29	79.854	48.345	3.055	16.405	12.39386318	1.106136824
4	30	45.29	79.854	48.537	3.247	16.213	12.32112238	1.178877617
5	30	45.29	79.854	48.751	3.461	15.999	12.23953727	1.260462727
6	30	45.29	79.854	48.974	3.684	15.776	12.15393834	1.346061658
7	30	45.29	79.854	49.169	3.879	15.581	12.07859011	1.421409885

Table 4-10 Flow diameter determination experiment (Run 1): results for the Remal oil sample at 35 °C

Time	T	Pipe Mass	Pipe+Oil+2 Plugs+Balloon	Pipe+Wax Layer	Wax Layer	Removed Oil	Flow Diameter	Wax Layer Thickness
hr	°C	g	Mass, g	Mass, g	Mass, g	Mass, g	mm	(2*hw), mm
1	35	45.38	79.954	48.341	2.961	16.509	12.43025106	1.069748944
2	35	45.38	79.954	48.638	3.258	16.212	12.31793233	1.182067667
3	35	45.38	79.954	48.867	3.487	15.983	12.23062544	1.26937456
4	35	45.38	79.954	49.092	3.712	15.758	12.14423226	1.35576774
5	35	45.38	79.954	49.343	3.963	15.507	12.04712482	1.452875184
6	35	45.38	79.954	49.581	4.201	15.269	11.95431826	1.545681736
7	35	45.38	79.954	49.847	4.467	15.003	11.84973317	1.650266829

The rest of tables are placed in Appendix A2

The data and calculation procedure is shown in the Tables A2-1 to Table A2-48 in Appendix 2. Table 4-8, Table 4-9 and Table 4-10 are a typical tables presented here. Table 4-8 shows that with the BP oil at 13 °C, the effective diameter after just half an hour shutdown time from the full diameter value of 13.5 mm down to 12.64 mm or a 6.4% decrease. After seven hours of shutdown time, the effective flow diameter is 12.18 mm or a reduction of nearly 10% from the full diameter. For the Mix oil at 30 °C as shown in Table 4-9, the corresponding diameters were 12.43 mm after half an hour shutdown and 12.07 mm after seven hours. With Remal oils as shown in Table 4-10, the effective flow diameter was at 35 °C, 12.43 and 11.83 mm after half an hour and seven hours shutdown respectively. The important observations in all this data is that there was a significant difference between the full and actual diameter which lead to a significant (proportional) difference in the calculated yield flow stress using:

$$\tau_{Y,D_e} = \frac{dp}{4L} D_e$$

Table 4-11 Accuracy of yield stress calculation for the BP oil sample at 13 °C using the actual flow diameter

Shutdown Time, hr	The Flow Diameter mm	0.16 °C/min			0.25 °C/min			0.5 °C/min			1 °C/min			2 °C/min		
		ΔP Pa	τ (a) Pa	τ (b) Pa	ΔP Pa	τ (a) Pa	τ (b) Pa	ΔP Pa	τ (a) Pa	τ (b) Pa	ΔP Pa	τ (a) Pa	τ (b) Pa	ΔP PSI	τ (a) Pa	τ (b) Pa
1	12.643764	34473.8	12.26	11.4791	24131.7	8.58	8.03535	24131.7	8.58	8.03535	17236.9	6.13	5.73954	15513.2	5.52	5.16558
2	12.560717	41368.6	14.71	13.6844	27579	9.81	9.12294	24131.7	8.58	7.98258	20684.3	7.36	6.84221	17236.9	2.5	5.70184
3	12.4974	44815.9	15.94	14.7501	30336.9	11.03	9.98465	27579	9.81	9.07696	20684.3	7.36	6.80772	20684.3	7.36	6.80772
4	12.442876	51710.7	18.39	16.945	34473.8	12.26	11.2967	27579	9.81	9.03735	24131.7	8.58	7.90769	20684.3	7.36	6.77802
5	12.340642	55158.1	19.61	17.9262	37921.2	13.48	12.3243	34473.8	12.26	11.2039	27579	9.81	8.9631	24131.7	8.58	7.84271
6	12.274044	55158.1	19.61	17.8295	41368.6	14.71	13.3721	34473.8	12.26	11.1434	31026.4	11.03	10.0291	24131.7	8.58	7.80039
7	12.149558	55158.1	19.61	17.6486	41368.6	14.71	13.2365	37921.2	13.48	12.1334	31026.4	11.03	9.92735	27579	9.81	8.82432

Table 4-12 Accuracy of yield stress calculation for the BP oil sample at 18 °C using the actual flow diameter

Shutdown Time, hr	The Flow Diameter mm	0.16 °C/min			0.25 °C/min			0.5 °C/min			1 °C/min			2 °C/min		
		ΔP Pa	τ (a) Pa	τ (b) Pa	ΔP Pa	τ (a) Pa	τ (b) Pa	ΔP Pa	τ (a) Pa	τ (b) Pa	ΔP Pa	τ (a) Pa	τ (b) Pa	ΔP Pa	τ (a) Pa	τ (b) Pa
1	13.009126	25855.4	9.19	8.85809	22408	7.97	7.67701	18960.6	6.74	6.49593	15513.2	5.52	5.31485	13789.5	4.9	4.72431
2	12.938939	27579	9.81	9.39765	25855.4	9.19	8.8103	20684.3	7.36	7.04824	17236.9	6.13	5.87353	17236.9	6.13	5.87353
3	12.815372	29302.7	10.42	9.88964	29302.7	10.42	9.88964	22408	7.97	7.56267	18960.6	6.74	6.39918	17236.9	6.13	5.81744
4	12.761314	31026.4	11.03	10.4272	31026.4	11.03	10.4272	22408	7.97	7.53077	20684.3	7.36	6.95148	18960.6	6.74	6.37219
5	12.617371	32750.1	11.65	10.8824	32750.1	11.65	10.8824	24131.7	8.58	8.01858	22408	7.97	7.44582	18960.6	6.74	6.30031
6	12.539467	34473.8	12.26	11.3844	34473.8	12.26	11.3844	24131.7	8.58	7.96907	24131.7	8.58	7.96907	20684.3	7.36	6.83063
7	12.49153	34473.8	12.26	11.3409	34473.8	12.26	11.3409	25855.4	9.19	8.50565	24131.7	8.58	7.93861	20684.3	7.36	6.80452

Table 4-13 Accuracy of yield stress calculation for the Mix oil sample at 30 °C using the actual flow diameter

Shutdown Time, hr	The Flow Diameter mm	0.16 °C/min			0.25 °C/min			0.5 °C/min			1 °C/min			2 °C/min		
		ΔP Pa	τ (a) Pa	τ (b) Pa	ΔP Pa	τ (a) Pa	τ (b) Pa	ΔP Pa	τ (a) Pa	τ (b) Pa	ΔP Pa	τ (a) Pa	τ (b) Pa	ΔP Pa	τ (a) Pa	τ (b) Pa
1	12.56717	93079.3	33.71	30.8058	87908.2	31.26	29.0943	12.75	31.26	29.0911	86184.5	30.65	28.5238	84460.8	30.03	27.9534
2	12.48333	98250.3	34.94	32.3003	89631.9	31.87	29.4669	13	31.87	29.4637	87908.2	31.26	28.9002	86184.5	30.65	28.3336
3	12.37058	106869	38	34.8163	91355.6	32.49	29.7623	13.25	32.49	29.759	89631.9	31.87	29.2007	87908.2	31.26	28.6392
4	12.30259	115487	41.07	37.4173	93079.3	33.1	30.1572	13.5	33.1	30.1539	91355.6	32.49	29.5987	91355.6	32.49	29.5987
5	12.2309	125829	44.74	40.5305	101698	36.16	32.7575	14	34.32	31.0885	94803	33.71	30.5367	93079.3	33.1	29.9815
6	12.15311	131000	46.58	41.9278	105145	37.39	33.6525	14.25	34.94	31.4424	94803	33.71	30.3425	93079.3	33.1	29.7908
7	12.07349	131000	46.58	41.6531	105145	37.39	33.4321	14.25	34.94	31.2364	94803	33.71	30.1437	93079.3	33.1	29.5956

Table 4-14 Accuracy of yield stress calculation for the Mix oil sample at 35 °C using the actual flow diameter

Shutdown Time, hr	The Flow Diameter mm	0.16 °C/min			0.25 °C/min			0.5 °C/min			1 °C/min			2 °C/min		
		ΔP Pa	τ (a) Pa	τ (b) Pa	ΔP Pa	τ (a) Pa	τ (b) Pa	ΔP Pa	τ (a) Pa	τ (b) Pa	ΔP Pa	τ (a) Pa	τ (b) Pa	ΔP Pa	τ (a) Pa	τ (b) Pa
1	12.789665	63776.5	22.68	21.4813	62052.8	22.07	20.9008	60329.2	21.45	20.3202	56881.8	20.23	19.159	55158.1	19.61	18.5785
2	12.706049	65500.2	23.29	21.9177	63776.5	22.68	21.3409	63776.5	22.68	21.3409	58605.5	20.84	19.6106	56881.8	20.23	19.0338
3	12.63897	68947.6	24.52	22.9494	65500.2	23.29	21.802	65500.2	23.29	21.802	60329.2	21.45	20.0808	60329.2	21.45	20.0808
4	12.573208	72395	25.74	23.9715	68947.6	24.52	22.83	67223.9	23.9	22.2593	62052.8	22.07	20.547	62052.8	22.09	20.547
5	12.521363	75842.4	26.99	25.0095	72395	25.74	23.8727	70671.3	25.13	23.3043	65500.2	23.29	21.5991	63776.5	22.68	21.0307
6	12.48188	79289.7	28.2	26.0638	72395	25.74	23.7974	72395	25.74	23.7974	67223.9	23.9	22.0976	65500.2	23.29	21.531
7	12.394337	79289.7	28.2	25.881	74118.7	26.36	24.1931	72395	25.74	23.6305	67223.9	23.9	21.9426	65500.2	23.29	21.38

Table 4-15 Accuracy of yield stress calculation for the Remal oil sample at 35 °C using the actual flow diameter

Shutdown Time, hr	The Flow Diameter mm	0.16 °C/min			0.25 °C/min			0.5 °C/min			1 °C/min			2 °C/min		
		ΔP Pa	τ (a) Pa	τ (b) Pa	ΔP Pa	τ (a) Pa	τ (b) Pa	ΔP Pa	τ (a) Pa	τ (b) Pa	ΔP Pa	τ (a) Pa	τ (b) Pa	ΔP Pa	τ (a) Pa	τ (b) Pa
1	12.429873	244764	87.04	80.1227	244764	82.13	80.1227	210290	74.78	68.8378	198224	70.49	447339	191330	68.04	62.6311
2	12.320319	251659	89.49	81.6536	251659	83.36	81.6536	213738	76.01	69.3496	203395	72.33	454963	196501	69.87	63.7569
3	12.226907	265448	94.4	85.4748	265448	85.81	85.4748	220632	78.56	71.044	210290	74.78	466819	203395	72.33	65.4936
4	12.147314	272343	96.84	87.124	272343	89.49	87.124	224080	79.68	71.6843	217185	77.23	478986	206843	73.55	66.1701
5	11.357593	275790	98.07	82.4911	275790	90.71	82.4911	227527	80.91	68.0551	224080	79.68	462063	210290	74.78	62.8994
6	11.952976	286133	100.75	90.0709	286133	93.17	90.0709	234422	83.36	73.7931	227527	80.91	493767	213738	76.01	67.2819
7	11.870894	293027	102.2	91.6079	293027	93.17	91.6079	234422	83.36	73.2863	227527	80.91	490376	213738	76.01	66.8199

Table 4-16 Accuracy of yield stress calculation for the Remal oil sample at 40 °C using the actual flow diameter

Shutdown Time, hr	The Flow Diameter mm	0.16 °C/min			0.25 °C/min			0.5 °C/min			1 °C/min			2 °C/min		
		ΔP Pa	τ (a) Pa	τ (b) Pa	ΔP Pa	τ (a) Pa	τ (b) Pa	ΔP Pa	τ (a) Pa	τ (b) Pa	ΔP Pa	τ (a) Pa	τ (b) Pa	ΔP Pa	τ (a) Pa	τ (b) Pa
1	12.42987	244764	87.04	80.1227	244764	82.13	80.123	210290	74.78	68.8378	198224	70.49	447339	191330	68.04	62.6311
2	12.32032	251659	89.49	81.6536	251659	83.36	81.654	213738	76.01	69.3496	203395	72.33	454963	196501	69.87	63.7569
3	12.22691	265448	94.4	85.4748	265448	85.81	85.475	220632	78.56	71.044	210290	74.78	466819	203395	72.33	65.4936
4	12.14731	272343	96.84	87.124	272343	89.49	87.124	224080	79.68	71.6843	217185	77.23	478986	206843	73.55	66.1701
5	11.35759	275790	98.07	82.4911	275790	90.71	82.491	227527	80.91	68.0551	224080	79.68	462063	210290	74.78	62.8994
6	11.95298	286133	100.75	90.0709	286133	93.17	90.071	234422	83.36	73.7931	227527	80.91	493767	213738	76.01	67.2819
7	11.87089	293027	102.2	91.6079	293027	93.17	91.608	234422	83.36	73.2863	227527	80.91	490376	213738	76.01	66.8199

Such data are now presented in Table 4-11 to Table 4-16 and for the 3 oils at the same conditions tested as described earlier and for which the yield stress was calculated using the full diameter. For ease of comparison, the yield stresses using both diameters are tabulated. Clearly because of the direct dependence on the diameter, the reduction in the yield stresses is proportional to the reduction in diameter. There is thus no change in the broad variation of the yield stress with cooling rate, shutdown time and temperature in both cases. Although the difference between the two yield stresses is not major (no more than 5 Pa which represent about 10%), it is significant, particularly in rheological terms when the quest is to get precise data. The importance of the work here is thus more about getting a more accurate measurement of the yield stress. Also the data gathered here can help develop models because the way in which the wax layer thickness develops in time has been measured. This will be an important recommendation for future work as the data here provide a comprehensive basis.

4.3.5 Conclusions

The important conclusion from this part of the research is that it is important to take into consideration the wax layer thickness in the evaluation of the yield flow stress as the build up of wax into a measurable layer has been established with three oil of different wax content ranging from 15 to 35%. In all cases, the layer thickness has significant effect but this effect on the yield stress is never more than 5 Pa (about 10%). The start-up pressures and corresponding yield flow stresses have been found to underpin the crystallisation process of the wax. Slow cooling rate produce stronger structures requiring higher stresses to fracture and flow. Longer shutdown times also render these structures even stronger require even larger stresses for flow to commence.

In principle this data can be used to guide operation at the large scales and as such they provide a good data basis to assess scaling up. The data on the evolution of the wax thickness in time with cooling rates, shutdown times and temperature also provide a good data basis to develop theoretical model that can predict start-up. Having measured these yield *flow* stresses or the stresses when the solid oil fracture and suddenly flow, it will be desirable to compare them with stresses measured in more precise rheological systems. This is undertaken in the following section.

4.4 RHEOLOGY IN OSCILLATORY FLOWS & YIELD STRESSES

4.4.1 Introduction

As explained in section 4.2, oscillatory flows are very well suited to the measurement of yield stress because if carried out properly, at low strain amplitude and frequency, they approach the yield region very progressively from the solid state. Measurement of how the shear storage modulus G' and loss modulus G" varies with increasing strain can then detect the end of the solid deformation and the entire yielding region until fracture of the material occurs. This is precisely what was tested with the BP oil sample in an effort to compare the yielding *flow* or fracture stresses measured in the pipeline rig using the superior method of using the effective flow diameter with the various stresses measured in oscillatory flow.

4.4.2 Test Data

Figure 4-23 presents the data for BP oil from a sample fully conditioned cooled from 70 ^{0}C down to various test temperatures at a controlled low cooling rate of 0.125^{0}C.

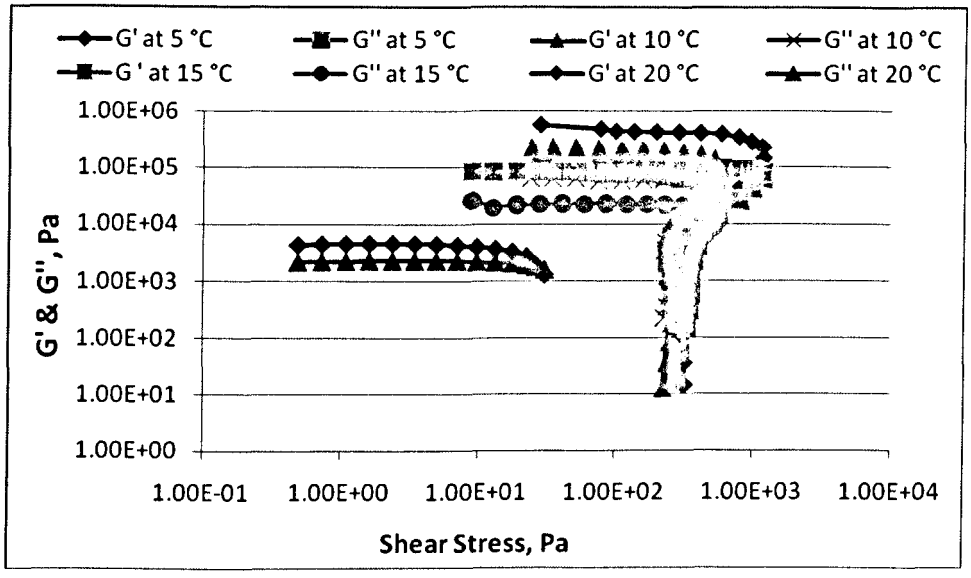

Figure 4-23 Shear stress vs. G' and G'' for the BP oil sample

Table 4-17 True yield and flow yield values for the BP oil sample

	Strain (1), %	True Yield , Pa	Strain (2), %	Flow yield, Pa
At 5 °C	0.147	581	3.16	952
At 10 °C	0.147	306	3.16	517
At 15 °C	0.147	119	3.16	226
At 20 °C	0.147	7.02	3.16	13.3

A plateau of constant shear storage modulus G' in the data signifies the oil is in the elastic region. Yielding is detected at values of strain and corresponding stresses when G' begins to drop with increasing stresses. This is the true yield stress (the true yield is starting once G' starts to leave the LVR), denoted here by τ_{Y*} which is at the intersection of the linear elastic region with the non linear region. Yielding is completed when G' and G" intersect that is when the fluid part of the material overtakes the solid part. This point is referred to as the flow point or yield point. Clearly, yielding here occurs over a wide range of value and in comparison with the experiments carried out in the pipe flow, the measured yield flow stress is the same

as the yield point or flow point measured in the oscillatory tests. On this basis, the data from the two tests can be compared. The results of Figure 4.23 are represented in Table 4.17; the different temperatures (5, 10, 15 and 20 °C) are applied to the sample from BP in order to determine/identify the true yield as well as the flow yield.

The figures obtained for 5 °C generated strain of 0.147% during which the oil commenced to leave the LVE region; similarly the oil also has a magnitude of shear stress of 581Pa

Furthermore, at the same time of applying the same temperature, the oil generated a strain level of 3.16% at which the oil completely began to move with a corresponding stress level of 952Pa

Additionally, figures were obtained at a temperature of 10 °C which gave a strain value of 0.147% which enabled the oil to depart the LVR region with corresponding value of 306 Pa and then for the strain of 3.16% together corresponding stress level of 517Pa

Likewise, figures were obtained at a temperature of 15 °C which gave a strain value of 0.147% which enabled the oil to depart the LVR region with corresponding value of 119 Pa and then for the strain of 3.16&% together corresponding stress level of 226Pa.

Similar figures and results were carried out and repeated for the temperature of 20 °C and are represented in the third and fourth row and column of Figure 4.23.

4.4.3 Conclusions

The conclusion to be derived from the oscillatory test results of Figure 4.23 and Table 4.17 are as follows:

There appears to be correlation between temperature and yield; that is with increase in temperature the yield point also increases.

There are two yield points; firstly, as soon as the oil commences to move, it is denoted by a lower magnitude of stress; which is called a true yield; when the oil is in motion with ease at normal flow rate the corresponding stress is higher.

4.5 SHEAR DATA IN ROTATIONAL FLOWS TO MEASURE THIXOTROPY, TIME DEPENDENCY & TEMPERATURE DEPENDENCY

4.5.1 Introduction

The start-up pressures and yield stresses are important design/operation of pipelines pumping waxy crude oils. When they are known, they guide safe operation of blocked pipelines which can be very expensive if not carried out quickly and appropriately. They do not however give complete information to manage the subsequent pressures once the start-up after shutdown has been successful. What is required is knowledge of the viscosity very near this state and how it can change with time so that the operating pressures can be reduced and consequently the cost kept to a minimum.

As established from above, waxy crude oil yield stress which develops strongly upon cooling when at rest is the result of structure build up due to crystallisation. Clearly, at restart, the application of a force equal or greater than the yield stress will result in flow. Because of the cost of pumping, restarting flow with minimum pressure requires application of a pressure force just equivalent to the measured yield stress. When this yield stress is applied, the structure will gradually

break in time until flow commences. Therefore a study of the thixotropic behaviour of the waxy oil is required. In shear flows, this can be achieved either by the application of a constant stress equivalent to the yield stress or by the application of the lowest permissible shear rate (depending on the accuracy of the rheometer).

In these experiments, the measurement of thixotropy was achieved by using the lowest shear rates permissible, typically $0.1s^{-1}$. If at this shear rate, very close to the restart (when the oil is constraint to move in the pipe), the oil is observed to drop significantly in viscosity with time, then the pressure can be reduced below the start-up values to maintain a desired flow rate in accordance with pipe flow theory (Hagen-Poiseuille equation for laminar flow) which links flow rate, Q pipe diameter D and length L with pressure drop, i.e.

$$Q = \frac{\Delta P}{L}\frac{\pi D^2}{128\mu_a}$$

This equation strictly applies to a Newtonian fluid in laminar flow but can be relaxed by using an apparent viscosity which can be measured from test data. Therefore in this section, we present data on the variation of the oil apparent viscosity with time at the lowest shear rate that happens immediately after start-up. Also and in order to measure thixotropic behaviour and illustrate the extent in the range of viscosities that can be attained after start-up, it is necessary to also observe the behaviour when the shear stress is increased drastically to a high value, say 1000 s^{-1} which will be typical of a full flow and brought down back to 0.1 s^{-1}. This will give the spread of the viscosities and are the necessary values to guide the setting up of pressures until full flow is reached. Because clearly, maintaining the pressure to the highest value is not only not necessary but also very expensive.

In order to complement the thixoropic data, it is also useful to measure the variation of apparent viscosity at constant temperature with shear rate when the shearing time is varied. Such information will provide a complete picture of the oil behaviour and will enable an optimisation of the pressure during start-up.

4.5.2 Measuring Technique

The technique used for thixotropic measurements here is simple and it seeks to mimic the gradual development of shear rate with time at the beginning of re-start from shutdown. Again a controlled cooling is applied to the samples which are brought down below the gel point to a test temperature. These conditions are similar to the one studied above. Therefore using a modern rheometer, one can programme first the control cooling of the sample from a high temperature to the test temperature, then set for the shear rate to be maintained at a very low value, 0.1 s^{-1} and measure the reduction of apparent viscosity in time. A step increase thereafter to 1000 s^{-1} would show the extent to which the apparent viscosity can really drop to and this will allow calculation of a whole set of pressures possible to operate the pipeline for a set flow rate. Also by programming a step decrease back to 0.1 s^{-1}, thixotropy and the increase in viscosity after shutdown can also be measured.

As for the measurement of time dependency at all shear rates, it was a simple matter to impose a shear rate and measure the variation of apparent viscosity in timer.

4.5.3 Thixotropy Data

Figures 4-24 to 4-47 present the data for the three oils studied in this research with tests conditions as follows:

First interval: shear rate $\dot{\gamma} = 0.1\ s^{-1}$ for 60 s

Second interval: shear rate $\dot{\gamma} = 1000\ s^{-1}$ (or another large value $3000\ s^{-1}$) for 60 s

Third interval: shear rate $\dot{\gamma} = 0.1\ s^{-1}$ for 600 s

All samples as explained earlier were cooled in the rheometer to a set temperature as was done in the tests described above.

This test attempted to ascertain the amount of residual wax that is retained after application of shear rate ranging from 1000 1/s – 3000 1/s ; (1000 1/s for BP oil sample and 3000 1/s for Remal and Mix).

In the first interval the applied shear rate was 0.1 1/s at temperature 5 °C, thereafter a shear rate of 1000 1/s is applied to the BP sample. Afterwards at the second interval the viscosity was recorded at almost zero.

At the third interval the load was withdrawn and the applied sheer rate was maintained at 0.1 1/s in order to see if the viscosity value would revert to the reference/ residual value obtained from the first interval.

The test results are plotted in three different graphs in order to demonstrate the data in sequencing order with a view illustrating the viscosity at various shear rate in given intervals.

The benefits of these tests can give the pipeline operator the required data regarding stress and viscosity to be able to operate the pipeline optimally from Health and safety and budgetary consideration.

In order to derive the utmost benefit to the pipeline operator from this test results (thixotropy), it can provide us with the yield stress that is needed to re-start the pipeline and furthermore if flow is curtailed for any reasons, it is possible to get the

maximum shear stress that can be applied to re-start the pipeline is thus identified as the highest sheer stress repeated in the third of Table 4-18.

It is evidently shown in Figure 4-25 for the first interval that the viscosity of the BP sample is thinning drastically; falling from approximately 795 Pa.s to a low figure of 755 Pa.s

Similarly, at the second interval, when the load of 1000 1/s, the viscosity is relatively thinner in comparison with the initial viscosity obtained from the initial phase. The low viscosity shown in Figure 4-26 illustrates that the oil flows easily.

Correspondingly, in the third interval the same slow rate of 0.1 1/s that was applied in the first interval gave the possibility to the wax structure/composition to re-formed, however it will not revert back to its initial viscosity as shown by the results in Figure 4.27. Accordingly, the same process is repeated at different temperature of 10, 15 and 20 °C.

At the same instance, the same effect was considered and applied to the two other oil samples; (*Mix* & Remal) at different test temperatures below the gel point temperature with similar characteristics exhibited in the results recorded. This is illustrated in more details in Table 4.19 for the sample referred to as *Mix;* the same results recorded are equally represented in Figure 4.32 and up to Figure 4.39 for the temperatures under consideration; namely 5 and 10 °C. The remainder of the graphs of the other temperatures (15, 20, 25 and up to 35 °C) are given in appendix III.

Similarly, the characteristics of the sample referred to as Remal is illustrated in tables 4.20, Figure 4.40 up to figure 4.47 for temperature under discussion/consideration 5 and 10 °C. The remainder of the graphs of the other temperatures (15, 20, 25 and up to 45 °C) are given in appendix III.

Table 4-18 Results of measurements of shear stress and viscosity obtained by the shear function step to measure thixotropic behaviour of BP oil sample

Test Temperature °C	Interval I		Interval III					
			(1)	(1)	(2)	(2)	(3)	(3)
	Reference Viscosity Pa.s	Yield Stress Pa	Apparent Viscosity Pa.s	Shear Stress Pa	Highest Viscosity Pa.s	Highest Stress Pa	Steady State Vis. Pa.s	Steady state Stress Pa
5	796	199	6.07	1.52	98	103	50.6	12.6
10	396	99.1	1.47	0.368	68.7	17.2	27.2	6.79
15	62	15.5	0.192	0.048	31	7.76	19.5	4.88
20	4.08	1.01	0.258	0.064	3.63	0.9	3.63	0.9
25	1.56	0.39	0.125	0.059	0.68	0.17	0.2	0.69

Table 4-19 Results of measurements of shear stress and viscosity obtained by the shear function step to measure thixotropic behaviour of Mix oil sample

Test Temperature °C	IntervalI		IntervalIII					
			(1)	(1)	(2)	(2)	(3)	(3)
	Reference Viscosity Pa.s	Yield Stress Pa	Apparent Viscosity Pa.s	Apparent Shear Stress Pa	Highest Viscosity Pa.s	Highest Stress Pa	Steady State Viscosity Pa.s	Steady state Shear Stress Pa
5	1520	1674	418	104	765	192	122	30.4
10	1360	1140	203	50.9	341	85.2	104	25.9
15	699	175	30.8	7.7	91.7	23	39.3	9.82
20	324	80.9	6.51	1.63	48.5	12.1	27.8	6.96
25	47.4	11.8	2.16	0.185	23.1	5.76	22.4	5.59
30	7.99	2	0.66	0.028	7.27	1.87	6.46	1.61
35	3.5	0.648	0.114	0.0285	2	0.501	2	0.501
40	0.161	0.0403	0.0496	0.0374	0.0797	0.0199	0.139	0.0347

Table 4-20 Results of measurements of shear stress and viscosity obtained by the shear function step to measure the thixotropic behaviour of Remal oil sample

Test Temperature ℃	Interval I		Interval III					
			(1)	(1)	(2)	(2)	(3)	(3)
	Reference Viscosity Pa.s	Yield Stress Pa	Apparent Viscosity Pa.s	Apparent Shear Stress Pa	Highest Viscosity Pa.s	Highest Shear Stress Pa	Steady State Viscosity Pa.s	Steady state Stress Pa
5	1600	1700	671	168	1220	306	970	243
10	1490	1373	390	97.5	502	87.9	208	52.1
15	1260	816	485	121	900	225	563	144
20	783	196	439	110	592	148	525	131
25	375	98.8	74.1	13.6	94.1	5.58	76.2	16.5
30	115	29.1	63	15.1	66.2	17.8	63	15.1
35	52.2	13.1	2.397	0.0994	10.6	2.69	10.6	2.69
40	46.7	11.7	1.68	0.419	13.9	3.48	12.9	3.22
45	10.7	2.43	0.141	0.0352	4.79	1.2	3.4	0.85

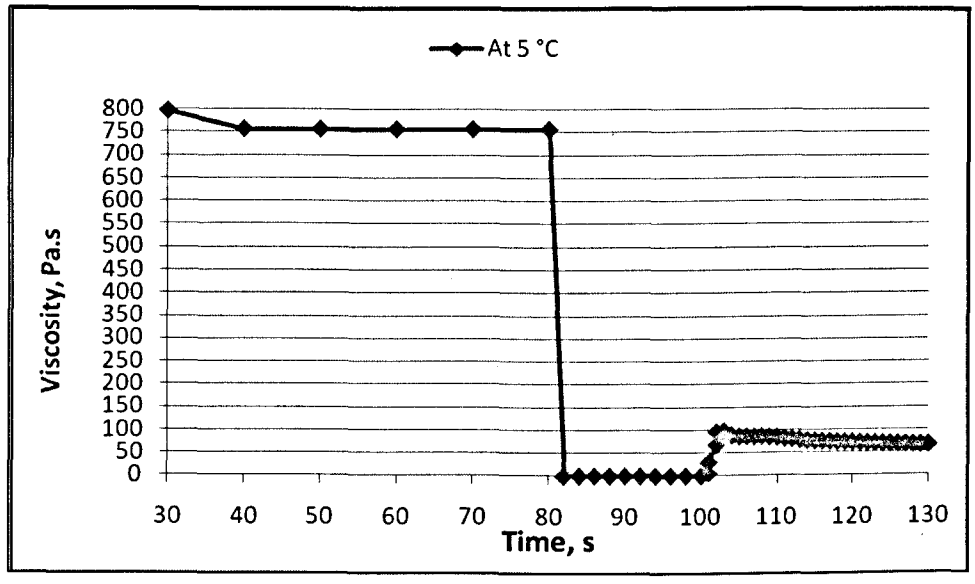

Figure 4-24 Time vs. viscosity: thixotropy phenomena test for BP sample under 0.1, 1000 and 0.1 1/s shear rates at 5 °C

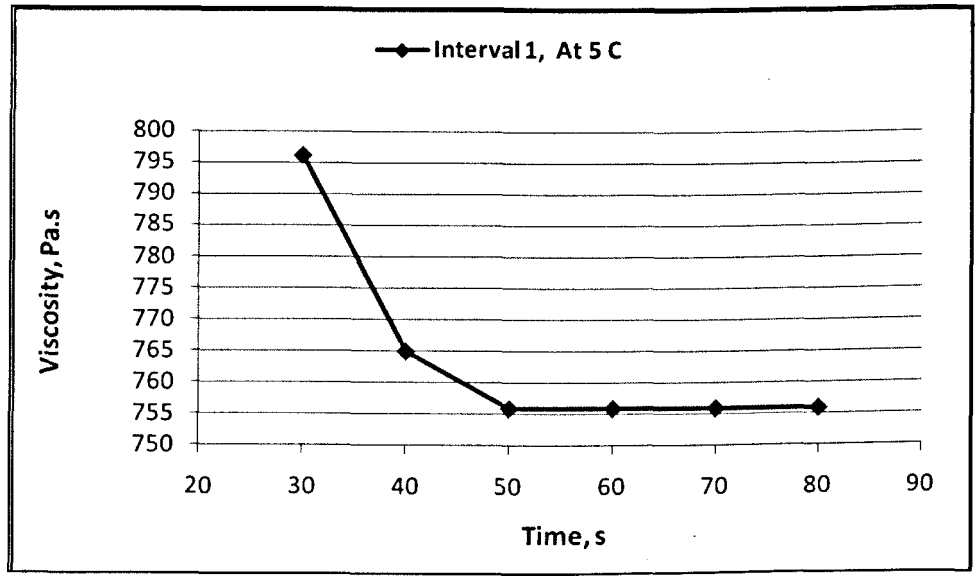

Figure 4-25 Magnification of the data shown in Figure 4.24 from time interval 20 to 80 second

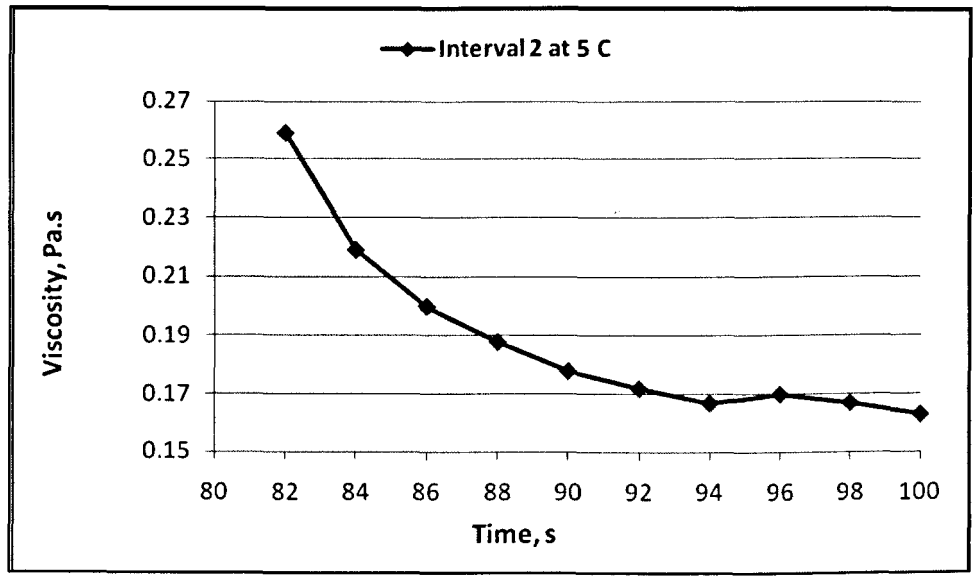

Figure 4-26 Magnification of the data shown in Figure 4.24 from time interval 80 to 100 second

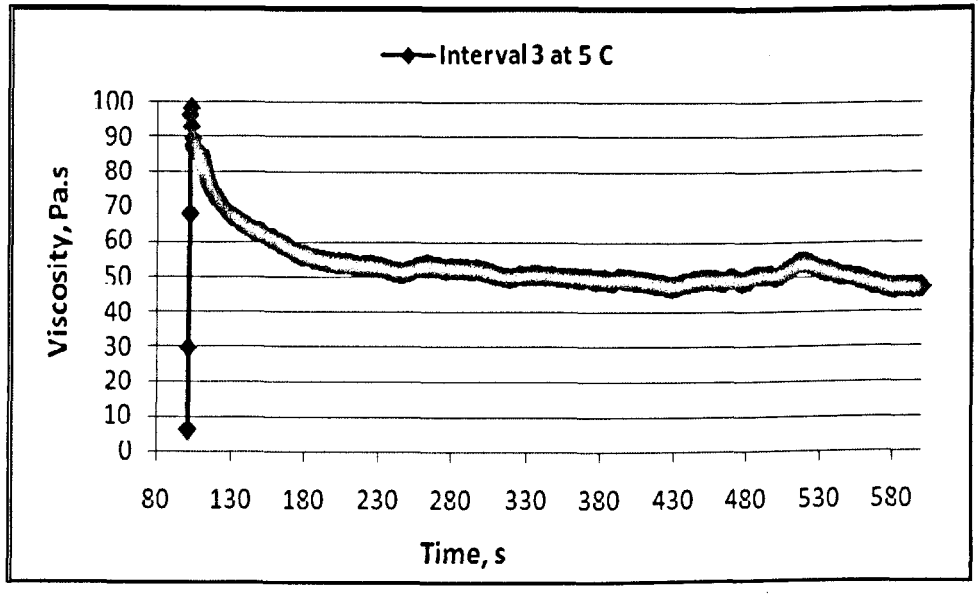

Figure 4-27 Magnification of the data shown in Figure 4.24 from time interval 100 to 580 second

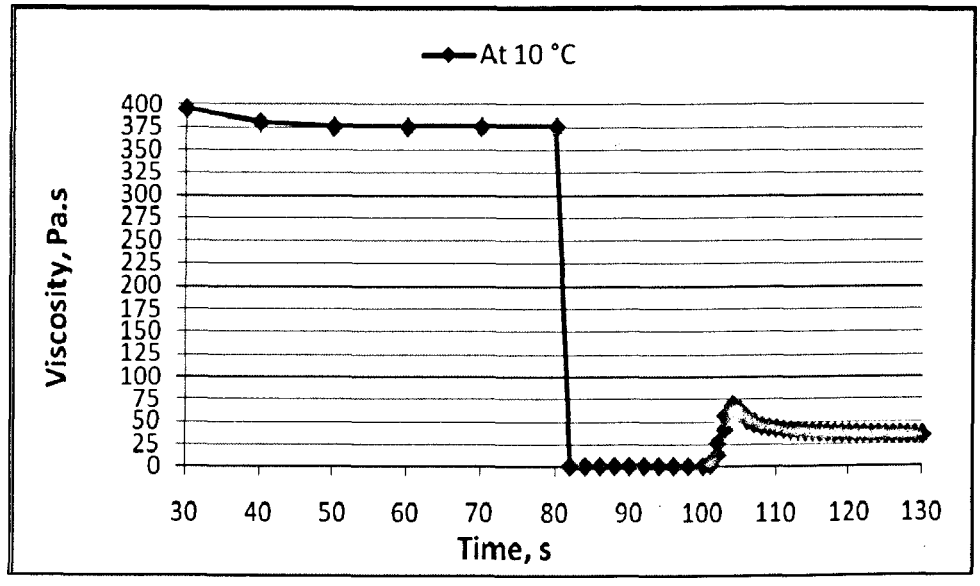

Figure 4-28 Time vs. viscosity: thixotropy phenomena test for BP sample under 0.1, 1000 and 0.1 1/s shear rates at 10 °C

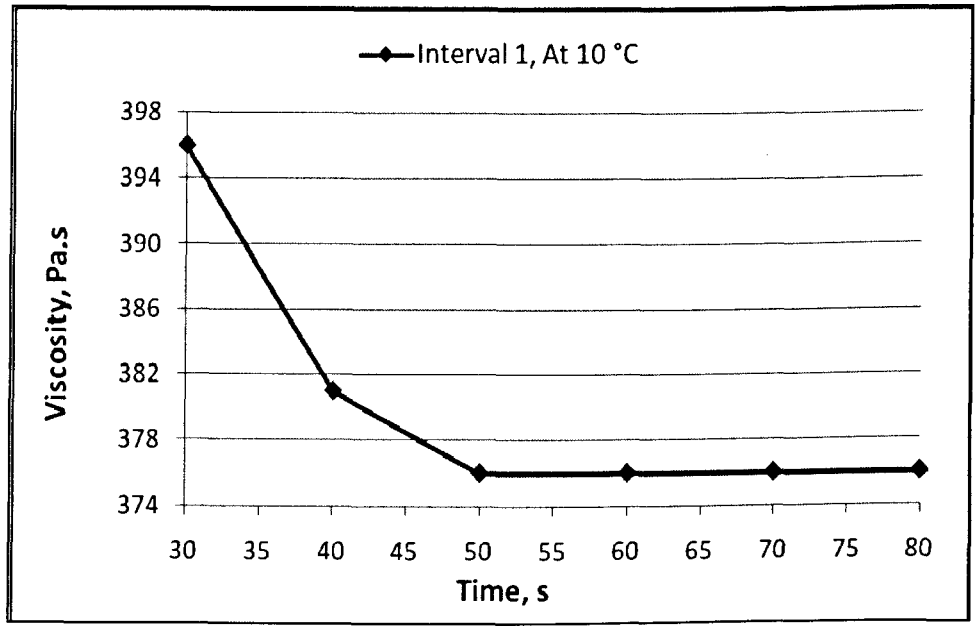

Figure 4-29 Magnification of the data shown in Figure 4.28 from time interval 20 to 80 second

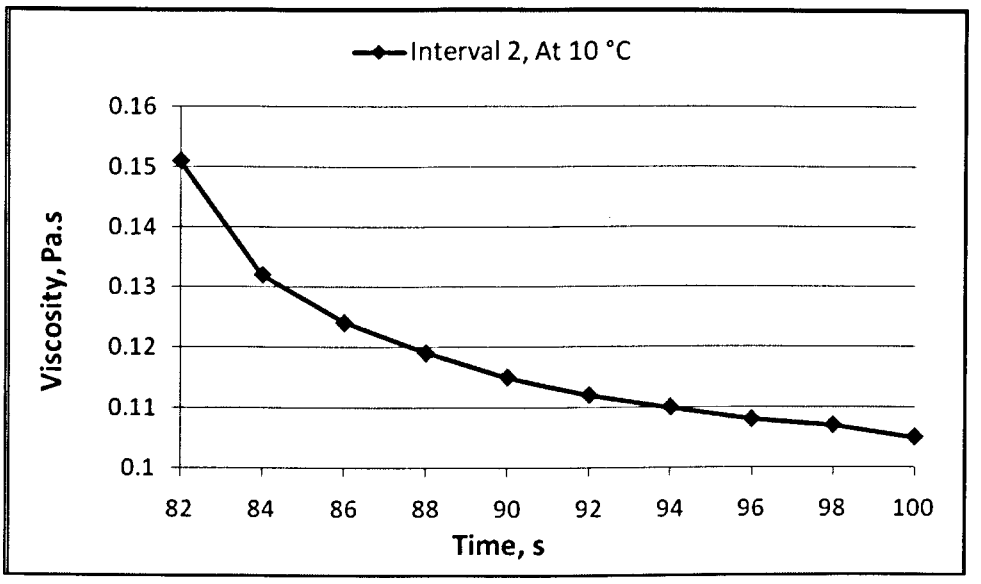

Figure 4-30 Magnification of the data shown in Figure 4.28 from time interval 80 to 100 second

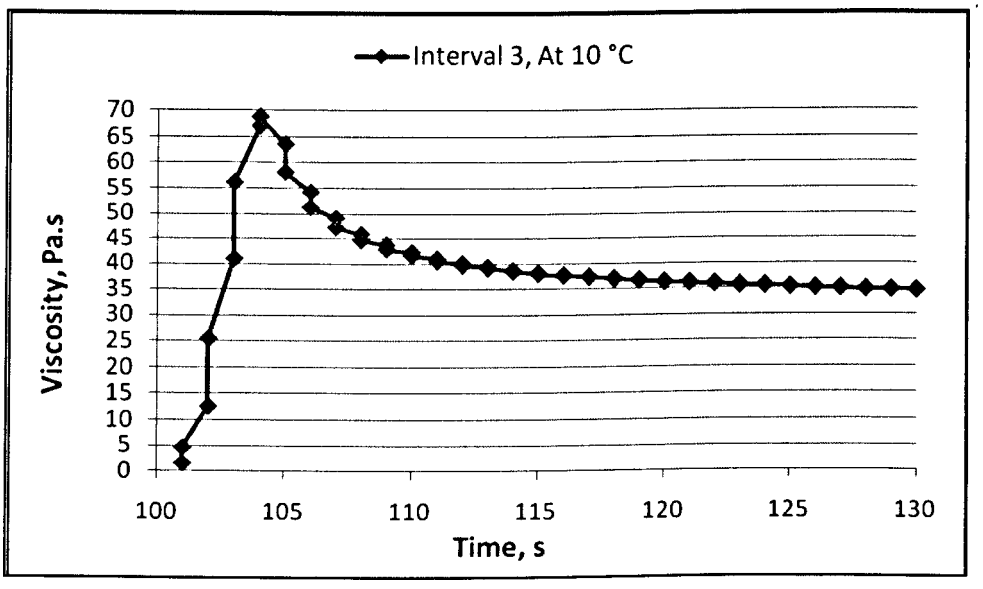

Figure 4-31 Magnification of the data shown in Figure 4.28 from time interval 100 to 580 second

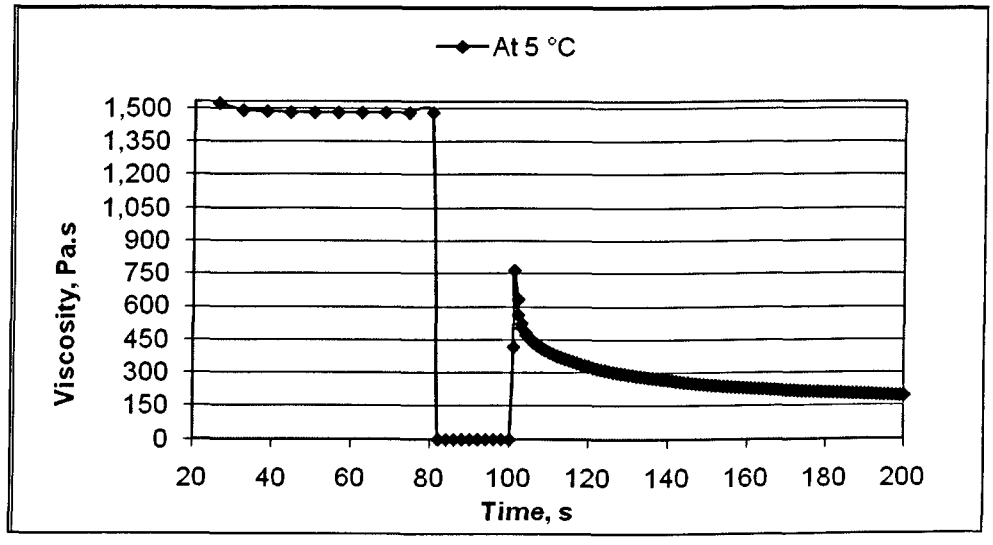

Figure 4-32 Time vs. viscosity: thixotropy phenomena test for Mix oil sample under 0.1, 1000 and 0.1 1/s shear rates at 5 °C

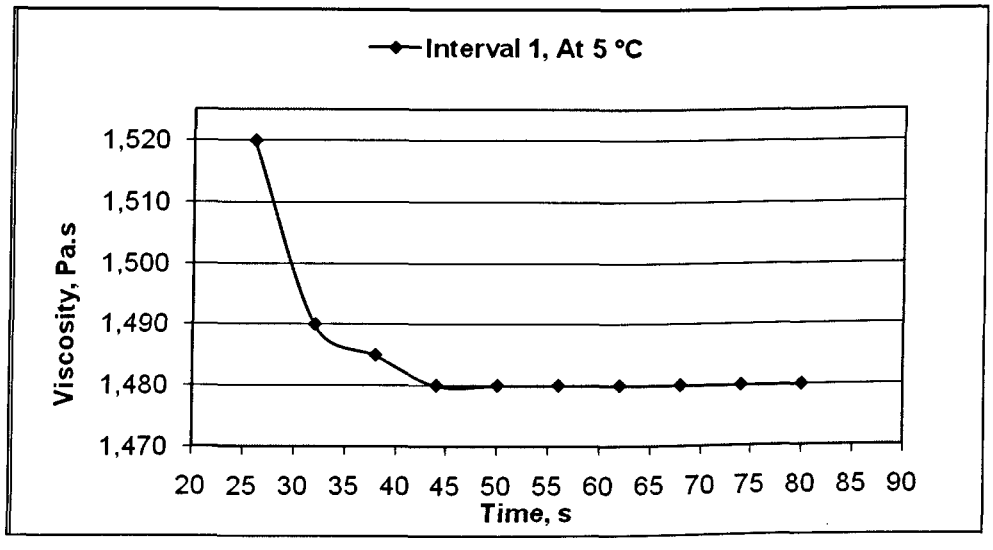

Figure 4-33 Magnification of the data shown in Figure 4.32 from time interval 20 to 80 second

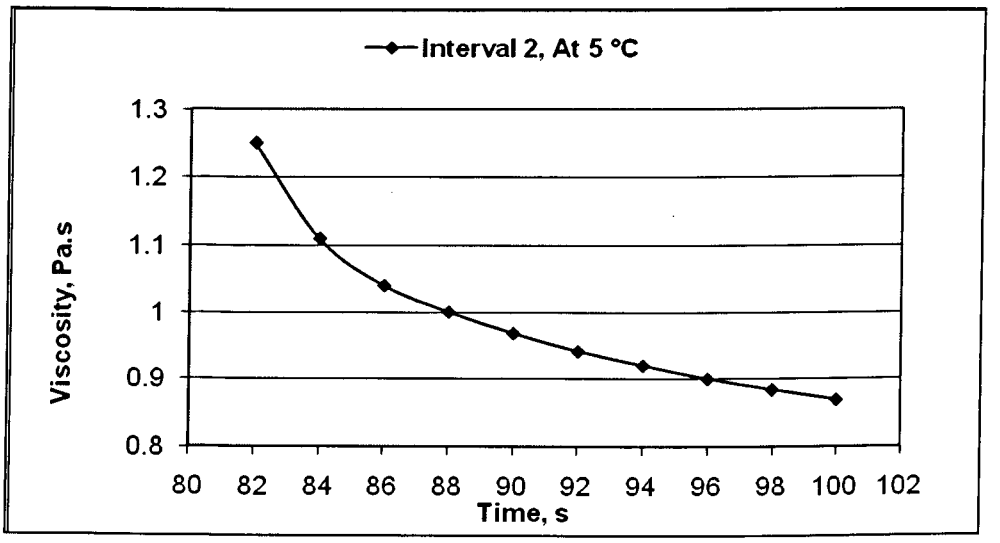

Figure 4-34 Magnification of the data shown in Figure 4.32 from time interval 80 to 100 second

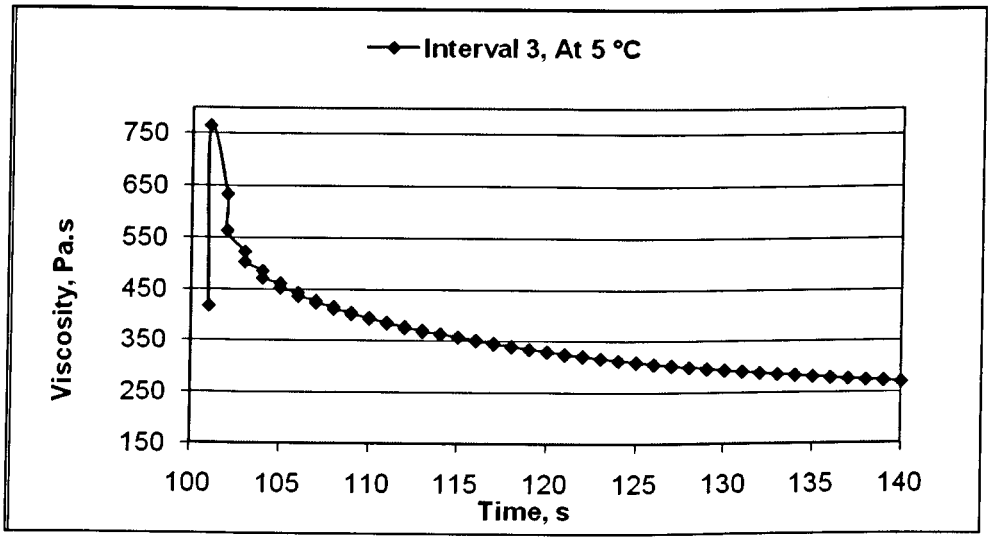

Figure 4-35 Magnification of the data shown in Figure 4.32 from time interval 100 to 580 second

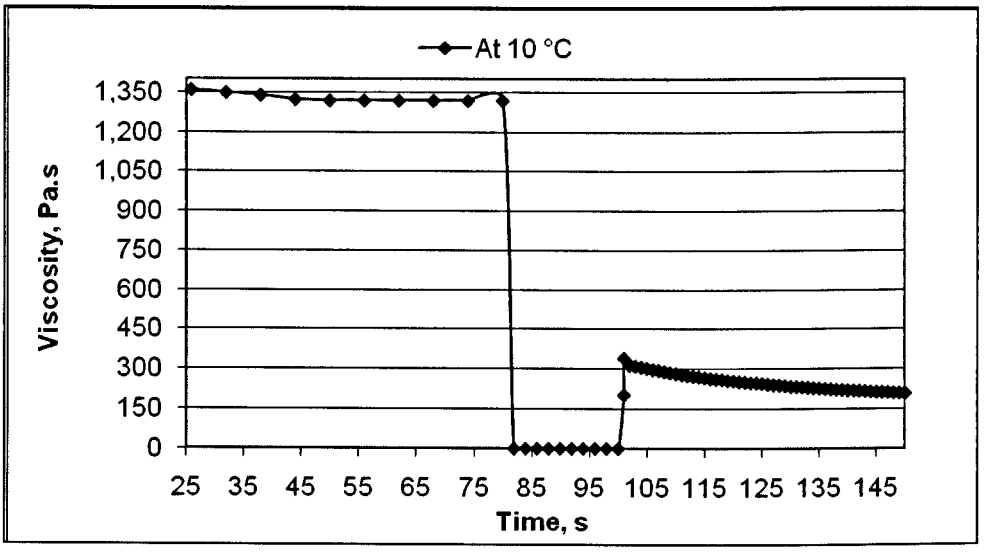

Figure 4-36 Time vs. viscosity: thixotropy phenomena test for Mix oil sample under 0.1, 1000 and 0.1 1/s shear rates at 10 °C

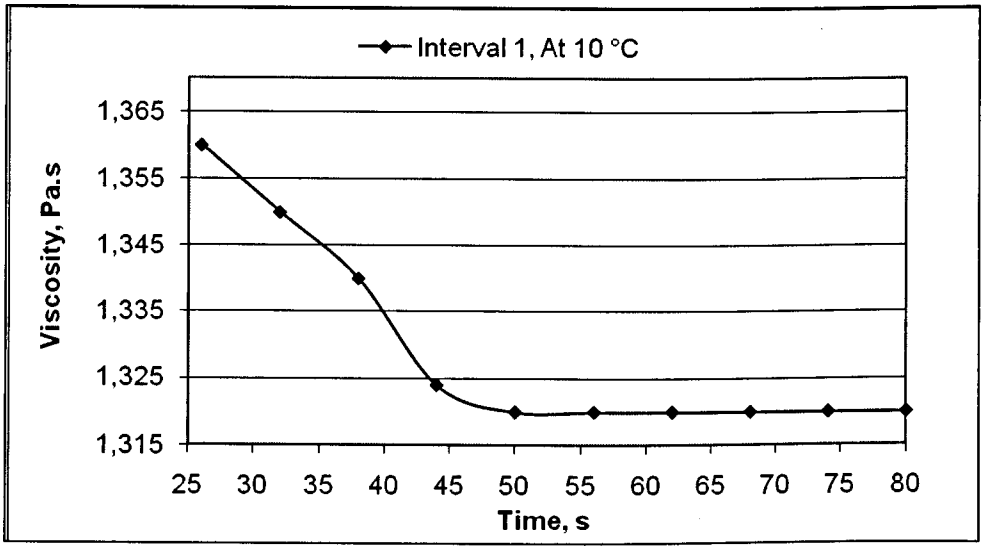

Figure 4-37 Magnification of the data shown in Figure 4.36 from time interval 20 to 80 second

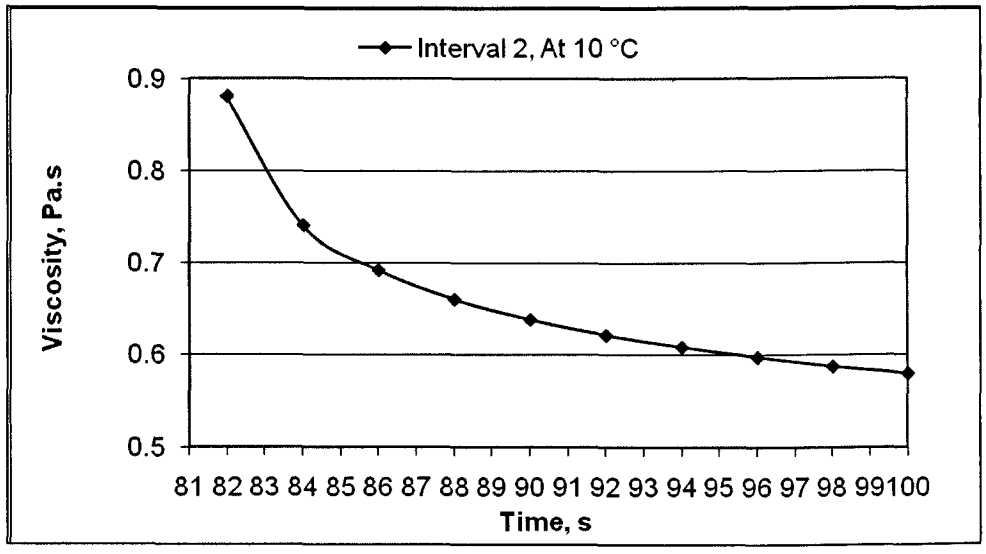

Figure 4-38 Magnification of the data shown in Figure 4.36 from time interval 80 to 100 second

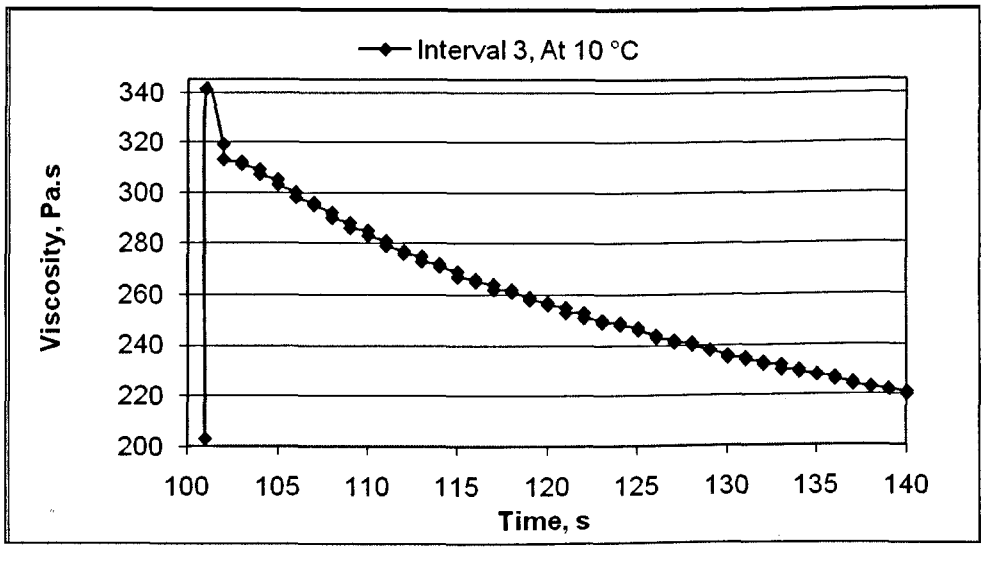

Figure 4-39 Magnification of the data shown in Figure 4.36 from time interval 100 to 580 second

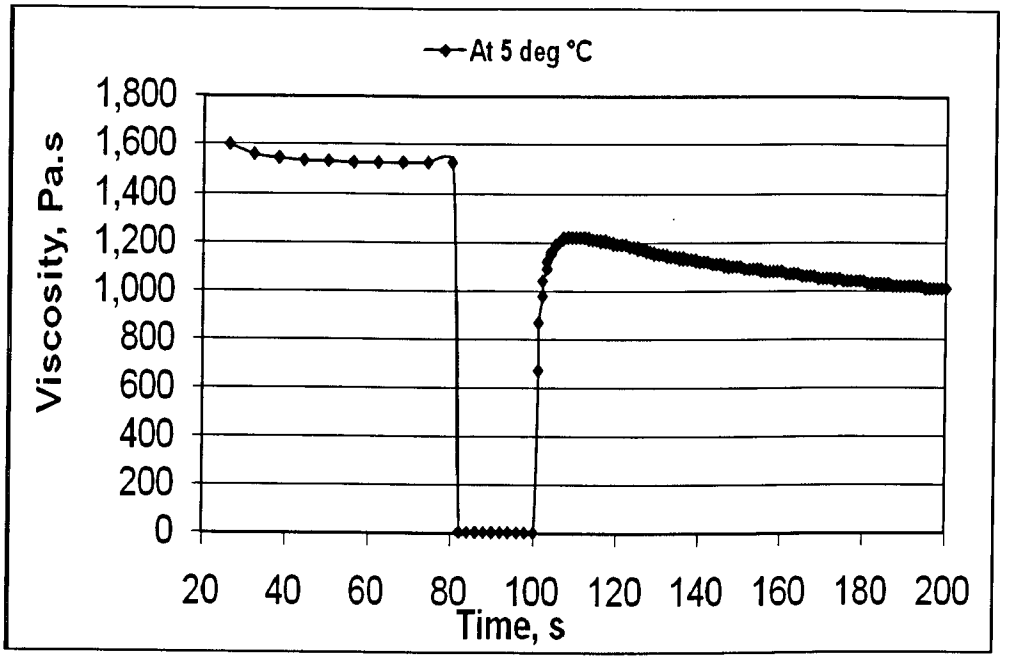

Figure 4-40 Time vs. viscosity: thixotropy phenomena test for Remal oil sample under 0.1, 1000 and 0.1 1/s shear rates at 5 °C

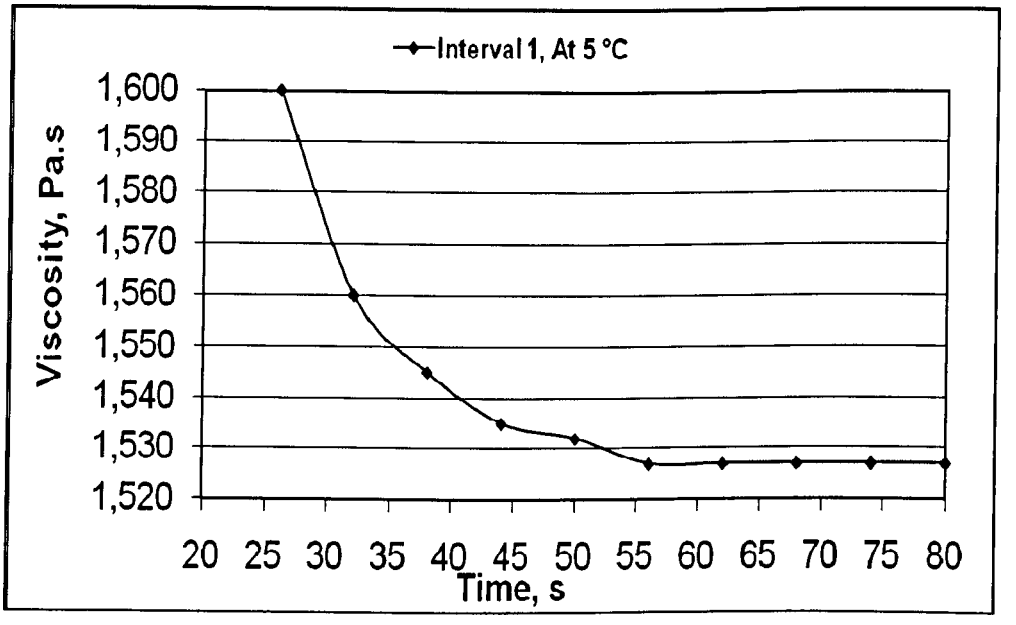

Figure 4-41 Magnification of the data shown in Figure 4.40 from time interval 20 to 80 second

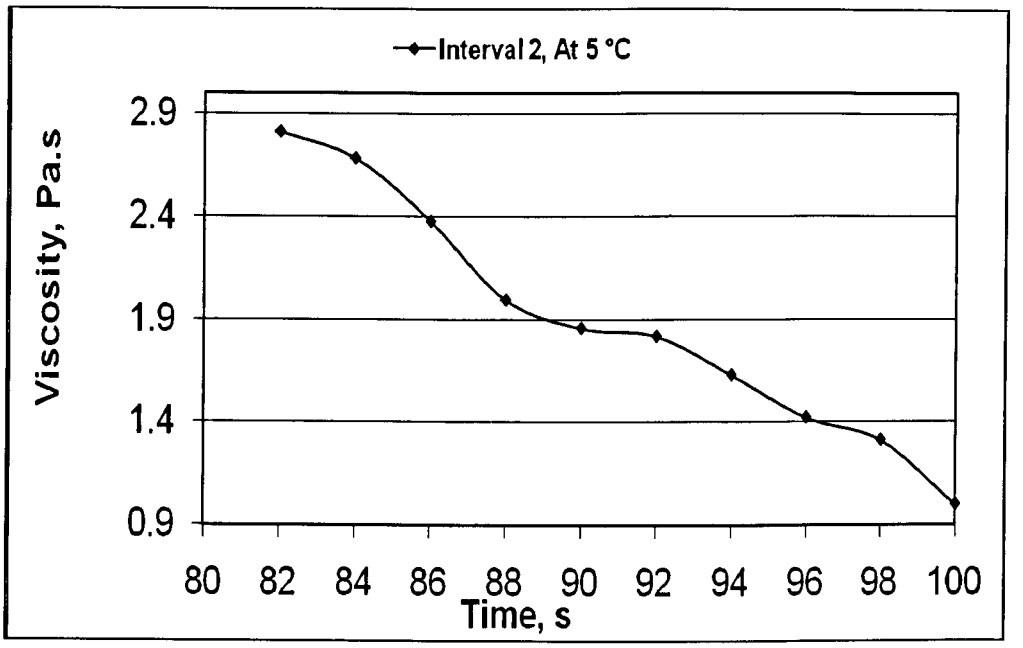

Figure 4-42 Magnification of the data shown in Figure 4.40 from time interval 80 to 100 second

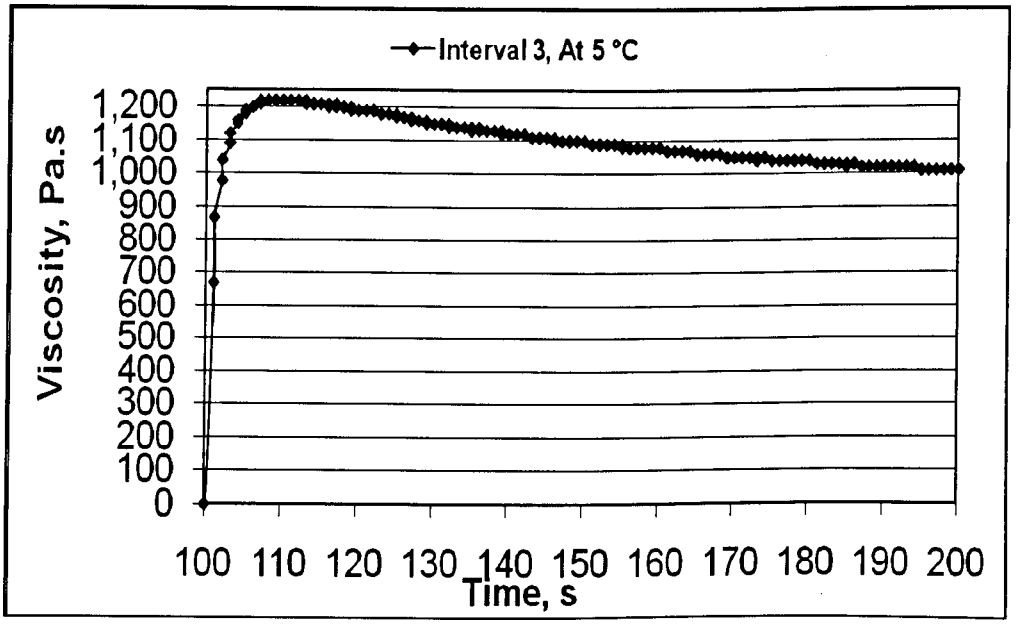

Figure 4-43 Magnification of the data shown in Figure 4.40 from time interval 100 to 580 second

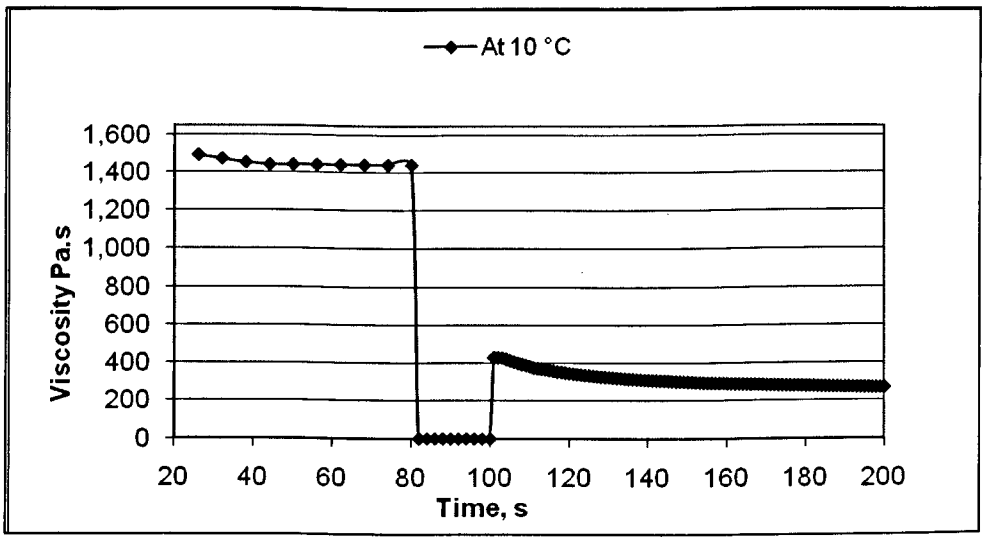

Figure 4-44 Time vs. viscosity: thixotropy phenomena test for Remal oil sample under 0.1, 1000 and 0.1 1/s shear rates at 10 °C

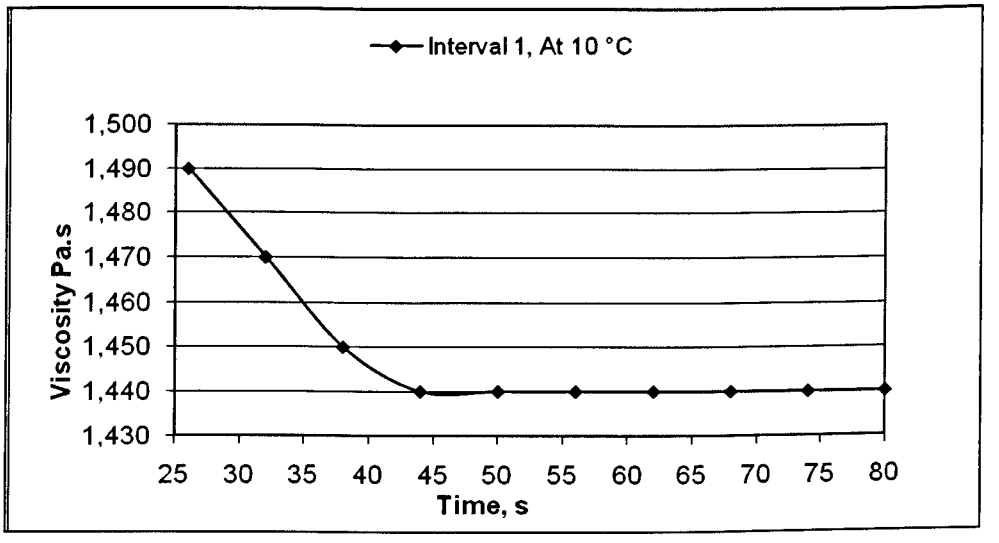

Figure 4-45 Magnification of the data shown in Figure 4.44 from time interval 20 to 80 second

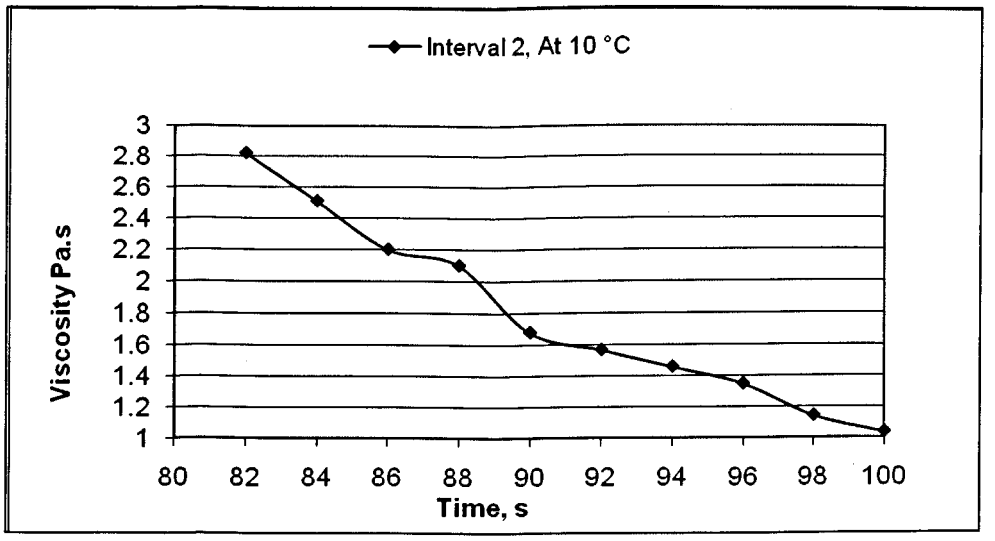

Figure 4-46 Magnification of the data shown in Figure 4.44 from time interval 80 to 100 second

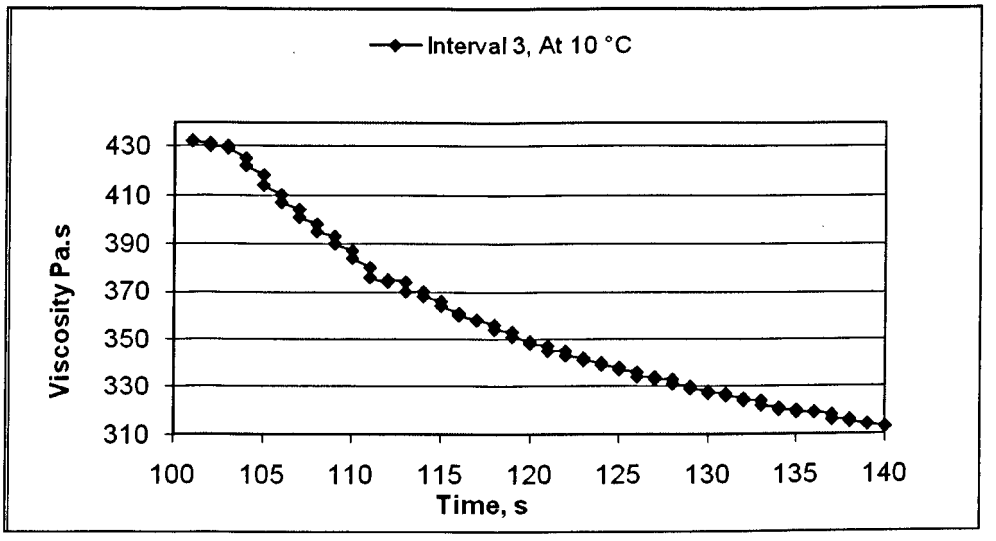

Figure 4-47 Magnification of the data shown in Figure 4.44 from time interval 100 to 580 second

The rest of the figures at the other temperature for all the samples are placed in Appendix A3

4.5.4 Time Dependency Data

Figures 4-48 to Figure 4-56 present the data for the three oils that were studied to determine the effect of shearing over time by applying a constant sheer rate at constant temperature. In all cases, the oils were cooled from the high temperature imposed so that no prior memory affects behaviour. These temperatures were 65^0C for BP oil, 75^0C for Remal oil and 75^0C for the Mix oil cooled thereafter at 0.5 °C/min down to the test temperatures of 5, 10, 15 , 20 and 25 °C for BP oil, 5, 10, , 15, 20, 25, 30, 35, 40, 45, 50 and 55 °C for Remal oil and 5, 10, , 15, 20, 25, 30, 35, 40 and 45°C for the Mix oil. The shear rates tested for each of these oils at each of these temperatures were 0.1, 1, 10, 20, 50, 100, 500, 1000, 1500, 2000 and 2500 s^{-1}. For each of these test conditions, the variation of the apparent viscosity with time was measured for a period of up to 20 minutes.

The results of these tests are presented in Figure 4-48 to Figure 4-56. However, the rest of the figures are presented in Appendix A4.

The outcome/result of the experiments is discussed and are as follows:

The shear rate load applied in this experiment ranges from 0.1$s^{-1}$and 2500 s^{-1}; at each instance, the load is applied over a period of 20 minutes. The viscosity of the oil showed a decline for the first few seconds and thereafter remained constant. It exhibited a shear thinning behaviour

For example, at the temperature of 5 °C using 0.1 s^{-1}, the viscosity decreased from 2000 Pa.s to approximately 900 Pa.s during the time interval of 30 seconds and thereafter remained constant. Similarly, at temperatures of 5 °C using 1 s^{-1}, the

viscosity also decreased from 900 Pa.s to 600 Pa.s during the time interval of 10 seconds and thereafter the viscosity remained constant.

In summary, in all the samples used during this experiments; the outcome observed and recorded are very similar and congruent; i.e. time dependency at the initial stages.

All the results for the BP sample in this experiment are given below; however, for the samples Mix and Remal, the results of 5°C and 10 °C degrees are given below with the remainder of the graphs presented in appendix

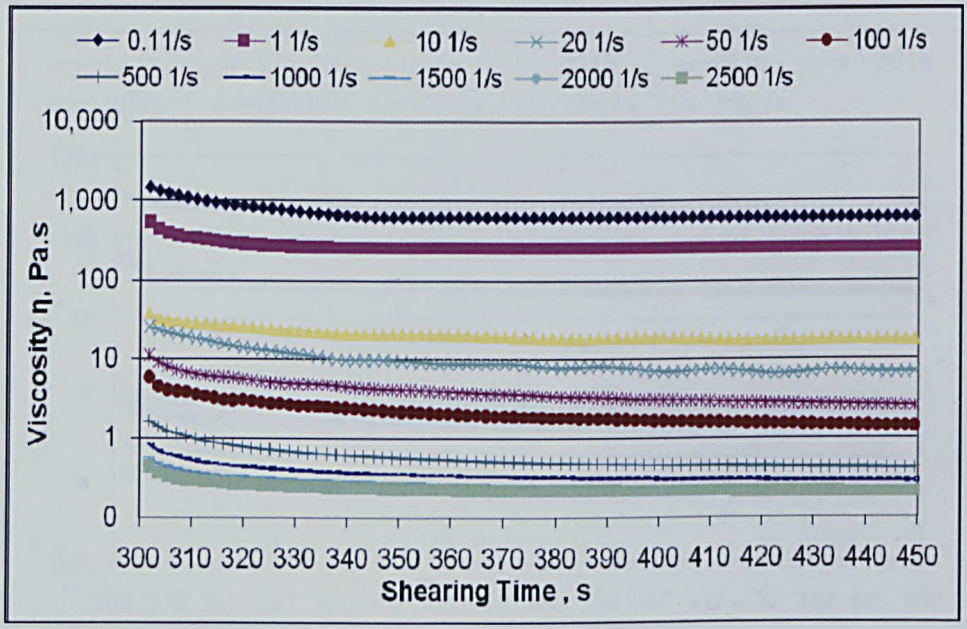

Figure 4-48 Time dependency data for the BP oil sample at 5 °C

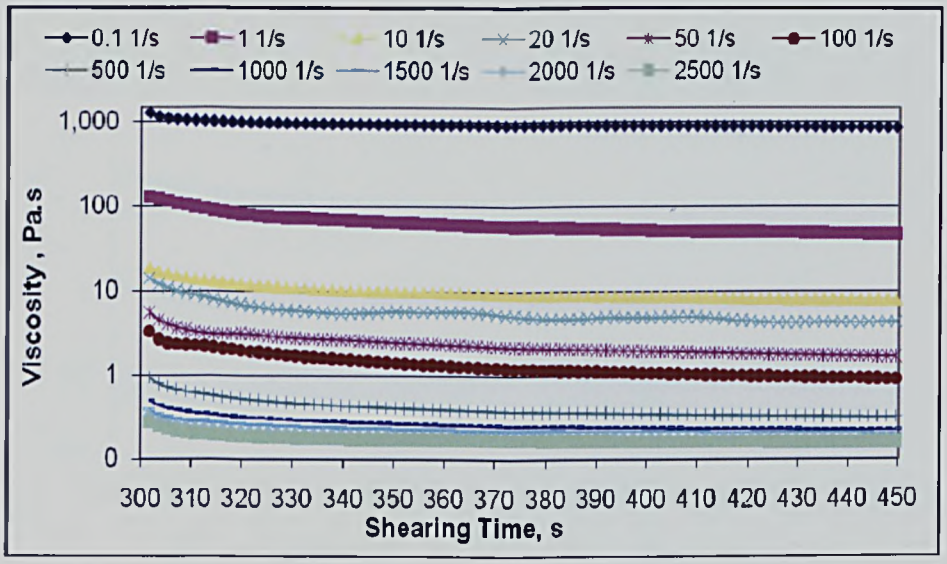

Figure 4-49 Time dependency data for the BP oil sample at 10 °C

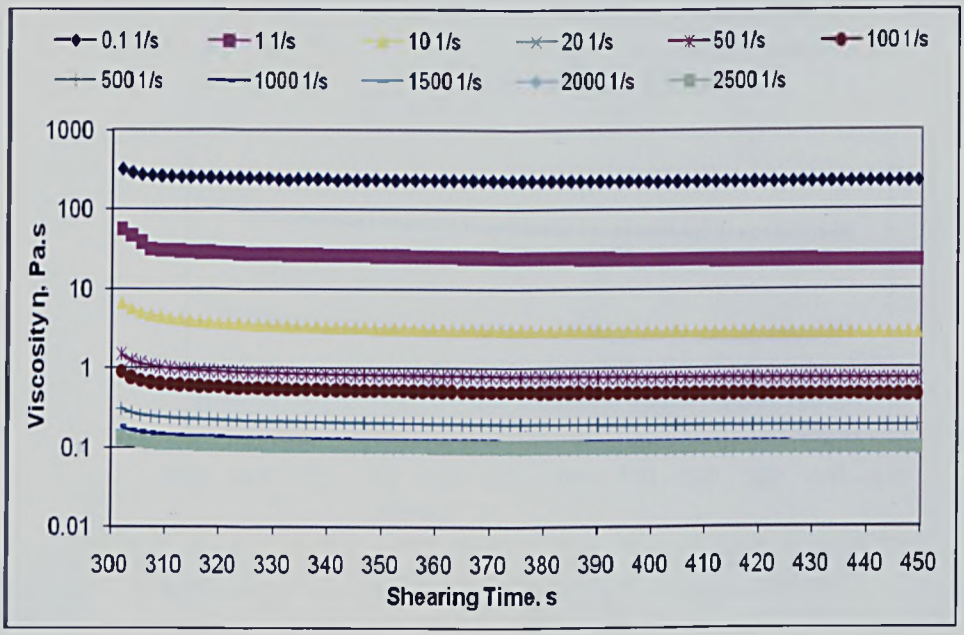

Figure 4-50 Time dependency data for the BP oil sample at 15 °C

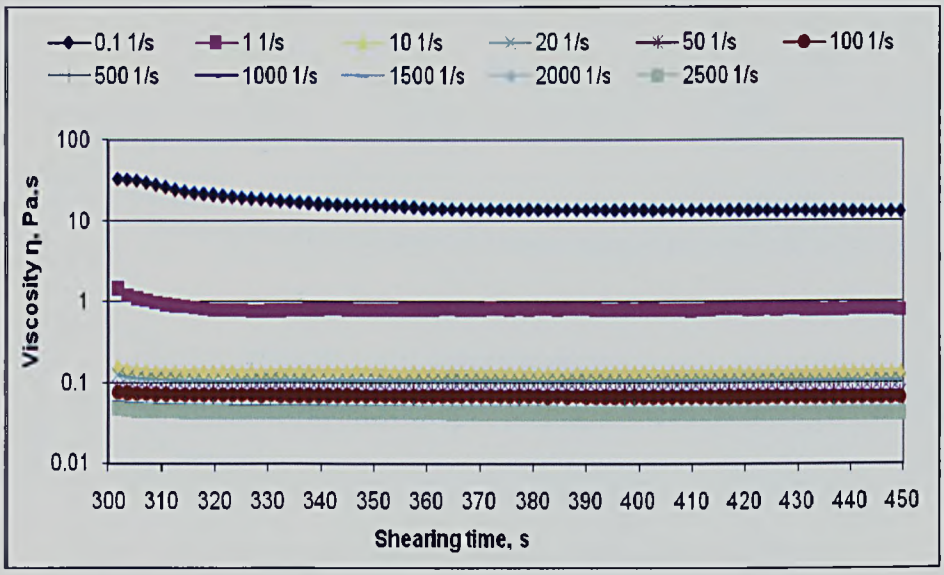

Figure 4-51 Time dependency data for the BP oil sample at 20 °C

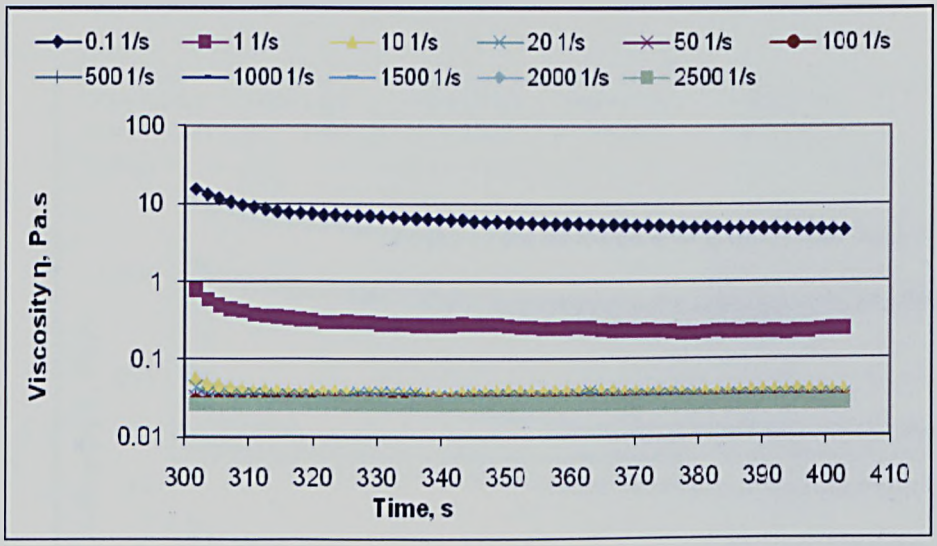

Figure 4-52 Time dependency data for the BP oil sample at 25 °C

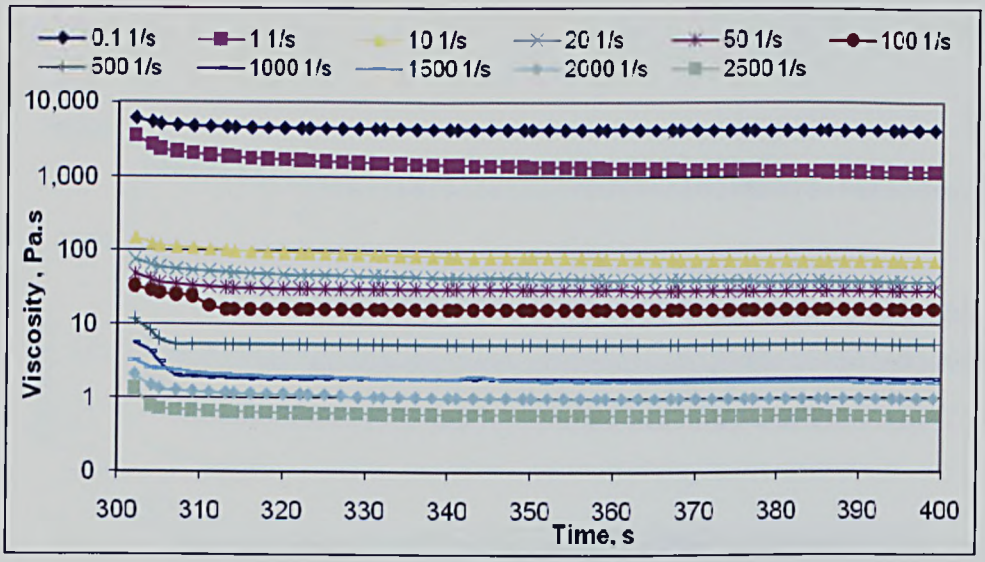

Figure 4-53 Time dependency data for the Mix oil sample at 5 °C

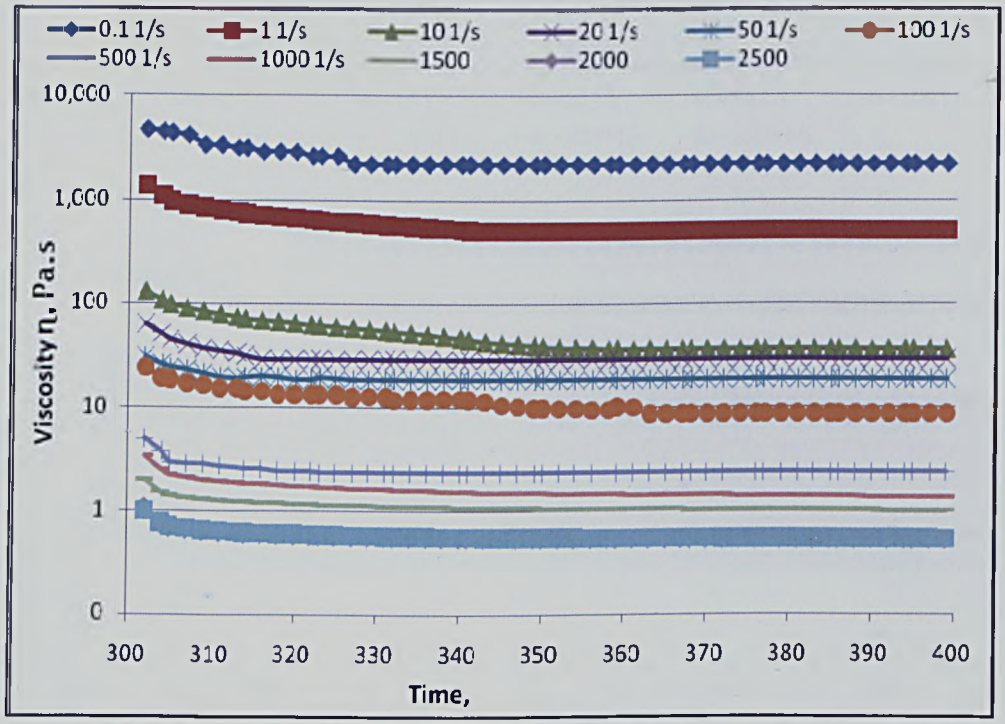

Figure 4-54 Time dependency data for the Mix oil sample at 10 °C

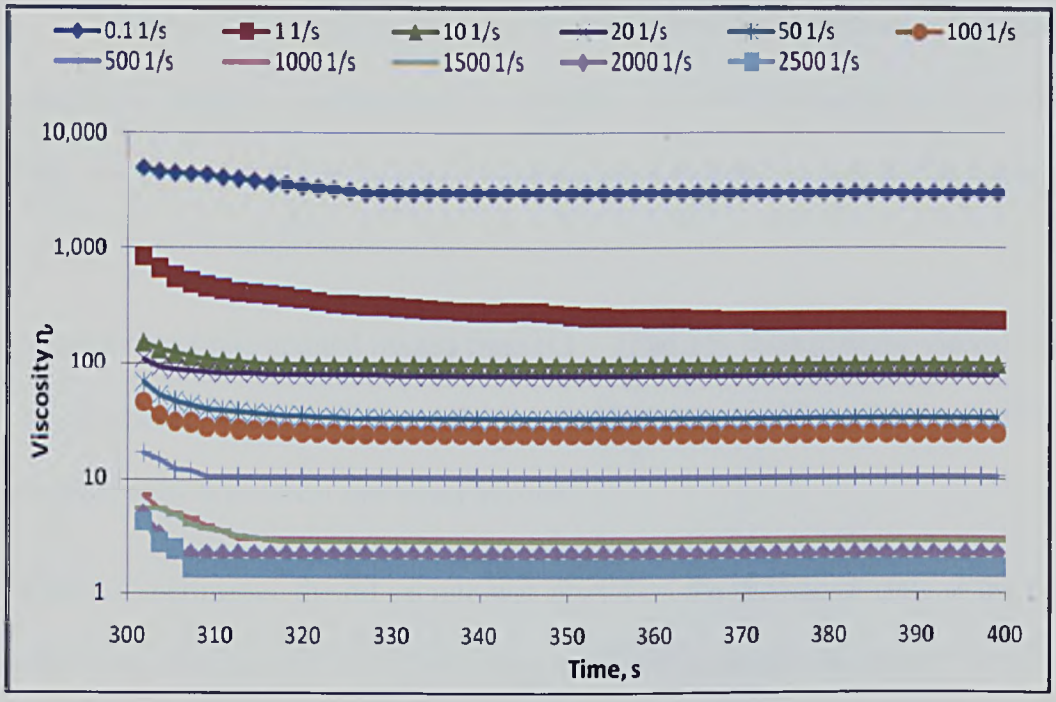

Figure 4-55 Time dependency data for the Mix oil sample at 5 °C

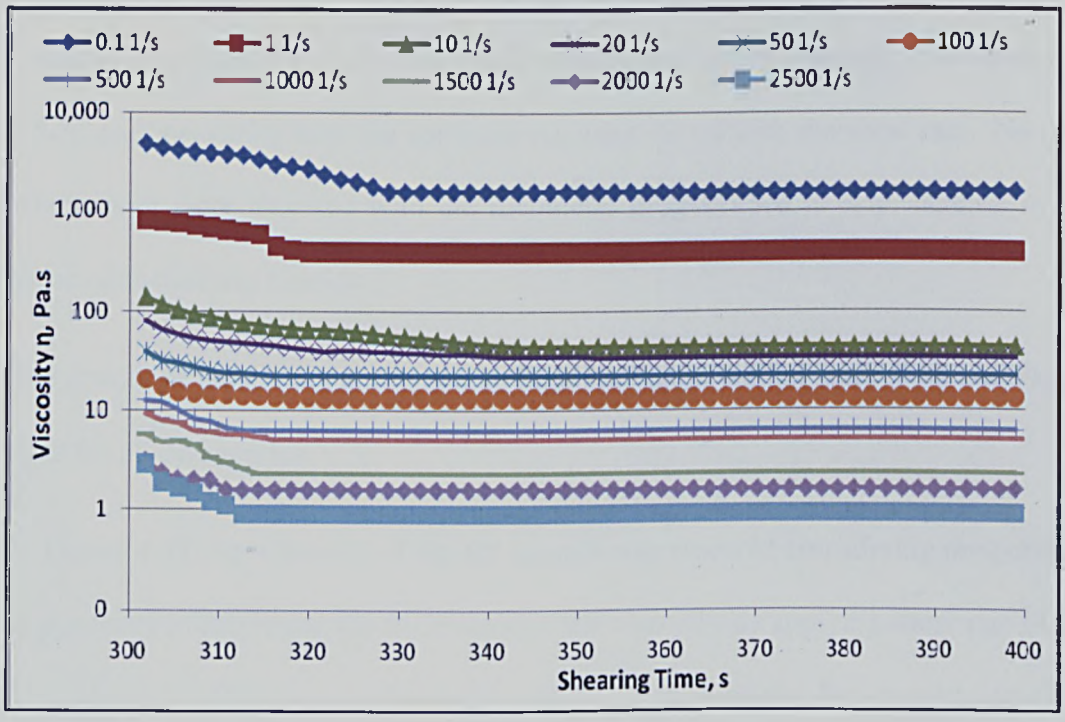

Figure 4-56 Time dependency data for the Mix oil sample at 10 °C

The rest of the graphs of Mix sample and Remal sample at different are presented in Appendix A4

4.5.5 Temperature Dependency Data

The data presented below gives apparent viscosities at various temperatures; however, in order to complement them further, data were collected for each of the three oils (BP, *Mix* and Remal) at temperatures we referred to here as the upper and lower pour point temperatures.

The sheer load rate applied ranged from 0.1 – 1500 1/s; thereafter the viscosity was measured every 0.25 seconds and the shear rate was increased by 1.5 1/s every 0.25 seconds, or by 6 1/s shear rate every second.

In these experiments, the oil sample was placed on the rheometer plate at the usual initial temperature well above the pour point; 65^0C for BP oil and 75^0C for the Remal and *Mix* oils, then cooled at a cooling rate of 0.5 °C/min down to 5 °C, a temperature much lower than any of the three oil's pour points. Assessment of temperature effects was then observed by evaluating the oil viscosity at increment of 2.5 °C and measuring how the apparent viscosity varied with the shear rate. No time effects here were assessed with the rheometer programmed to step increase in the shear rate relatively quickly.

The results of these tests are shown in Figures, Figure 4-57, Figure 4-58 and Figure 4-59 for all oil samples.

In Figure 4.57, the viscosity of the BP sample was assessed considering temperature dependency to determine the fluctuation of the viscosity by applying shear rate of 0.1 1/s and up to 1500 1/s at a temperature of 5 °C. It showed that the viscosity declined drastically from 1000 Pa.s to 100 Pa.s within the first amount of 3 1/s.

Subsequently with the proportional increase in the shear rate; 90 1/s, the viscosity remained constant.

As the temperature is considered as the key variable in this experiment, the test were repeated under similar operating conditions but at temperature of 25 °C; although similar characteristics were observed, the viscosity degradation was not as drastic in comparison to the cooler temperature (5 °C). In effect, the evidence suggests that there is shear thinning in all the samples studied.

Additionally, the same experiments of temperature dependency tests were repeated for the oil sample *Remal, at* a temperature of 5 °C- 50 °C; considering that the pour point of *Remal* is 42 °C. In the graph in Figure 4.58, the viscosity of the oil was observed when we applied shear rate of 0.1 1/s to 1500 1/s; at 5 °C the continued drop in viscosity was only apparent up to 205 Pa.s and beyond this figure it remained constant.

Similarly, the same tests were repeated at a temperature of 50 °C regarding the viscosity of the oil sample *Remal.* It is clearly shown that the continuous drop in viscosity was observed within the first 5 1/s sheer rate amount beyond which it remained relatively constant. Remarkably, the characteristics observed for the oil sample referred to as *Mix* is given in Figure 4.59.

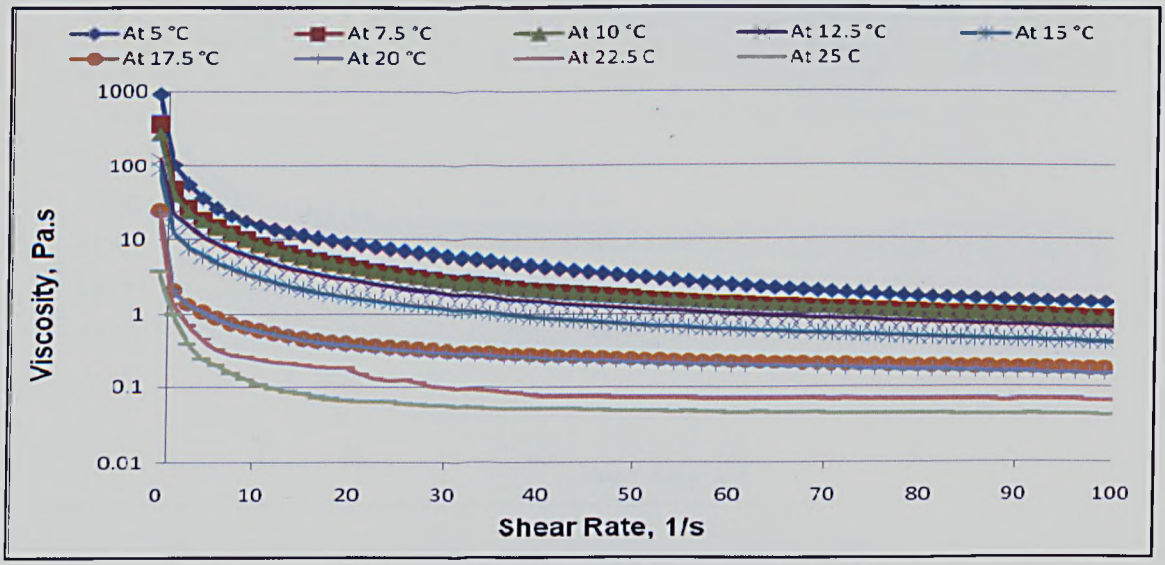

Figure 4-57 Temperature dependency data of viscosity for BP sample

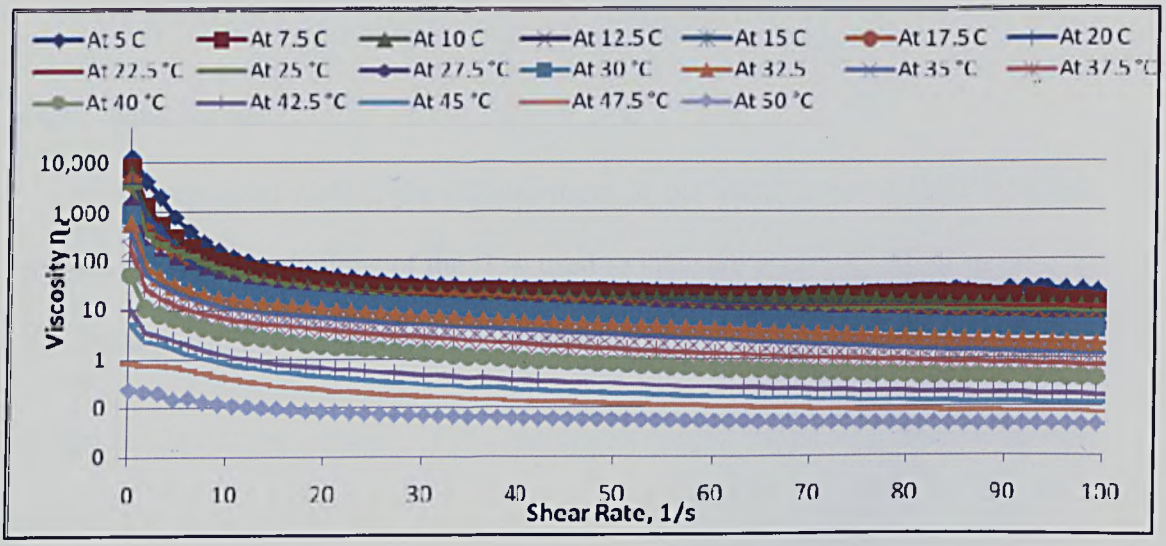

Figure 4-58 Temperature dependency data of viscosity for Remal sample

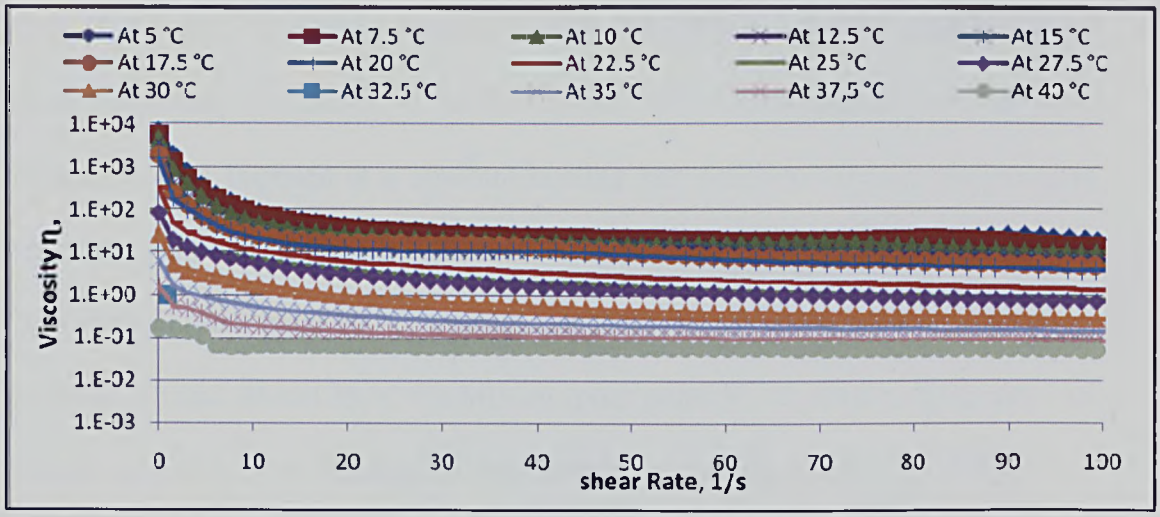

Figure 4-59 Temperature dependency data of viscosity for Mix sample

4.6 RHEOLOGY IN ROTATIONAL FLOWS BY APPLYING A RANGE OF STRESS

4.6.1 Introduction

As explained earlier, the measurement of the yield stress is a difficult task because of (i) the limitations of the flow used to measure it such as the possibility of slip, non uniform flow, varying shear stresses or rates.

(ii) the resolution and accuracy of the instrument variables such as torque, shear rate, cooling rate and temperature.

With the advent of new technology, modern instruments are allowing researchers to obtain more accurate data and this is one of the achievements claimed in this research. Here the Anton Paar Physica MCR series (2004) was used in the constant stress mode to provide a reliable and direct measurement of yield stress of three oil samples investigated. As with the other methods described in this thesis, these oils are first brought from a state of no prior flow memory (sheared at low shear rate for

3 hours at elevated temperature of 65^0C for BP oil and 75^0C for the Remal and Mix oils). A sample is then taken from this stock and deposited on the rheometer plate set at these temperatures, 65^0C for BP oil and 75^0C for the Remal and Mix oils. Cooling is then imposed at a constant cooling rate down to the test temperatures below the gel point of the oils. Two such temperatures are investigated, 13 and 18 °C for BP oil (pour point 20 °C, wax content 15%), 35 and 40 °C for Remal oil (pour point 42 °C) and 30 and 35 °C for Mix oil (pour point 37 °C). The cooling rates can also be varied to assess further this important effect and they were 0.16, 0.25, 0.5, 1 and 2 °C/min. It important to note that this schedule resembles what occurs in practice when a pipeline is shutdown and cools before it is restarted. Once the conditions of the tests were met, shearing was started by imposing a constant stress programmed to start from a low value of 10 Pa as indicated from the earlier capillary and oscillatory tests. To ascertain that the experiments were started from a very low point of stress, this applied stress of 10 Pa was applied for 3 hours (with no deformation observed by the rheometer) before it was very slowly increased until yielding was picked up by the rheometer. The stress was increased further gradually up to a higher value, 800 Pa in these experiment to obtain apparent viscosity data in full shear flow to compare with those obtained from the other techniques tested in this research.

4.6.2 Yield Stress Data

Figures 4-60 to Figure 4-89 show the yielding of the oils tested which enabled to locate the critical shear stress value at which it began and how yielding progress with time. This value is defined as the true yield stress, τ_y^* i.e. the end of elastic deformation and the beginning of the yielding. The data, as shown in these Figures, also identify the fracture yield stress, τ_y^f which is the stress at which big

changes in deformation are observed indicating the change from solid creeping behaviour to viscous flow.

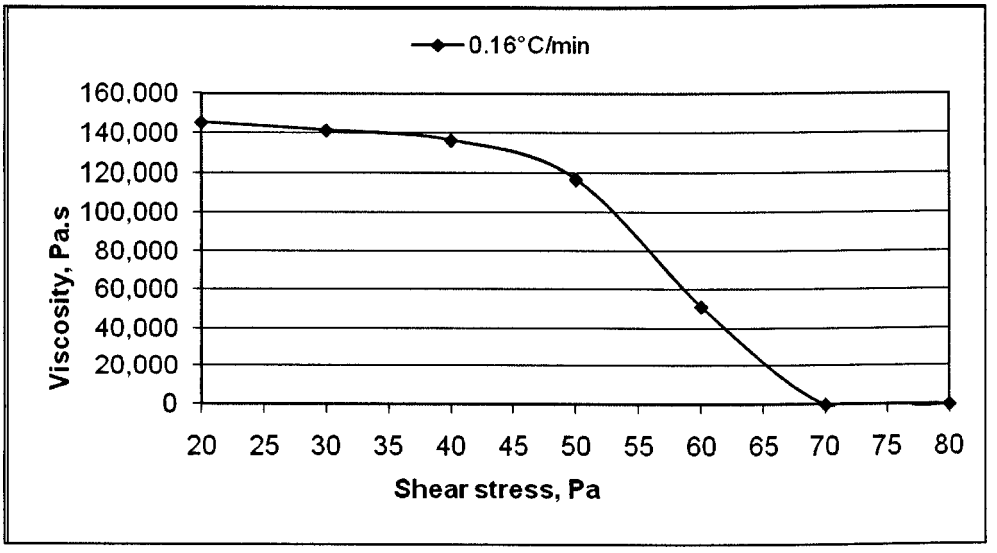

Figure 4-60 True yield stress and fracture yield stress of the BP oil sample at 13 °C, cooled at 0.16 °C/min

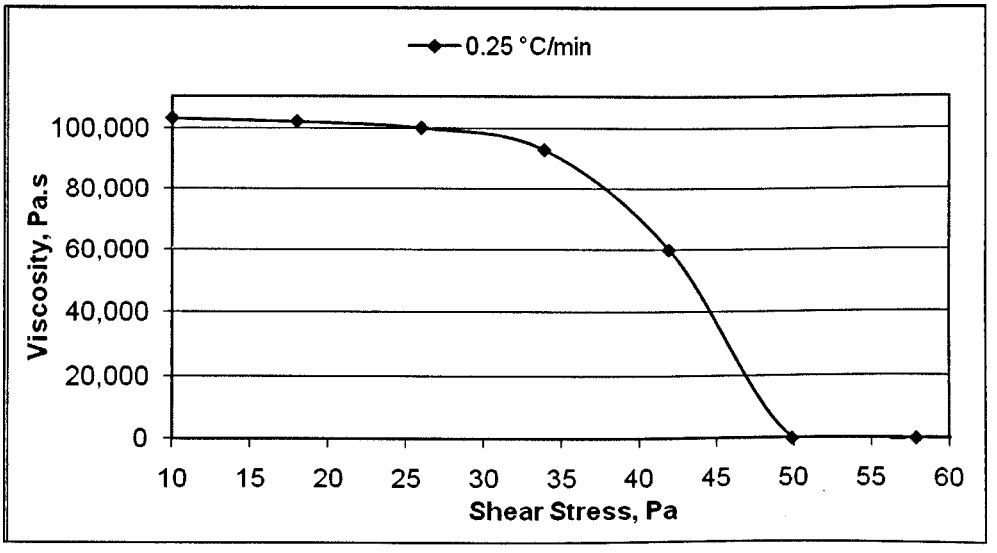

Figure 4-61 True yield stress and fracture yield stress of the BP oil sample at 13 °C, cooled at 0.25 °C/min

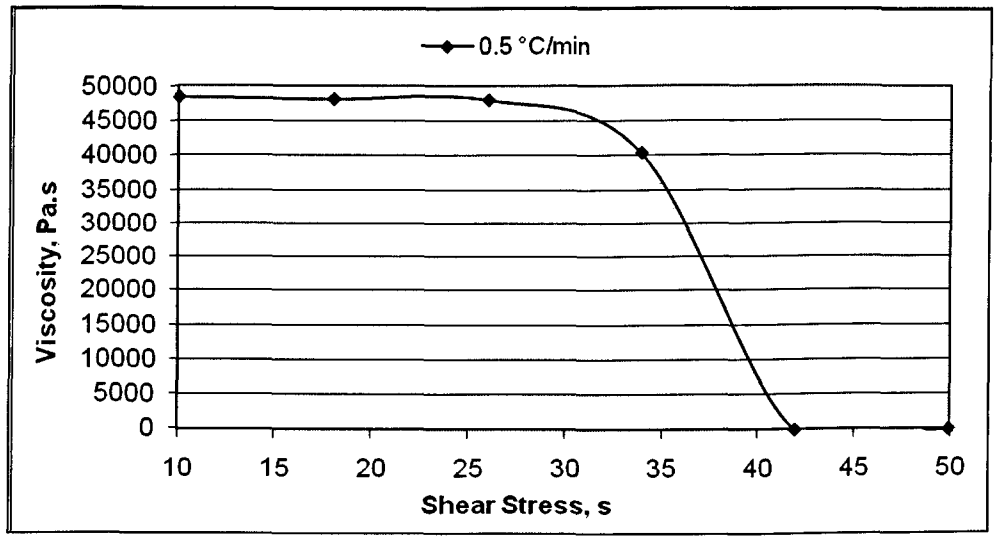

Figure 4-62 True yield stress and fracture yield stress of the BP oil sample at 13 °C, cooled at 0.5 °C/min

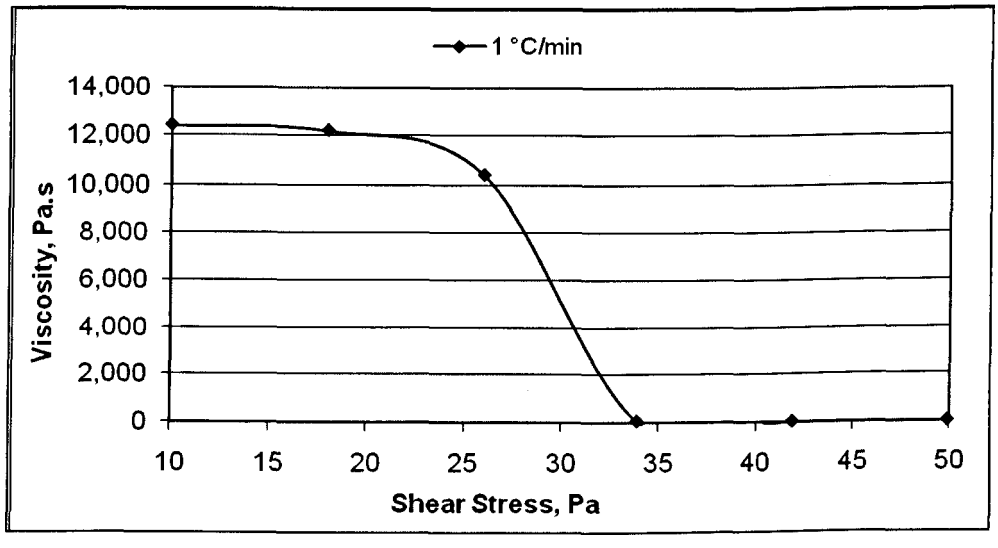

Figure 4-63 True yield stress and fracture yield stress of the BP oil sample at 13 °C, cooled at 1 °C/min

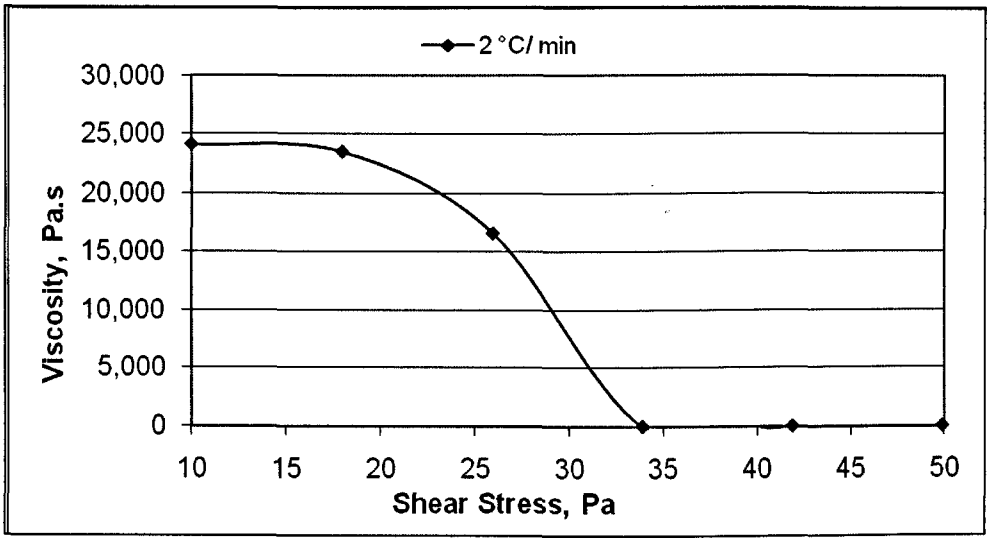

Figure 4-64 True yield stress and fracture yield stress of the BP oil sample at 13 °C, cooled at 2 °C/min

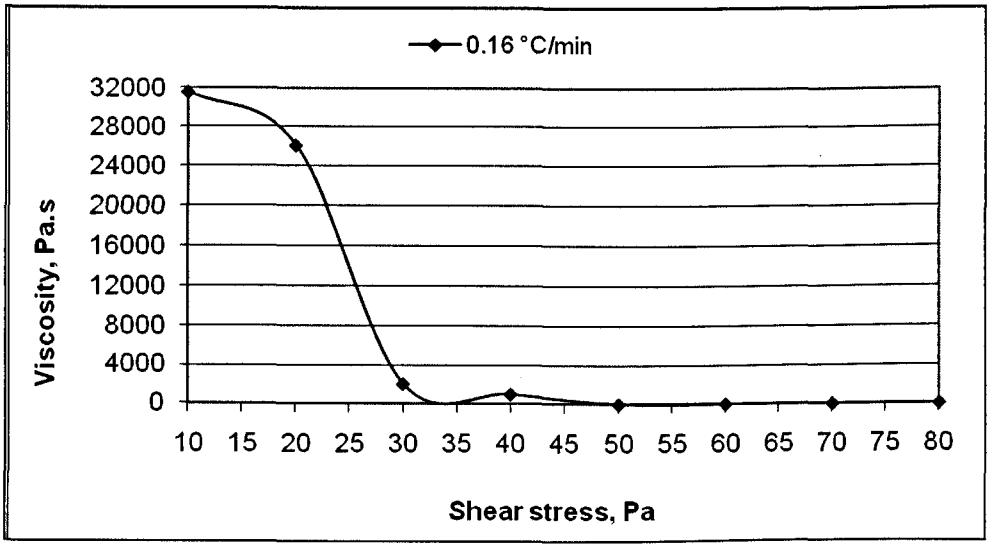

Figure 4-65 True yield stress and fracture yield stress of the BP oil sample at 18 °C, cooled at 0.16 °C/min

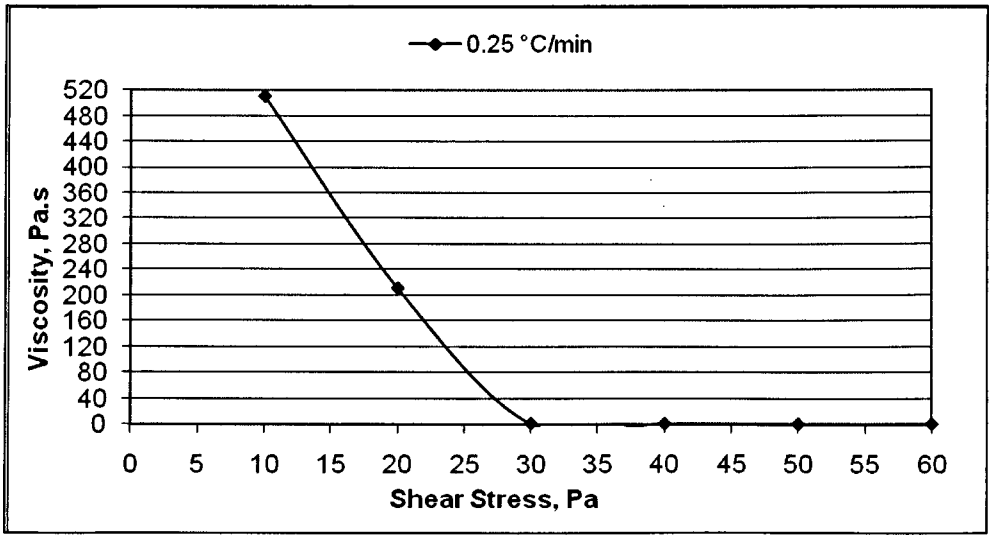

Figure 4-66 True yield stress and fracture yield stress of the BP oil sample at 18 °C, cooled at 0.25 °C/min

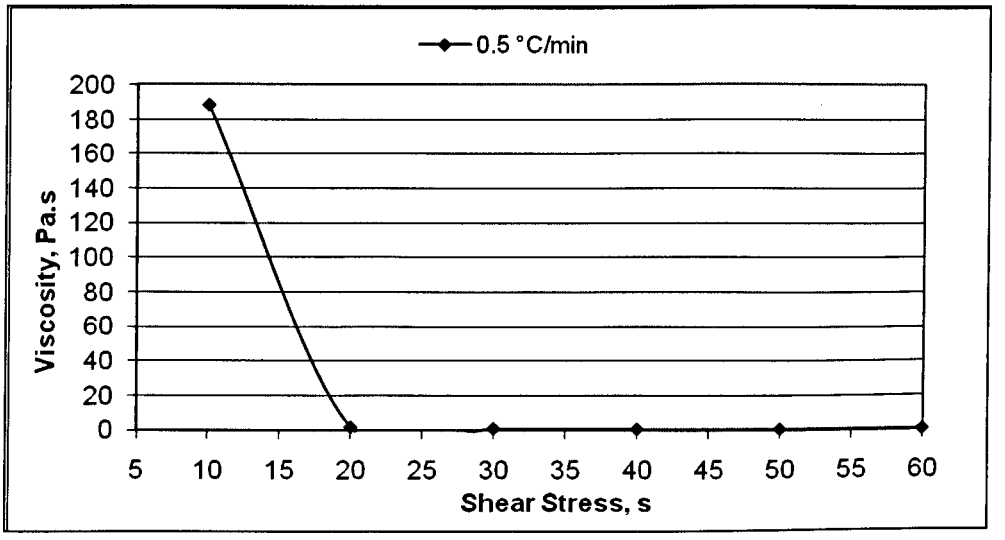

Figure 4-67 True yield stress and fracture yield stress of the BP oil sample at 18 °C, cooled at 0.5 °C/min

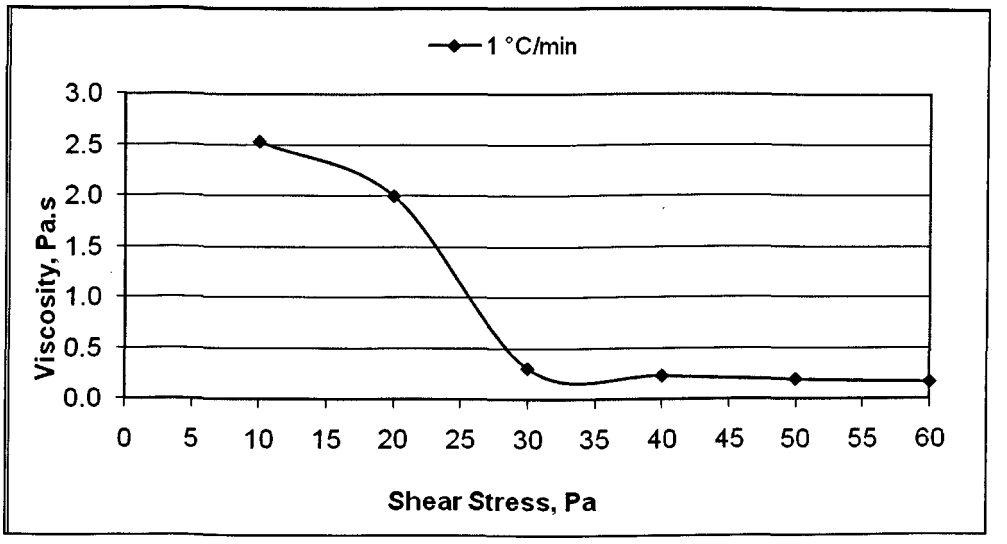

Figure 4-68 True yield stress the fracture yield stress of the BP oil sample at 18 °C, cooled at 1 °C/min

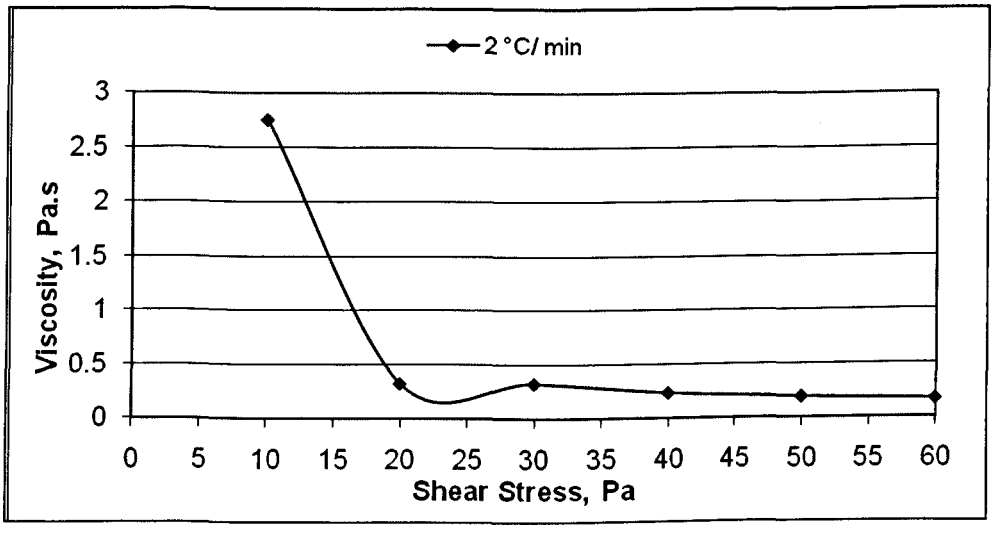

Figure 4-69 True yield stress and fracture yield stress of the BP oil sample at 18 °C, cooled at 2 °C/min

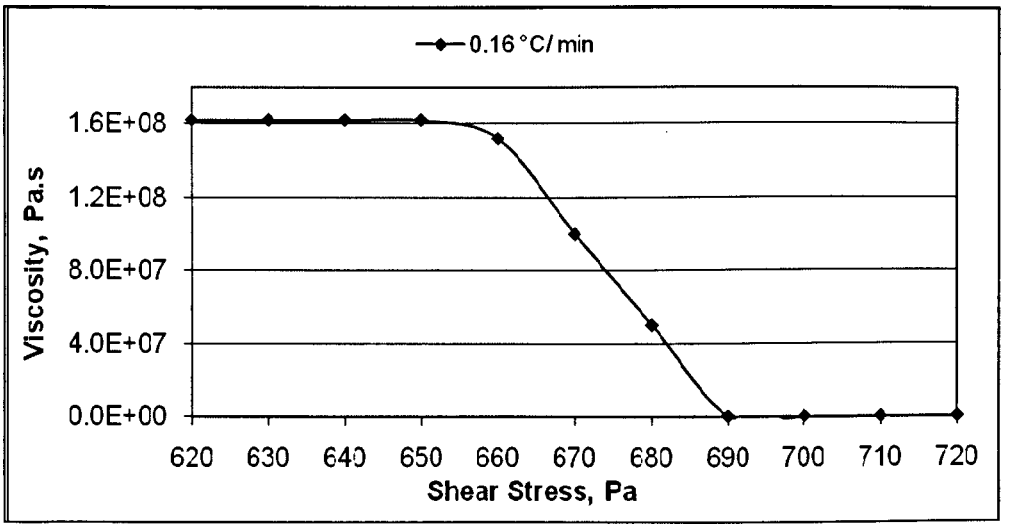

Figure 4-70 True yield stress and fracture yield stress of the Mix oil sample at 30 °C, cooled at 0.16 °C/min

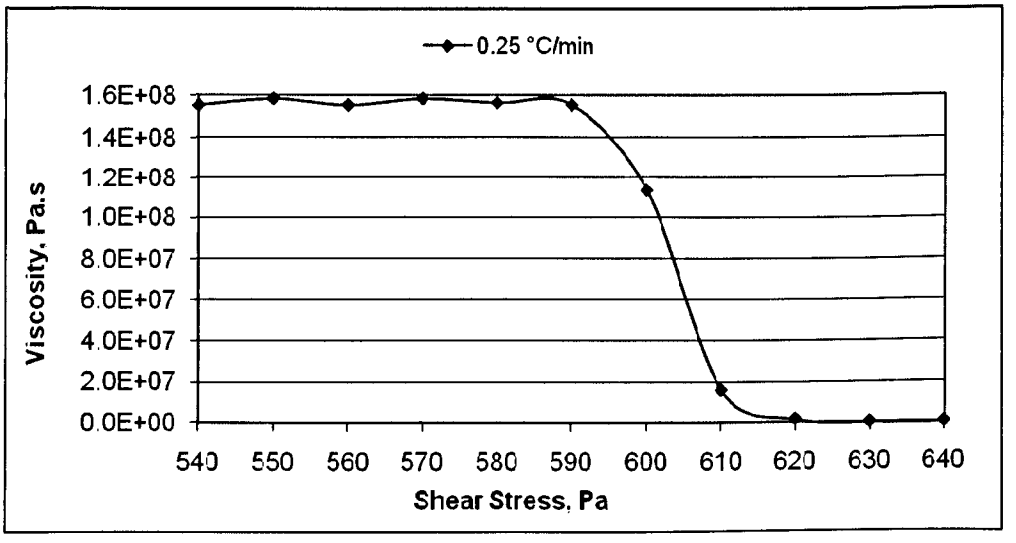

Figure 4-71 True yield stress and fracture yield stress of the Mix oil sample at 30 °C, cooled at 0.25 °C/min

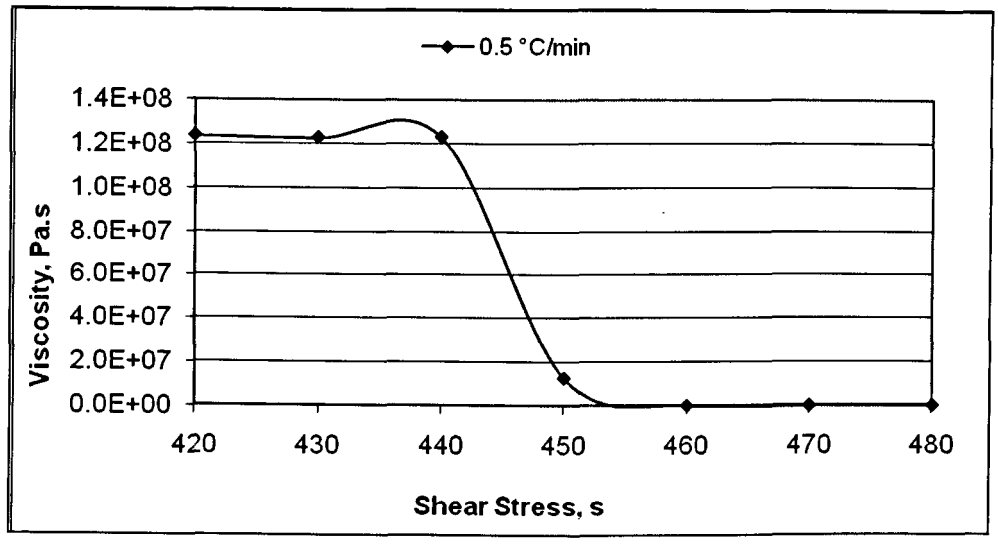

Figure 4-72 True yield stress and fracture yield stress of the Mix oil sample at 30 °C, cooled at 0.5 °C/min

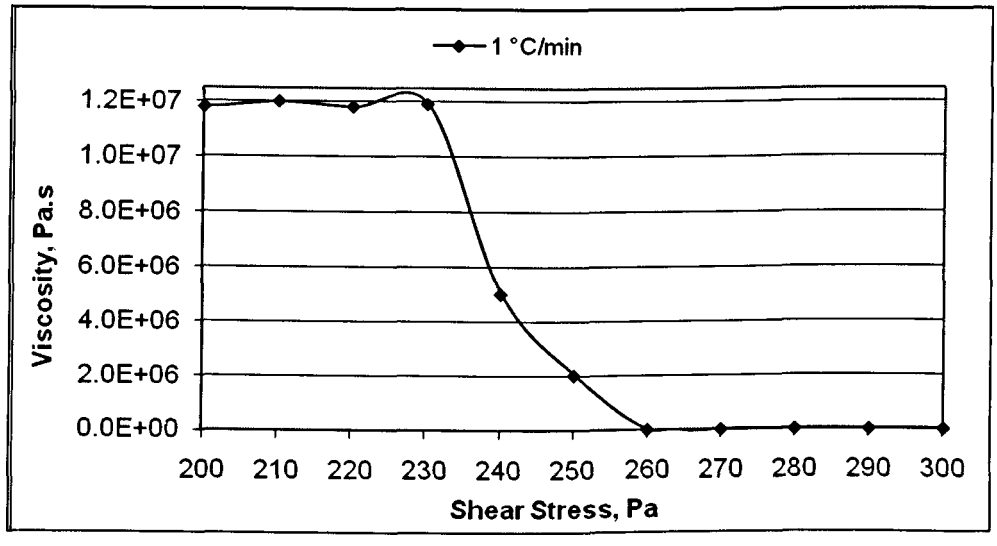

Figure 4-73 True yield stress and fracture yield stress of the Mix oil sample at 30 °C, cooled at 1 °C/min

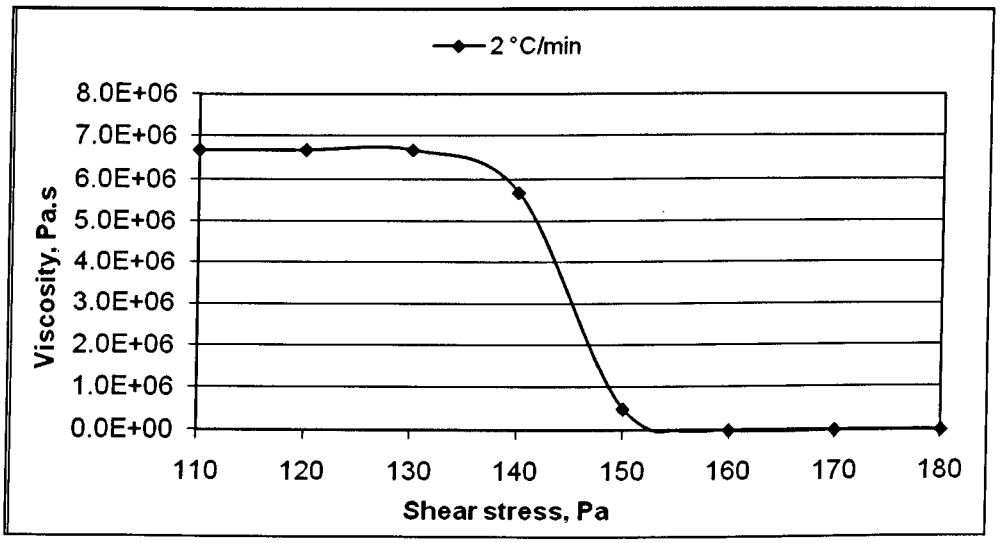

Figure 4-74 True yield stress and fracture yield stress of the Mix oil sample at 30 °C, cooled at 2 °C/min

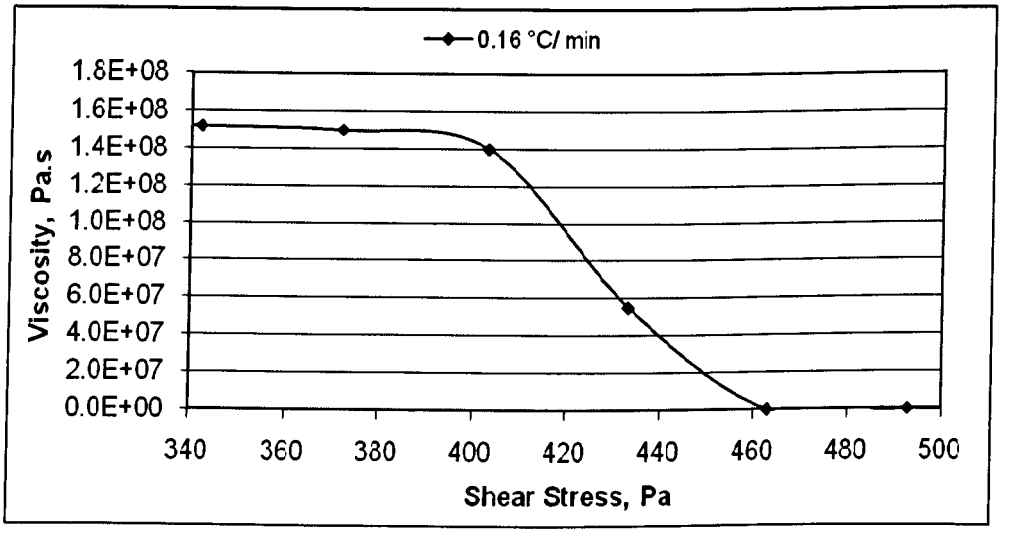

Figure 4-75 True yield stress and fracture yield stress of the Mix oil sample at 35 °C, cooled at 0.16 °C/min

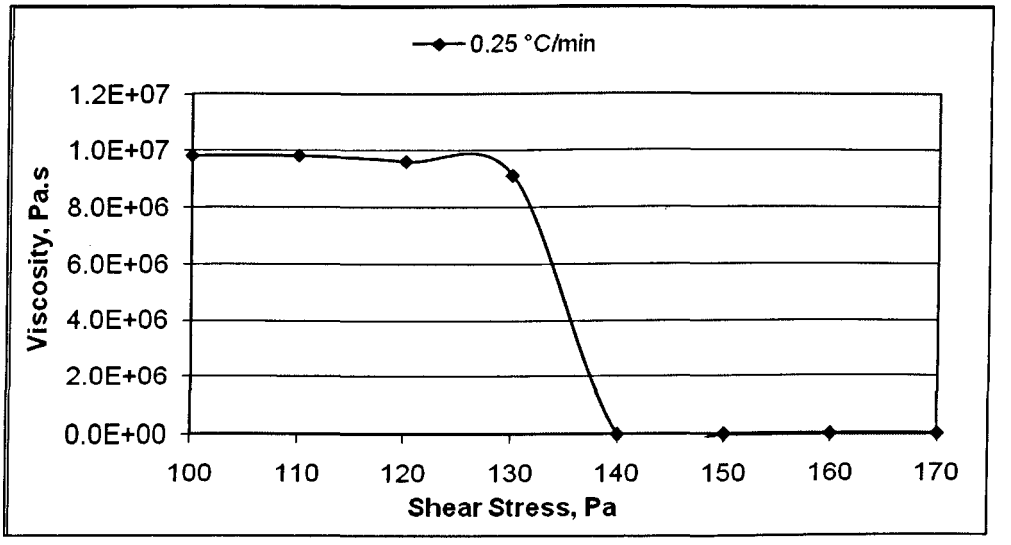

Figure 4-76 True yield stress and fracture yield stress of the Mix oil sample at 35 °C, cooled at 0.25 °C/min

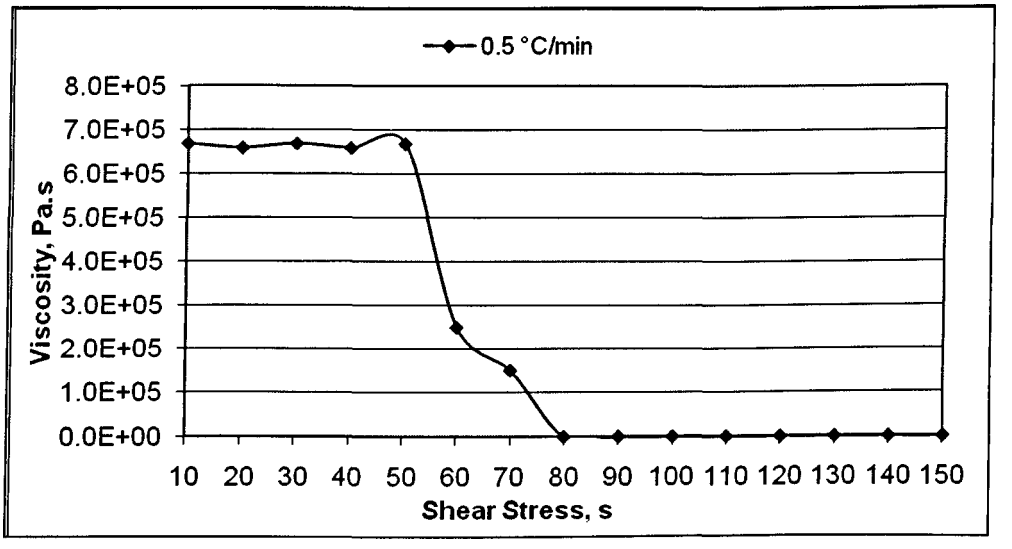

Figure 4-77 True yield stress and fracture yield stress of the Mix oil sample at 35 °C, cooled at 0.5 °C/min

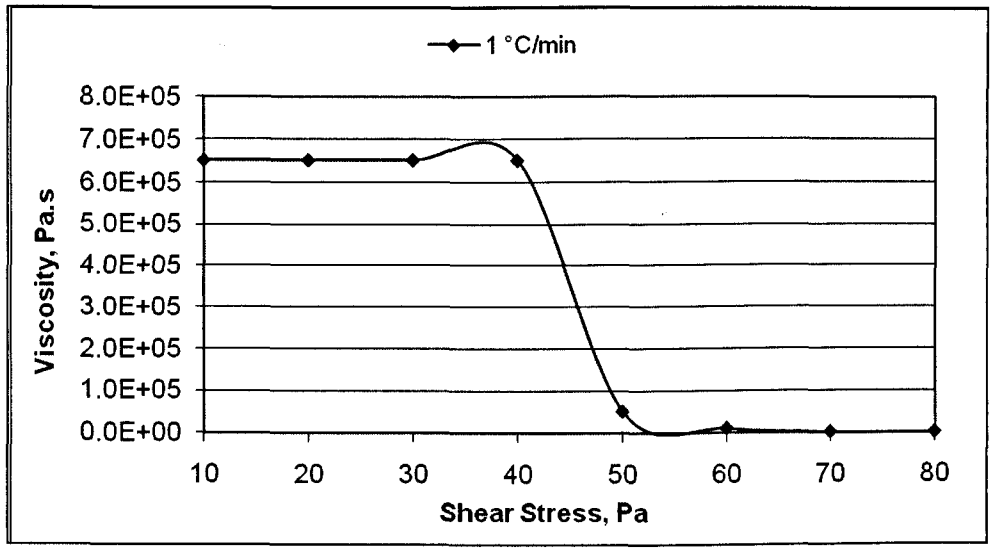

Figure 4-78 True yield stress and fracture yield stress of the Mix oil sample at 35 °C, cooled at 1 °C/min

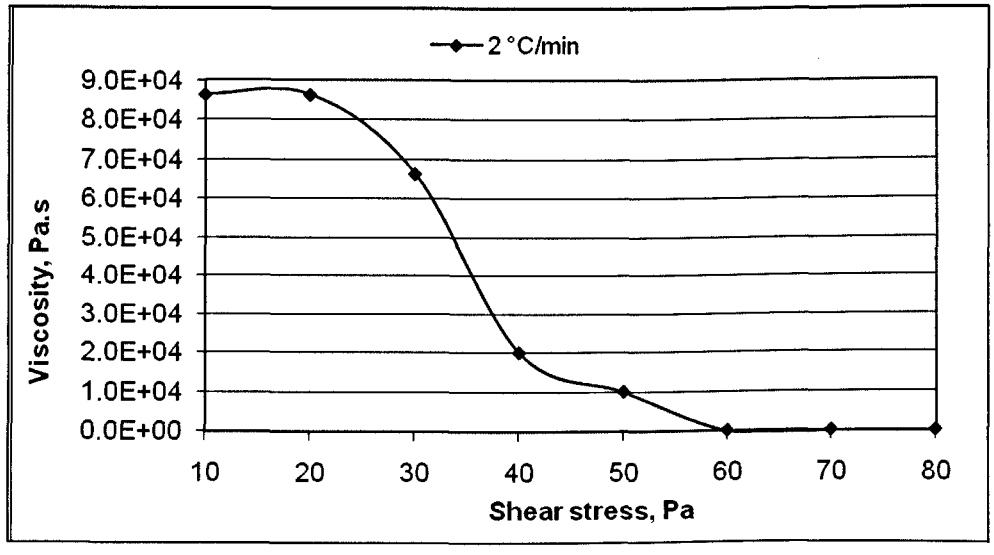

Figure 4-79 True yield stress and fracture yield stress of the Mix oil sample at 35 °C, cooled at 2 °C/min

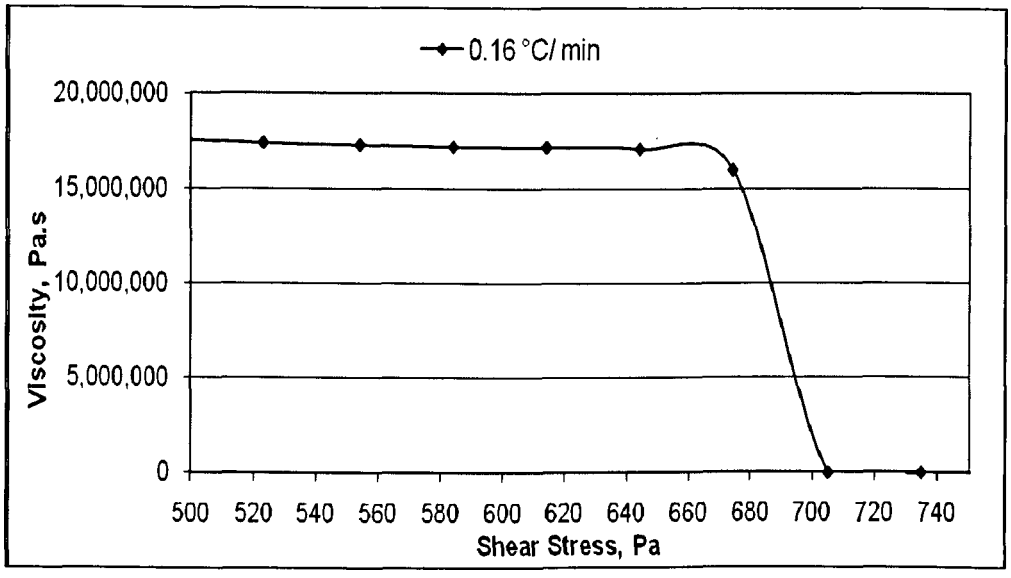

Figure 4-80 True yield stress and fracture yield stress of the Remal oil sample at 35 °C, cooled at 0.16 °C/min

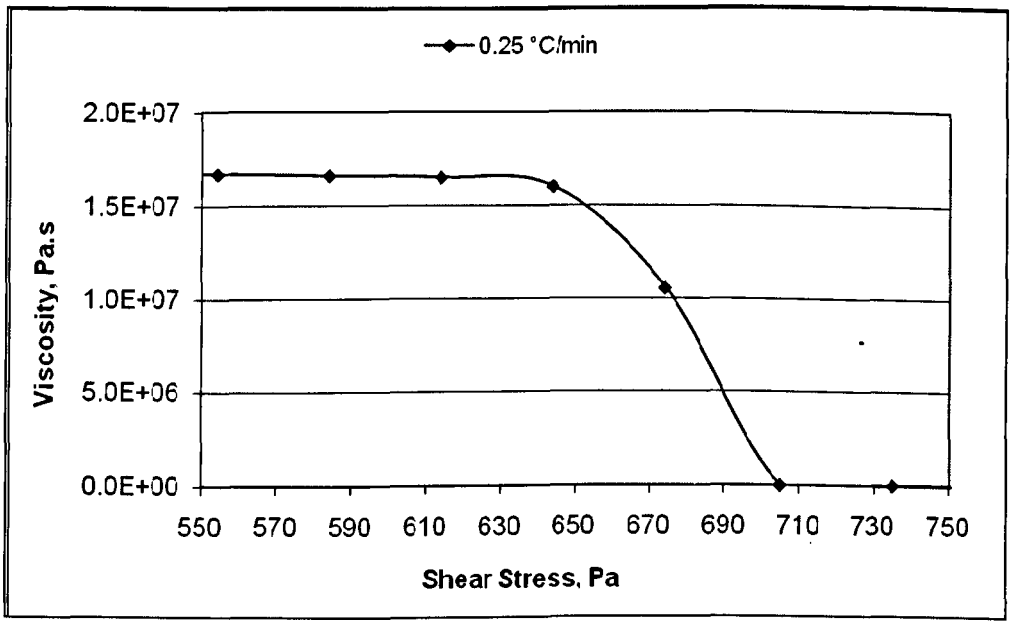

Figure 4-81 True yield stress and fracture yield stress of the Remal oil sample at 35 °C, cooled at 0.25 °C/min

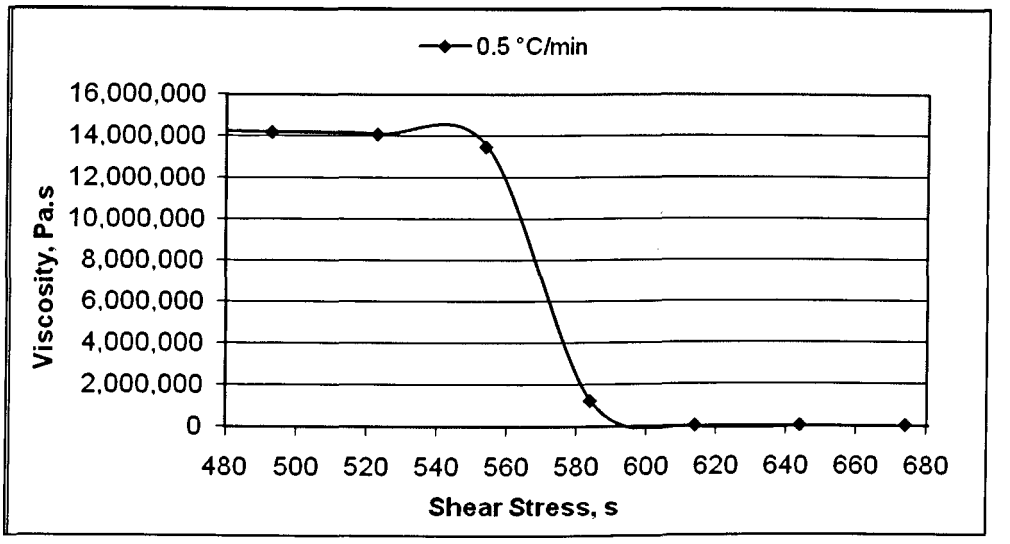

Figure 4-82 True yield stress and fracture yield stress of the Remal oil sample at 35 °C, cooled at 0.5 °C/min

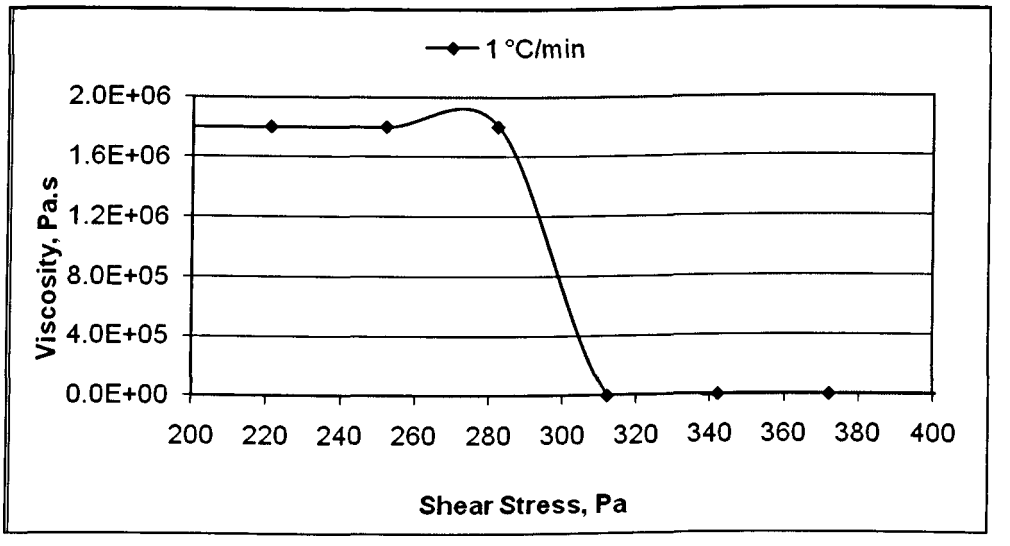

Figure 4-83 True yield stress and fracture yield stress of the Remal oil sample at 35 °C, cooled at 1 °C/min

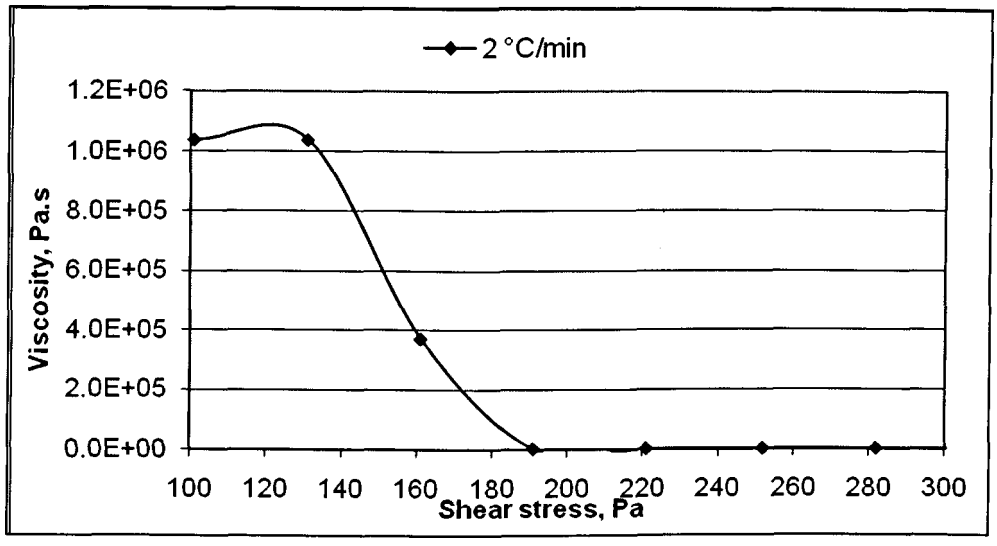

Figure 4-84 True yield stress and fracture yield stress of the Remal oil sample at 35 °C, cooled at 2 °C/min

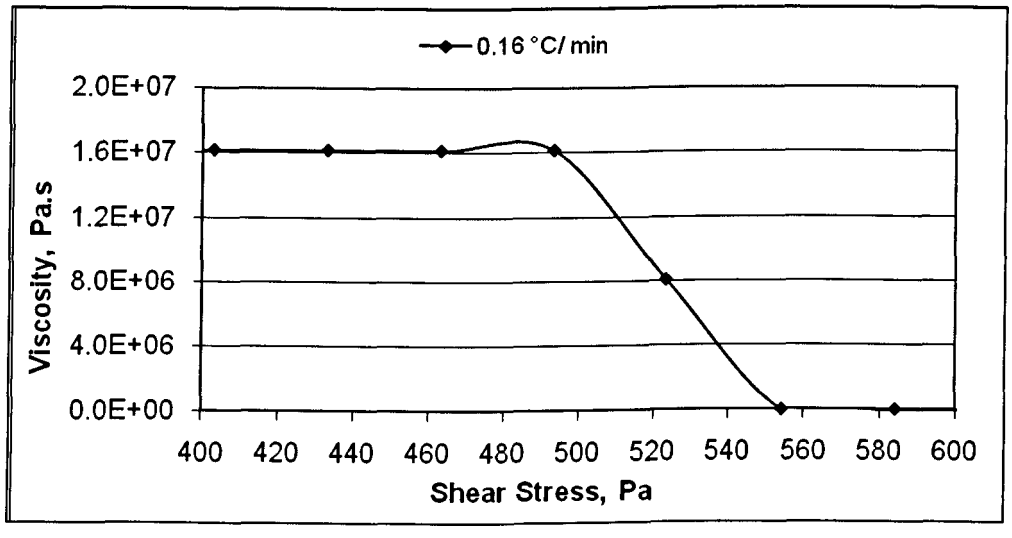

Figure 4-85 True yield stress and fracture yield stress of the Remal oil sample at 40 °C, cooled at 0.16 °C/min

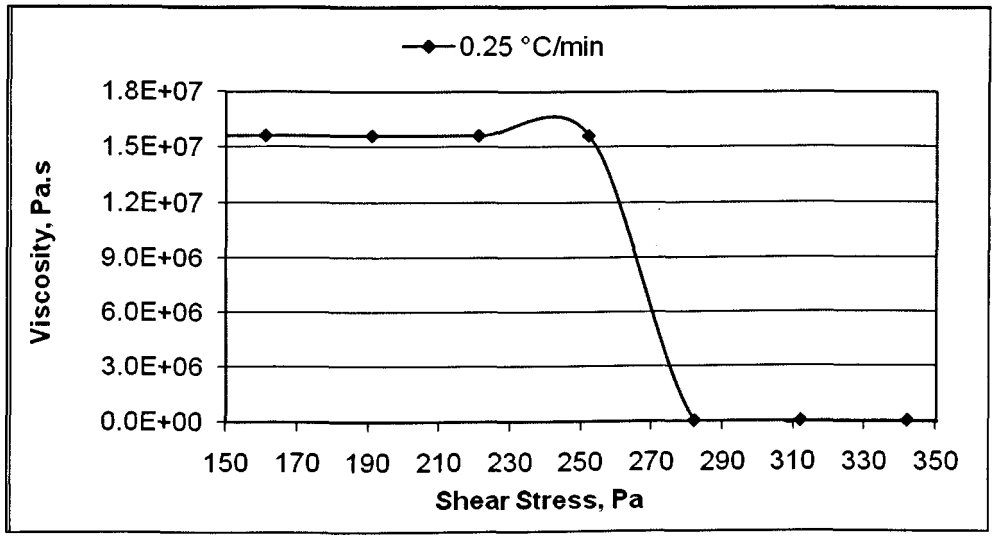

Figure 4-86 True yield stress and fracture yield stress of the Remal oil sample at 40 °C, cooled at 0.25 °C/min

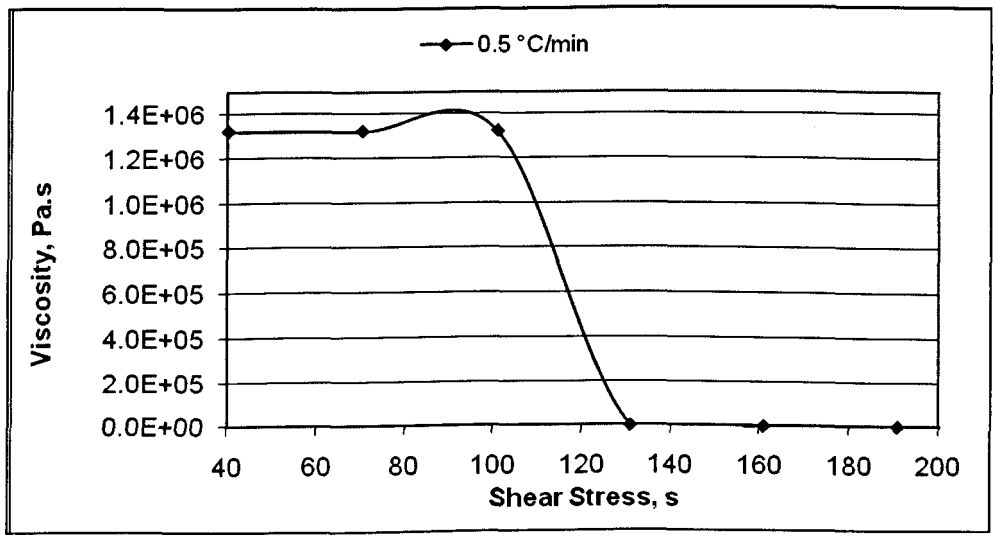

Figure 4-87 True yield stress and fracture yield stress of the Remal oil sample at 40 °C, cooled at 0.5 °C/min

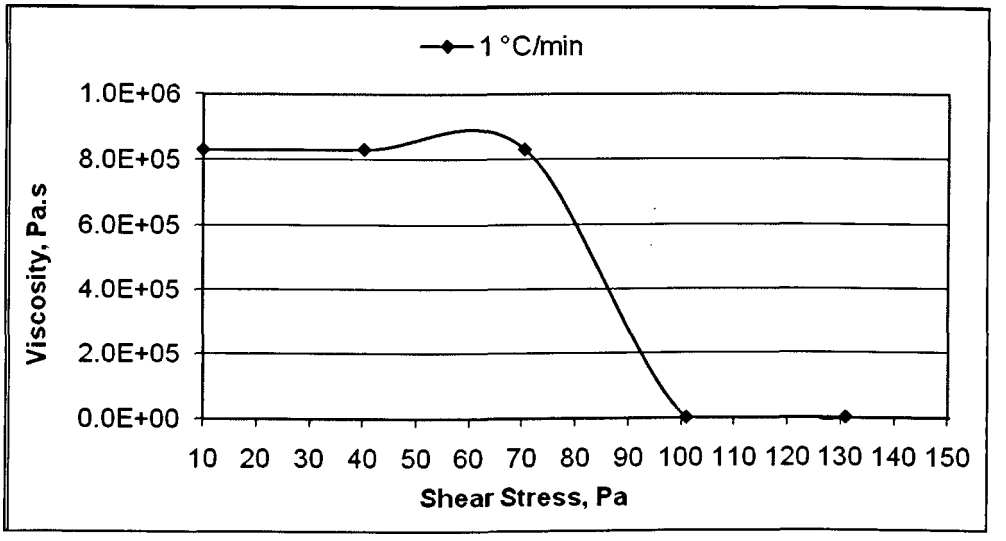

Figure 4-88 True yield stress and fracture yield stress of the Remal oil sample at 40 °C, cooled at 1 °C/min

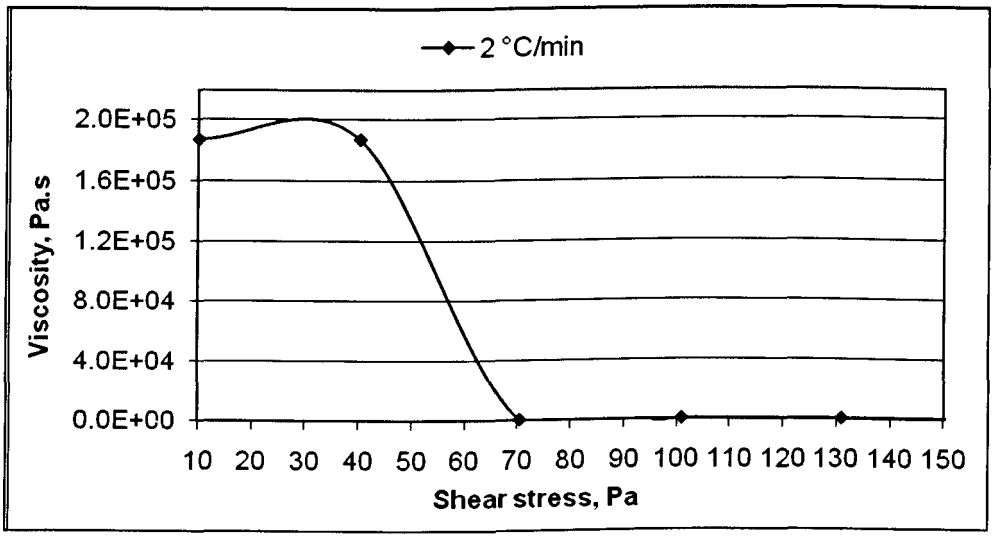

Figure 4-89 True yield stress and fracture yield stress of the Remal oil sample at 40 °C, cooled at 2 °C/min

Table 4-21 Results of two yielding stress points of all samples

Sample	Test Temp., °C	Cooling Rates, °C/min									
		0.16		0.25		0.5		1		2	
		τ_y^* Pa	$\tau_{y,f}^*$ Pa	τ_y^* Pa	$\tau_{y,f}^*$ Pa	τ_y^* Pa	$\tau_{y,f}^*$ Pa	τ_y^* Pa	$\tau_{y,f}^*$ Pa	τ_y^* Pa	$\tau_{y,f}^*$ Pa
BP	13	40	60	30	50	25	42	25	37	20	34
	18	15	30	13	20	10	18	10	16	10	14
Mix	30	660	690	590	615	440	450	230	255	130	150
	35	390	450	130	140	55	75	40	55	25	50
Remal	35	680	700	640	690	550	580	290	310	140	180
	40	510	540	260	275	110	120	75	95	45	60

The data in Table 4-21 of the yield stress experiments results give apparent viscosity data once full viscous flow has been established. The following observations can be made:

- *BP Oil & Effect of Cooling Rates and Cooling Temperatures*: Figure 4.60 to Figure 4.64 show the yield point of the BP sample cooled to 13 °C under five cooling rates of 0.16, 0.25, 0.5, 1 and 2°C/min. The lowest cooling rate produces the largest yield value of 60 Pa with values of 40, 30, 36 and 18 Pa at the cooling rates of 0.25, 0.5, 1 and 2°C/min

respectively. This variation trend with cooling rate, also observed with the Remal and Mix oils is consistent with crystallization kinetics: larger crystals and stronger structures progressively forms as the cooling rate is lowered. Table 4-21 shows similar data as just described but for sample cooled at 18 rather than 13 °C. The yield stress measured are lower in comparison 30, 20, 18, 10 and 10 for cooling rates of 0.16, 0.25, 0.5, 1 and 2°C/min respectively. This confirms the first observation that lower cooling rates result with stronger structures. It also shows that yield stresses diminish in value as we approach the gel and pour point which is to be expected. It is interesting that at the lowest cooling rate of 0.16°C/min, the yield stress is very large, three times as much as those at the lowest rates which show here comparatively less variation. The important observation here is the data themselves and how they can help to construct a full representation (non-linear) of how the yield stress varies with cooling rates and temperatures. This is essential for mathematical modelling which can only describes trend and not real values.

- *Remal Oil in comparison with BP and Mix Oil:* Table 4-21 lists the values of the yield stresses τ_y^* and τ_y^f of the three oils for the various cooling rates and temperatures tested. The cooling temperatures are different but reflect the variation near the respective pour or gel point of each of the three oils. Remal display relatively higher yield stresses (700 to 45 Pa) than BP (60 to 10 Pa) and the Mix oil (670 to 28 Pa) falls in between which is consistent with the wax content of the oils, 15, 30 and 35 % for BP, Mix and Remal respectively.

The yielding stress points of the BP oil sample of the experiment are presented in Table 4.21 which summarised the content of Figures 4.60 and Figure 4.89. The tests started at temperature 13 °C for the BP sample at cooling rate of 0.16 °C/minute at initial yield stress τ_y^* 40 Pa and final yield stress $\tau_{y,f}^*$, 60 Pa. At cooling rate 0.25 °C/minute, the yield stress τ_y^* and $\tau_{y,f}^*$, are recorded as 30 Pa and 50 Pa respectively; similarly at 2 °C/minute, the yield stress τ_y^* and $\tau_{y,f}^*$, are 20 Pa and 34 Pa accordingly.

By contrast, obtained for the oil sample referred to as Remal; the values for τ_y^* and $\tau_{y,f}^*$ as shown in Table 4-24 , is recorded as 680 Pa and 700 Pa at temperature at cooling rate of 0.16 °C/minute. Similarly, the values of τ_y^* and $\tau_{y,f}^*$ *at* cooling rate of 2 °C/minute equalled 140 Pa and 180 Pa. Furthermore, at the temperature of 40 °C and with cooling rate of 0.16 °C/minute, the values recorded for τ_y^* and $\tau_{y,f}^*$, is 510 Pa and 540 Pa, and also at a cooling rate 2 °C/minute, the value of τ_y^* and $\tau_{y,f}^*$, was 140 Pa and 180 Pa.

4.7 Comparison of the CSS and pipeline test results for all samples after applying 3 hours shutdown time

In Table 4.22, the results obtained of the comparison that was made of pipeline test and control sheer tests after application shut down time of 3 hours at the following temperatures 13 °C and 18 °C at various cooling rate which is given s 0.16, 0.25, 0.5, 1 and 2 °C/minutes in respect of the BP oil sample.

The CSS test is considered to be more effective in determining the yield point test by providing us with two yield points; namely $\tau_y a$ and $\tau_y b$, where as the pipeline test only provides the flow yield point.

The values recorded in the CSS test at cooling rate of 0.16 °C/minute for $\tau_y a$ and $\tau_y b$ are given as 15.95 Pa and 14.75 Pa at the temperature of 13 °C; whereas for the pipeline test the value of $\tau_y b$ (flow yield point) for the same temperature 13 °C is given as 60 Pa.

Similarly, the values recorded in the same experiment (CSS tests) at temperature of 18 °C at cooling rate 0.16 °C/minutes for $\tau_y a$ and $\tau_y b$ are given as 10.42 Pa and 9.89 Pa, by contrast in the pipeline test at 18 °C, the $\tau_y b$ (flow yield point) is given as 30 Pa.

Furthermore, the values recoded in the same test (CSS test) at temperature of 13C at cooling rate 2 °C/minutes for $\tau_y a$ and $\tau_y b$ are given as 7.36 Pa and 6.81Pa, by contrast in the pipeline test the $\tau_y b$ (flow yield point) 34 Pa.

It is shown that in both tests (CSS and Pipeline) with the increase in the cooling rate, the yield point decreases. Similar tests (CSS and Pipeline) were carried out for the two other oil samples (*Remal and Mix*) and the results are shown in Table 4-23 and Table 4-24 respectively.

Table 4-22 Comparison between the CSS and pipeline tests results for the BP oil sample after applying 3 hours shutdown (S/D) time

Cooling Rate °C/min	**Pipe Line Test (after 3 hr S/D)**		**CSS Test (after 3 hr S/D)**			
	At 13 , °C	**At 18, °C**	**At 13 , °C**		**At 18 , °C**	
	$\tau_y b$,**Pa**	$\tau_y b$, **Pa**	$\tau_y a$, **Pa**	$\tau_y b$, **Pa**	$\tau_y a$, **Pa**	$\tau_y b$, **Pa**
0.16	60	30	15.95	14.75	10.42	9.89
0.25	50	20	11.03	9.98	10.42	9.89
0.5	42	18	9.81	9.07	7.97	7.56
1	37	10	7.36	6.81	6.74	6.39
2	34	10	7.36	6.81	6.13	5.82

Table 4-23 Comparison between the CSS and pipeline results for the Mix oil sample after applying 3 hours shutdown (S/D) time

Cooling Rate °C/min	**CSS Test (after 3 hr S/D)**		**Pipe Line Test (after 3 hr S/D)**			
	At 30 °C	**At 35 °C**	**At 30 °C**		**At 35 °C**	
	$\tau_y b$ **Pa**	$\tau_y b$ **Pa**	$\tau_y a$ **Pa**	$\tau_y b$ **Pa**	$\tau_y a$ **Pa**	$\tau_y b$ **Pa**
0.16	690	450	38	34.81	24.52	22.95
0.25	615	140	32.49	29.76	23.29	21.8
0.5	450	75	32.49	29.76	23.29	21.8
1	255	55	31.87	29.19	21.45	20
2	150	50	31.26	28.64	21.45	20

Table 4-24 Comparison between CSS test and pipeline results for the Remal oil sample after applying 3 hours shutdown (S/D) time

Cooling Rate °C/min	CSS Test (after 3 hr S/D)		Pipe Line Test (after 3 hr S/D)			
	At 35 °C	At 40 °C	At 35 °C		At 40 °C	
	$\tau_y b$ Pa	$\tau_y b$ Pa	$\tau_y a$ Pa	$\tau_y b$ Pa	$\tau_y a$ Pa	$\tau_y b$ Pa
0.16	700	540	94.4	85.47	78.46	72.48
0.25	690	275	85.81	77.7	73.55	67.95
0.5	580	120	78.56	71.04	72.33	66.82
1	310	95	74.78	67.71	68.65	63.42
2	180	60	72.33	65.49	66.81	61.73

4.8 CONCLUSIONS

In summarising the outcome and content of the experiments of comparing CSS and Pipeline tests; at different testing temperature under varying cooling rates; it has clearly been demonstrated that the CSS tests has more efficacy in determining both the initial yield point $\tau_y a$ and flow yield point $\tau_y b$; where as the pipeline test only gives the flow yield point $\tau_y b$.

Furthermore, it is evident in this experiment that with the increase in the cooling rate, the yield decreases.

4.9 Mathematical Modeling

In this section, we demonstrate how the rheological data obtained can be processed into constitutive equations which can then be used to carry out mathematical modelling of the flow of these waxy crude oils, in pipe or other flows.

Let us consider as an example, Remal oil. The pipe line tests showed that the yield stress measured were as follows (see Table 4.24):

4.25 Yield stress data for Remal sample cooled from 70 °C to 35 °C and 40 °C

The Yield Stress Pa	Test Temperature °C	
	40	35
τ_y	72.33*	78.56*

*Measured at cooling rate of 0.5 °C/minute , and holding up time of 3 hours

Clearly from the data, there is a whole range of yield stress values depending on cooling rate and hold up time. The rheological data obtained with the rheometer can now be used to extract the corresponding data value as a set of $(\tau, \dot{\gamma})$ for Remal cooled from 70 °C to 40 °C at cooling rate of 0.5 °C/minute with a hold up of 3 hours. The same can be done for the same sample cooled from 70 °C to 35 °C at cooling rate of 0.5 °C/minute with hold up of 3 hours. These data is plotted in the next two graphs, ,Figure 4.90 and Figure 4.91 for Remal samples cooled from 70 °C to 40 °C and 35 °C respectively.

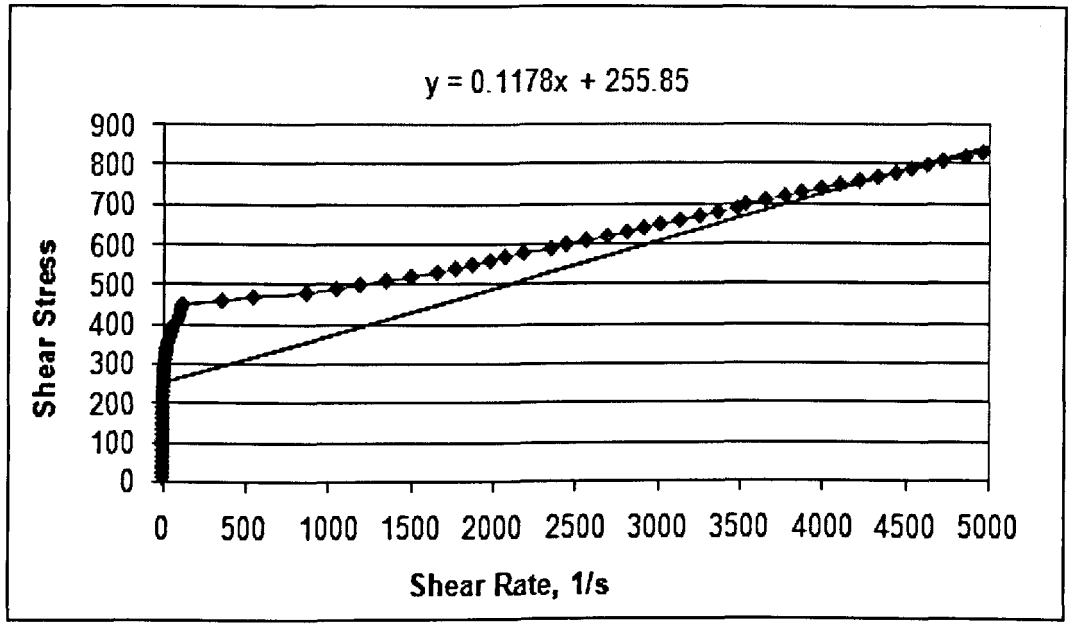

Figure 4.90 Shear stress vs shear rate for Remal sample cooled from 75 °C to 40 °C

From this data, we can obtain the corresponding constitutive equation which was found to be:

$$\tau = \tau_y + k\dot{\gamma}^n$$

at 40 °C for cooling rate of 0.5 °C/ minutes, and where n = 1, the equation is:

$$\tau = 255.85 + 0.1178\ \dot{\gamma}$$

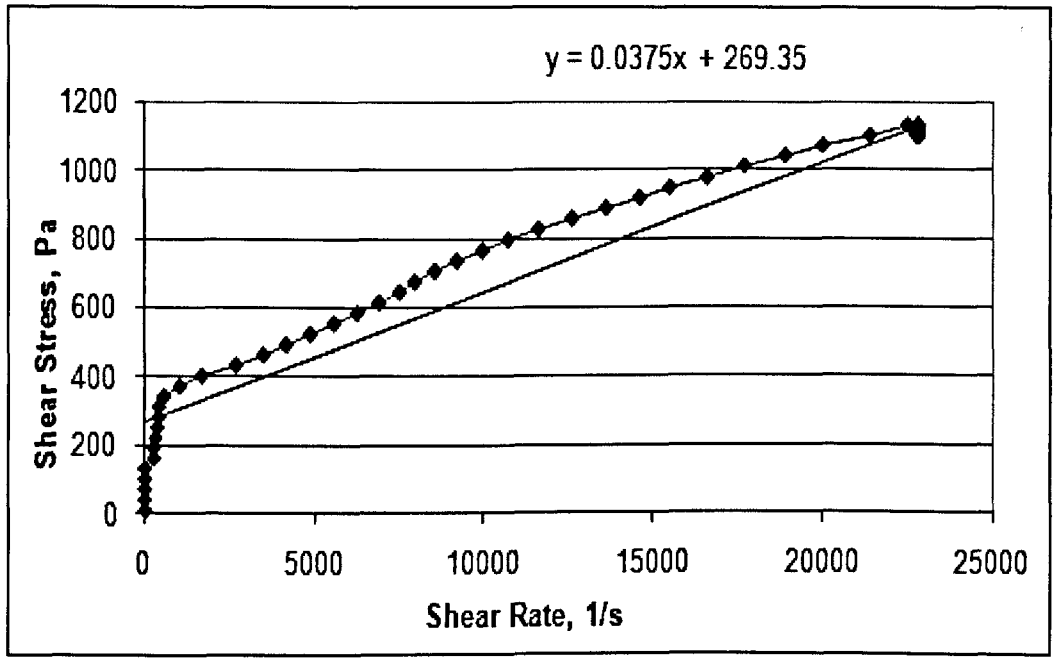

Figure 4.91Shear stress vs shear rate for Remal sample cooled from 75 °C to 35 °C

$$\tau = \tau_y + k\dot{\gamma}^n$$

at 35 °C for cooling rate of 0.5 °C/ minutes, and where n = 1, the equation is:

$$\tau = 269.35 + 0.375\ \dot{\gamma}$$

We clearly observe from this, the fit between the data obtained from the pipeline rig and from the rheological instrument. Clearly we can do the same with all the data and use them for pipeline calculation. Also thesis can be done for BP and Mix waxy samples.

From this data, we can fit constitutive equations of the type that that considers yield stress, for example:

$$\tau = \tau_y + \mu a \dot{\gamma}^n \qquad \text{(Bingham Plastic)} \qquad (1)$$

$$\tau = \tau_y + k \dot{\gamma}^n \qquad \text{(General Bingham Plastic)} \qquad (2)$$

We observe from Figure 4.90, that rather of these equation fit completely the data and we can either use a best fit of all the data or truncate the data into a set at low shear rate (0-10 $\sec^{-1}$) and a pet at larger shear rate (10 $\sec^{-1}$). At the larger shear rate, Equation 2 is appropriate where in the larger shear rate, a Bingham Plastic constitutive equation holds.

Using this approach, we can summarise all the data we obtained with these equations that can be used for mathematical modelling of flow of these waxy crude fluids in pipelines.

CHAPTER 5: CONCLUSIONS AND RECOMMENDATIONS

5.1 CONCLUSION

5.1.1 Introduction

This chapter presents the conclusions derived from the work that has been presented in the previous chapters and also recommendations for future research. A novel method has been developed to measure the thickness of wax deposited on the pipe wall and this has enabled the calculation of more accurate values of wall shear stress. Also thixotropy measurements have been used for the first time in this field to understand the flow behaviour of the waxy oils in the transportation pipeline.

5.1.2 Start-up Pressures & Yield Flow Stress Data at Effective Flow Diameter

- It is crucial to take into account the wax layer deposited on the wall during the precipitation of the wax near and below the gel point especially when the shutdown time increases. Measurements of the wax layer thickness give a true flow diameter and hence a more accurate calculation of the yield stress during start up.
- In all cases, the layer thickness has significant effect on the yield stress and start-up pressures and corresponding yield flow stresses have been found to underpin the crystallisation process of the wax.
- Slow cooling rate produce stronger structures requiring higher stresses to fracture and induce flow.

- Longer shutdown times make these structures even stronger and therefore require even larger stresses for flow to commence.
- This data can be used to guide operation at the large scales and as such they provide a good data basis to assess scaling up. The data on the evolution of the wax thickness as a function of time, cooling rate and temperature also provide a good basis to develop theoretical model that can predict start-up.

5.1.3 The Gelation Point

- For all the oil samples studied the storage modulus G' and the loss modulus increase with the decreasing of the gel strength.
- In addition, the gel point temperature and strength of the wax crystal decreases with increasing cooling rate and vice versa. The obtained data showed a linear variation of the gel point temperature with cooling rate. Most of the results of the samples show that the gelation point temperature under slow cooling rates i.e. 0.125 °C/min, 0.25 °C/min and 0.5 °C/min is higher than the pour point. However, at high cooling rates; 1, 2 °C/minutes to 5 °C/minutes, the gelation point temperature is close to the pour point temperature.

5.1.4 The Thixotropy Behaviour

- The shear step function method was used in this research to study the thixotropic behaviour of the oil samples. The results of this test showed a very clear thixotropic behaviour for all the oils tested. The viscosity of the oil in first two intervals decreases with the increasing of the temperature. However, in the third interval the viscosity reverts back to a value which is the reference viscosity of the first interval.

- Also, most of the test results show that the oils exhibit a shear thinning behaviour in the beginning of the first interval.

5.1.5 Time Dependency

- The results from the study show that the apparent viscosity of each sample decreases sharply in the first minute of shearing and then remains constant until the end of the test. This means that the structure of wax is affected by the shearing time for the beginning period of time.

5.1.6 Temperature Dependency

- The waxy oils viscosity decreases with increasing the temperature. This means that increasing the temperature makes the wax structure weak.
- At constant temperature, the results show that the apparent viscosity of each sample decreases at the beginning of the shearing time and then the viscosity remains constant until the end of the test.
- The data show that waxy oils display shear thinning behaviour. As the temperature passes the limit of the gelation point, the wax particles give the sample its non-Newtonian behaviour.
- As the temperature increases above the gel point temperature, the wax melts and the shear dependence of the sample is reduced. At higher temperature the oils exhibit Newtonian behaviour.

5.1.7 Shear Thinning Behaviour

- The data showed that waxy oils show shear thinning behaviour. The effect of the temperature is as expected; near the gelation point temperature the wax particles give the oil its non-Newtonian behaviour. As the temperature

exceeds the pour point temperature, the wax crystals melt thereby exhibiting a Newtonian behaviour.

5.1.8 Rheometer Yield Stress

- The rheometer is capable of making sensitive measurements and able to track yielding which is something that the pipeline rig cannot do. A rheometer is thus able to provide a better method of detecting yielding which is helpful to develop models of yielding.
- The yield stress of the gelled waxy oils is a complex function of gel composition and shear and thermal histories under which the gel has been formed.
- The wax crystals are observed to form a wax network that inhibits the flow. When the gel is formed under quiescent cooling, the yield stress decreases with an increasing cooling rate.
- The wax crystal network formed at a lower cooling rate is stronger due to the formation of larger wax crystal plates. However, when the gel is formed under high cooling rate, the gel is weaker.
- The yield stress of the gel increases with an increasing cooling rate. The yield stress in controlled not only by the strength of the wax structure in the oil but also by the time scale of yielding. This is advantageous in the design and operation of the pipelines where a lower level of applied stress may produce movement if applied over an appropriate period of time. However, as the yield stress increases with shutdown time, a larger pressure will be needed to restart the pipeline operation.
- Oil temperature and the ambient temperature are very important critical factors that control the yield stress point of the gelled waxy oil. The closer to

the lower the pour point *(PP)*, the larger the yield stress will be. Furthermore, the composition of the gel also affects the yield stress. As expected, it was found that the higher the wax content, the larger the yield stress required to induce flow.

5.1.9 Yield Stress Obtained by the Oscillatory Test

- There are two yield points; firstly, the oil starts to move at a lower magnitude of stress which is called the true yield; the second yield point is when the oil is completely in motion at normal flow rate and the corresponding stress is higher.

5.2 RECOMMENDATIONS FOR FURTHER STUDIES

On the basis of this study and understanding of the rheology and pumping of waxy crude oils, the following recommendations are made with respect to future work:

- According to the measurements of the thixotropic behaviour of the waxy crude oils, this versatile test could accommodate most behaviours inherent in waxy crude oils.
- The step function test could be used in future under different cooling rates and different shear rates to measure most of the parameters e.g. apparent viscosity, shear thinning behaviour, apparent yield stress etc.
- Measurement of the actual flow diameter by another means (e.g. ultrasound) could enable more accurate calculation of the pressure needed by pumps to break down the yield stress of the cooled waxy oil gels.
- The yield stress measurement with and without the waxy layer would help developing a model of the yield stress for waxy oils with different wax content.

- Measurement of pressure drop should also be carried out on actual pipelines which have been partially blocked. This would help with scale up issues.

References

Abdel-Waly, A. A. (1997). "NewCorrelation Estimates Viscosity of Paraffinic Stocks." Oil and Gas Journal **95**(24): 61-65.

Ahmad, T., Ed. (2000). Wax Deposetion. T. Ahmad. Jalo, Agip Oil Company.

Ahn, S., K. S. Wang, et al. (2005). "Paraffin Crystal and Deposition Control By

Amhammed, A. (2009). Rheology and re-start pressure of waxy oils, University of Bradford, Bradford. Thesis, PhD

Emulsification." Society of Petroleum Engineering SPE **93357**(2005): 9.

Alboudwarej, H., A. Shahraki, et al. (2007). "Rheology of Heavy-Oil Emulsions." Society of Petroleum Engineering SPE **97886**(2007).

Anderson, M. I. (1997). "Ultrasonic Instrumentation for On-Line Monitoring of Solid Deposition in Pipes." Society of Petroleum Engineering SPE **37437**(1997): 7.

Al-Roomi, Y., R. George, et al. (2004). "Use of a novel surfactant for improving the transportability/transportation of heavy/viscous crude oils." Journal of Petroleum Science and Engineering **42**(2-4): 235-243.

Al-Zahrani, S. M. and T. F. Al-Fariss (1998). "A general model for the viscosity of waxy oils." Chemical Engineering and Processing **37**(5): 433-437.

Barry, E. G. (1971). "Pumping Non-Newtonian Waxy Crude Oils." J. Inst. Pet. **57**(554): 11.

Becker, J. R. (1997). Crude Oil Waxes, Emulsions and Asphalrenes. Oklahoma, Penn Well Publishing Company.

Bell, H. S. (1963). Petroleum Transportation Handbook. New York.

Benallal, A., P. Maurel, et al. (2008). "Wax deposit accumulation in a "cylindrical Couette" geometry." Comptes Rendus Mécanique **336**(11-12): 835-839.

Billington, E. W. (1960). "Some Measurements of the Time Dependence of the Viscosity of Thixotropic Fluids." Proc. Phys Soc. **75**: 10.

Bomba, J. G. (1986). "Offshore Pipeline Transport of Waxy Crude Oils." Society of Petroleum Engineering SPE **14622**(1986): 250-256.

Borghi, G.-P., S. Correra, et al. (2003). "Prediction and Scaleup of Waxy Oil Restart Behavior." Society of Petroleum Engineering SPE **80259**(2003): 5.

Bot, A., U. Erle, et al. (2004). "Influence of crystallisation conditions on the large deformation rheology of inulin gels." Food Hydrocolloids **18**(4): 547-556.

Boukadi, A. and H. Amri (2005). "Flow Improvement of a Waxy Oil by Chemical Additive Utilization." Pakistan Journal of Biological Scientific Information **8**(8): 6.

Brown, T. S., V. G. Niesen, et al. (1993). "Measurement and Prediction of the Kinetics of Paraffin Deposition " Society of Petroleum Engineering SPE **29976**(1993).

Cawkwell, M. G. and M. E. Charles (1989). Journal of Pipelines **7**: 251-264.

Chang, C., Q. D. Nguyen, et al. (1999). "Isothermal start-up of pipeline transporting waxy crude oil." Journal of Non-Newtonian Fluid Mechanics **87**(2-3): 127-154.

Chang, C. and D. V. Boger (1998). "The Yielding of Waxy Crude Oils." Iddustrial & Engineering Chemistry Research **37**: 9.

Chen, X. T., T. Butler, et al. (1997). "Thechniques for Measuring Wax Thickness During Sigle and Multiphase Flow." Society of Petroleum Engineering **2**: 7.

Chin, W. C. (2001). Computational rheology for pipeline and annular flow, Elsevier Inc.

Couto, G. H., H. Chen, et al. (2008). "An Investigation of Two-Phase Oil/Water Paraffin Deposition " Society of Petroleum Engineering SPE **114735**(2008).

Dante, R. C., E. Geffroy-Aguilar, et al. (2006). "Viscoelastic models for Mexican heavy crude oil and comparison with a mixture of heptadecane and eicosane. Part I." Fuel **85**(4): 559-568.

Davidson, M. R., Q. Dzuy Nguyen, et al. (2004). "A model for restart of a pipeline with compressible gelled waxy crude oil." Journal of Non-Newtonian Fluid Mechanics **123**(2-3): 269-280.

Davidson, M. R., Q. D. Nguyen, et al. (2007). "Restart model for a multi-plug gelled waxy oil pipeline." Journal of Petroleum Science and Engineering **59**(1-2): 1-16.

Deshmukh, S. and D. P. Bharambe (2008). "Synthesis of polymeric pour point depressants for Nada crude oil (Gujarat, India) and its impact on oil rheology." Fuel Processing Technology **89**(3): 227-233.

Durand, S., C. Garnier, et al. (2006). "Rheology-structure properties of waxy maize starch-gellan mixtures." Food Hydrocolloids **20**(8): 1223-1230.

El-Eman, N., A. Bayoumi, et al. (1993). "Study on the suitable techniques for improving the flow properties of the Egyptian waxy crude oils." Revue de l'Institut Francais du Petrole **48**(4): 371-382.

El-Gamal, I. M. and E. A. M. Gad (1997). "Low Temperature rheolgical behavior of Umbaraka waxy crude and influence of flow improver." Elsevier **131**: 10.

El-Gamal, I. M. (1998). "Combined effects of shear and flow improvers: the optimum solution for handling waxy crudes below pour point." Colloids and Surfaces A: Physicochemical and Engineering Aspects **135**(1-3): 283-291.

Elsharkawy, A. M., T. A. Al-Sahhaf, et al. (1999). "Determination and Prediction of Wxy Deposition from Kuwaiti Crude Oils." Society of Petroleum Engineering SPE **54006**(1999): 10.

Etoumi, A. (2007). "Microbial treatment of waxy crude oils for mitigation of wax precipitation." Journal of Petroleum Science and Engineering **55**(1-2): 111-121.

Fusi, L. (2003). "On the Stationary Flow of a Waxy Crude Oil with Deposition Mechanisims " Nonlinear Analysis **53**: 20.

Fingas, M. and B. Fieldhouse (2009). "Studies on crude oil and petroleum product emulsions: Water resolution and rheology." Colloids and Surfaces A: Physicochemical and Engineering Aspects **333**(1-3): 67-81.

Frigaard, I., G. Vinay, et al. (2007). "Compressible displacement of waxy crude oils in long pipeline startup flows." Journal of Non-Newtonian Fluid Mechanics **147**(1-2): 45-64.

Garcia, M. d. C. (2001). "Paraffin Deposition in Oil Production " Society of Petroleum Engineering SPE **64992**(20017).

Govier, G. W. and M. Fogarasi (1972). "The Interpretation of Data on the Rheological Behaviour of Thixotropic Crude Oils " J. Can. Pet. Technol. (Montreal)(42-48).

Guo, X. and R. K. Prud'homme (2005). "Crystal structure of mixed paraffins and rheological behavior of model waxy oils." American Chemical Society, Division of Petroleum Chemistry, Preprints **50**(1): 81-83.

Guozhong, Z. and L. Gang (2008). "Study on the wax Deposition of Waxy Crude in Pipelines and its application." Journal of Petroleum Science and Engineering **1629**(2008): 33.

Hammami, A., D. B. Robinson, et al. (1997). "Paraffin Deposition From Crude Oils: Comparison of Laboratory Results to Field Data." Society of Petroleum Engineering SPE **SPE 38776**(1097): 15.

Hangs, F. E. (1963). Crude Oil and Refined Product Pipelines Petroleum Transportation Handbook

H. S. Bell. Houston, McGraw-Hill Book Company, INC 54.

Hemandez, O. C., H. Hensley, et al. (2004). "Improvement in Single-Phase Paraffin Deposition Modeling." Society of Petroleum Engineering SPE **84502**(2004): 237-244.

Hernandez, O. C., H. Hensley, et al. (2003). "Improvements in Single-Phase Paraffin Deposition Modeling." Society of Petroleum Engineering SPE **84502**(2003): 9.

Herring, J. D. (1974). "Design Concepts for High Wax Crude Oil Pipelines." Pipeline Gas J **31**(36): 4.

Hsu, J. J. C. and J. P. Brubaker (1995). "Wax Deposition Measurement and Scale-Up Modeling for Waxy Live Crudes under Turbulent Flow Conditions." Society of Petroleum Engineering SPE **29976**(1995): 241-250.

Hsu, J. J. C., S. J. Lian, et al. (1998). "Validation of Wax Deposition Model by a Field \test " Society of Petroleum Engineering SPE **48867**(1998): 371-381`.

Hsu, J. J. C., M. M. Santamaria, et al. (1994). "Wax Deposition of Waxy Live Crudes under Turbulent Flow Conditions " Society of Petroleum Engineering SPE **28480**(1994).

Hsu, J. J. C., M. M. Santamaria, et al. (1994). "Wax Deposition and Gel Strength of Waxy Live Crudes." OTC **7573**(1994).

Irani, C. and J. Zajac (1982). "Handling of High Pour Point West African Crude Oils." J. Inst. Pet.Technol. **34**: 9.

Johnsen, E. E. and H. P. Rønningsen (2003). "Viscosity of [`]live' water-in-crude-oil emulsions: experimental work and validation of correlations." Journal of Petroleum Science and Engineering **38**(1-2): 23-36.

Kané, M., M. Djabourov, et al. (2004). "Rheology and structure of waxy crude oils in quiescent and under shearing conditions." Fuel **83**(11-12): 1591-1605.

Kané, M., M. Djabourov, et al. (2003). "Morphology of paraffin crystals in waxy crude oils cooled in quiescent conditions and under flow." Fuel **82**(2): 127-135.

Kane, M., M. Djabourov, et al. (2004). "Rheology and Structure of Waxy Crude Oils in Quiescent and under Shearing Condsitions." Fuel Journal **83**(2004): 1591-1605.

Lei, H. and Z. Jin-jun (2007). "New Method for rapid thixotropy measurement of waxy crude " Journal Central South University **14 part 1**: 3.

Lie, H. and Z. Jin-jun (2007). "Viscoelasticity of Gelled Waxy Crude Oil." J. Cent. Univ. Technol.(Springer) **1**: 4.

Li, H. and J. Zhang (2003). "A generalized model for predicting non-Newtonian viscosity of waxy crudes as a function of temperature and precipitated wax[small star, filled]." Fuel **82**(11): 1387-1397.

Li, C., Q. Yang, et al. (2009). "Effect of Stress and Oscillatory Frequency on the Structural Properties of Daqing Gelled Crude Oil at Different Temperature." Journal of Petroleum Science and Engineering **65**(2009): 167-170.

Letoffe, J. M., P. Claudy, et al. (1994). "Crude Oils: Characterization of Waxes Precipitated on cooling by D.S.C and Thermomicroscopy." Fuel Journal **74**(6): 810-817.

Luo, K., S. Li, et al. (2001). "Phase Behavior of Highly Waxy Gas Condensate Systems." Society of Petroleum Engineering SPE **68228**(2001): 7.

M. A, H. (1981). "Deposition of Paraffin Wax from its Solutions with Hydrocarbons." Society of Petroleum Engineering SPE **10541**(1981): 11.

Manning, F. S. and R. E. Thompson (1995). Oil Field Processing: Crude Oil. Oklahoma, Penn Well Publishing Company.

Marsden, S., I. Kiyoshi, et al. (1988). "Slurries and Emulsions of Waxy and Heavy Crude Oils for Pipeline Transportation of Crude Oil." Colloids and Surfaces **29**: 13.

Masson, J. F., G. M. Polomark, et al. (2006). "Melting and glass transitions in paraffinic and naphthenic oils." Thermochimica Acta **440**(2): 132-140.

Matlach, W. J., M. E. Newberry, et al. (1983). "Paraffin Deposition and Rheological Evaluation of High Wax Content Altamont Crude Oils." Society of Petroleum Engineering SPE **11851**(1983): 9.

Mcketta, J. J. (1993). Encyclopedia of Chemical Processing and design. J. J. Mcketta. New York, Marcel Dekker Inc. **36**.

Mewis, J. and N. J. Wagner (1999). "Thixotropy." Advances in Colloid and Interface Science **In Press, Corrected Proof**.

Mezger, T. G. (2006). Rheology Handbook.

Mohamed, F. (2003). Rheology of Waxy crude Oils. EDT. Bradford, University of Bradford. **MSC**.

Monger, T. G., J. E. Tackett, et al. (1997). "DeepStar Comparisons of Cloud Point Measurment and Paraffin Prediction Methods." Society of Petroleum Engineering SPE **38774**(1997): 257-272.

Mozes, G. (1982). Paraffin Products. New York, Elsevier.

Narjes (2003). Wax deposition of waxy crude oils. Glasco. **MSc.**

Owodunni, O. L. and J. A. Ajienka (2007). "Use of Thermal Insulation to Prevent Hydrate and Paraffin Wax Deposition " Society of Petroleum Engineering SPE **111903**(2007): 20.

Perkins, T. K. and J. B. Turner (1971). "Starting Behaviour of Gathering Lines and Pipelines Filld with Gelled Prudhoe Bay Oil." J. Petr. Technolo.: 301-308.

Pilehari, P. E., B. Saadevandi, et al. (1988). "Oil/Water Emulsion for Pipeline Transport pf Viscous Crude Oils." Society of Petroleum Engineering SPE **18218**(1988): 393-403.

Qabazard, H. M. (2008). Annual Statistical Bulletin. Vina.

Rashidah, A. (2005). Flow a non-Newtonian Bingham Palstic fluid over a rotational disk. , University of Saskatchewan, Saskatchewan. PhD

Razavi, S. M. A. and H. Karazhiyan (2009). "Flow properties and thixotropy of selected hydrocolloids: Experimental and modeling studies." Food Hydrocolloids **23**(3): 908-912.

Ribeiro, F. S., P. R. Souza Mendes, et al. (1997). "Obstruction of pipelines due to paraffin deposition during the flow of crude oils." International Journal of Heat and Mass Transfer **40**(18): 4319-4328.

(Ribeiro, Souza Mendes et al. 1997; Vinay, Wachs et al. 2005; Masson, Polomark et al. 2006; Vinay, Wachs et al. 2006; Wang, Huang et al. 2006; Savreux, Jay et al. 2007; Vinay, Wachs et al. 2007; Yu, Wang et al. 2008; Razavi and Karazhiyan 2009)

Ronningsen, H. P. (1992). "Rheolgical Behavior of Gelled, Waxy North Sea Crude Oils." J. Pet. Sci. Eng. **7**.

Ronningsen, H. P. (1992). Journal of Petroleum Science and Engineering **7**: 177-231.

Rocha, N. O., C. N. Khalil, et al. (2003). "A Thermochemical Process for Wax Damage Removal." Society of Petroleum Engineering SPE **80266**(2003): 6.

Russell, R. J. and E. D. Chapman (1971). Journal of the Institute of Petroleum **57**:

117-12

Sadeghazad, A. and N. Ghaemi (2003). "Microbial Prevention of Wax Precipitation in Crude Oil by Biodegradation Mechanism." Society of Petroleum Engineering SPE **80529**(2003)

Santay Maria, S. Baruah, et al. (1994). "Paraffin Problems in Crude Oil Production and Transpotation; A Review." Society of Petroleum Engineering SPE **28181**(1994): 50-54.

Savreux, F., P. Jay, et al. (2007). "Viscoplastic fluid mixing in a rotating tank." Chemical Engineering Science **62**(8): 2290-2301.

Singh, P., R. Venkatesan, et al. (2000). A.I.Ch.E Journal **46**: 1059-1074.

Skelland, A. H. P. (1967). "Non-Newtonian Flow and Heat Transfer " John Wiley & Sons, Inc. New York.

Smith, B. (1979a). "Pumping Heavy Crude-1Guidelines Set Out for Pumping Heavy Crudes " Oil Gas J **77**(27): 4.

Smith, B. (1979b). "Pumping Heavy Crude-2 Steps for finding Crude." Oil Gas J **77**(27): 2.

Straub, T. J. and G. E. King (1998). "An Investigation into Practical Removal of Downhole Paraffin by Thermal Method and Chemical Solvent." Society of Petroleum Engineering SPE **18889**(1989): 8.

Thomas, O. C. (1988). "Selection of Paraffin Control Products and Applications."

Society of Petroleum Engineering SPE **17626**(1988): 811-819.

Tower, B. F., A. K. Chejara, et al. (2007). "Experimental Investigations of Ultrasonic Waves Effects on Wax Deposition During Crude-Oil Production." Society of Petroleum Engineering SPE **109505**(2007): 9.

Venkatesan, R., N. R. Nagarajan, et al. (2005). "The strength of paraffin gels formed under static and flow conditions." Elsevier **60 (2005)**: 12.

Vinay, G., A. Wachs, et al. (2005). "Numerical simulation of non-isothermal viscoplastic waxy crude oil flows." Journal of Non-Newtonian Fluid Mechanics **128**(2-3): 144-162.

Vinay, G., A. Wachs, et al. (2006). "Numerical simulation of weakly compressible Bingham flows: The restart of pipeline flows of waxy crude oils." Journal of Non-Newtonian Fluid Mechanics **136**(2-3): 93-105.

Vinay, G., A. Wachs, et al. (2007). "Start-up transients and efficient computation of isothermal waxy crude oil flows." Journal of Non-Newtonian Fluid Mechanics **143**(2-3): 141-156.

Wang, S., Y. Huang, et al. (2006). "Experimental and theoretical investigation of the Zaoyuan field heavy oil flow through porous media." Journal of Petroleum Science and Engineering **50**(2): 83-101.

Wardhaugh, L. T. (1990). The Rheology of Waxy Crude Oil. Chemical Engineering. Parkville, Victoria, Australia, The University of Melbourne. **PhD:** 344.

Wardhaugh, L. T. and D. V. Boger (1990). "Rheology of waxy crude oils. An overview." European Rheology Conference: 501.

Wardhaugh, L. T., D. V. Boger, et al. (1988). "Rheology of Waxy Crude Oils (SPE 17625)." Proc. SPE Int. Meet. Petr. Eng. : 7.

Weingarten, J. S. and J. A. Euchner (1988). "Methods for Predicting Wax Precipitation and Deposition." Society of Petroleum Engineering SPE **15654**(1988).

Yu, B., Y. Wang, et al. (2008). "Thermal impact of the products pipeline on the crude oil pipeline laid in one ditch - The effect of pipeline interval." International Journal of Heat and Mass Transfer **51**(3-4): 597-609.

Zougari, M. I. (2009). "Shear Driven Crude Oil Wax Deposition Evaluation." Journal of Petroleum Science and Engineering(2009).

Appendix 1

Gelation Point graphs of Mix Sample

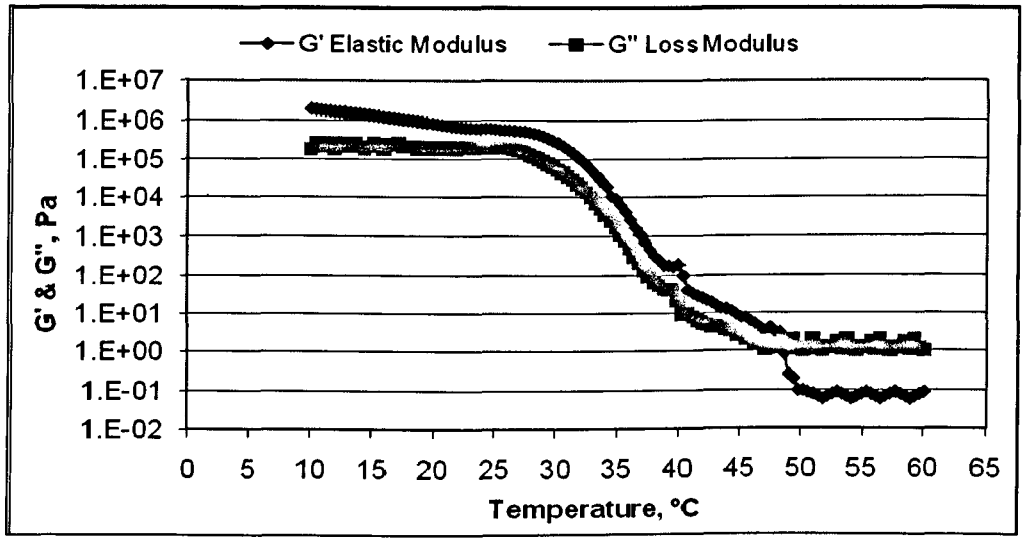

Figure A1. 1 Temperature vs. $G^{'}$ and $G^{''}$ for the Mix sample at cooling rate of 0.125 °C/min

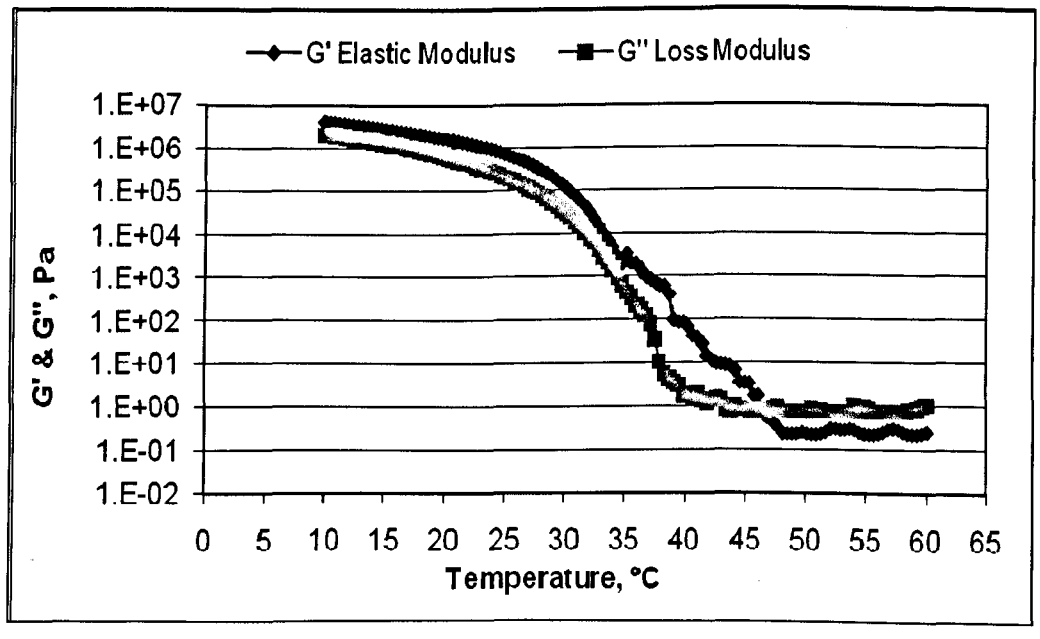

Figure A1. 2 Temperature vs. $G^{'}$ and $G^{''}$ for the Mix sample at cooling rate of 0.25 °C/min

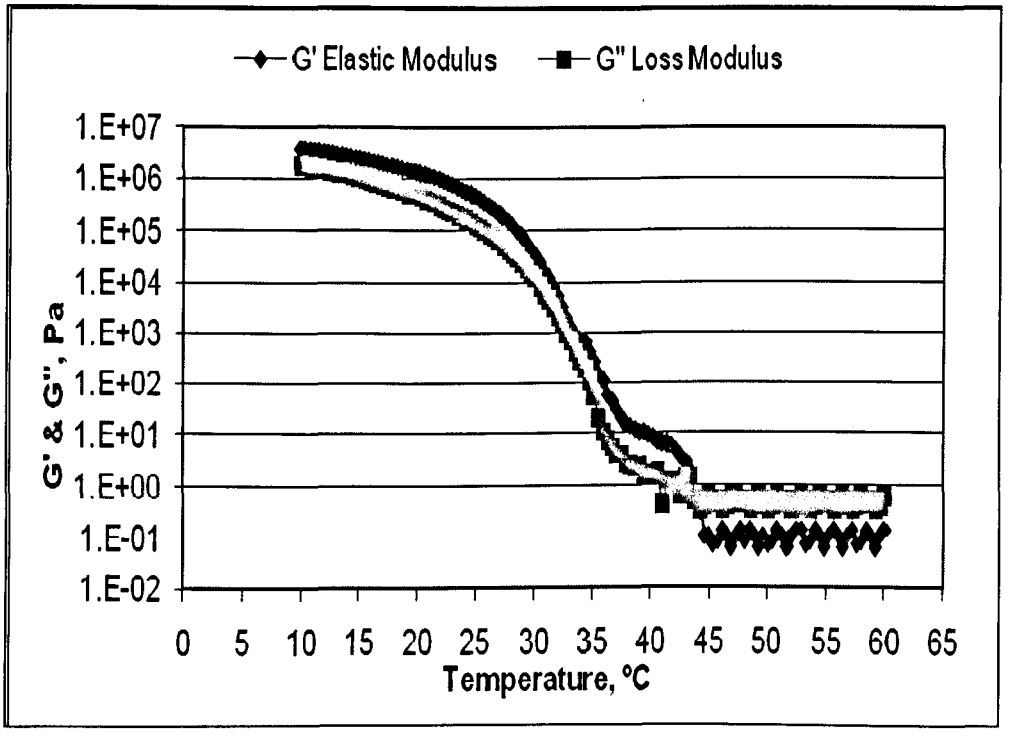

Figure A1. 3 Temperature vs. $G^{'}$ and $G^{"}$ for the Mix sample at cooling rate of 0.5 °C/min

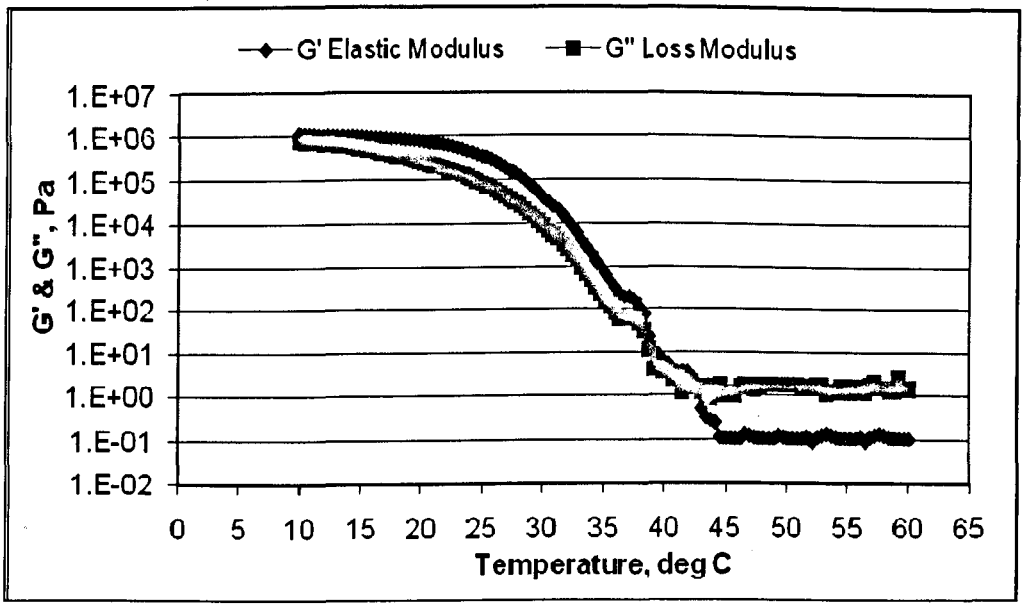

Figure A1. 4 Temperature vs. $G^{'}$ and $G^{"}$ for the Mix sample at cooling rate of 1 °C/min

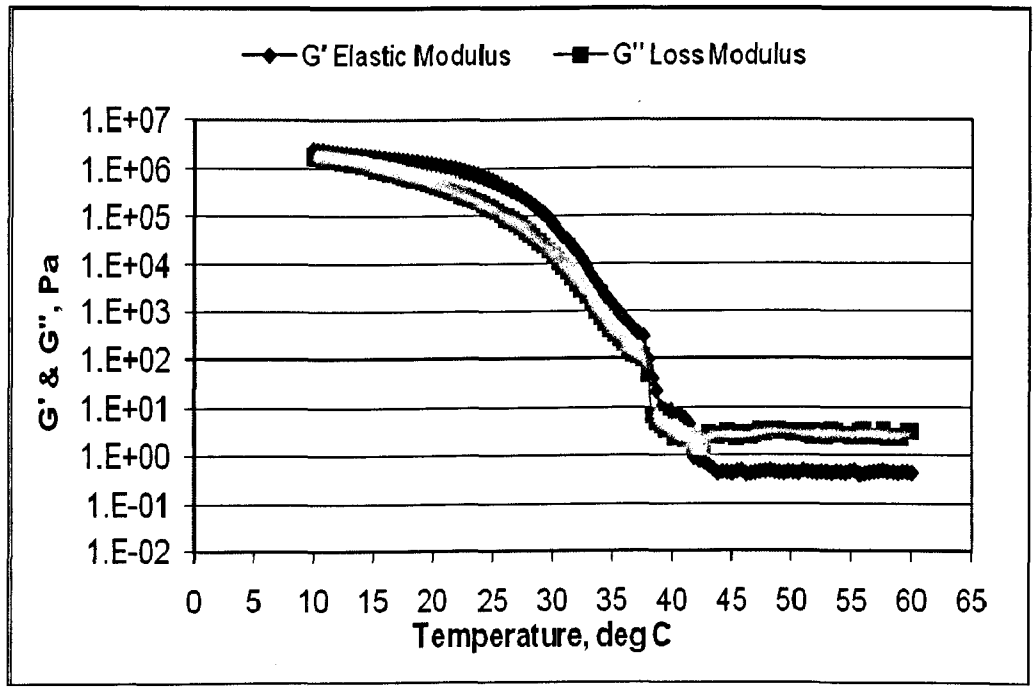

Figure A1. 5 Temperature vs. $G^{'}$ and $G^{"}$ for the Mix sample at cooling rate of 2 °C/min

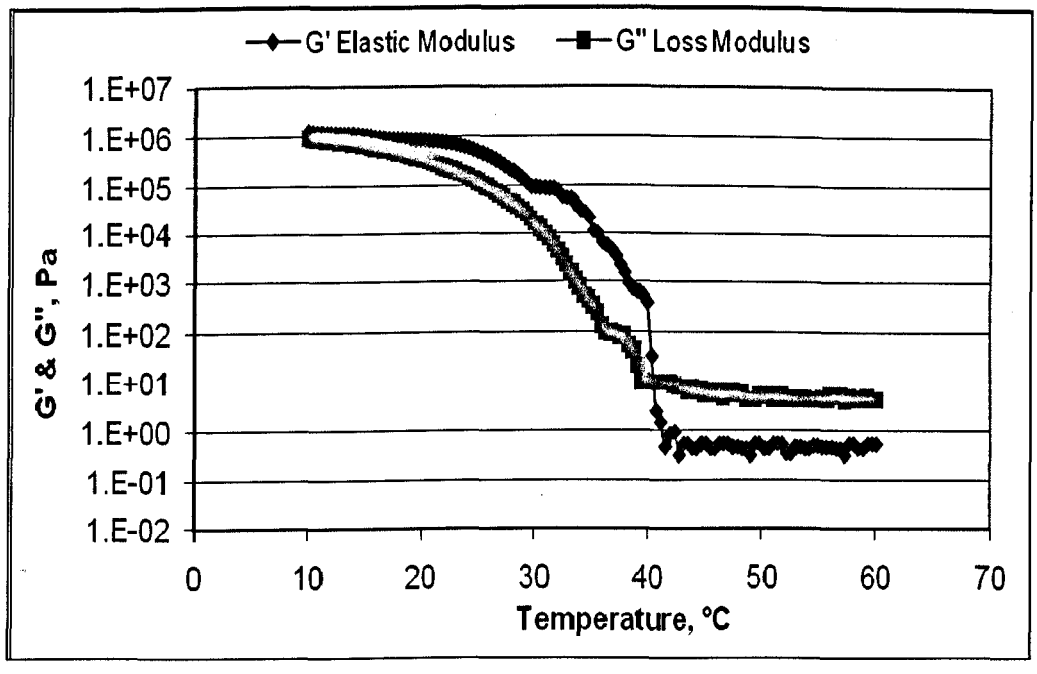

Figure A1. 6 Temperature vs. $G^{'}$ and $G^{"}$ for the Mix sample at cooling rate of 5 °C/min

Gelation Point graphs of Remal Sample

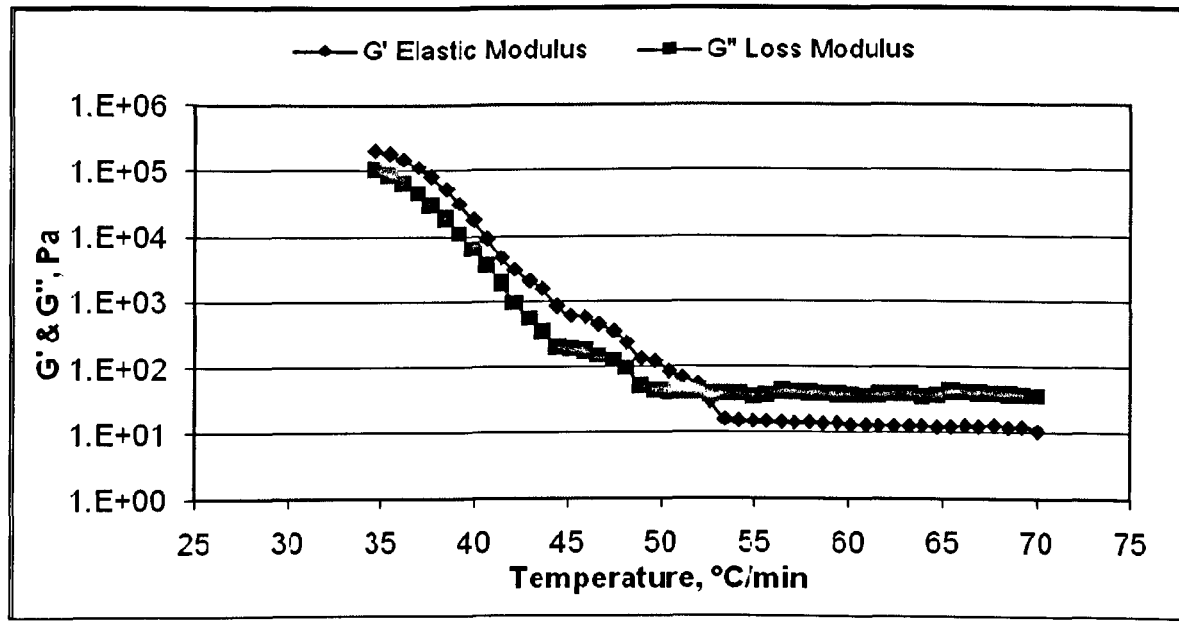

Figure A1. 7 Temperature vs. G' and G'' for the Remal sample at cooling rate of 0.125 °C/min

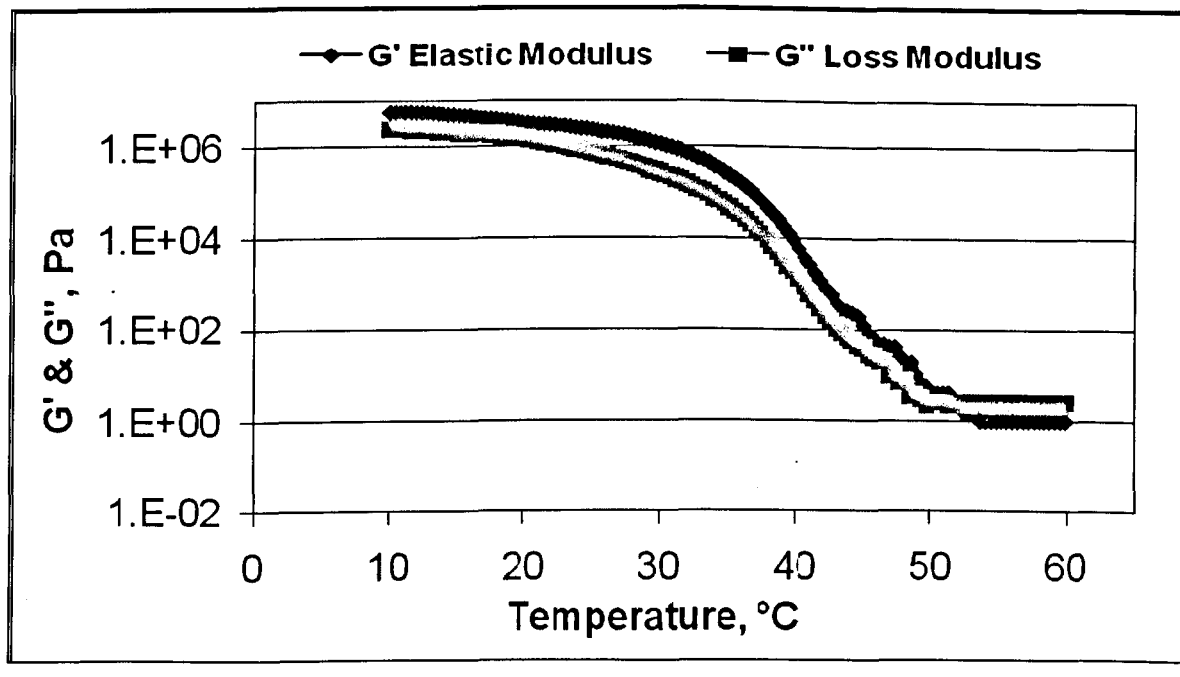

Figure A1. 8 Temperature vs. G' and G'' for the Remal sample at cooling rate of 0.25 °C/

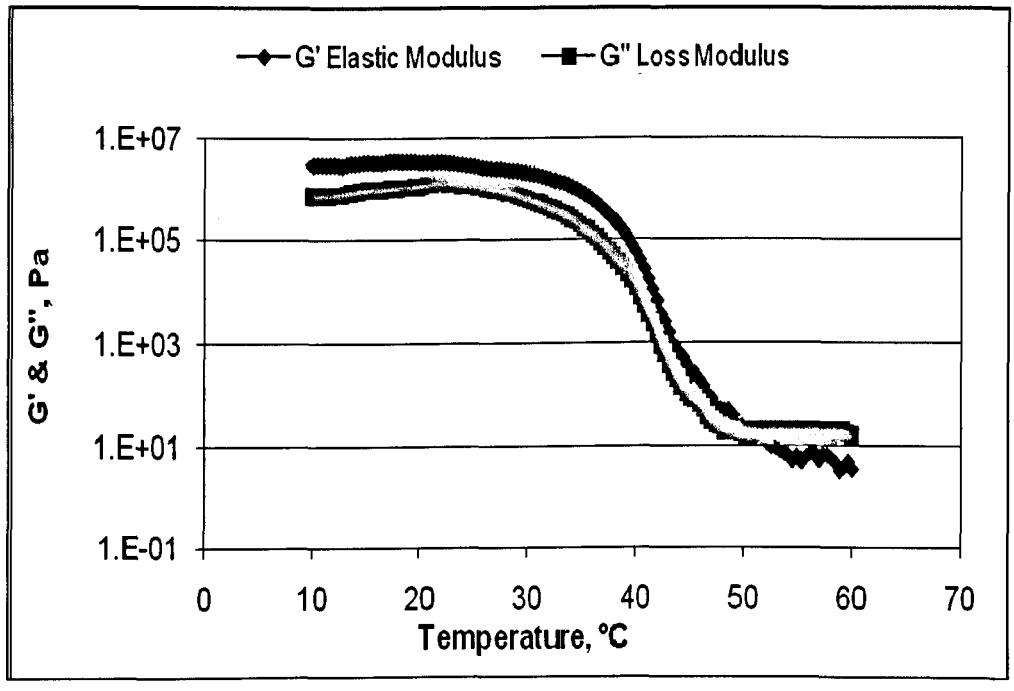

Figure A1. 9 Temperature vs. $G^{'}$ and $G^{''}$ for the Remal sample at cooling rate of 0.5 °C/min

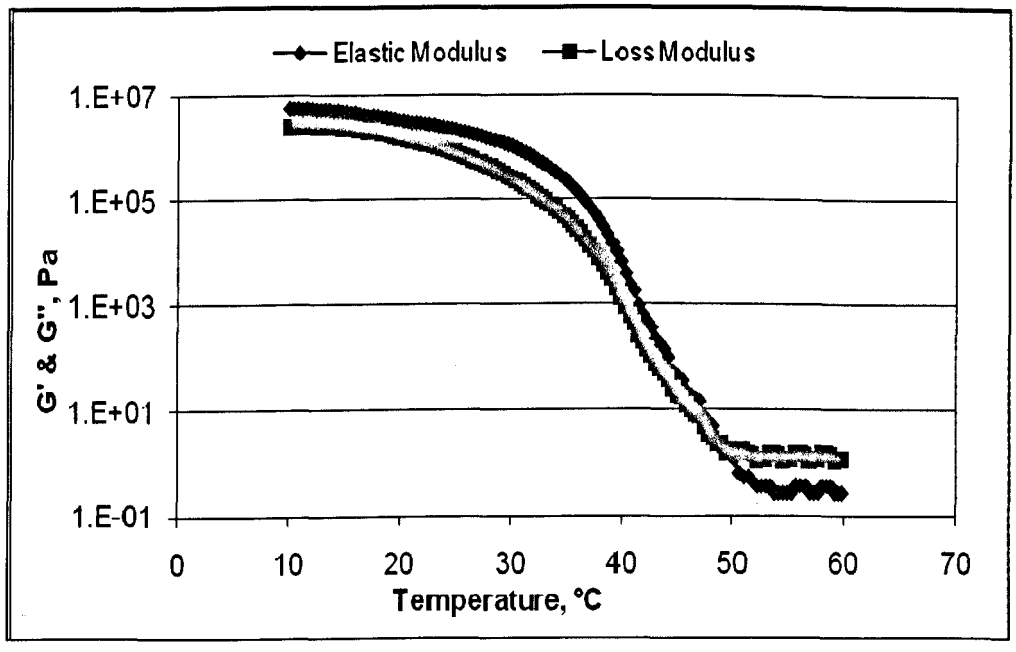

Figure A1. 10 Temperature vs. $G^{'}$ and $G^{''}$ for the Remal sample at cooling rate of 1 °C/min

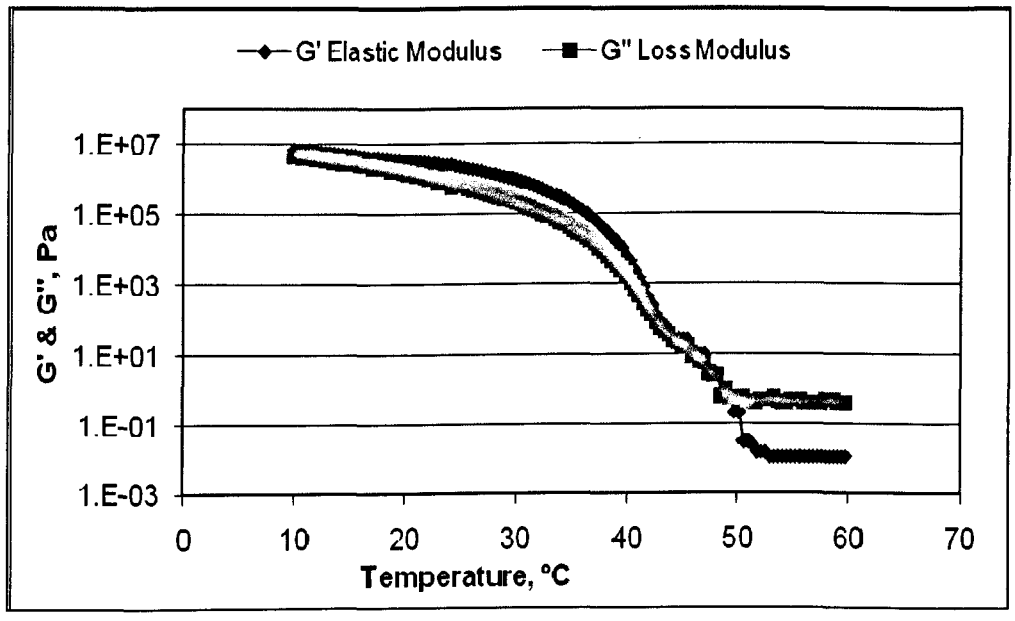

Figure A1. 11 Temperature vs. $G^{'}$ and $G^{"}$ for the Remal sample at cooling rate of 2 °C/min

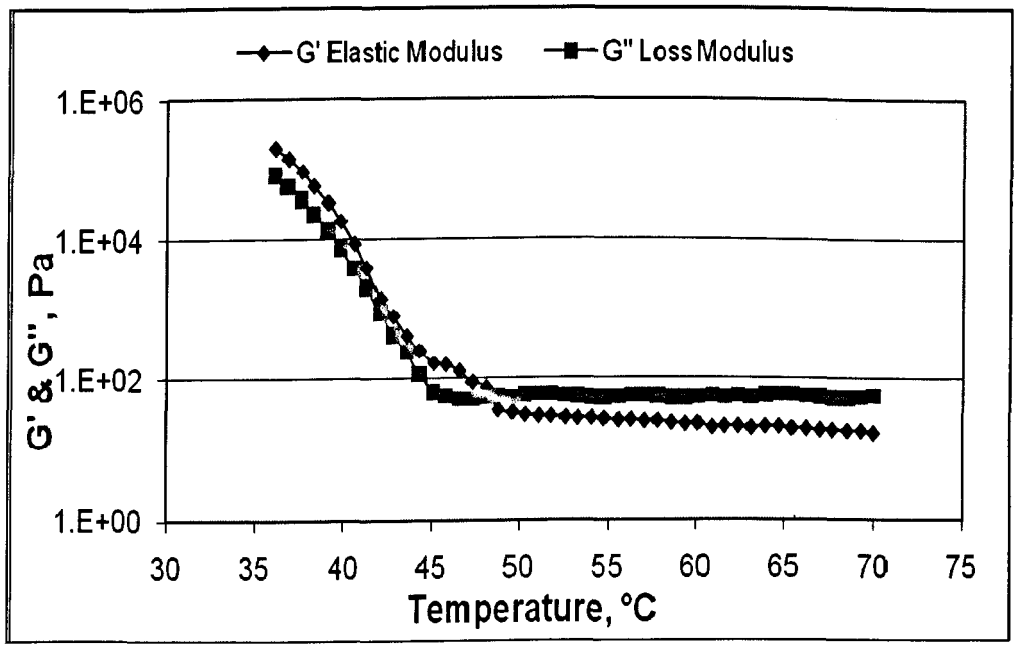

Figure A1.12: Temperature vs. $G^{'}$ and $G^{"}$ for the Remal sample at cooling rate of 5 °C/min

Appendix 2: The data for the calculation of determining the actual flow diameter

1. For BP Sample

- **At 13 °C**

Table A2. 1 Flow diameter determination experiment (Run 1): results for the BP oil sample at 13 °C

Time	T	Pipe mass	Pipe+oil+2 plugs+Balloon	Pipe+wax layer	Layer mass	Removed oil	flow diameter	Wax layer thickness
hr	°C	g	mass, g	mass, g	g	mass, g	mm	(2*hw), mm
1	13	47.108	81.736	49.488	2.38	17.144	12.64903721	0.850962786
2	13	47.108	81.736	49.718	2.61	16.914	12.56390241	0.936097589
3	13	47.108	81.736	49.858	2.75	16.774	12.51179761	0.988202391
4	13	47.108	81.736	50.058	2.95	16.574	12.43698351	1.063016489
5	13	47.108	81.736	50.338	3.23	16.294	12.33148126	1.16851874
6	13	47.108	81.736	50.488	3.38	16.144	12.27458918	1.225410816
7	13	47.108	81.736	50.718	3.61	15.914	12.18683884	1.313161157

Table A2.2 Flow diameter determination experiment (Run 2): results for the BP oil sample at 13 °C

Time	T	Pipe mass	Pipe+oil+2 plugs+Balloon	Pipe+wax layer	Layer mass	Removed oil	flow diameter	Wax layer thickness
hr	°C	g	mass, g	mass, g	g	mass, g	mm	(2*hw), mm
1	13	47.108	81.736	49.538	2.43	17.094	12.63057846	0.869421537
2	13	47.108	81.736	49.728	2.62	16.904	12.56018781	0.939812192
3	13	47.108	81.736	49.898	2.79	16.734	12.49687062	1.00312938
4	13	47.108	81.736	50.038	2.93	16.594	12.44448516	1.05551484
5	13	47.108	81.736	50.348	3.24	16.284	12.32769662	1.172303377
6	13	47.108	81.736	50.488	3.38	16.144	12.27458918	1.225410816
7	13	47.108	81.736	50.918	3.81	15.714	12.11001736	1.389982641

Table A2.3 Flow diameter determination experiment (Run 3): results for the BP oil sample at 13 °C

Time	T	Pipe mass	Pipe+oil+2 plugs+Balloon	Pipe+wax layer	Layer mass	Removed oil	flow diameter	Wax layer thickness
hr	°C	g	mass, g	mass, g	g	mass, g	mm	(2*hw), mm
1	13	47.108	81.736	49.498	2.39	17.134	12.64534762	0.854652381
2	13	47.108	81.736	49.698	2.59	16.934	12.57132832	0.928671675
3	13	47.108	81.736	49.928	2.82	16.704	12.48566367	1.014336333
4	13	47.108	81.736	50.058	2.95	16.574	12.43698351	1.063016489
5	13	47.108	81.736	50.298	3.19	16.334	12.34660821	1.153391795
6	13	47.108	81.736	50.528	3.42	16.104	12.25937337	1.240626626
7	13	47.108	81.736	50.818	3.71	15.814	12.14848882	1.351511176

Table A2.4 Flow diameter determination experiment (Run 4): results for the BP oil sample at 13 °C

Time	T	Pipe mass	Pipe+oil+2 plugs+Balloon	Pipe+wax layer	Layer mass	Removed oil	flow diameter	Wax layer thickness
hr	°C	g	mass, g	mass, g	g	mass, g	mm	(2*hw), mm
1	13	47.108	81.736	49.508	2.4	17.124	12.64165695	0.858343052
2	13	47.108	81.736	49.758	2.65	16.874	12.5490374	0.950962599
3	13	47.108	81.736	49.888	2.78	16.744	12.50060404	0.999395962
4	13	47.108	81.736	50.038	2.93	16.594	12.44448516	1.05551484
5	13	47.108	81.736	50.158	3.05	16.474	12.39940719	1.100592814
6	13	47.108	81.736	50.488	3.38	16.144	12.27458918	1.225410816
7	13	47.108	81.736	50.838	3.73	15.794	12.14080428	1.359195716

Table A2.5 Flow diameter determination experiment (Run 5): results for the BP oil sample at 13 °C

Time	T	Pipe mass	Pipe+oil+2 plugs+Balloon	Pipe+wax layer	Layer mass	Removed oil	flow diameter	Wax layer thickness
hr	°C	g	mass, g	mass, g	g	mass, g	mm	(2*hw), mm
1	13	47.108	81.736	49.488	2.38	17.144	12.64903721	0.850962786
2	13	47.108	81.736	49.718	2.61	16.914	12.56390241	0.936097589
3	13	47.108	81.736	49.858	2.75	16.774	12.51179761	0.988202391
4	13	47.108	81.736	50.058	2.95	16.574	12.43698351	1.063016489
5	13	47.108	81.736	50.338	3.23	16.294	12.33148126	1.16851874
6	13	47.108	81.736	50.488	3.38	16.144	12.27458918	1.225410816
7	13	47.108	81.736	50.718	3.61	15.914	12.18683884	1.313161157

Table A2.6 Flow diameter determination experiment (Run 6): results for the BP oil sample at 13 °C

Time	T	Pipe mass	Pipe+oil+2 plugs+Balloon	Pipe+wax layer	Layer mass	Removed oil	flow diameter	Wax layer thickness
hr	°C	g	mass, g	mass, g	g	mass, g	mm	(2*hw), mm
1	13	47.108	81.736	49.478	2.37	17.154	12.65272573	0.847274267
2	13	47.108	81.736	49.738	2.63	16.894	12.55647211	0.943527894
3	13	47.108	81.736	49.918	2.81	16.714	12.48940044	1.010599565
4	13	47.108	81.736	50.008	2.9	16.624	12.45572916	1.044270837
5	13	47.108	81.736	50.358	3.25	16.274	12.32391082	1.176089176
6	13	47.108	81.736	50.458	3.35	16.174	12.28598867	1.214011325
7	13	47.108	81.736	50.868	3.76	15.764	12.12926834	1.370731656

Table A2.7 Flow diameter determination experiment (Run 7): results for the BP oil sample at 13 °C

Time	T	Pipe mass	Pipe+oil+2 plugs+Balloon	Pipe+wax layer	Layer mass	Removed oil	flow diameter	Wax layer thickness
hr	°C	g	mass, g	mass, g	g	mass, g	mm	(2*hw), mm
1	13	47.108	81.736	49.518	2.41	17.114	12.6379652	0.862034802
2	13	47.108	81.736	49.728	2.62	16.904	12.56018781	0.939812192
3	13	47.108	81.736	49.928	2.82	16.704	12.48566367	1.014336333
4	13	47.108	81.736	50.038	2.93	16.594	12.44448516	1.05551484
5	13	47.108	81.736	50.358	3.25	16.274	12.32391082	1.176089176
6	13	47.108	81.736	50.488	3.38	16.144	12.27458918	1.225410816
7	13	47.108	81.736	50.828	3.72	15.804	12.14464716	1.355352838

Table A2.8 Average of flow diameter of all runs of the BP oil sample at 13 °C

Time, hr	T, °C	Rnu 1	Rnu 2	Rnu 3	Rnu 4	Rnu 5	Rnu 6	Rnu 7	Avarge flow diameter mm
1	13	12.64903721	12.63057846	12.64534762	12.64165695	12.64903721	12.65272573	12.6379652	12.64376406
2	13	12.56390241	12.56018781	12.57132832	12.5490374	12.56390241	12.55647211	12.56018781	12.5607169
3	13	12.51179761	12.49687062	12.48566367	12.50060404	12.51179761	12.48940044	12.48566367	12.49739966
4	13	12.43698351	12.44448516	12.43698351	12.44448516	12.43698351	12.45572916	12.44448516	12.44287645
5	13	12.33148126	12.32769662	12.34660821	12.39940719	12.33148126	12.32391082	12.32391082	12.34064231
6	13	12.27458918	12.27458918	12.25937337	12.27458918	12.27458918	12.28598867	12.27458918	12.274044
7	13	12.18683884	12.11001736	12.14848882	12.14080428	12.18683884	12.12926834	12.14464716	12.14955767

Table A2.9 Flow diameter determination experiment (Run 1): results for the BP oil sample at 18 °C

Time	T	Pipe mass	Pipe+oil+2 plugs+Balloon	Pipe+wax layer	Layer mass	Removed oil	flow diameter	Wax layer thickness
hr	°C	g	mass, g	mass, g	g	mass, g	mm	(2*hw), mm
1	18	47.108	81.736	48.508	1.4	18.124	13.00554086	0.494459135
2	18	47.108	81.736	48.708	1.6	17.924	12.93358313	0.566416868
3	18	47.108	81.736	49.908	2.8	16.724	12.49313609	1.006863914
4	18	47.108	81.736	49.208	2.1	17.424	12.75191245	0.748087546
5	18	47.108	81.736	49.608	2.5	17.024	12.6046908	0.895309202
6	18	47.108	81.736	49.808	2.7	16.824	12.53043134	0.969568661
7	18	47.108	81.736	49.958	2.85	16.674	12.47444665	1.025553354

Table A2.10 Flow diameter determination experiment: (Run 2) results for the BP oil sample at 18 °C

Time	T	Pipe mass	Pipe+oil+2 plugs+Balloon	Pipe+wax layer	Layer mass	Removed oil	flow diameter	Wax layer thickness
hr	°C	g	mass, g	mass, g	g	mass, g	mm	(2*hw), mm
1	18	47.108	81.736	48.458	1.35	18.174	13.02346818	0.476531824
2	18	47.108	81.736	48.648	1.54	17.984	12.95521242	0.544787582
3	18	47.108	81.736	48.888	1.78	17.744	12.86847715	0.631522852
4	18	47.108	81.736	49.188	2.08	17.444	12.75922895	0.740771055
5	18	47.108	81.736	49.548	2.44	17.084	12.62688347	0.873116526
6	18	47.108	81.736	49.778	2.67	16.854	12.54159829	0.958401712
7	18	47.108	81.736	49.858	2.75	16.774	12.51179761	0.988202391

Table A2.11 Flow diameter determination experiment (Run 3): results for the BP oil sample at 18 °C

Time	T	Pipe mass	Pipe+oil+2 plugs+Balloon	Pipe+wax layer	Layer mass	Removed oil	flow diameter	Wax layer thickness
hr	°C	g	mass, g	mass, g	g	mass, g	mm	(2*hw), mm
1	18	47.108	81.736	48.528	1.42	18.104	12.99836302	0.501636983
2	18	47.108	81.736	48.738	1.63	17.894	12.92275491	0.577245087
3	18	47.108	81.736	48.898	1.79	17.734	12.86485049	0.635149511
4	18	47.108	81.736	49.198	2.09	17.434	12.75557122	0.744428776
5	18	47.108	81.736	49.518	2.41	17.114	12.6379652	0.862034802
6	18	47.108	81.736	49.728	2.62	16.904	12.56018781	0.939812192
7	18	47.108	81.736	49.898	2.79	16.734	12.49687062	1.00312938

Table A2.12 Flow diameter determination experiment (Run 4): results for the BP oil sample at 18 °C

Time	T	Pipe mass	Pipe+oil+2 plugs+Balloon	Pipe+wax layer	Layer mass	Removed oil	flow diameter	Wax layer thickness
hr	°C	g	mass, g	mass, g	g	mass, g	mm	(2*hw), mm
1	18	47.108	81.736	48.498	1.39	18.134	13.0091283	0.490871697
2	18	47.108	81.736	48.688	1.58	17.944	12.94079691	0.559203089
3	18	47.108	81.736	48.898	1.79	17.734	12.86485049	0.635149511
4	18	47.108	81.736	49.168	2.06	17.464	12.76654124	0.733458756
5	18	47.108	81.736	49.588	2.48	17.044	12.6120927	0.887907305
6	18	47.108	81.736	49.798	2.69	16.834	12.53415476	0.965845239
7	18	47.108	81.736	49.928	2.82	16.704	12.48566367	1.014336333

Table A2.13 Flow diameter determination experiment (Run 5): results for the BP oil sample at 18 °C

Time	T	Pipe mass	Pipe+oil+2 plugs+Balloon	Pipe+wax layer	Layer mass	Removed oil	flow diameter	Wax layer thickness
hr	°C	g	mass, g	mass, g	g	mass, g	mm	(2*hw), mm
1	18	47.108	81.736	48.518	1.41	18.114	13.00195244	0.498047564
2	18	47.108	81.736	48.694	1.586	17.938	12.9386332	0.561366801
3	18	47.108	81.736	48.888	1.78	17.744	12.86847715	0.631522852
4	18	47.108	81.736	49.228	2.12	17.404	12.74459176	0.755408239
5	18	47.108	81.736	49.568	2.46	17.064	12.61949025	0.880509748
6	18	47.108	81.736	49.788	2.68	16.844	12.53787708	0.962122923
7	18	47.108	81.736	49.918	2.81	16.714	12.48940044	1.010599565

Table A2.14 Flow diameter determination experiment (Run 6): results for the BP oil sample at 18 °C

Time	T	Pipe mass	Pipe+oil+2 plugs+Balloon	Pipe+wax layer	Layer mass	Removed oil	flow diameter	Wax layer thickness
hr	°C	g	mass, g	mass, g	g	mass, g	mm	(2*hw), mm
1	18	47.108	81.736	48.488	1.38	18.144	13.01271475	0.487285247
2	18	47.108	81.736	48.678	1.57	17.954	12.94440229	0.555597708
3	18	47.108	81.736	48.918	1.81	17.714	12.8575941	0.6424059
4	18	47.108	81.736	49.158	2.05	17.474	12.77019582	0.729804177
5	18	47.108	81.736	49.628	2.52	17.004	12.59728455	0.902715449
6	18	47.108	81.736	49.758	2.65	16.874	12.5490374	0.950962599
7	18	47.108	81.736	49.938	2.83	16.694	12.48192578	1.01807422

Table A2.15 Flow diameter determination experiment (Run 7): results for the BP oil sample at 18 °C

Time	T	Pipe mass	Pipe+oil+2 plugs+Balloon	Pipe+wax layer	Layer mass	Removed oil	flow diameter	Wax layer thickness
hr	°C	g	mass, g	mass, g	g	mass, g	mm	(2*hw), mm
1	18	47.108	81.736	48.488	1.38	18.144	13.01271475	0.487285247
2	18	47.108	81.736	48.698	1.59	17.934	12.93719052	0.562809476
3	18	47.108	81.736	48.828	1.72	17.804	12.89021568	0.60978432
4	18	47.108	81.736	49.128	2.02	17.504	12.78115329	0.718846709
5	18	47.108	81.736	49.558	2.45	17.074	12.6231874	0.876812596
6	18	47.108	81.736	49.828	2.72	16.804	12.52298117	0.977018826
7	18	47.108	81.736	49.888	2.78	16.744	12.50060404	0.999395962

Table A2.16 Average of flow diameter determination of all runs for the BP oil sample at 18°C

Time, hr	T°C	Rnu 1	Rnu 2	Rnu 3	Rnu 4	Rnu 5	Rnu 6	Rnu 7	Avarge flow diameter mm
1	17	13.00554	13.02347	12.99836	13.00913	13.00195	13.01271	13.01271	13.00912604
2	17	12.93358	12.95521	12.92275	12.9408	12.93863	12.9444	12.93719	12.93893906
3	17	12.49314	12.86848	12.86485	12.86485	12.86848	12.85759	12.89022	12.81537159
4	17	12.75191	12.75923	12.75557	12.76654	12.74459	12.7702	12.78115	12.76131353
5	17	12.60469	12.62688	12.63797	12.61209	12.61949	12.59728	12.62319	12.61737062
6	17	12.53043	12.5416	12.56019	12.53415	12.53788	12.54904	12.52298	12.53946684
7	17	12.47445	12.5118	12.49687	12.48566	12.4894	12.48193	12.5006	12.49152983

2. For MIX Sample

Table A2.17 Flow diameter determination experiment (Run 1): results for the Mix oil sample at 30 °C

Time	T	Pipe Mass	Pipe+Oil+2 Plugs+Balloon	Pipe+Wax Layer	Wax Layer	Removed Oil	Flow Diameter	Wax Layer Thickness
hr	°C	g	Mass, g	Mass, g	Mass, g	Mass, g	mm	(2*hw), mm
1	30	45.29	79.854	47.893	2.603	16.857	12.56344444	0.936555562
2	30	45.29	79.854	48.114	2.824	16.636	12.48081759	1.019182412
3	30	45.29	79.854	48.345	3.055	16.405	12.39386318	1.106136824
4	30	45.29	79.854	48.537	3.247	16.213	12.32112238	1.178877617
5	30	45.29	79.854	48.751	3.461	15.999	12.23953727	1.260462727
6	30	45.29	79.854	48.974	3.684	15.776	12.15393834	1.346061658
7	30	45.29	79.854	49.169	3.879	15.581	12.07859011	1.421409885

Table A2.18 Flow diameter determination experiment (Run 2): results for the Mix oil sample at 30 °C

Time	T	Pipe Mass	Pipe+Oil+2 Plugs+Balloon	Pipe+Wax Layer	Wax Layer	Removed Oil	Flow Diameter	Wax Layer Thickness
hr	°C	g	Mass, g	Mass, g	Mass, g	Mass, g	mm	(2*hw), mm
1	30	45.29	79.854	47.882	2.592	16.868	12.56754289	0.932457106
2	30	45.29	79.854	48.135	2.845	16.615	12.47293769	1.027062309
3	30	45.29	79.854	48.425	3.135	16.325	12.36360652	1.136393478
4	30	45.29	79.854	48.592	3.302	16.158	12.30020591	1.199794086
5	30	45.29	79.854	48.771	3.481	15.979	12.23188469	1.268115308
6	30	45.29	79.854	48.973	3.683	15.777	12.15432354	1.345676461
7	30	45.29	79.854	49.187	3.897	15.563	12.07161118	1.428388816

Table A2.19 Flow diameter determination experiment (Run 3): results for the Mix oil sample at 30 °C

Time	T	Pipe Mass	Pipe+Oil+2 Plugs+Balloon	Pipe+Wax Layer	Wax Layer	Removed Oil	Flow Diameter	Wax Layer Thickness
hr	°C	g	Mass, g	Mass, g	Mass, g	Mass, g	mm	(2*hw), mm
1	30	45.29	79.854	47.886	2.596	16.864	12.5660527	0.933947299
2	30	45.29	79.854	48.121	2.831	16.629	12.47819151	1.021808491
3	30	45.29	79.854	48.394	3.104	16.356	12.37533975	1.124660246
4	30	45.29	79.854	48.542	3.252	16.208	12.31922235	1.180777646
5	30	45.29	79.854	48.762	3.472	15.988	12.23532895	1.264671055
6	30	45.29	79.854	48.969	3.679	15.781	12.15586421	1.344135793
7	30	45.29	79.854	49.193	3.903	15.557	12.06928398	1.430716024

Table A2.20 Flow diameter determination experiment (Run 4): results for the Mix oil sample at 30 °C

Time	T	Pipe Mass	Pipe+Oil+2 Plugs+Balloon	Pipe+Wax Layer	Wax Layer	Removed Oil	Flow Diameter	Wax Layer Thickness
hr	°C	g	Mass, g	Mass, g	Mass, g	Mass, g	mm	(2*hw), mm
1	30	45.29	79.854	47.892	2.602	16.858	12.56381708	0.93618292
2	30	45.29	79.854	48.103	2.813	16.647	12.48494317	1.015056832
3	30	45.29	79.854	48.427	3.137	16.323	12.36284916	1.137150843
4	30	45.29	79.854	48.624	3.334	16.126	12.28801995	1.211980051
5	30	45.29	79.854	48.793	3.503	15.957	12.22346132	1.276538681
6	30	45.29	79.854	49.002	3.712	15.748	12.14314786	1.356852144
7	30	45.29	79.854	49.195	3.905	15.555	12.06850814	1.431491859

Table A2.21 Flow diameter determination experiment (Run 5): results for the Mix oil sample at 30 °C

Time	T	Pipe Mass	Pipe+Oil+2 Plugs+Balloon	Pipe+Wax Layer	Wax Layer	Removed Oil	Flow Diameter	Wax Layer Thickness
hr	°C	g	Mass, g	Mass, g	Mass, g	Mass, g	mm	(2*hw), mm
1	30	45.29	79.854	47.879	2.589	16.871	12.56866042	0.931339577
2	30	45.29	79.854	48.086	2.796	16.664	12.49131638	1.008683615
3	30	45.29	79.854	48.419	3.129	16.331	12.36587834	1.134121661
4	30	45.29	79.854	48.611	3.321	16.139	12.29297195	1.207028046
5	30	45.29	79.854	48.774	3.484	15.976	12.23073639	1.269263609
6	30	45.29	79.854	48.964	3.674	15.786	12.15778977	1.342210234
7	30	45.29	79.854	49.159	3.869	15.591	12.08246556	1.417534443

Table A2.22 Flow diameter determination experiment (Run 6): results for the Mix oil sample at 30 °C

Time	T	Pipe Mass	Pipe+Oil+2 Plugs+Balloon	Pipe+Wax Layer	Wax Layer	Removed Oil	Flow Diameter	Wax Layer Thickness
hr	°C	g	Mass, g	Mass, g	Mass, g	Mass, g	mm	(2*hw), mm
1	30	45.29	79.854	47.871	2.581	16.879	12.57164001	0.928359986
2	30	45.29	79.854	48.074	2.784	16.676	12.49581317	1.004186831
3	30	45.29	79.854	48.421	3.131	16.329	12.36512111	1.134878887
4	30	45.29	79.854	48.599	3.309	16.151	12.29754127	1.202458734
5	30	45.29	79.854	48.795	3.505	15.955	12.22269527	1.27730473
6	30	45.29	79.854	48.981	3.691	15.769	12.15124162	1.348758381
7	30	45.29	79.854	49.193	3.903	15.557	12.06928398	1.430716024

Table A2.23 Flow diameter determination experiment (Run 7): results for the Mix oil sample at 30 °C

Time	T	Pipe Mass	Pipe+Oil+2 Plugs+Balloon	Pipe+Wax Layer	Wax Layer	Removed Oil	Flow Diameter	Wax Layer Thickness
hr	°C	g	Mass, g	Mass, g	Mass, g	Mass, g	mm	(2*hw), mm
1	30	45.29	79.854	47.878	2.588	16.872	12.56903291	0.93096709
2	30	45.29	79.854	48.118	2.828	16.632	12.47931704	1.020682961
3	30	45.29	79.854	48.415	3.125	16.335	12.36739265	1.132607348
4	30	45.29	79.854	48.595	3.305	16.155	12.29906399	1.200936007
5	30	45.29	79.854	48.769	3.479	15.981	12.23265017	1.267349835
6	30	45.29	79.854	48.97	3.68	15.78	12.15547906	1.344520942
7	30	45.29	79.854	49.179	3.889	15.571	12.07471343	1.425286571

Table A2.24 Average of flow diameter determination of all runs for the Mix oil sample at 30°C

Time Hr	T°C	Rnu 1	Rnu 2	Rnu 3	Rnu 4	Rnu 5	Rnu 6	Rnu 7	Avarge of Flow Diameter mm
1	30	12.56344444	12.56754289	12.5660527	12.56381708	12.56866042	12.57164001	12.56903291	12.56717007
2	30	12.48081759	12.47293769	12.47819151	12.48494317	12.49131638	12.49581317	12.47931704	12.48333379
3	30	12.39386318	12.36360652	12.37533975	12.36284916	12.36587834	12.36512111	12.36739265	12.37057867
4	30	12.32112238	12.30020591	12.31922235	12.28801995	12.29297195	12.29754127	12.29906399	12.30259254
5	30	12.23953727	12.23188469	12.23532895	12.22346132	12.23073639	12.22269527	12.23265017	12.23089915
6	30	12.15393834	12.15432354	12.15586421	12.14314786	12.15778977	12.15124162	12.15547906	12.15311206
7	30	12.07859011	12.07161118	12.06928398	12.06850814	12.08246556	12.06928398	12.07471343	12.07349377

Table A2.25 Flow diameter determination experiment (Run 1): results for Mix sample at 35 °C

Time	T	Pipe Mass	Pipe+Oil+2 Plugs+Balloon	Pipe+Wax Layer	Wax Layer	Removed Oil	Flow Diameter	Wax Layer Thickness
hr	°C	g	Mass, g	Mass, g	Mass, g	Mass, g	mm	(2*hw), mm
1	35	45.29	79.854	47.241	1.951	17.509	12.80410572	0.695894279
2	35	45.29	79.854	47.491	2.201	17.259	12.71236618	0.787633816
3	35	45.29	79.854	47.672	2.382	17.078	12.64553141	0.854468591
4	35	45.29	79.854	47.805	2.515	16.945	12.59619475	0.903805252
5	35	45.29	79.854	47.977	2.687	16.773	12.53210294	0.967897062
6	35	45.29	79.854	48.093	2.803	16.657	12.48869251	1.011307487
7	35	45.29	79.854	48.325	3.035	16.425	12.4014158	1.098584195

Table A2.26 Flow diameter determination experiment (Run 2) results for the Mix oil sample at 35 °C

Time	T	Pipe Mass	Pipe+Oil+2 Plugs+Balloon	Pipe+Wax Layer	Wax Layer	Removed Oil	Flow Diameter	Wax Layer Thickness
hr	°C	g	Mass, g	Mass, g	Mass, g	Mass, g	mm	(2*hw), mm
1	35	45.29	79.854	47.241	1.951	17.509	12.80410572	0.695894279
2	35	45.29	79.854	47.491	2.201	17.259	12.71236618	0.787633816
3	35	45.29	79.854	47.672	2.382	17.078	12.64553141	0.854468591
4	35	45.29	79.854	47.805	2.515	16.945	12.59619475	0.903805252
5	35	45.29	79.854	47.977	2.687	16.773	12.53210294	0.967897062
6	35	45.29	79.854	48.093	2.803	16.657	12.48869251	1.011307487
7	35	45.29	79.854	48.325	3.035	16.425	12.4014158	1.098584195

Table A2.27 Flow diameter determination experiment (Run 3): results for the Mix oil sample at 35 °C

Time	T	Pipe Mass	Pipe+Oil+2 Plugs+Balloon	Pipe+Wax Layer	Wax Layer	Removed Oil	Flow Diameter	Wax Layer Thickness
hr	°C	g	Mass, g	Mass, g	Mass, g	Mass, g	mm	(2*hw), mm
1	35	45.29	79.854	47.3	2.01	17.45	12.78251455	0.717485453
2	35	45.29	79.854	47.544	2.254	17.206	12.69283222	0.807167782
3	35	45.29	79.854	47.693	2.403	17.057	12.63775421	0.862245785
4	35	45.29	79.854	47.875	2.585	16.875	12.57015031	0.929849693
5	35	45.29	79.854	48.041	2.751	16.709	12.50817099	0.99182901
6	35	45.29	79.854	48.133	2.843	16.617	12.47368837	1.026311628
7	35	45.29	79.854	48.398	3.108	16.352	12.37382641	1.126173586

Table A2.28 Flow diameter determination experiment (Run 4): results for Mix sample at 35 °C

Time	T	Pipe Mass	Pipe+Oil+2 Plugs+Balloon	Pipe+Wax Layer	Wax Layer	Removed Oil	Flow Diameter	Wax Layer Thickness
hr	°C	g	Mass, g	Mass, g	Mass, g	Mass, g	mm	(2*hw), mm
1	35	45.29	79.854	47.222	1.932	17.528	12.81105106	0.688948935
2	35	45.29	79.854	47.517	2.227	17.233	12.70278724	0.797212763
3	35	45.29	79.854	47.681	2.391	17.069	12.64219891	0.857801088
4	35	45.29	79.854	47.777	2.487	16.973	12.60659746	0.893402541
5	35	45.29	79.854	47.983	2.693	16.767	12.52986126	0.97013874
6	35	45.29	79.854	48.088	2.798	16.662	12.49056676	1.009433236
7	35	45.29	79.854	48.275	2.985	16.475	12.42027728	1.079722715

Table A2.29 Flow diameter determination experiment (Run 5): results for the Mix oil sample at 35 °C

Time	T	Pipe Mass	Pipe+Oil+2 Plugs+Balloon	Pipe+Wax Layer	Wax Layer	Removed Oil	Flow Diameter	Wax Layer Thickness
hr	°C	g	Mass, g	Mass, g	Mass, g	Mass, g	mm	(2*hw), mm
1	35	45.29	79.854	47.259	1.969	17.491	12.79752244	0.702477555
2	35	45.29	79.854	47.487	2.197	17.263	12.71383923	0.786160772
3	35	45.29	79.854	47.698	2.408	17.052	12.6359018	0.864098204
4	35	45.29	79.854	47.971	2.681	16.779	12.53434422	0.965655784
5	35	45.29	79.854	47.985	2.695	16.765	12.52911394	0.970886056
6	35	45.29	79.854	48.075	2.785	16.675	12.4954385	1.004561501
7	35	45.29	79.854	48.321	3.031	16.429	12.40292578	1.097074221

Table A2.30 Flow diameter determination experiment (Run 6): results for the Mix oil sample at 35 °C

Time	T	Pipe Mass	Pipe+Oil+2 Plugs+Balloon	Pipe+Wax Layer	Wax Layer	Removed Oil	Flow Diameter	Wax Layer Thickness
hr	°C	g	Mass, g	Mass, g	Mass, g	Mass, g	mm	(2*hw), mm
1	35	45.29	79.854	47.302	2.012	17.448	12.781782	0.718217996
2	35	45.29	79.854	47.519	2.229	17.231	12.7020501	0.797949904
3	35	45.29	79.854	47.725	2.435	17.025	12.62589404	0.87410596
4	35	45.29	79.854	47.958	2.668	16.792	12.53919894	0.960801058
5	35	45.29	79.854	48.085	2.795	16.665	12.49169118	1.008308821
6	35	45.29	79.854	48.093	2.803	16.657	12.48869251	1.011307487
7	35	45.29	79.854	48.341	3.051	16.409	12.39537407	1.10462593

Table A2.31 Flow diameter determination experiment (Run 7): results for Mix sample at 35 °C

Time	T	Pipe Mass	Pipe+Oil+2 Plugs+Balloon	Pipe+Wax Layer	Wax Layer	Removed Oil	Flow Diameter	Wax Layer Thickness
hr	°C	g	Mass, g	Mass, g	Mass, g	Mass, g	mm	(2*hw), mm
1	35	45.29	79.854	47.398	2.108	17.352	12.74657042	0.753429584
2	35	45.29	79.854	47.508	2.218	17.242	12.70610384	0.793896156
3	35	45.29	79.854	47.687	2.397	17.063	12.63997676	0.860023242
4	35	45.29	79.854	47.876	2.586	16.874	12.56977785	0.930222148
5	35	45.29	79.854	47.992	2.702	16.758	12.52649799	0.97350201
6	35	45.29	79.854	48.203	2.913	16.547	12.44738761	1.052612395
7	35	45.29	79.854	48.421	3.131	16.329	12.36512111	1.134878887

Table A2.32 Average of flow diameter determination of all runs for the Mix oil sample at 35°C

Time Hr	T °C	Rnu 1	Rnu 2	Rnu 3	Rnu 4	Rnu 5	Rnu 6	Rnu 7	Avarge flow diameter mm
1	35	12.80410572	12.80410572	12.78251455	12.81105106	12.79752244	12.781782	12.74657042	12.78966456
2	35	12.71236618	12.71236618	12.69283222	12.70278724	12.71383923	12.7020501	12.70610384	12.70604928
3	35	12.64553141	12.64553141	12.63775421	12.64219891	12.6359018	12.62589404	12.63997676	12.63896979
4	35	12.59619475	12.59619475	12.57015031	12.60659746	12.53434422	12.53919894	12.56977785	12.57320832
5	35	12.53210294	12.53210294	12.50817099	12.52986126	12.52911394	12.49169118	12.52649799	12.52136303
6	35	12.48869251	12.48869251	12.47368837	12.49056676	12.4954385	12.48869251	12.44738761	12.48187983
7	35	12.4014158	12.4014158	12.37382641	12.42027728	12.40292578	12.39537407	12.36512111	12.39433661

3. For Remal Sample

Table A2.33 Flow diameter determination experiment (Run 1): results for the Remal oil sample at 35 °C

Time	T	Pipe Mass	Pipe+Oil+2 Plugs+Balloon	Pipe+Wax Layer	Wax Layer	Removed Oil	Flow Diameter	Wax Layer Thickness
hr	°C	g	Mass, g	Mass, g	Mass, g	Mass, g	mm	(2*hw), mm
1	35	45.38	79.954	48.341	2.961	16.509	12.43025106	1.069748944
2	35	45.38	79.954	48.638	3.258	16.212	12.31793233	1.182067667
3	35	45.38	79.954	48.867	3.487	15.983	12.23062544	1.26937456
4	35	45.38	79.954	49.092	3.712	15.758	12.14423226	1.35576774
5	35	45.38	79.954	49.343	3.963	15.507	12.04712482	1.452875184
6	35	45.38	79.954	49.581	4.201	15.269	11.95431826	1.545681736
7	35	45.38	79.954	49.847	4.467	15.003	11.84973317	1.650266829

Table A2.34 Flow diameter determination experiment (Run 2): results for the Remal oil sample at 35 °C

Time	T	Pipe Mass	Pipe+Oil+2 Plugs+Balloon	Pipe+Wax Layer	Wax Layer	Removed Oil	Flow Diameter	Wax Layer Thickness
hr	°C	g	Mass, g	Mass, g	Mass, g	Mass, g	mm	(2*hw), mm
1	35	45.38	79.954	48.344	2.964	16.506	12.4291216	1.070878402
2	35	45.38	79.954	48.624	3.244	16.226	12.32324981	1.176750191
3	35	45.38	79.954	48.872	3.492	15.978	12.22871222	1.271287777
4	35	45.38	79.954	49.075	3.695	15.775	12.1507812	1.349218803
5	35	45.38	79.954	49.319	3.939	15.531	12.05644381	1.443556192
6	35	45.38	79.954	49.593	4.213	15.257	11.94961986	1.550380145
7	35	45.38	79.954	49.871	4.491	14.979	11.84025149	1.659748514

Table A2.35 Flow diameter determination experiment (Run 3): results for the Remal oil sample at 35 °C

Time	T	Pipe Mass	Pipe+Oil+2 Plugs+Balloon	Pipe+Wax Layer	Wax Layer	Removed Oil	Flow Diameter	Wax Layer Thickness
hr	°C	g	Mass, g	Mass, g	Mass, g	Mass, g	mm	(2*hw), mm
1	35	45.38	79.954	48.326	2.946	16.524	12.43589681	1.064103192
2	35	45.38	79.954	48.611	3.231	16.239	12.32818541	1.171814589
3	35	45.38	79.954	48.864	3.484	15.986	12.23177323	1.268226773
4	35	45.38	79.954	49.081	3.701	15.769	12.14847021	1.35152979
5	35	45.38	79.954	49.313	3.933	15.537	12.05877243	1.44122757
6	35	45.38	79.954	49.578	4.198	15.272	11.95549258	1.544507422
7	35	45.38	79.954	49.822	4.442	15.028	11.85960186	1.640398136

Table A2.36 Flow diameter determination experiment (Run 4): results for the Remal oil sample at 35 °C

Time	T	Pipe Mass	Pipe+Oil+2 Plugs+Balloon	Pipe+Wax Layer	Wax Layer	Removed Oil	Flow Diameter	Wax Layer Thickness
hr	°C	g	Mass, g	Mass, g	Mass, g	Mass, g	mm	(2*hw), mm
1	35	45.38	79.954	48.329	2.949	16.521	12.43476786	1.065232138
2	35	45.38	79.954	48.626	3.246	16.224	12.32249031	1.17750969
3	35	45.38	79.954	48.882	3.502	15.968	12.22488489	1.275115111
4	35	45.38	79.954	49.084	3.704	15.766	12.14731455	1.352685448
5	35	45.38	79.954	49.347	3.967	15.503	12.04557095	1.45442905
6	35	45.38	79.954	49.575	4.195	15.275	11.95666678	1.543333224
7	35	45.38	79.954	49.782	4.402	15.068	11.87537472	1.624625284

Table A2.37 Flow diameter determination experiment (Run 5): results for the Remal oil sample at 35 °C

Time	T	Pipe Mass	Pipe+Oil+2 Plugs+Balloon	Pipe+Wax Layer	Wax Layer	Removed Oil	Flow Diameter	Wax Layer Thickness
hr	°C	g	Mass, g	Mass, g	Mass, g	Mass, g	mm	(2*hw), mm
1	35	45.38	79.954	48.338	2.958	16.512	12.43138041	1.068619589
2	35	45.38	79.954	48.631	3.251	16.219	12.32059136	1.179408642
3	35	45.38	79.954	48.868	3.488	15.982	12.23024282	1.26975718
4	35	45.38	79.954	49.069	3.689	15.781	12.15309174	1.346908256
5	35	45.38	79.954	59.337	13.957	5.513	7.183126467	6.316873533
6	35	45.38	79.954	49.585	4.205	15.265	11.95275233	1.547247667
7	35	45.38	79.954	49.781	4.401	15.069	11.87576877	1.624231231

Table A2.38 Flow diameter determination experiment (Run 6): results for the Remal oil sample at 35 °C

Time	T	Pipe Mass	Pipe+Oil+2 Plugs+Balloon	Pipe+Wax Layer	Wax Layer	Removed Oil	Flow Diameter	Wax Layer Thickness
hr	°C	g	Mass, g	Mass, g	Mass, g	Mass, g	mm	(2*hw), mm
1	35	45.38	79.954	48.378	2.998	16.472	12.41631389	1.083686108
2	35	45.38	79.954	48.661	3.281	16.189	12.30919149	1.190808507
3	35	45.38	79.954	48.902	3.522	15.948	12.21722663	1.282773374
4	35	45.38	79.954	49.098	3.718	15.752	12.14192003	1.358079973
5	35	45.38	79.954	49.319	3.939	15.531	12.05644381	1.443556192
6	35	45.38	79.954	49.591	4.211	15.259	11.95040305	1.549596948
7	35	45.38	79.954	49.638	4.258	15.212	11.93198434	1.568015656

Table A2.39 Flow diameter determination experiment (Run 7): results for the Remal oil sample at 35 °C

Time	T	Pipe Mass	Pipe+Oil+2 Plugs+Balloon	Pipe+Wax Layer	Wax Layer	Removed Oil	Flow Diameter	Wax Layer Thickness
hr	°C	g	Mass, g	Mass, g	Mass, g	Mass, g	mm	(2*hw), mm
1	35	45.38	79.954	48.338	2.958	16.512	12.43138041	1.068619589
2	35	45.38	79.954	48.631	3.251	16.219	12.32059136	1.179408642
3	35	45.38	79.954	48.882	3.502	15.968	12.22488489	1.275115111
4	35	45.38	79.954	49.089	3.709	15.761	12.14538821	1.354611789
5	35	45.38	79.954	49.321	3.941	15.529	12.0556675	1.4443325
6	35	45.38	79.954	49.588	4.208	15.262	11.95157775	1.54842225
7	35	45.38	79.954	49.812	4.432	15.038	11.86354704	1.636452957

Table A2.40 Average of flow diameter determination of all runs for the Remal oil sample at 35°C

Time Hr	T °C	Rnu 1	Rnu 2	Rnu 3	Rnu 4	Rnu 5	Rnu 6	Rnu 7	Avarge flow diameter mm
1	35	12.43025106	12.4291216	12.43589681	12.43476786	12.43138041	12.41631389	12.43138041	12.42987315
2	35	12.31793233	12.32324981	12.32818541	12.32249031	12.32059136	12.30919149	12.32059136	12.32031887
3	35	12.23062544	12.22871222	12.23177323	12.22488489	12.23024282	12.21722663	12.22488489	12.22690716
4	35	12.14423226	12.1507812	12.14847021	12.14731455	12.15309174	12.14192003	12.14538821	12.14731403
5	35	12.04712482	12.05644381	12.05877243	12.04557095	7.183126467	12.05644381	12.0556675	11.35759283
6	35	11.95431826	11.94961986	11.95549258	11.95666678	11.95275233	11.95040305	11.95157775	11.9529758
7	35	11.84973317	11.84025149	11.85960186	11.87537472	11.87576877	11.93198434	11.86354704	11.87089448

Table A2.41 Flow diameter determination experiment (Run 1): results for the Remal oil sample at 40 °C

Time	T	Pipe Mass	Pipe+Oil+2 Plugs+Balloon	Pipe+Wax Layer	Wax Layer	Removed Oil	Flow Diameter	Wax Layer Thickness
hr	°C	g	Mass, g	Mass, g	Mass, g	Mass, g	mm	(2*hw), mm
1	40	45.38	79.954	47.812	2.432	17.038	12.62783281	0.872167186
2	40	45.38	79.954	48.124	2.744	16.726	12.51167811	0.98832189
3	40	45.38	79.954	48.427	3.047	16.423	12.39783245	1.102167546
4	40	45.38	79.954	48.726	3.346	16.124	12.28445549	1.215544506
5	40	45.38	79.954	49.035	3.655	15.815	12.16617655	1.333823446
6	40	45.38	79.954	49.297	3.917	15.553	12.06497989	1.435020107
7	40	45.38	79.954	49.631	4.251	15.219	11.93472936	1.565270643

Table A2.42 Flow diameter determination experiment (Run 2): results for the Remal oil sample at 40 °C

Time	T	Pipe Mass	Pipe+Oil+2 Plugs+Balloon	Pipe+Wax Layer	Wax Layer	Removed Oil	Flow Diameter	Wax Layer Thickness
hr	°C	g	Mass, g	Mass, g	Mass, g	Mass, g	mm	(2*hw), mm
1	40	45.38	79.954	47.778	2.398	17.072	12.6404262	0.859573796
2	40	45.38	79.954	48.102	2.722	16.748	12.51990382	0.980096179
3	40	45.38	79.954	48.503	3.123	16.347	12.36911273	1.130887265
4	40	45.38	79.954	48.728	3.348	16.122	12.2836936	1.216306404
5	40	45.38	79.954	49.041	3.661	15.809	12.16386849	1.336131507
6	40	45.38	79.954	49.282	3.902	15.568	12.07079649	1.429203509
7	40	45.38	79.954	49.612	4.232	15.238	11.94217693	1.557823073

Table A2.43 Flow diameter determination experiment (Run 3): results for the Remal oil sample at 40 °C

Time	T	Pipe Mass	Pipe+Oil+2 Plugs+Balloon	Pipe+Wax Layer	Wax Layer	Removed Oil	Flow Diameter	Wax Layer Thickness
hr	°C	g	Mass, g	Mass, g	Mass, g	Mass, g	mm	(2*hw), mm
1	40	45.38	79.954	47.99	2.61	16.86	12.56169665	0.938303346
2	40	45.38	79.954	48.105	2.725	16.745	12.51878245	0.981217549
3	40	45.38	79.954	48.501	3.121	16.349	12.36986937	1.130130629
4	40	45.38	79.954	48.712	3.332	16.138	12.28978745	1.210212546
5	40	45.38	79.954	49.081	3.701	15.769	12.14847021	1.35152979
6	40	45.38	79.954	49.277	3.897	15.573	12.07273473	1.427265266
7	40	45.38	79.954	49.496	4.116	15.354	11.98754594	1.512454058

Table A2.44 Flow diameter determination experiment (Run 4): results for the Remal oil sample at 40 °C

Time	T	Pipe Mass	Pipe+Oil+2 Plugs+Balloon	Pipe+Wax Layer	Wax Layer	Removed Oil	Flow Diameter	Wax Layer Thickness
hr	°C	g	Mass, g	Mass, g	Mass, g	Mass, g	mm	(2*hw), mm
1	40	45.38	79.954	47.805	2.425	17.045	12.6304266	0.869573402
2	40	45.38	79.954	48.092	2.712	16.758	12.52364099	0.976359006
3	40	45.38	79.954	48.493	3.113	16.357	12.37289545	1.127104546
4	40	45.38	79.954	48.704	3.324	16.146	12.29283325	1.207166749
5	40	45.38	79.954	49.042	3.662	15.808	12.16348377	1.336516227
6	40	45.38	79.954	49.29	3.91	15.56	12.06769465	1.432305346
7	40	45.38	79.954	49.623	4.243	15.227	11.93786574	1.562134258

Table A2.45 Flow diameter determination experiment (Run 5): results for the Remal oil sample at 40 °C

Time	T	Pipe Mass	Pipe+Oil+2 Plugs+Balloon	Pipe+Wax Layer	Wax Layer	Removed Oil	Flow Diameter	Wax Layer Thickness
hr	°C	g	Mass, g	Mass, g	Mass, g	Mass, g	mm	(2*hw), mm
1	40	45.38	79.954	47.779	2.399	17.071	12.64005599	0.859944011
2	40	45.38	79.954	47.977	2.597	16.873	12.5665386	0.933461395
3	40	45.38	79.954	46.466	1.086	18.384	13.11715112	0.382848875
4	40	45.38	79.954	48.678	3.298	16.172	12.30272688	1.197273119
5	40	45.38	79.954	49.021	3.641	15.829	12.17156033	1.328439671
6	40	45.38	79.954	49.283	3.903	15.567	12.07040881	1.429591195
7	40	45.38	79.954	49.609	4.229	15.241	11.94335243	1.556647565

Table A2.46 Flow diameter determination experiment (Run 6): results for the Remal oil sample at 40 °C

Time	T	Pipe Mass	Pipe+Oil+2 Plugs+Balloon	Pipe+Wax Layer	Wax Layer	Removed Oil	Flow Diameter	Wax Layer Thickness
hr	°C	g	Mass, g	Mass, g	Mass, g	Mass, g	mm	(2*hw), mm
1	40	45.38	79.954	47.785	2.405	17.065	12.63783447	0.862165527
2	40	45.38	79.954	48.077	2.697	16.773	12.52924466	0.970755336
3	40	45.38	79.954	48.581	3.201	16.269	12.33956773	1.160432271
4	40	45.38	79.954	48.707	3.327	16.143	12.29169117	1.208308835
5	40	45.38	79.954	49.019	3.639	15.831	12.17232925	1.327670755
6	40	45.38	79.954	49.304	3.924	15.546	12.06226452	1.437735479
7	40	45.38	79.954	49.625	4.245	15.225	11.93708172	1.562918277

Table A2.47 Flow diameter determination experiment (Run 7): results for the Remal oil sample at 40 °C

Time	T	Pipe Mass	Pipe+Oil+2 Plugs+Balloon	Pipe+Wax Layer	Wax Layer	Removed Oil	Flow Diameter	Wax Layer Thickness
hr	°C	g	Mass, g	Mass, g	Mass, g	Mass, g	mm	(2*hw), mm
1	40	45.38	79.954	47.8	2.42	17.05	12.63227897	0.867721026
2	40	45.38	79.954	48.182	2.802	16.668	12.48996618	1.010033821
3	40	45.38	79.954	48.509	3.129	16.341	12.36684255	1.133157452
4	40	45.38	79.954	48.71	3.33	16.14	12.29054897	1.209451026
5	40	45.38	79.954	49.047	3.667	15.803	12.16155999	1.338440007
6	40	45.38	79.954	49.271	3.891	15.579	12.07506022	1.424939785
7	40	45.38	79.954	49.7	4.32	15.15	11.90764375	1.592356254

Table A2. 48 Average of flow diameter determination of all runs for the Remal oil sample at 40°C

Time Hr	T °C	Rnu 1	Rnu 2	Rnu 3	Rnu 4	Rnu 5	Rnu 6	Rnu 7	Avarge flow diameter mm
1	40	12.62783281	12.6404262	12.56169665	12.6304266	12.64005599	12.63783447	12.63227897	12.62436453
2	40	12.51167811	12.51990382	12.51878245	12.52364099	12.5665386	12.52924466	12.48996618	12.52282212
3	40	12.39783245	12.36911273	12.36986937	12.37289545	13.11715112	12.33956773	12.36684255	12.47618163
4	40	12.28445549	12.2836936	12.28978745	12.29283325	12.30272688	12.29169117	12.29054897	12.29081955
5	40	12.16617655	12.16386849	12.14847021	12.16348377	12.17156033	12.17232925	12.16155999	12.16392123
6	40	12.06497989	12.07079649	12.07273473	12.06769465	12.07040881	12.06226452	12.07506022	12.06913419
7	40	11.93472936	11.94217693	11.98754594	11.93786574	11.94335243	11.93708172	11.90764375	11.94148512

Appendix 3: Thixotropy Test Results

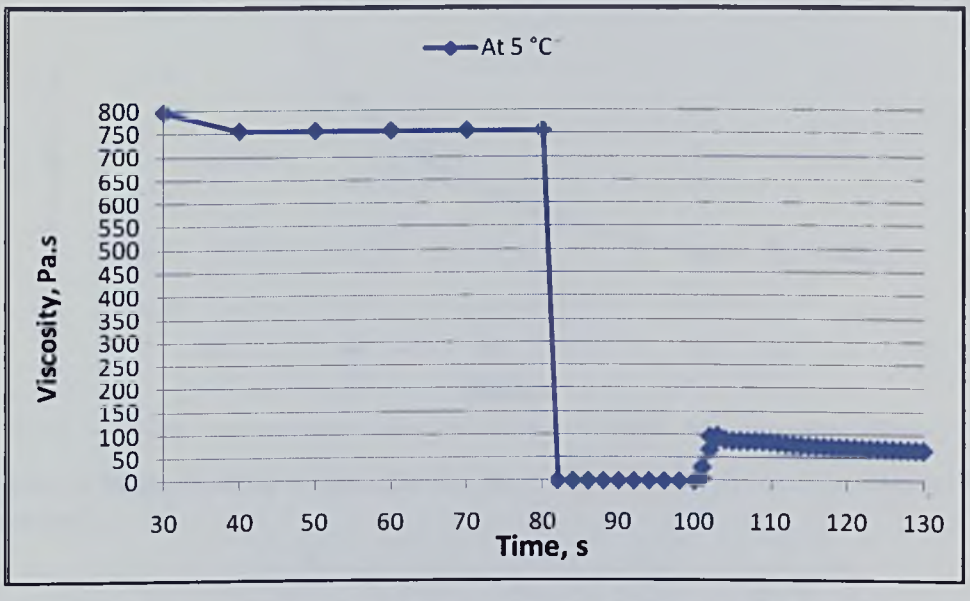

Figure A3.1 Time vs. viscosity: thixotropy phenomena test for BP oil sample under 0.1, 1000 and 0.1 1/s shear rates at 5 °C

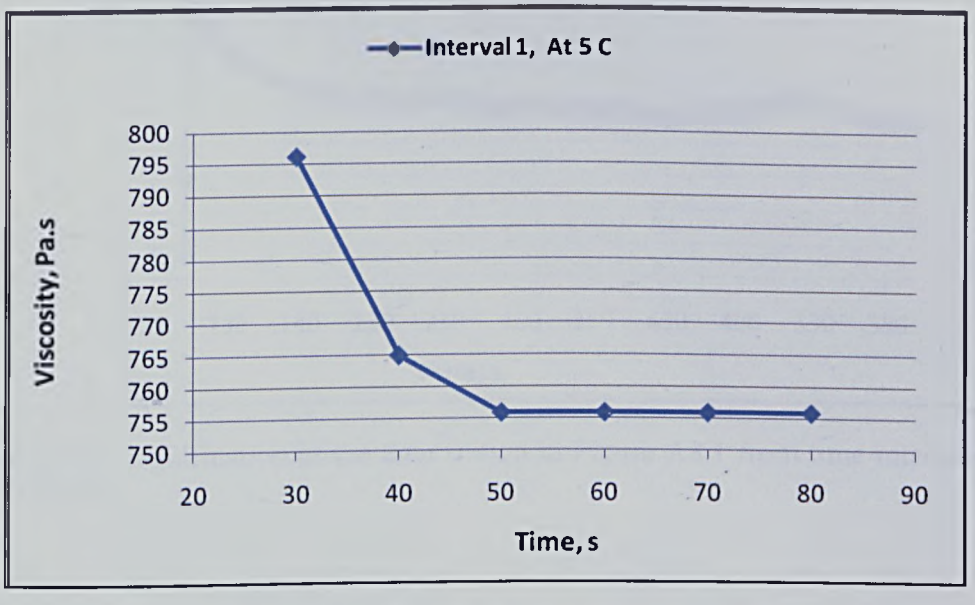

Figure A3.2 Magnification of the data shown in Figure A3.1 from time interval 20 to 80 second

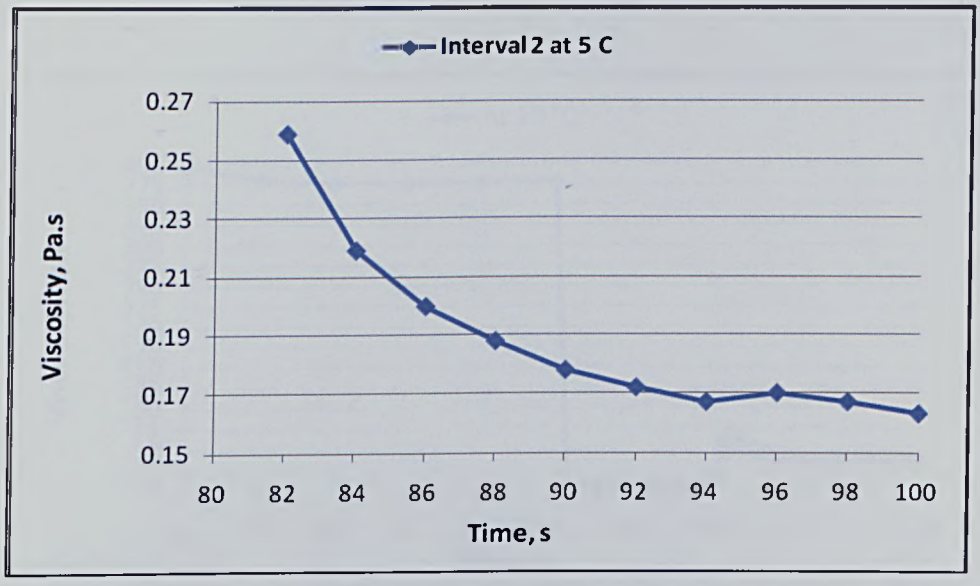

FigureA3.3 Magnification of the data shown in Figure A3.1 from time interval 80 to 100 second

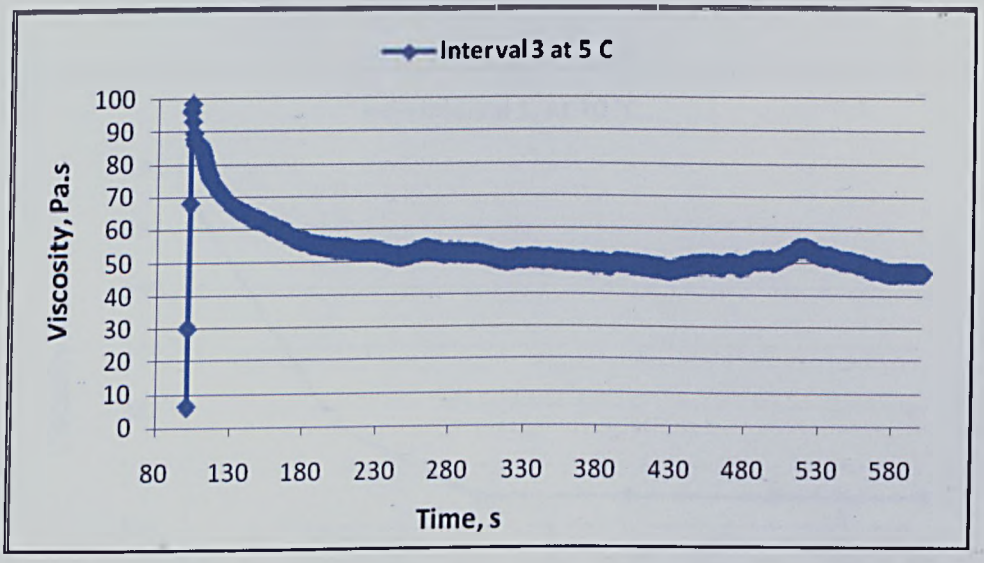

Figure A3.4 Magnification of the data shown in Figure A3.1 from time interval 100 to 580 second

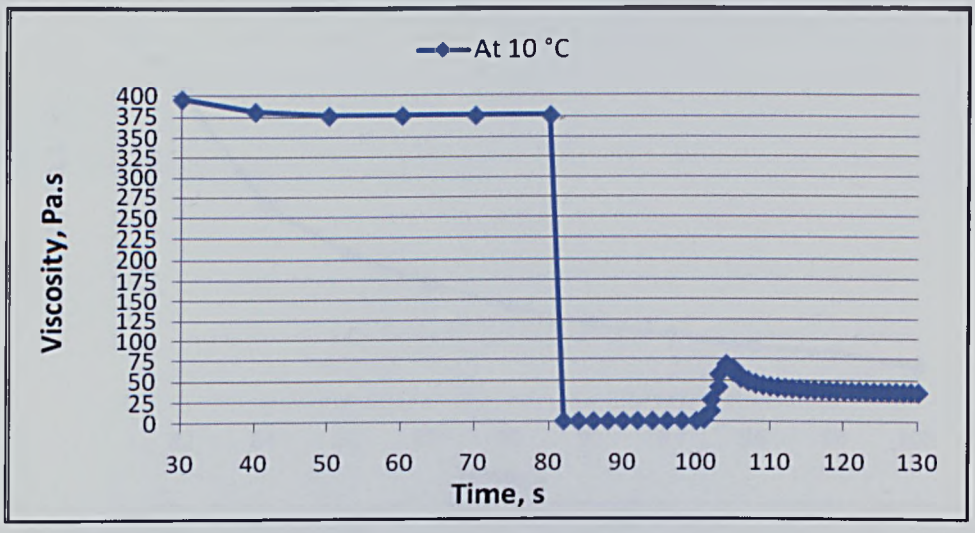

Figure A3.5 Time vs. viscosity: thixotropy phenomena test for BP oil sample under 0.1, 1000 and 0.1 1/s shear rates at 10 °C

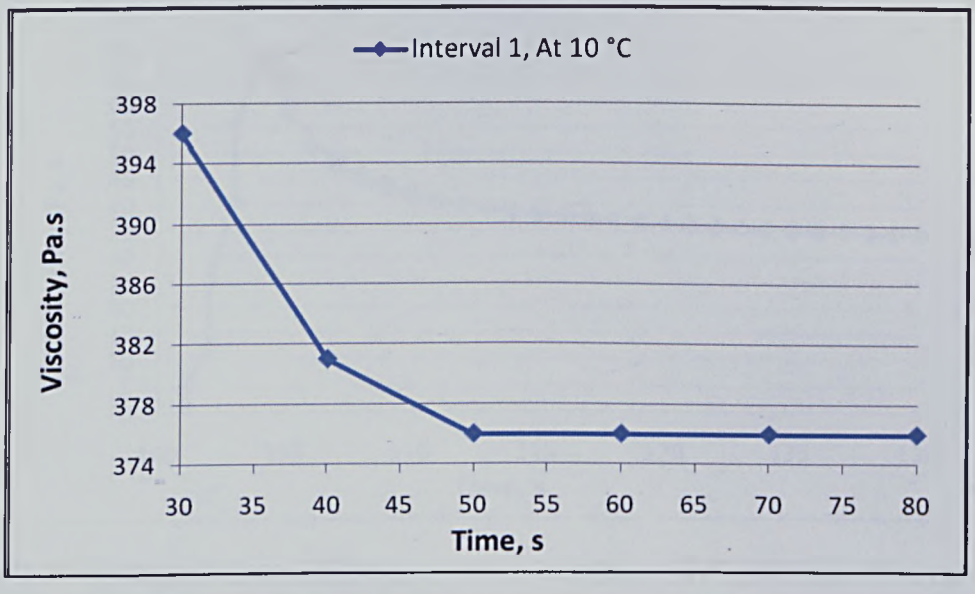

Figure A3.6 Magnification of the data shown in Figure A3.5 from time interval 20 to 80 second

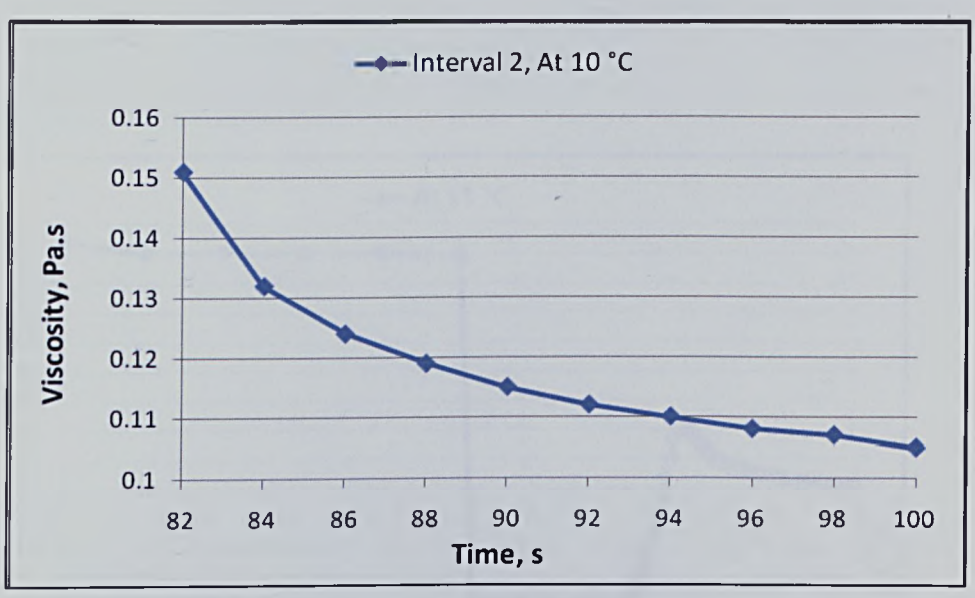

Figure A3.7 Magnification of the data shown in Figure A3.5 from time interval 80 to 100 second

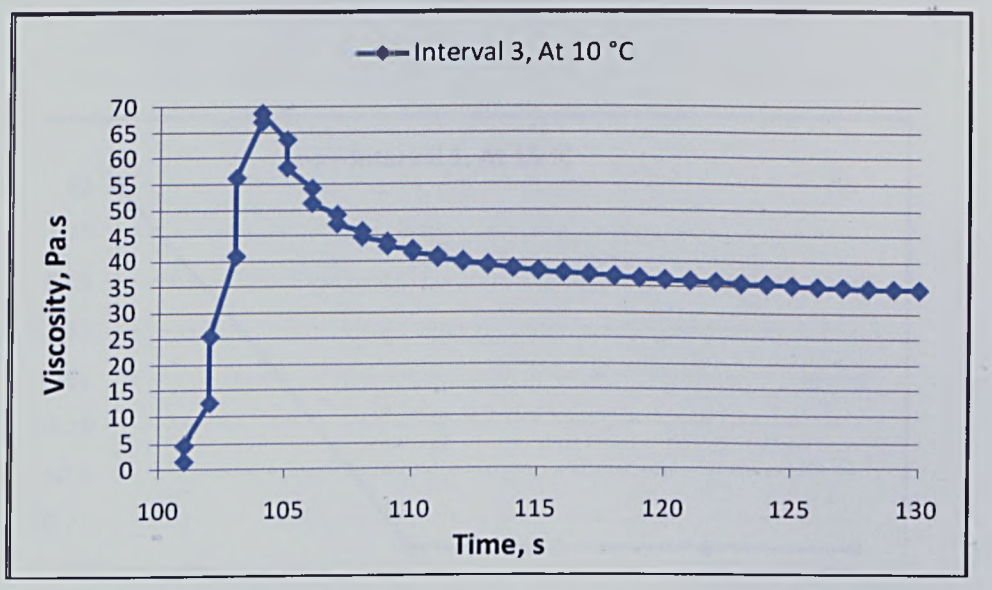

Figure A3.8 Magnification of the data shown in Figure A3.5 from time interval 100 to 130 second

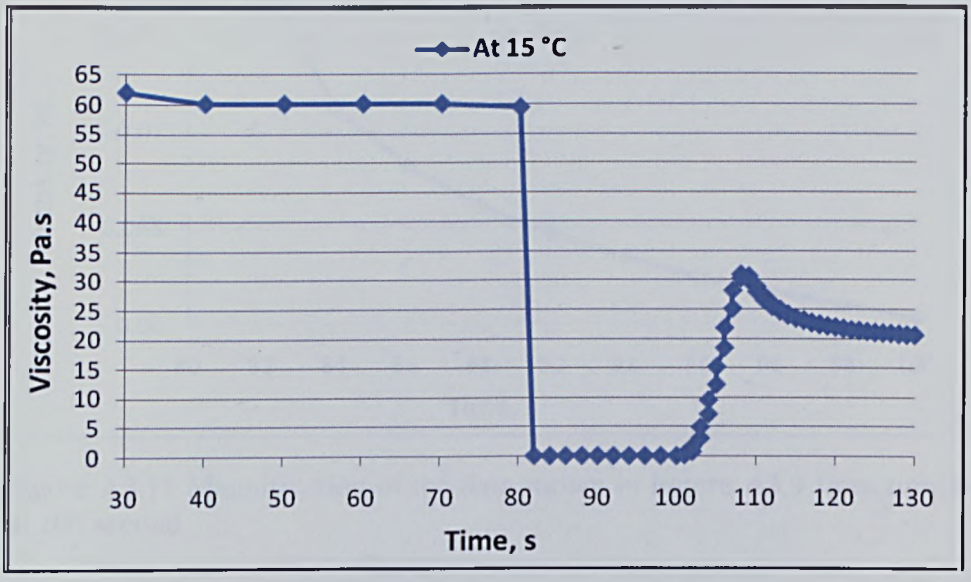

Figure A3.9 Time vs. viscosity: thixotropy phenomena test for BP oil sample under 0.1, 1000 and 0.1 1/s shear rates at 15 °C

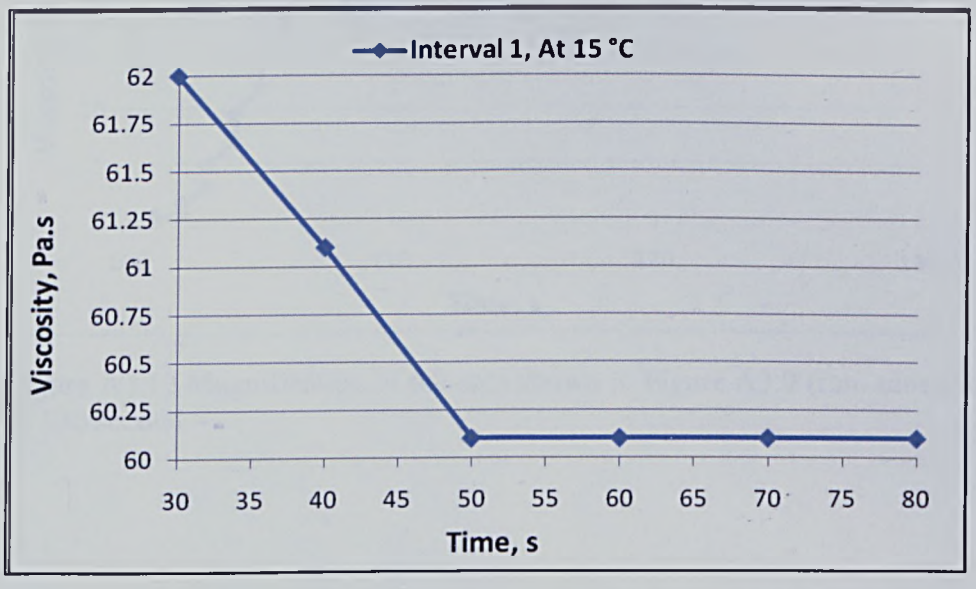

Figure A3.10 Magnification of the data shown in Figure A3.9 from time interval 20 to 80 second

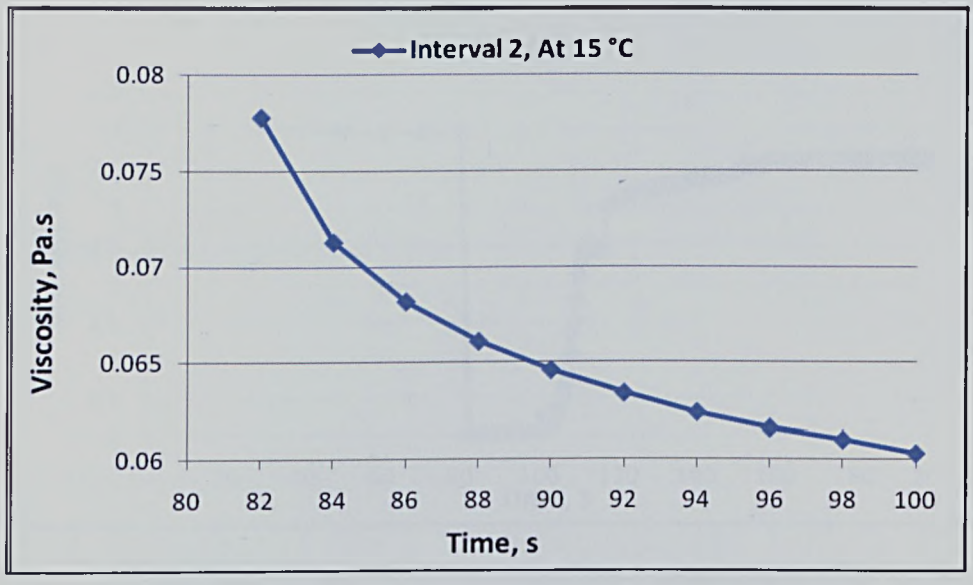

Figure A3.11 Magnification of the data shown in Figure A3.9 from time interval 80 to 100 second

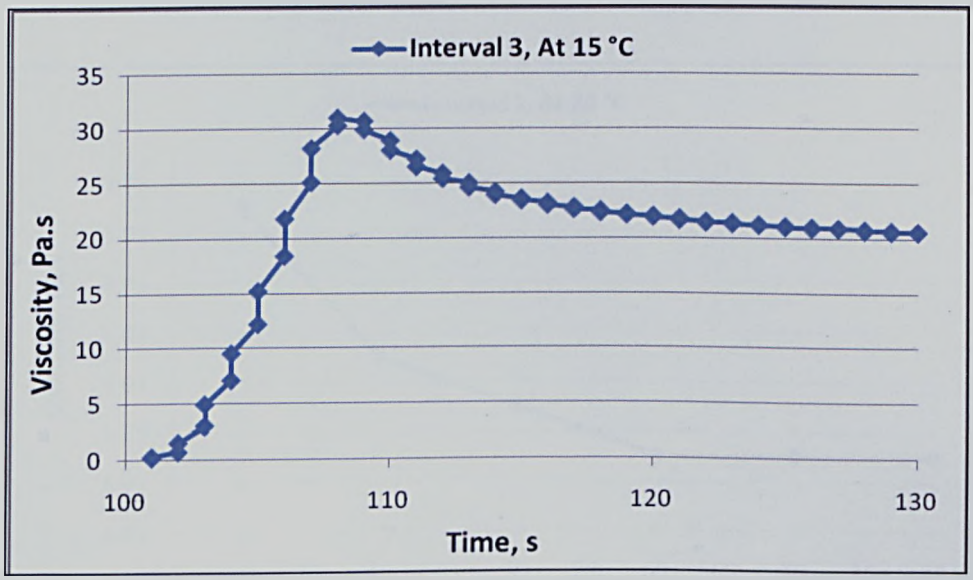

Figure A3.12 Magnification of the data shown in Figure A3.9 from time interval 100 to 130 second

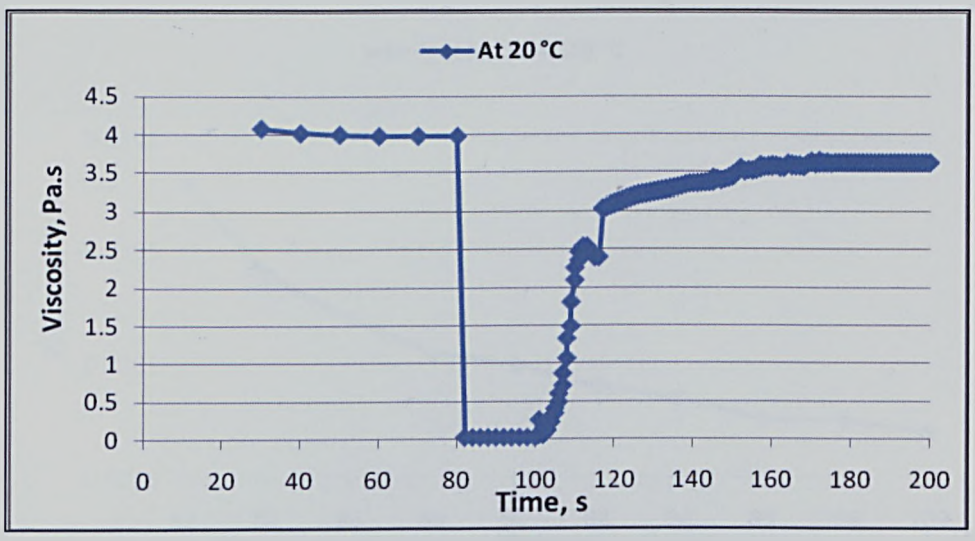

Figure A3.13 Time vs. viscosity: thixotropy phenomena test for BP oil sample under 0.1, 1000 and 0.1 1/s shear rates at 20 °C

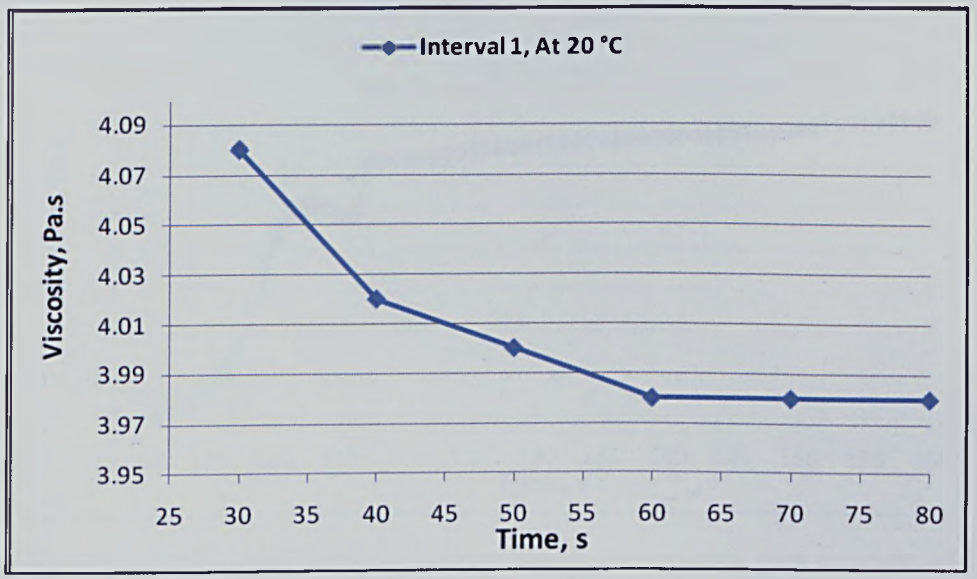

Figure A3.14 Magnification of the data shown in Figure A3.13 from time interval 20 to 80 second

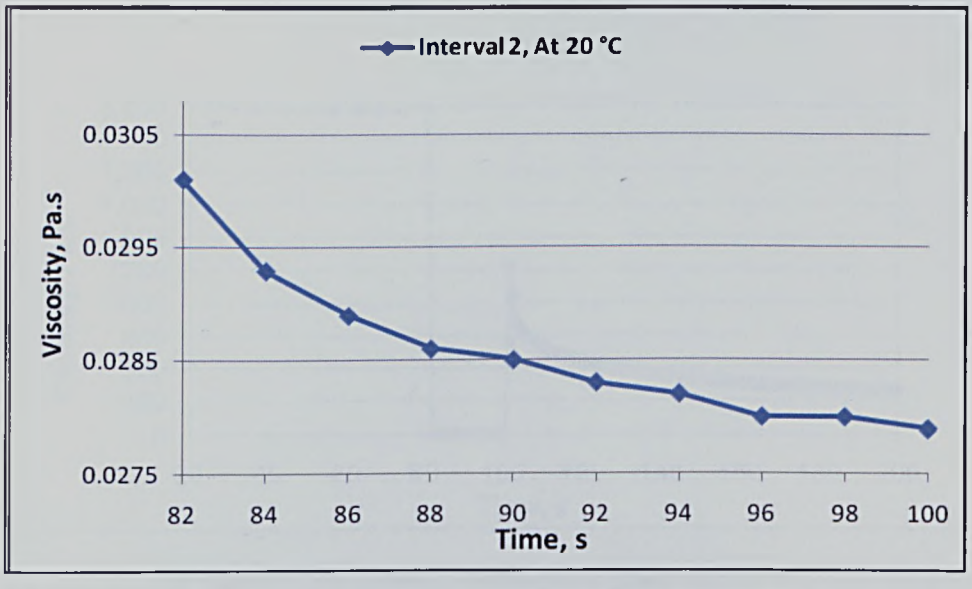

Figure A3.15 Magnification of the data shown in Figure A3.13 from time interval 80 to 100 second

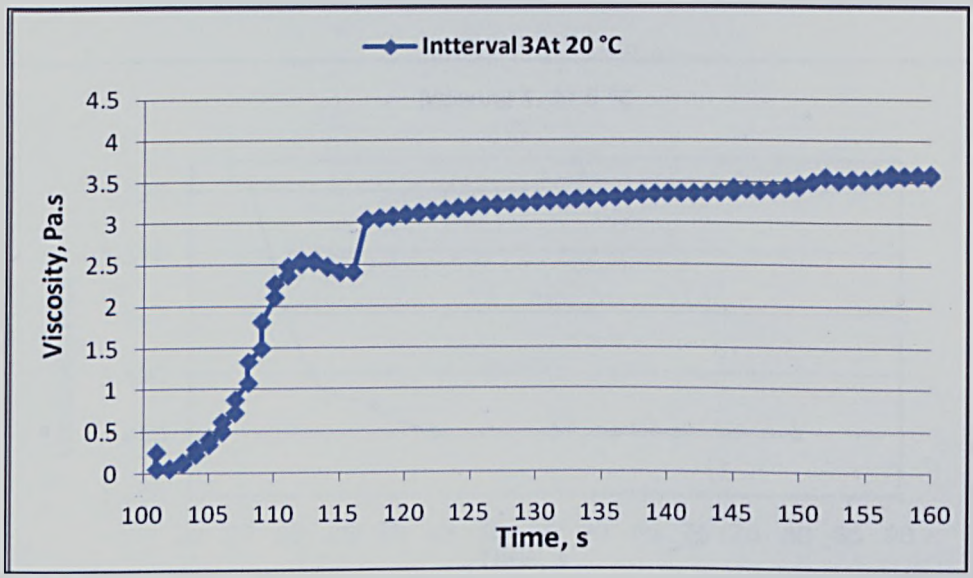

Figure A3.16 Magnification of the data shown in Figure A3.13 from time interval 20 to 80 second

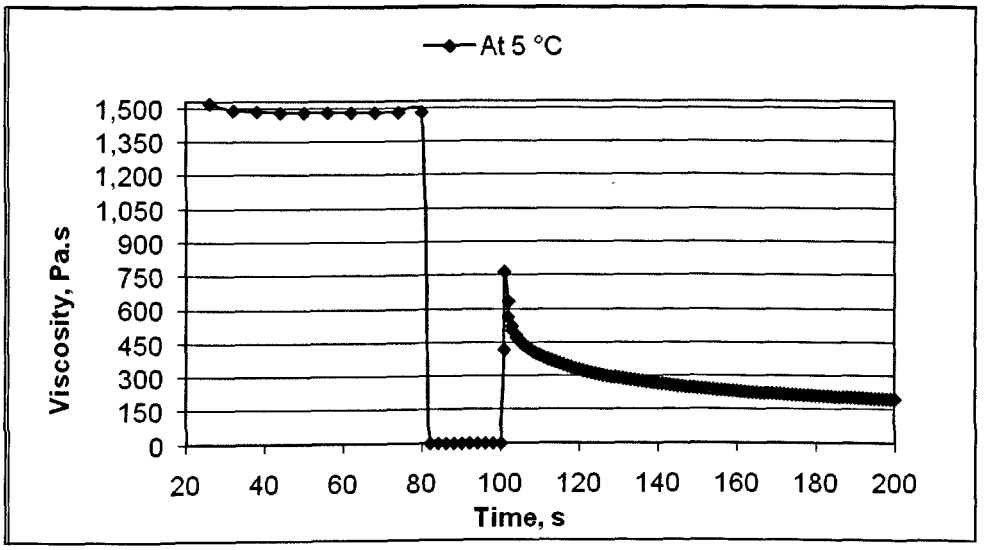

Figure A3.17 Time vs. viscosity: thixotropy phenomena test for Mix oil sample under 0.1, 1000 and 0.1 1/s shear rates at 5 °C

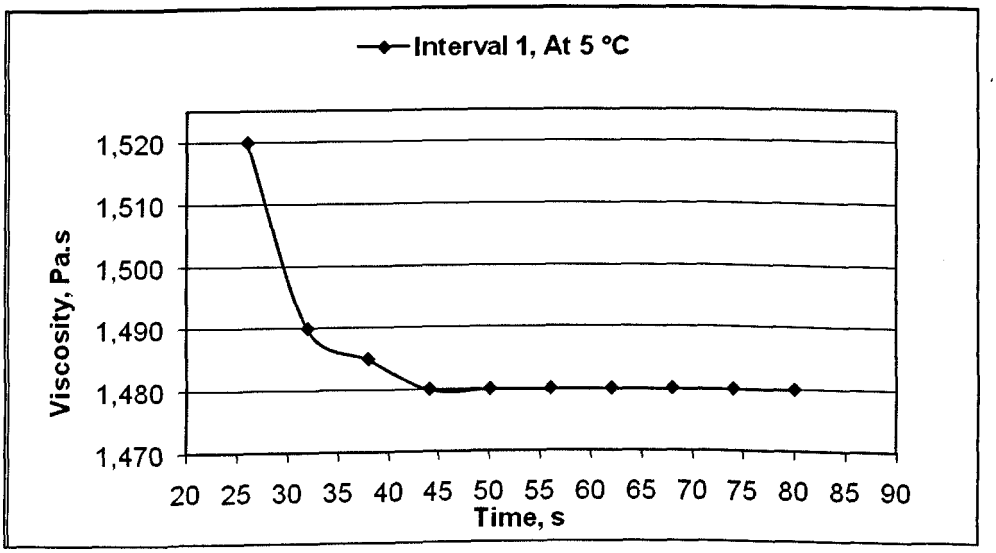

Figure A3.18 Magnification of the data shown in Figure A3.17 from time interval 20 to 80 second

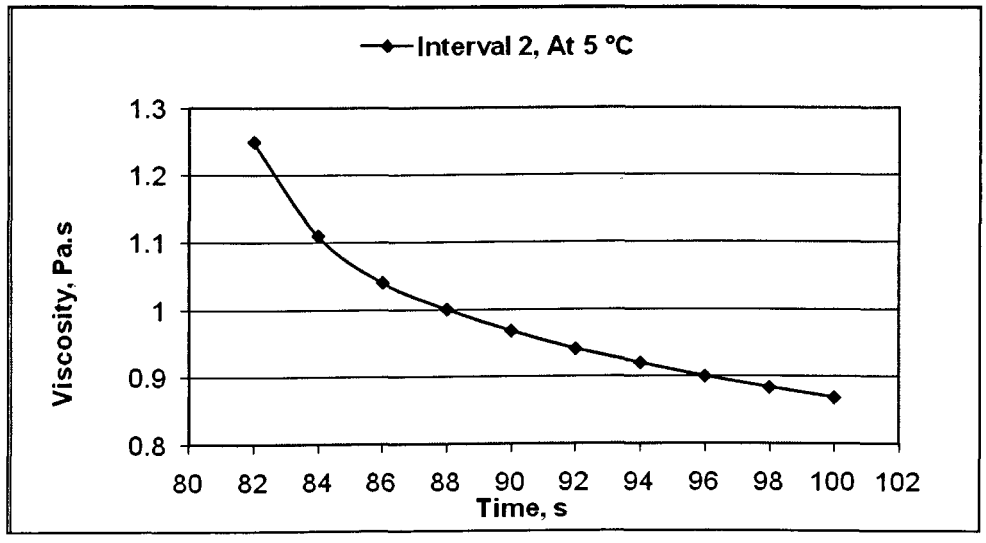

Figure A3.19 Magnification of the data shown in Figure A3.17 from time interval 80 to 100 second

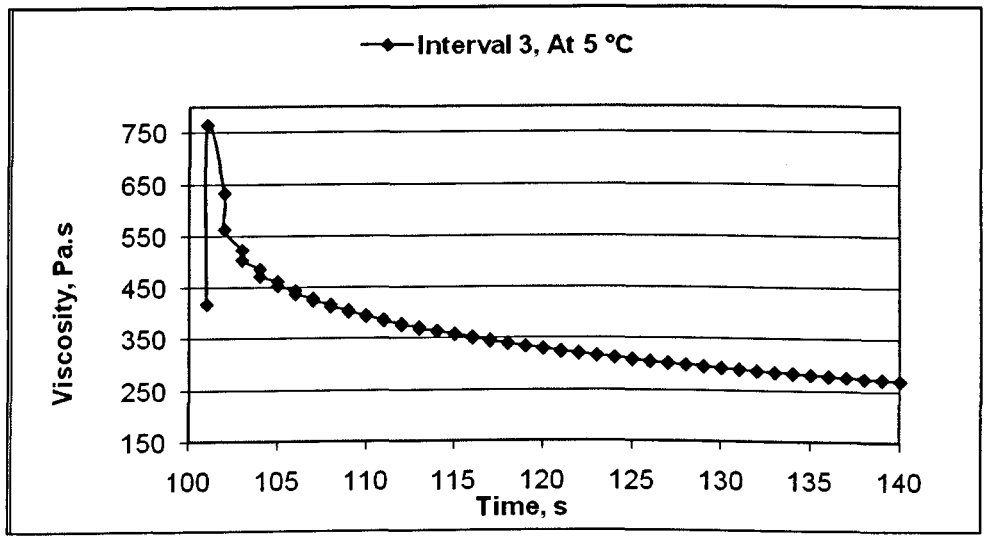

Figure A3.20 Magnification of the data shown in Figure A3.1 from time interval 100 to 140 second

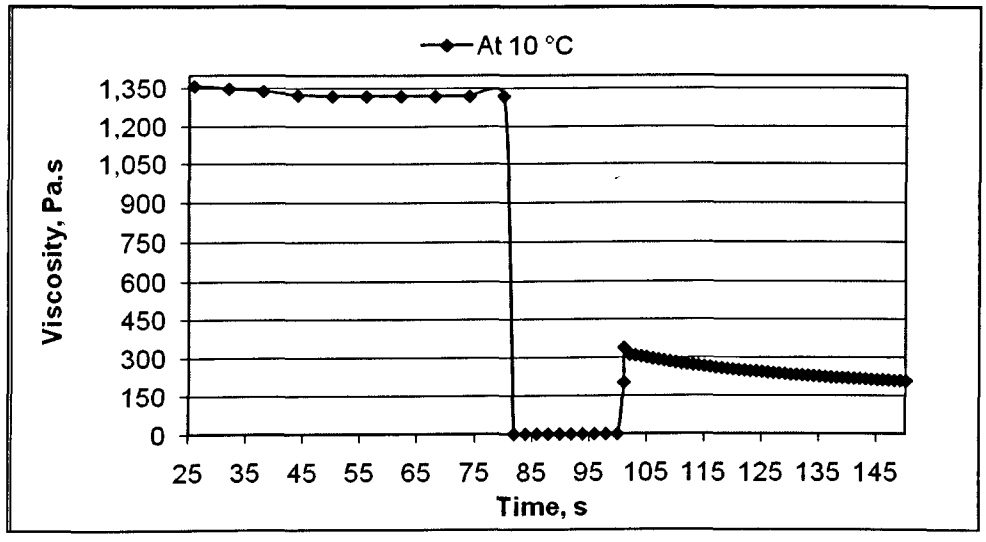

Figure A3.21 Time vs. viscosity: thixotropy phenomena test for Mix oil sample under 0.1, 1000 and 0.1 1/s shear rates at 10 °C

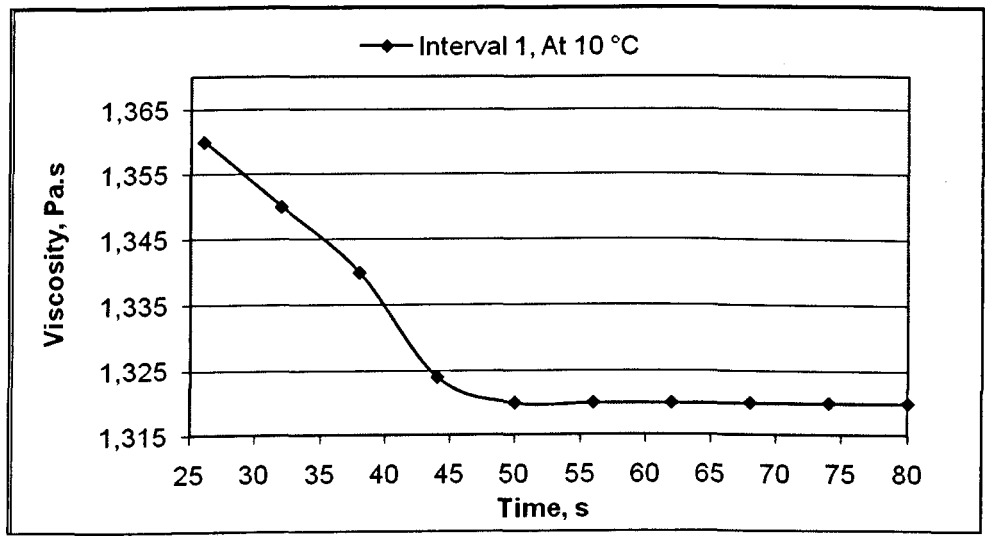

Figure A3.22 Magnification of the data shown in Figure A3.21 from time interval 20 to 80 second

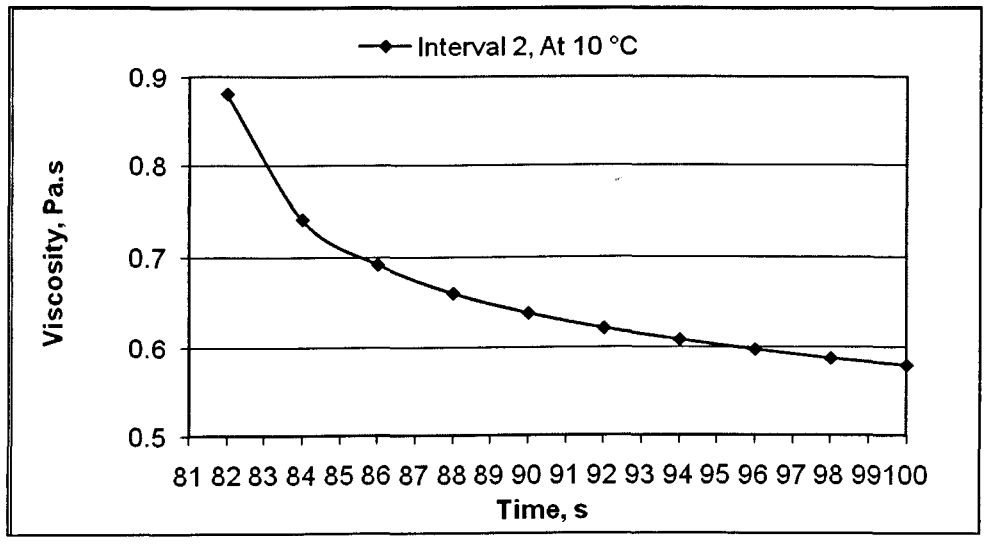

Figure A3.23 Magnification of the data shown in Figure A3.21 from time interval 80 to 100 second

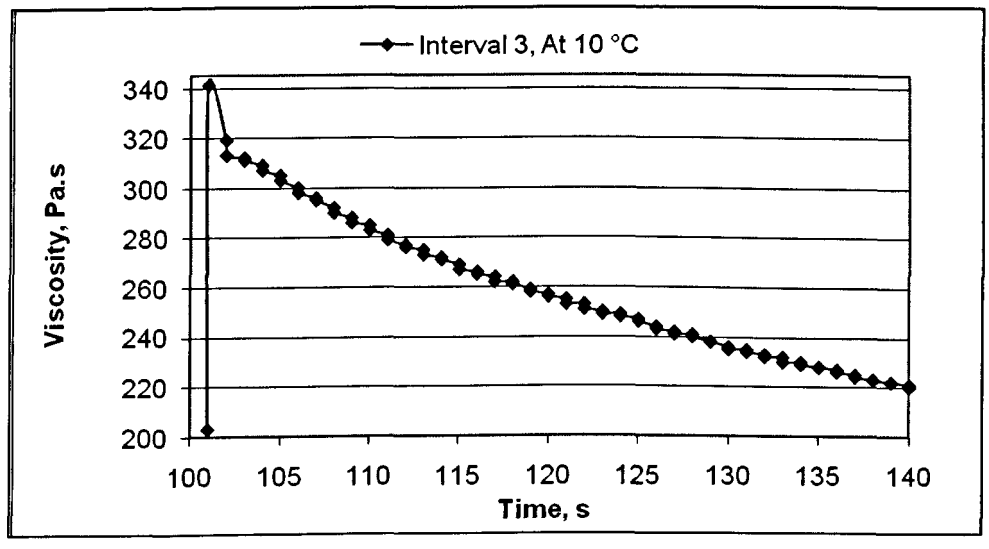

Figure A3.24 Magnification of the data shown in Figure A3.21 from time interval 100 to 140 second

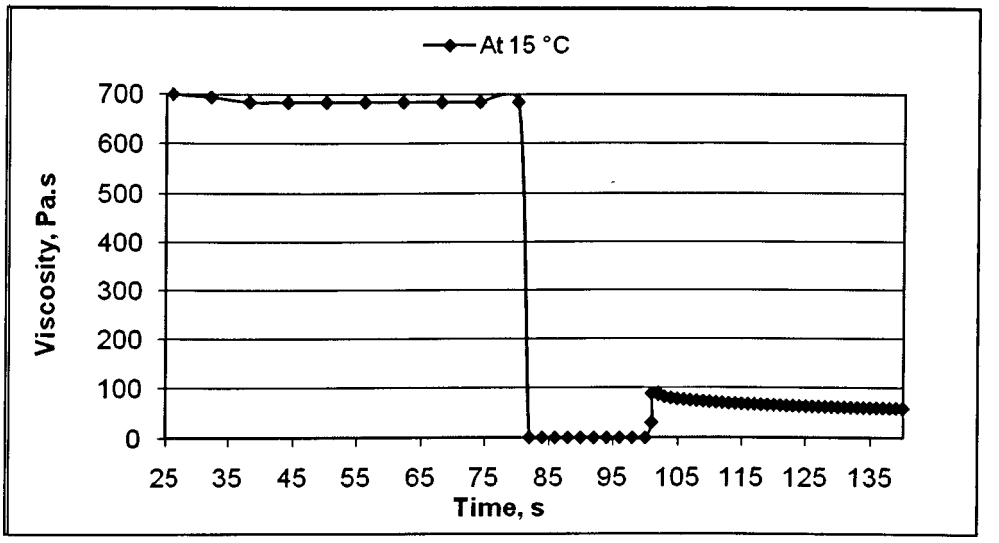

Figure A3.25 Time vs. viscosity: thixotropy phenomena test for Mix oil sample under 0.1, 1000 and 0.1 1/s shear rates at 15 °C

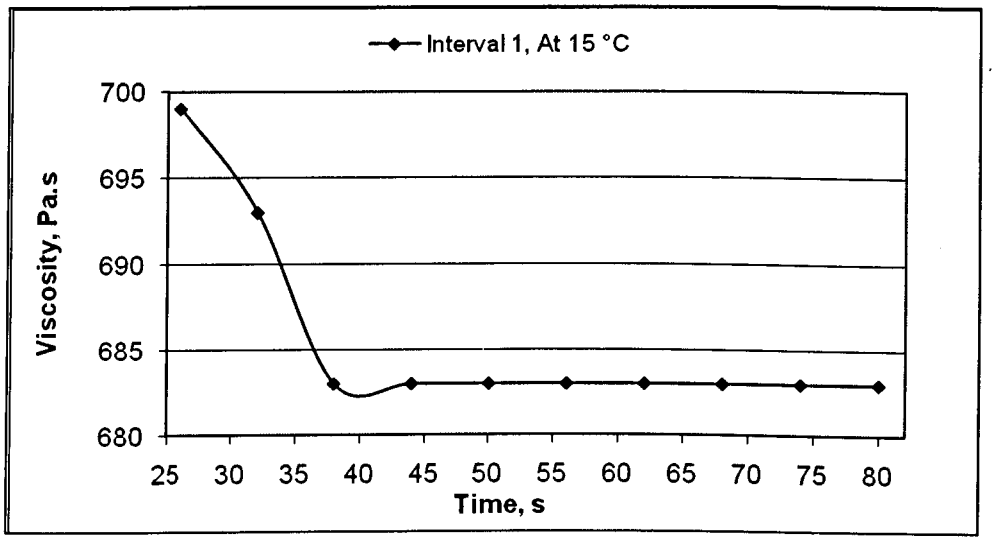

Figure A3.26 Magnification of the data shown in Figure A3.25 from time interval 20 to 80 second

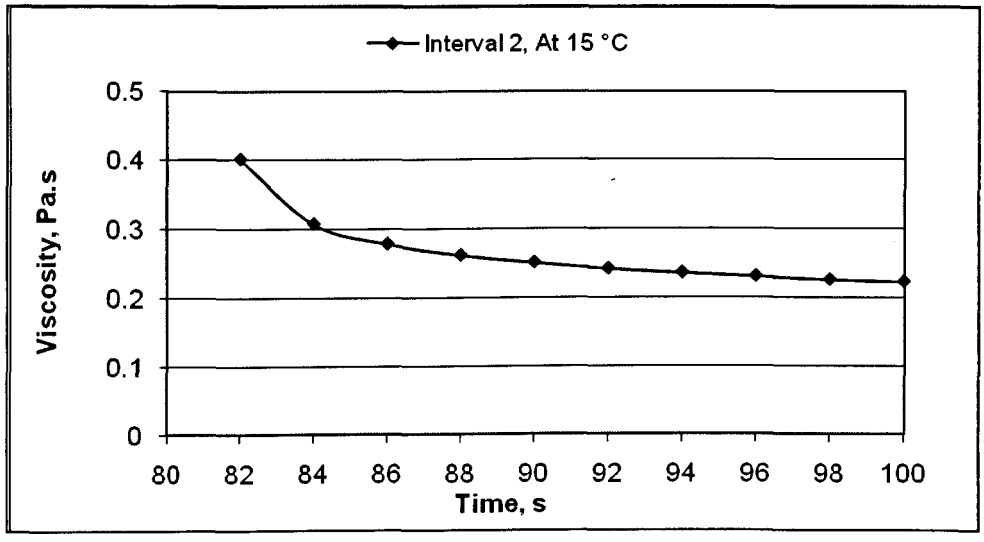

Figure A3.27 Magnification of the data shown in Figure A3.25 from time interval 80 to 100 second

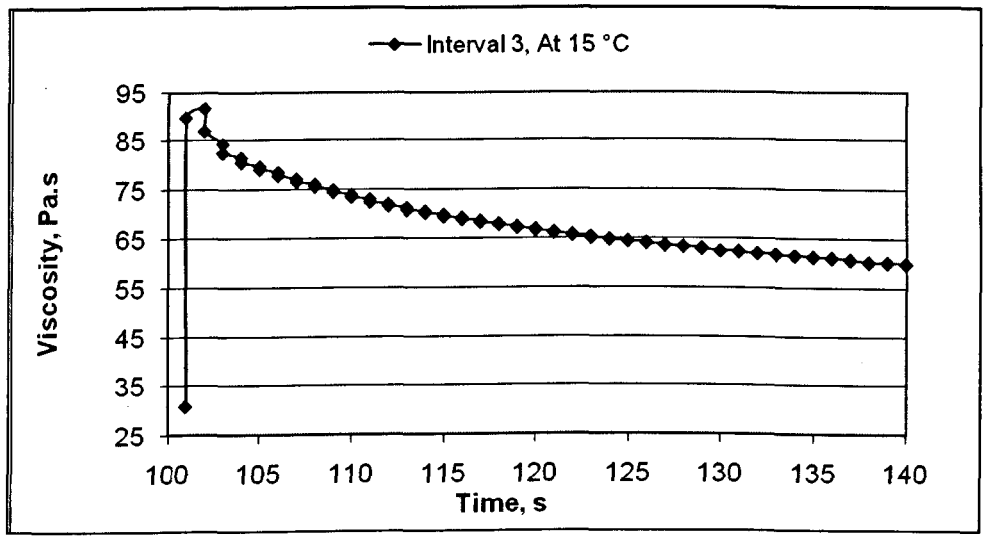

Figure A3.28 Magnification of the data shown in Figure A3.25 from time interval 100 to 140 second

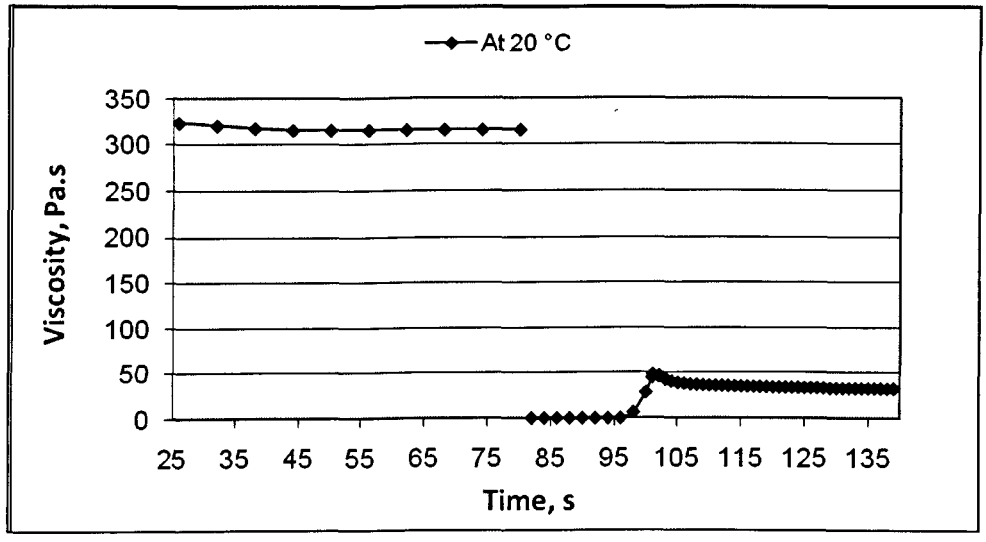

Figure A3.29 Time vs. viscosity: thixotropy phenomena test for Mix oil sample under 0.1, 1000 and 0.1 1/s shear rates at 20 °C

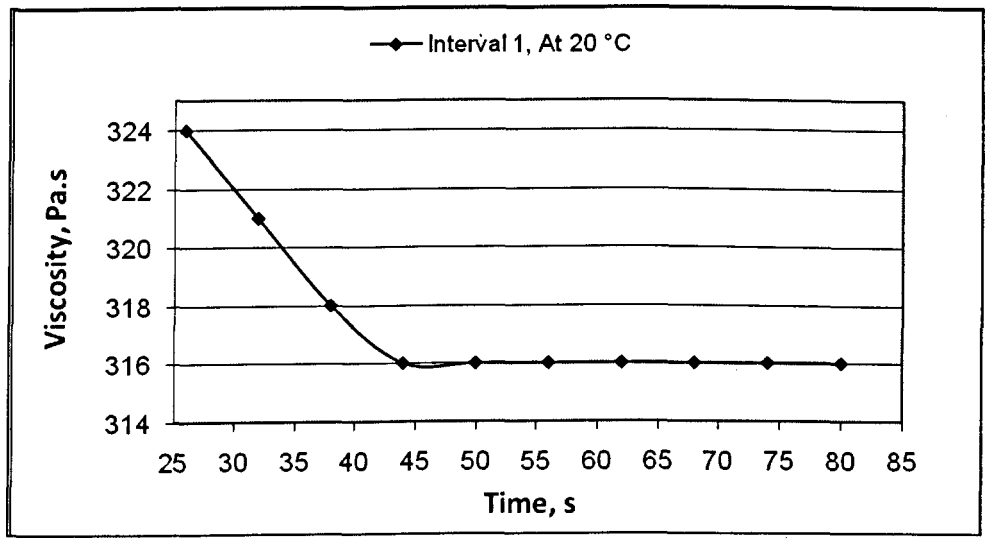

Figure A3.30 Magnification of the data shown in Figure A3.29 from time interval 20 to 80 second

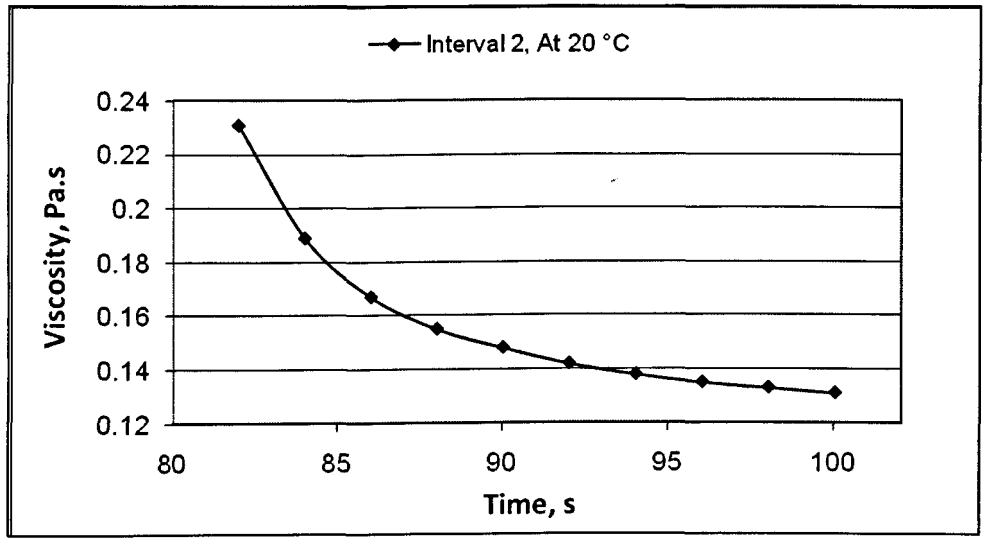

Figure A3.31 Magnification of the data shown in Figure A3.29 from time interval 80 to 100 second

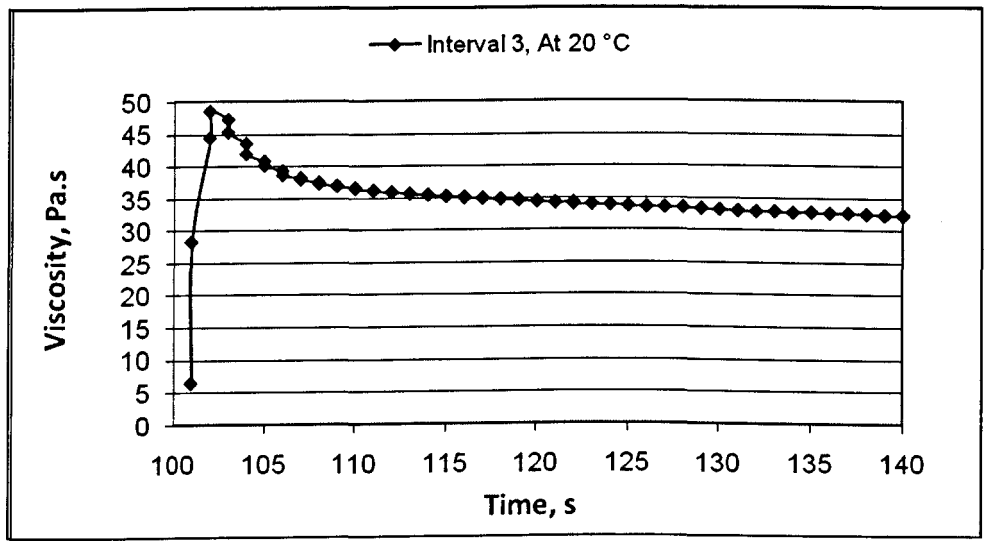

Figure A3.32 Magnification of the data shown in Figure A3.29 from time interval 100 to 140 second

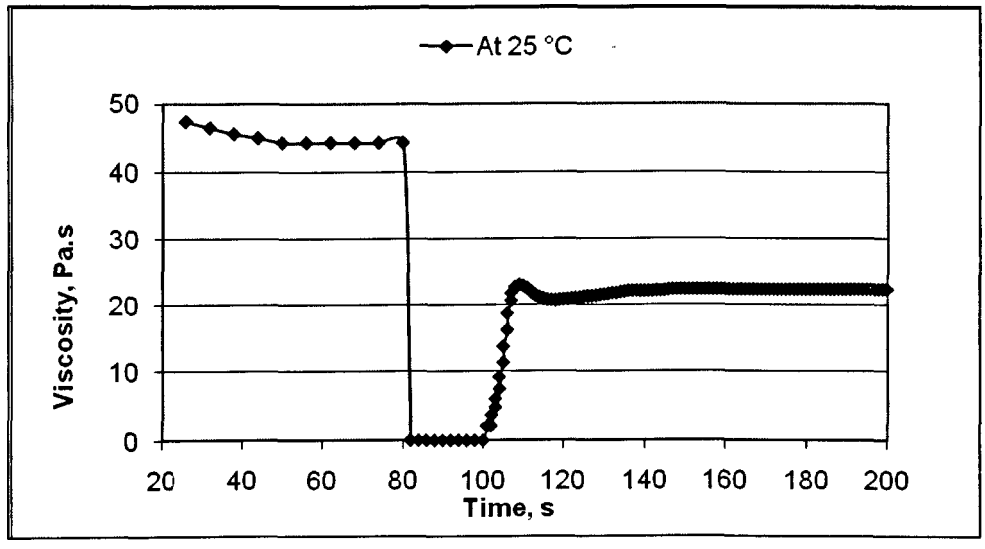

Figure A3.33 Time vs. viscosity: thixotropy phenomena test for Mix oil sample under 0.1, 1000 and 0.1 1/s shear rates at 25 °C

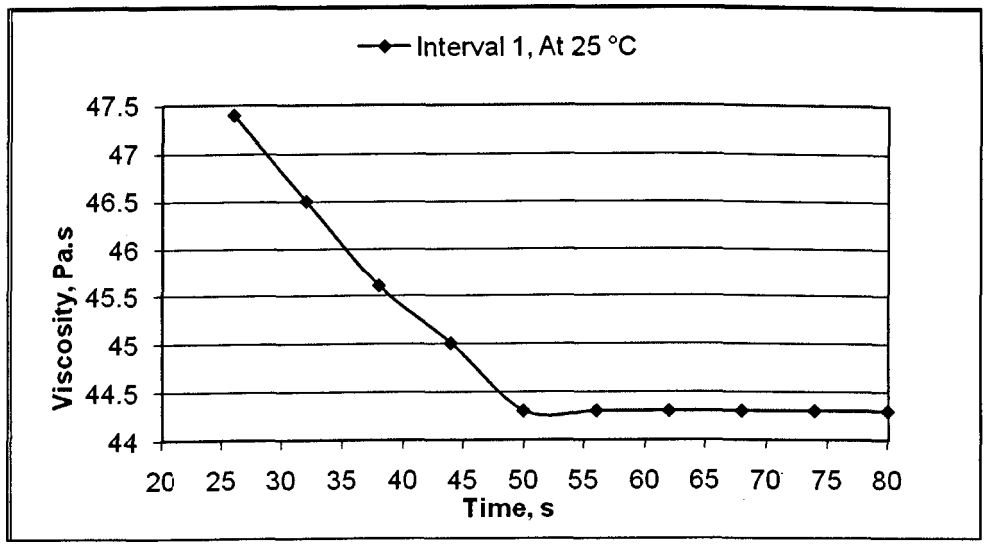

Figure A3. 34 Magnification of the data shown in Figure A3.33 from time interval 20 to 80 second

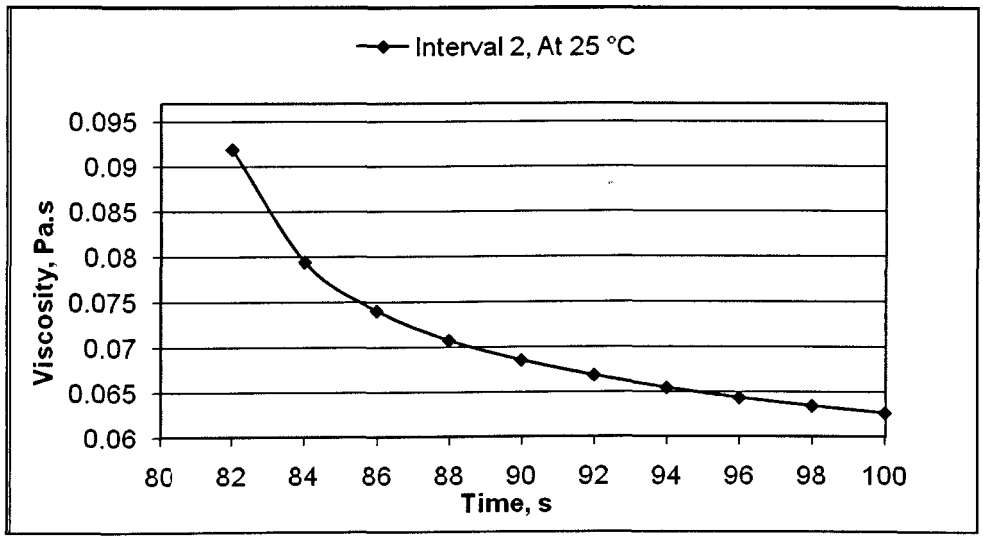

Figure A3.35 Magnification of the data shown in Figure A3.33 from time interval 80 to 100 second

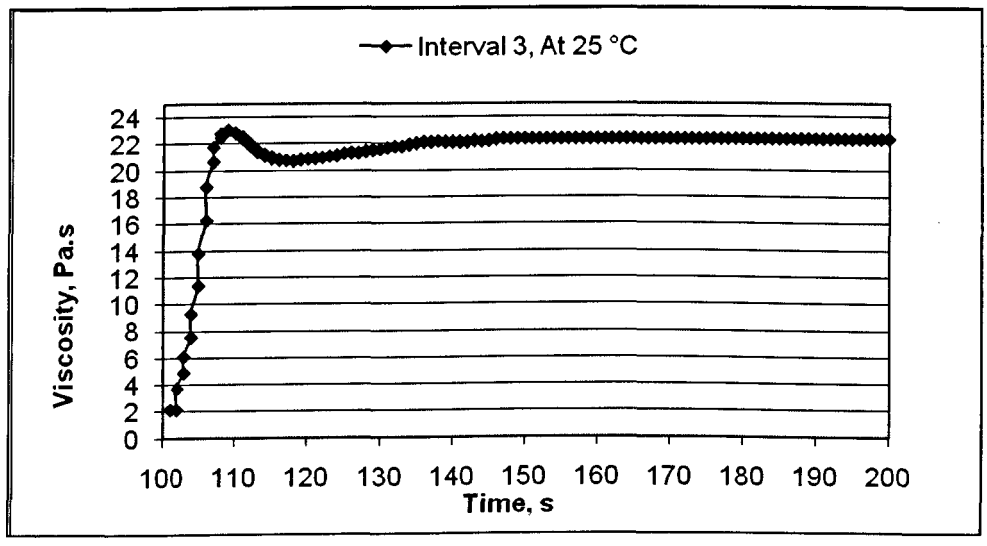

Figure A3.36 Magnification of the data shown in Figure A3.33 from time interval 20 to 80 second

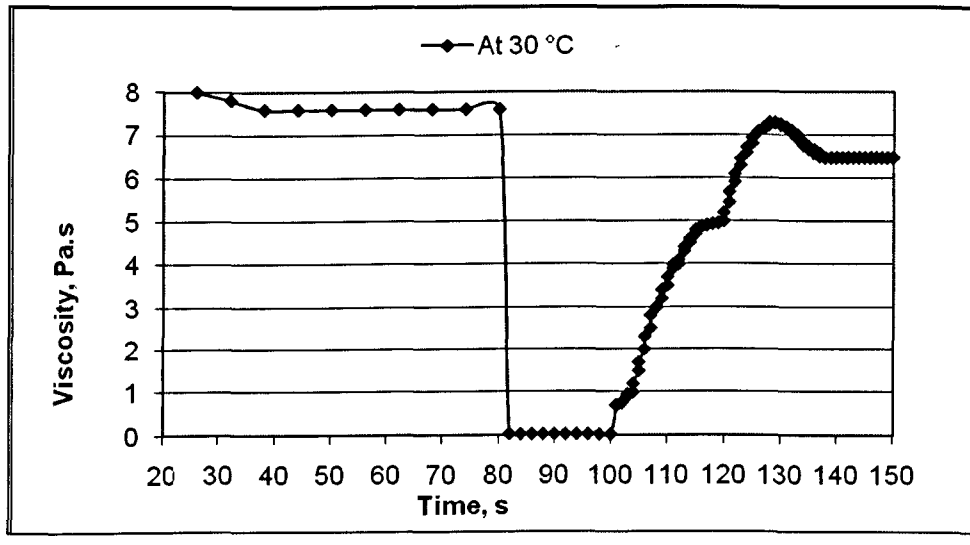

Figure A3.37 Time vs. viscosity: thixotropy phenomena test for Mix oil sample under 0.1, 1000 and 0.1 1/s shear rates at 30 °C

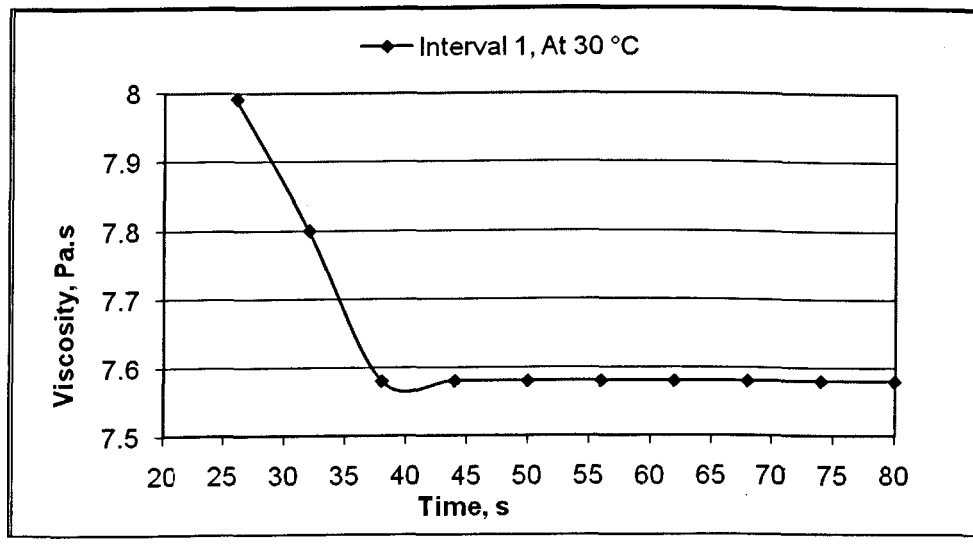

Figure A3.38 Magnification of the data shown in Figure A3.37 from time interval 20 to 80 second

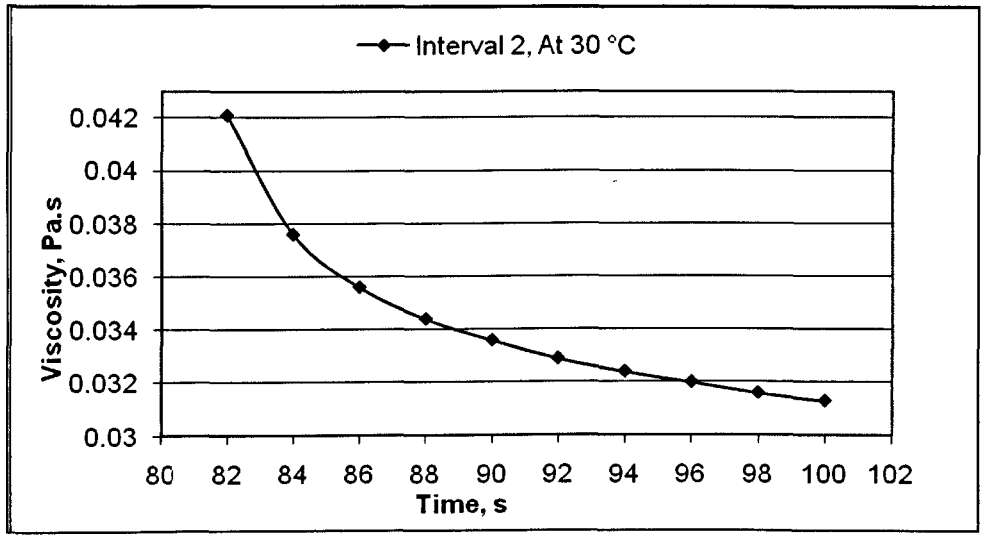

Figure A3.39 Magnification of the data shown in Figure A3.37 from time interval 80 to 100 second

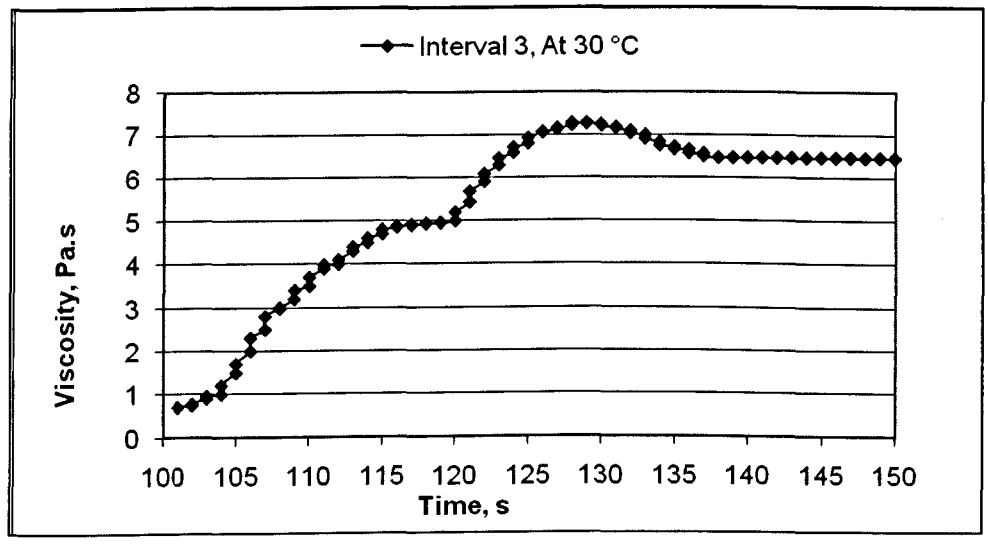

Figure A3.40 Magnification of the data shown in Figure A3.37 from time interval 100 to 150 second

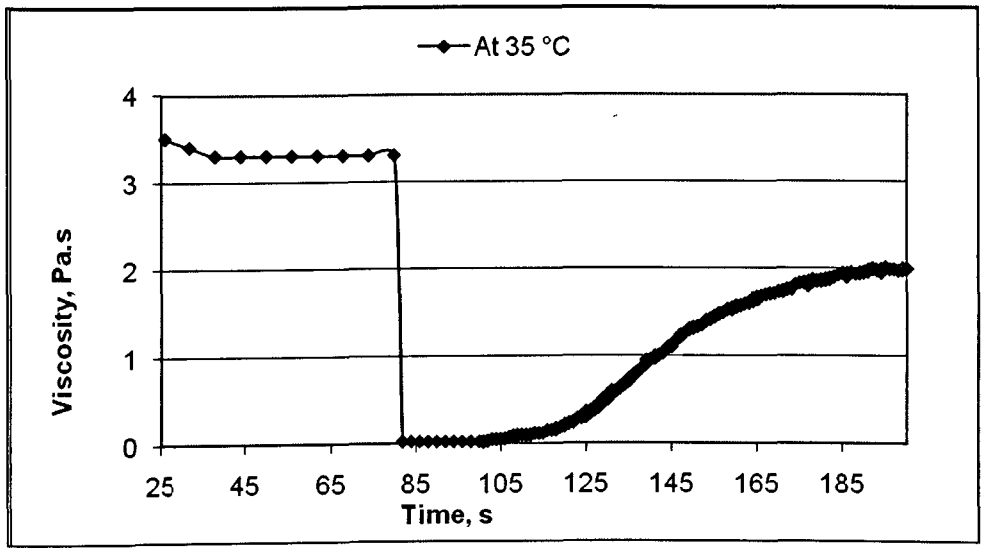

Figure A3.41 Time vs. viscosity: thixotropy phenomena test for Mix oil sample under 0.1, 1000 and 0.1 1/s shear rates at 35 °C

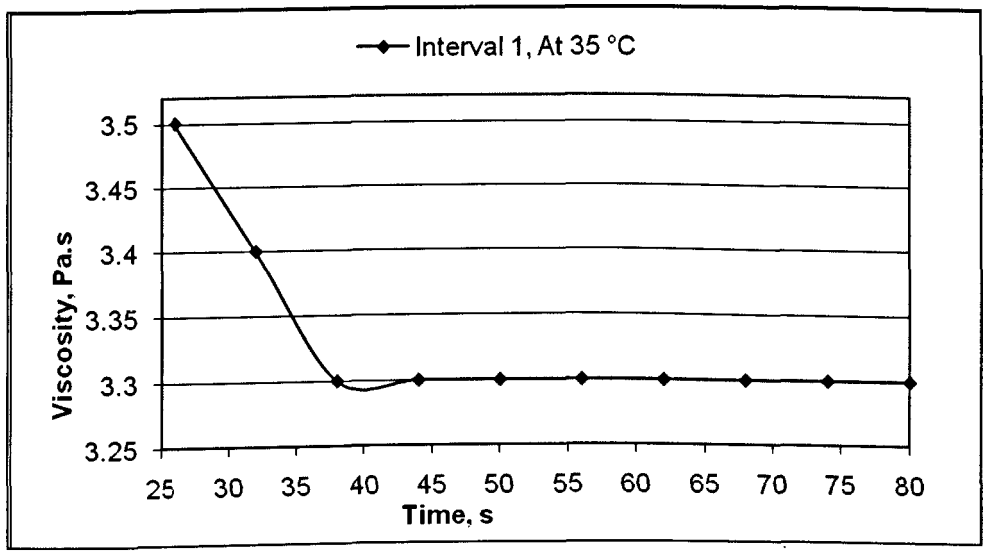

Figure A3.42 Magnification of the data shown in Figure A3.41 from time interval 20 to 80 second

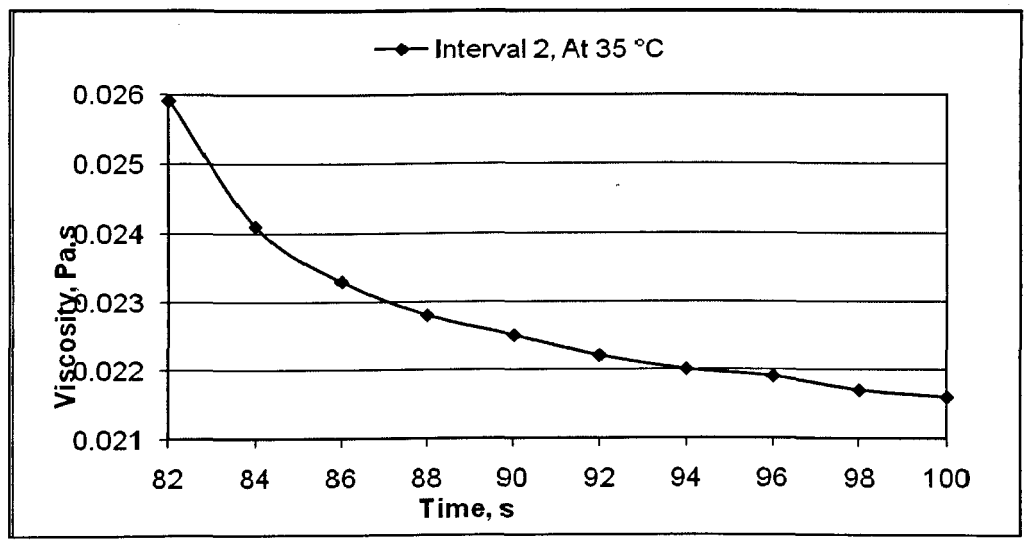

Figure A3.43 Magnification of the data shown in Figure A3.41 from time interval 80 to 100 second

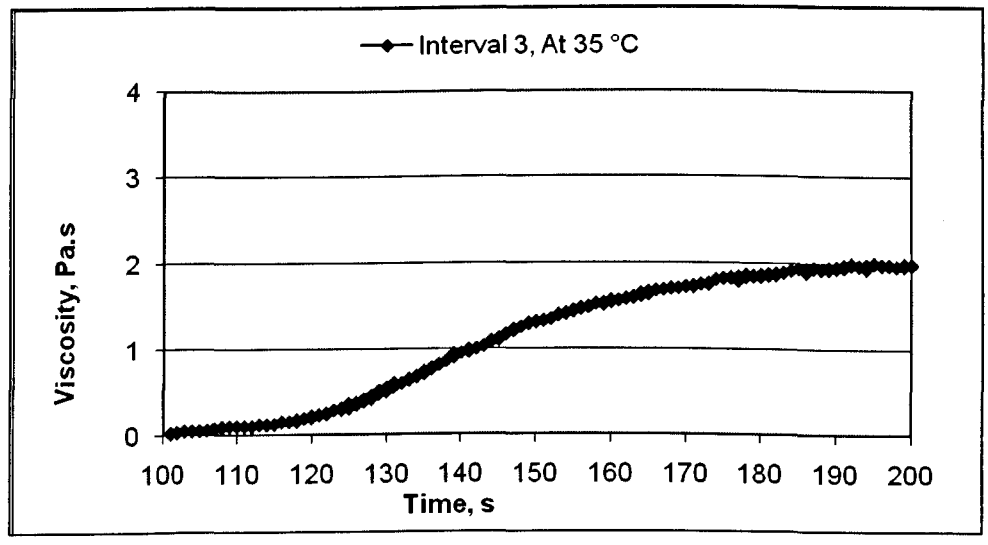

Figure A3.44 Magnification of the data shown in Figure A3.41 from time interval 100 to 200 second

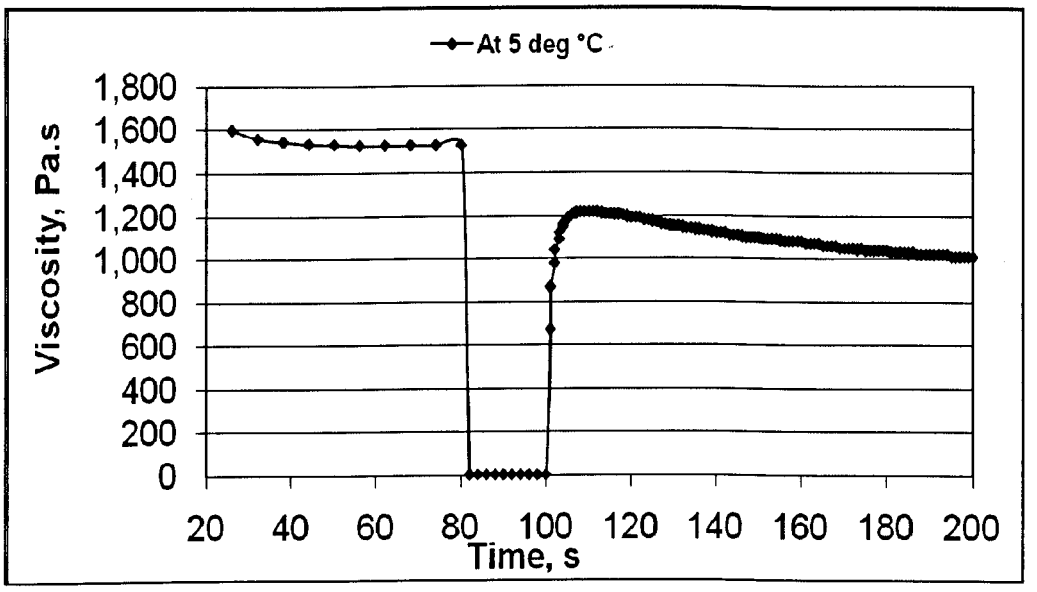

Figure A3.45 Time vs. viscosity: thixotropy phenomena test for Remal oil sample under 0.1, 1000 and 0.1 1/s shear rates at 5 °C

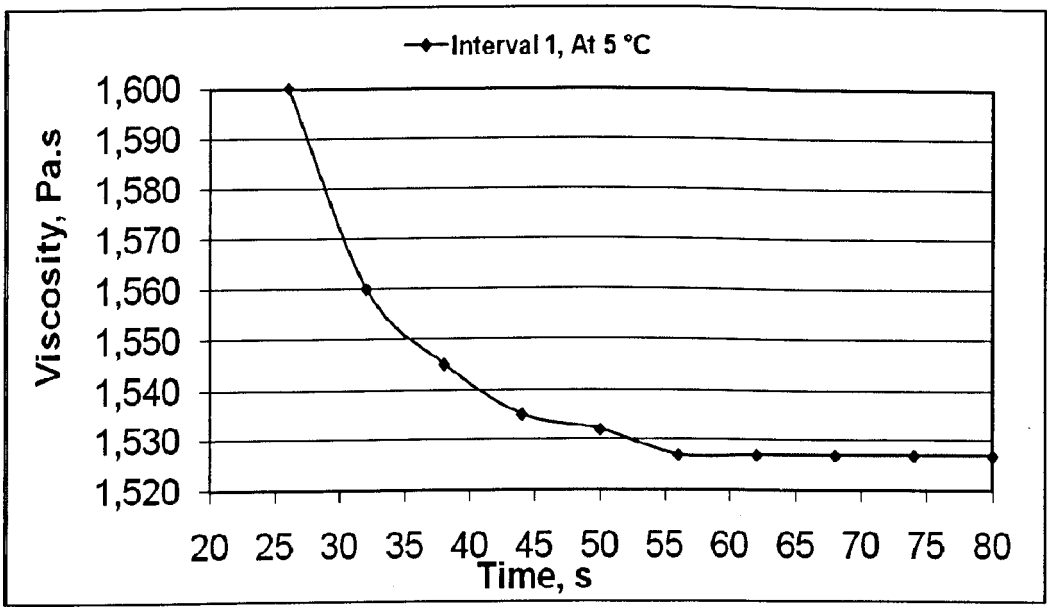

Figure A3.46 Magnification of the data shown in Figure A3.45 from time interval 20 to 80 second

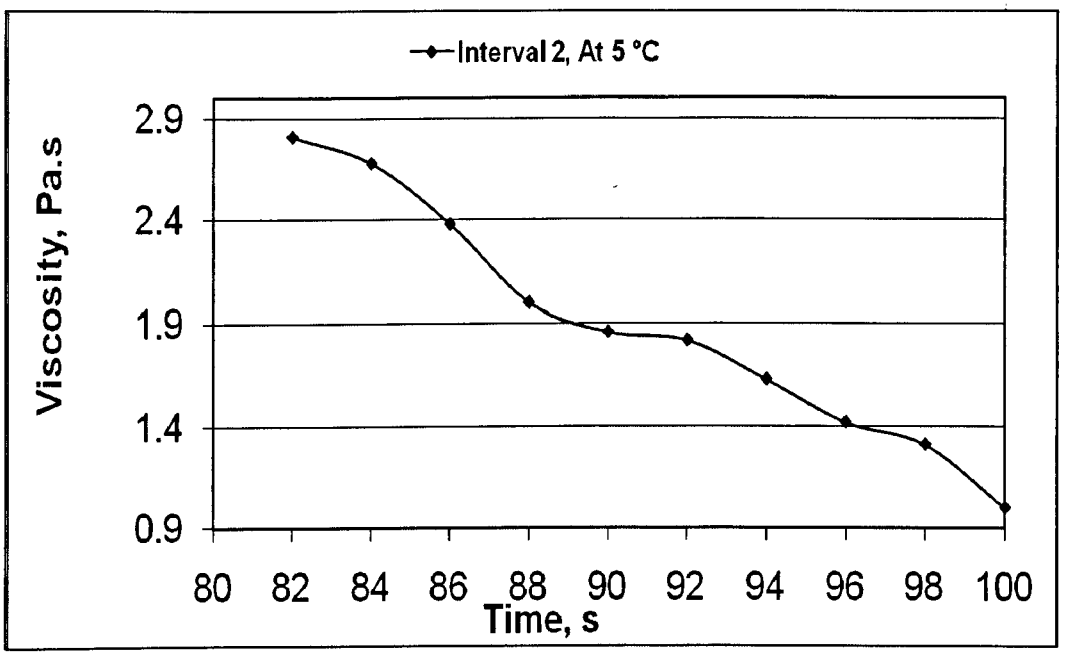

Figure A3.47 Magnification of the data shown in Figure A3.45 from time interval 80 to 100 second

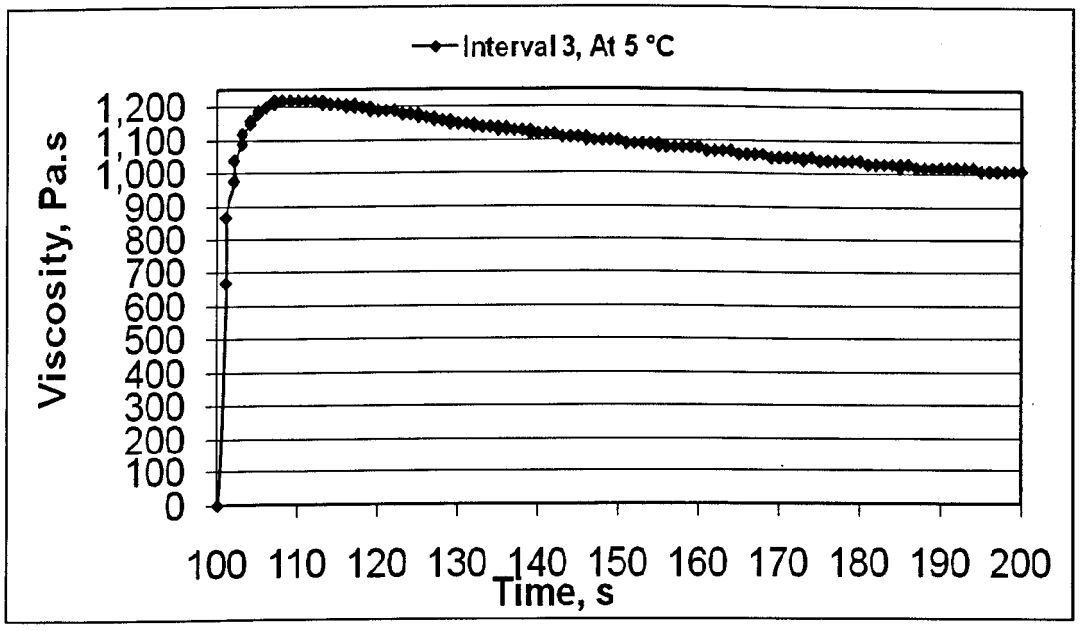

Figure A3.48 Magnification of the data shown in Figure A3.45 from time interval 100 to 200 second

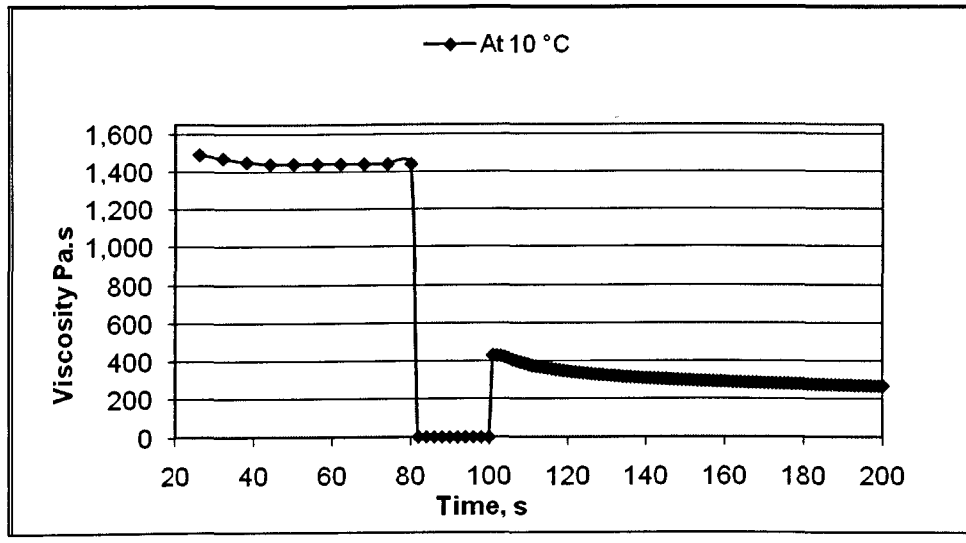

Figure A3.49 Time vs. viscosity: thixotropy phenomena test for Remal oil sample under 0.1, 1000 and 0.1 1/s shear rates at 10 °C

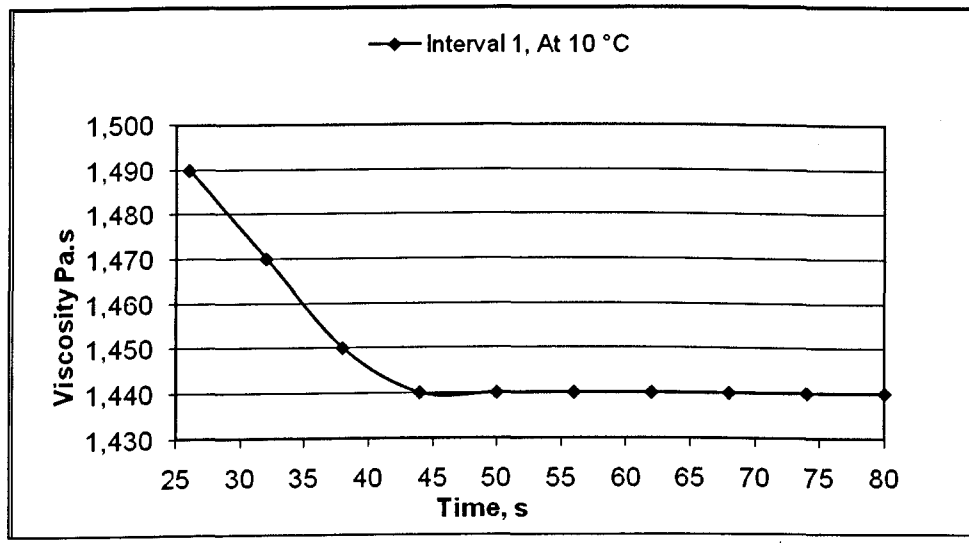

Figure A3.50 Magnification of the data shown in Figure A3.49 from time interval 20 to 80 second

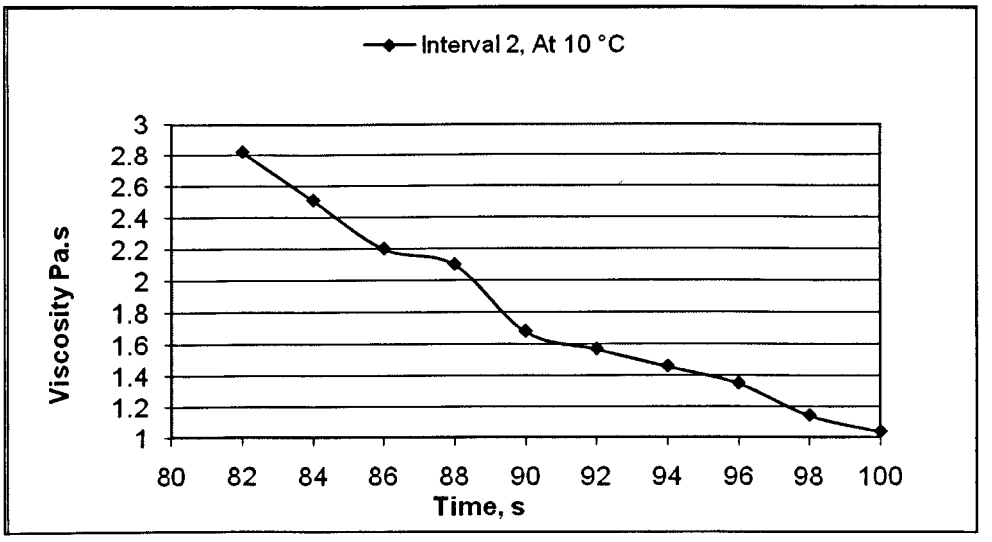

Figure A3.51 Magnification of the data shown in Figure A3.49 from time interval 80 to 100 second

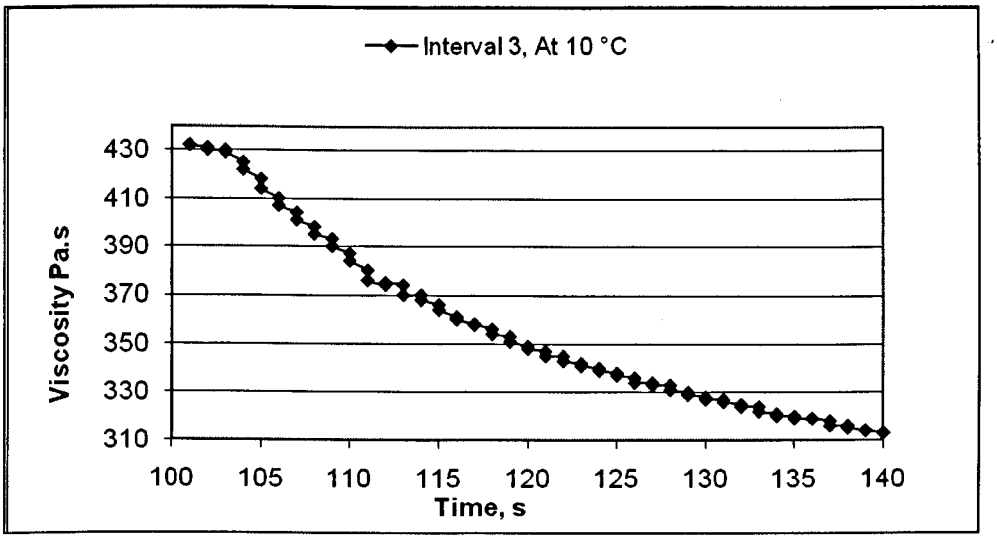

Figure A3.52 Magnification of the data shown in Figure A3.49 from time interval 100 to 140 second

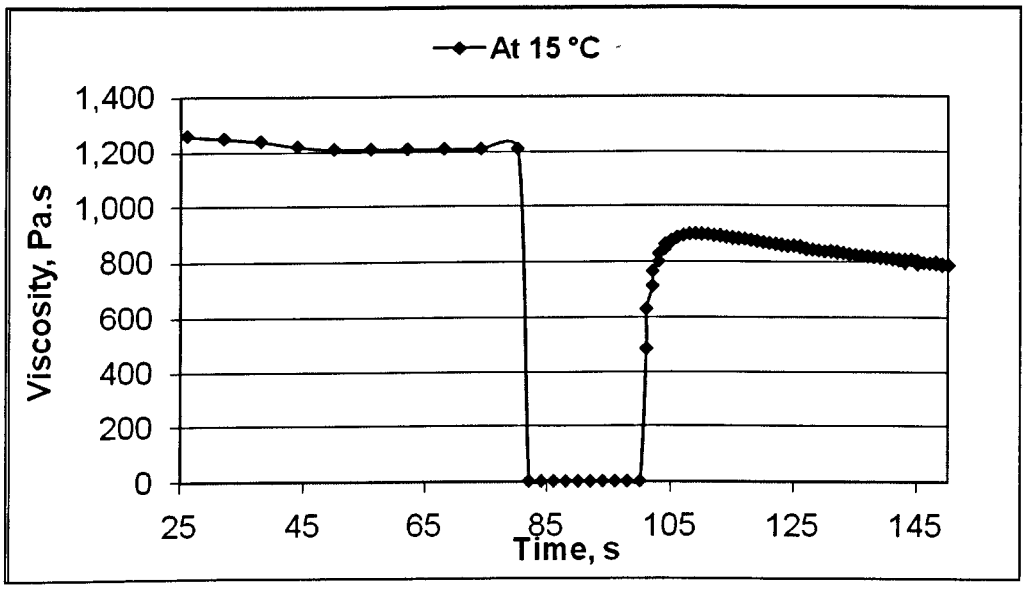

Figure A3.53 Time vs. viscosity: thixotropy phenomena test for Remal oil sample under 0.1, 1000 and 0.1 1/s shear rates at 15 °C

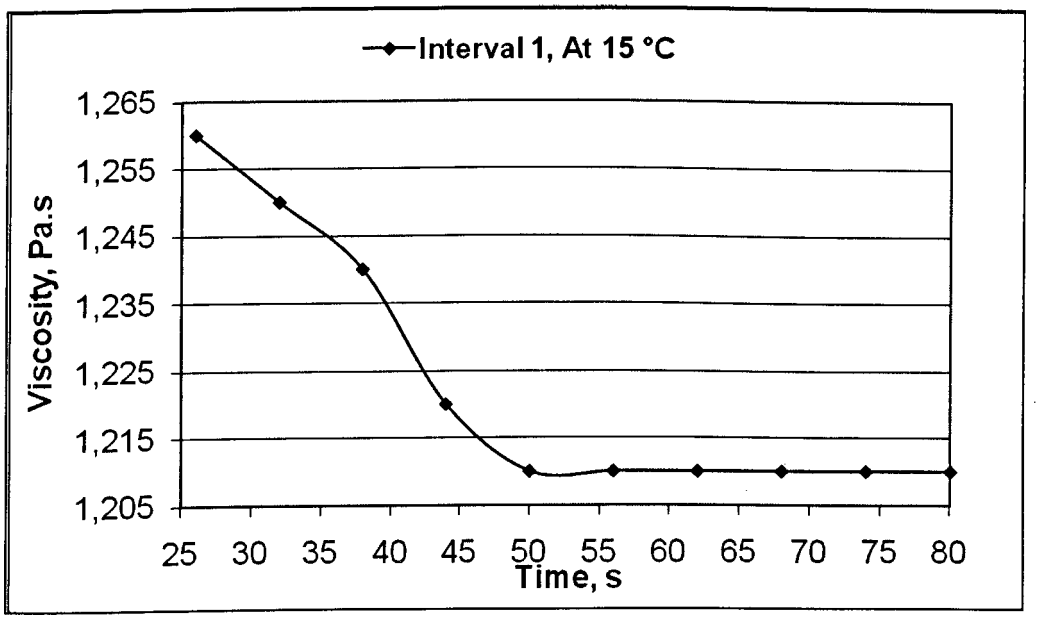

Figure A3.54 Magnification of the data shown in Figure A3.53 from time interval 20 to 80 second

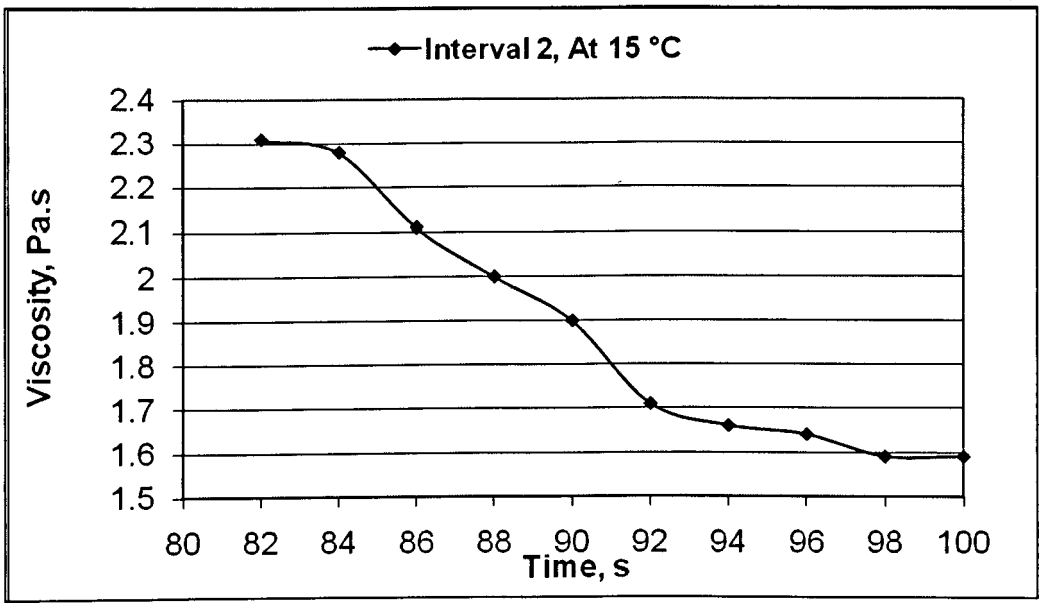

Figure A3.55 Magnification of the data shown in Figure A3.53 from time interval 80 to 100 second

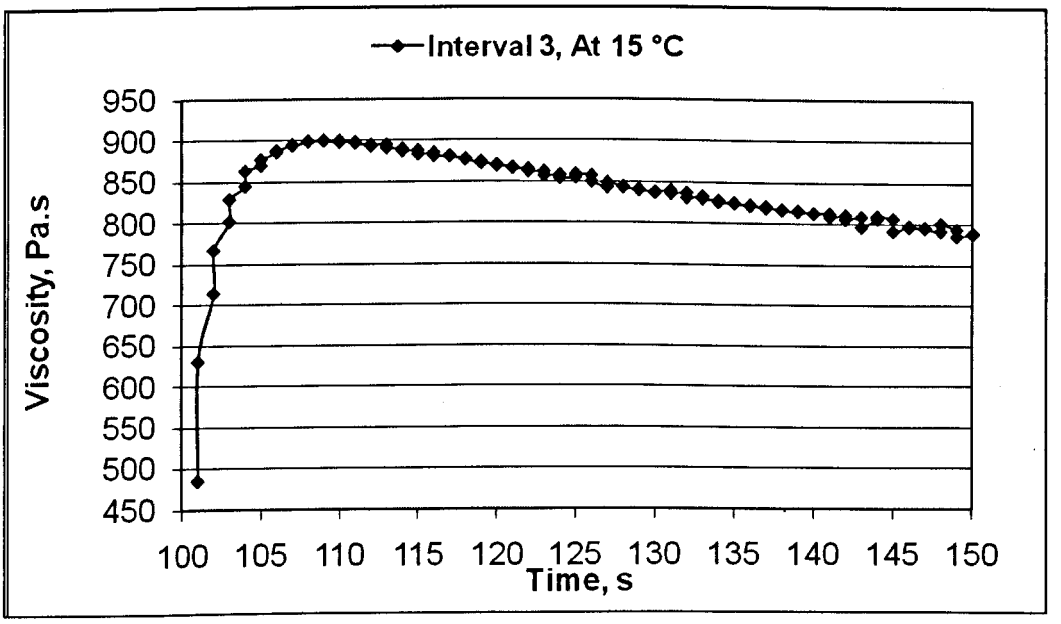

Figure A3.56 Magnification of the data shown in Figure A3.53 from time interval 100 to 150 second

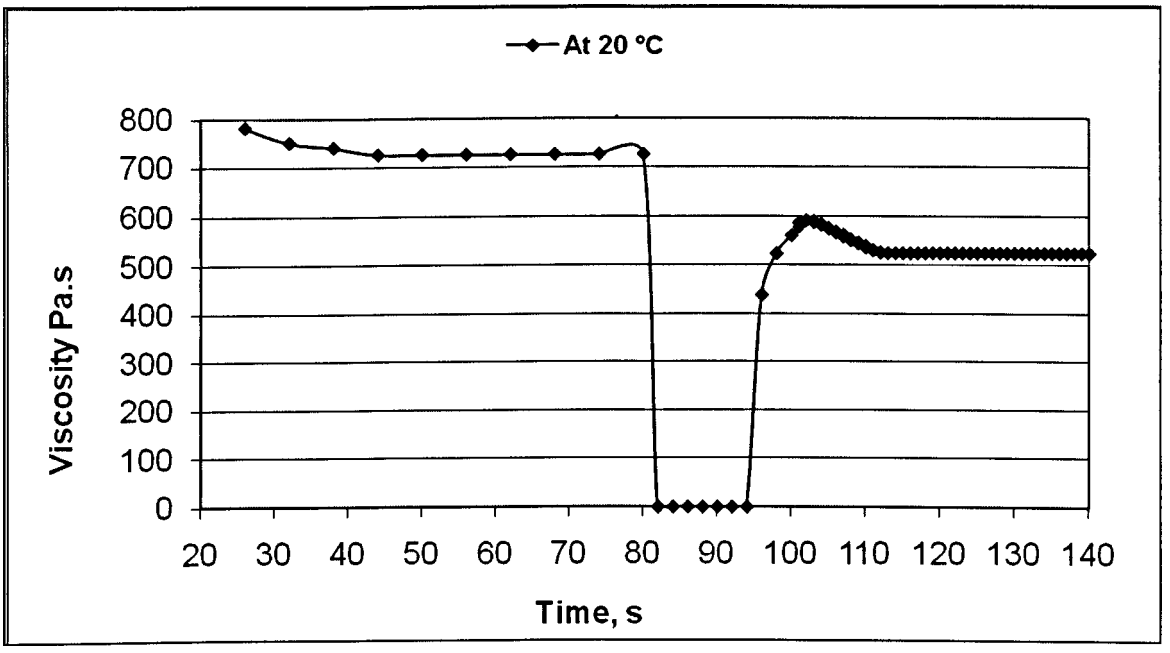

Figure A3.57 Time vs. viscosity: thixotropy phenomena test for Remal oil sample under 0.1, 1000 and 0.1 1/s shear rates at 20 °C

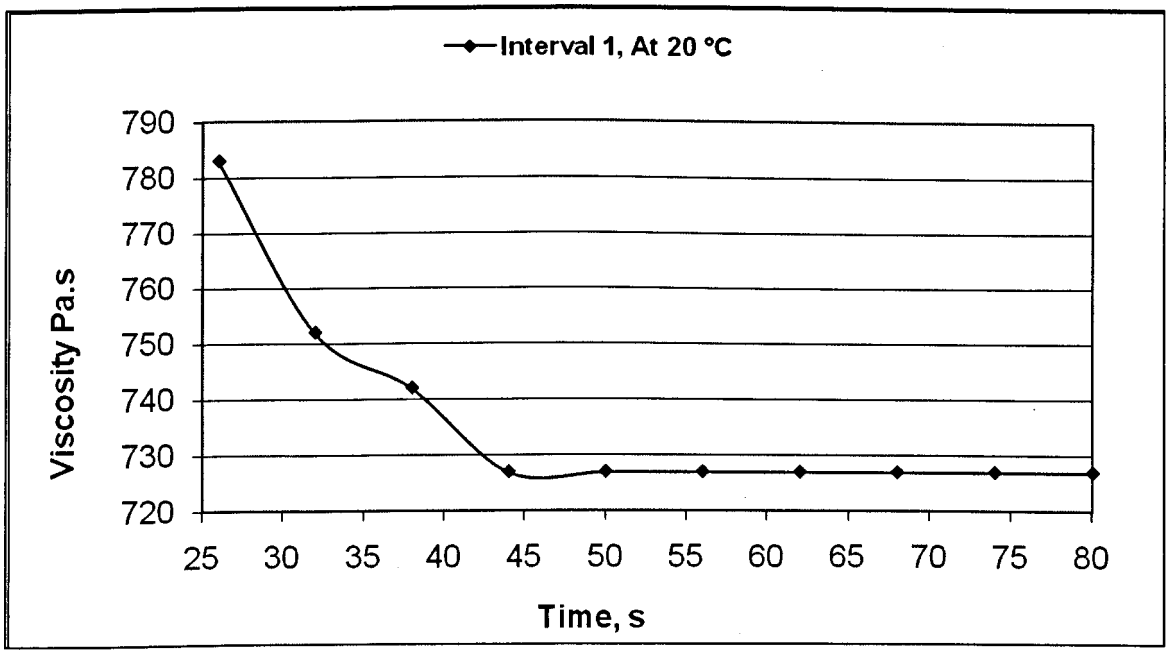

Figure A3.58 Magnification of the data shown in Figure A3.57 from time interval 20 to 80 second

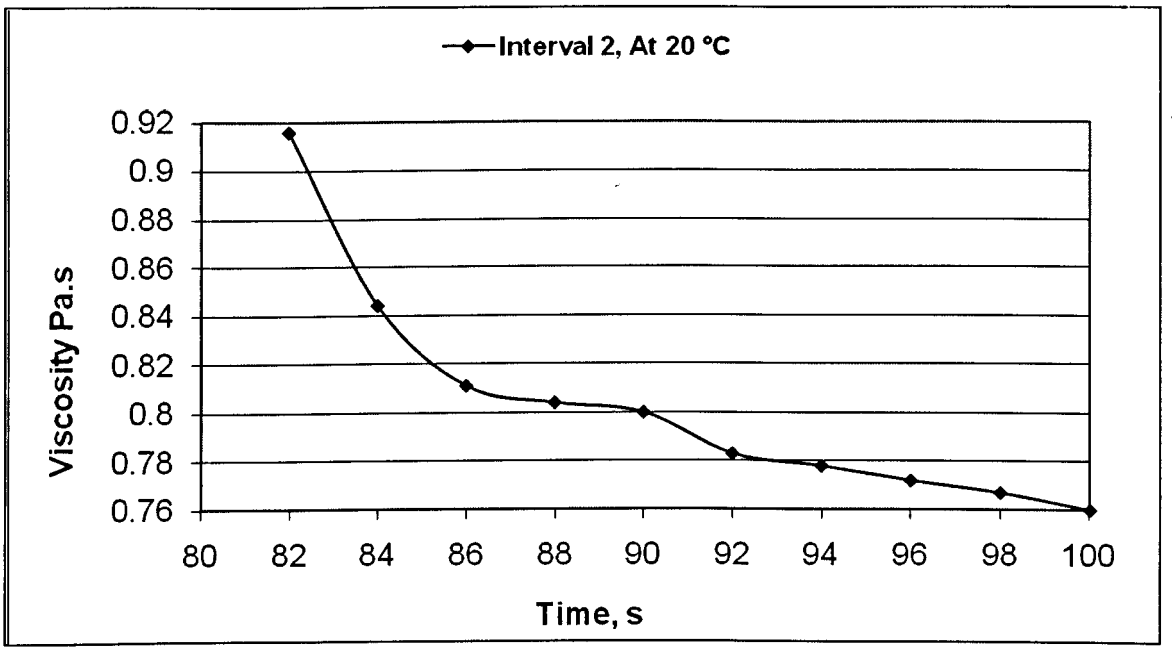

Figure A3.59 Magnification of the data shown in Figure A3.57 from time interval 80 to 100 second

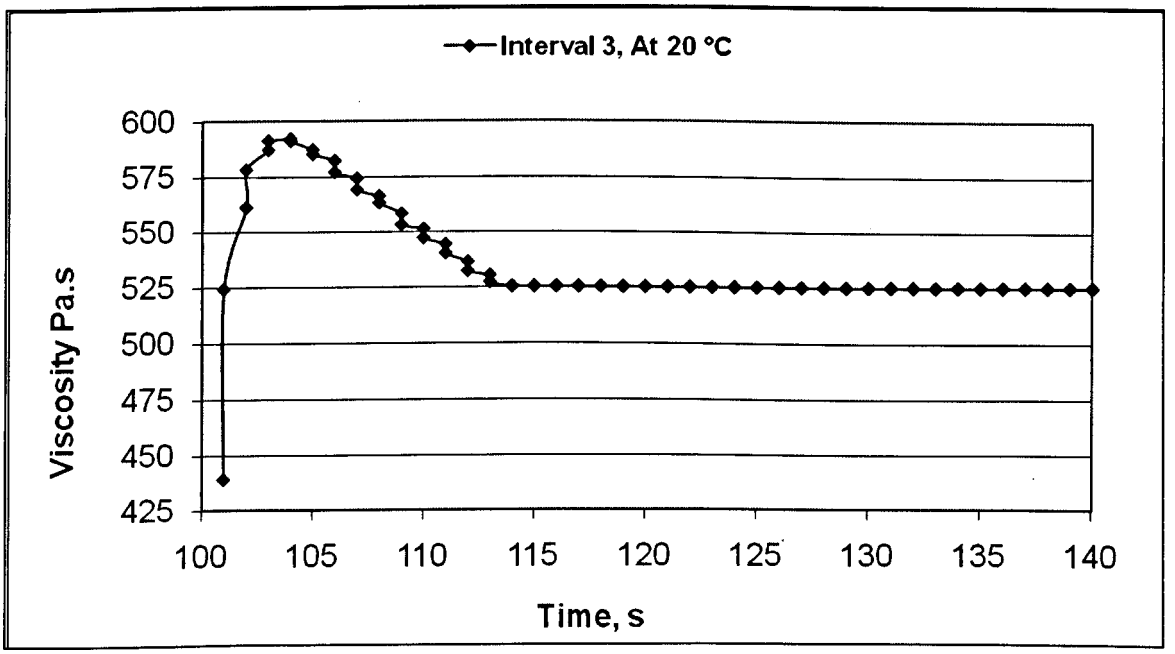

Figure A3.60 Magnification of the data shown in Figure A3.57 from time interval 20 to 80 second

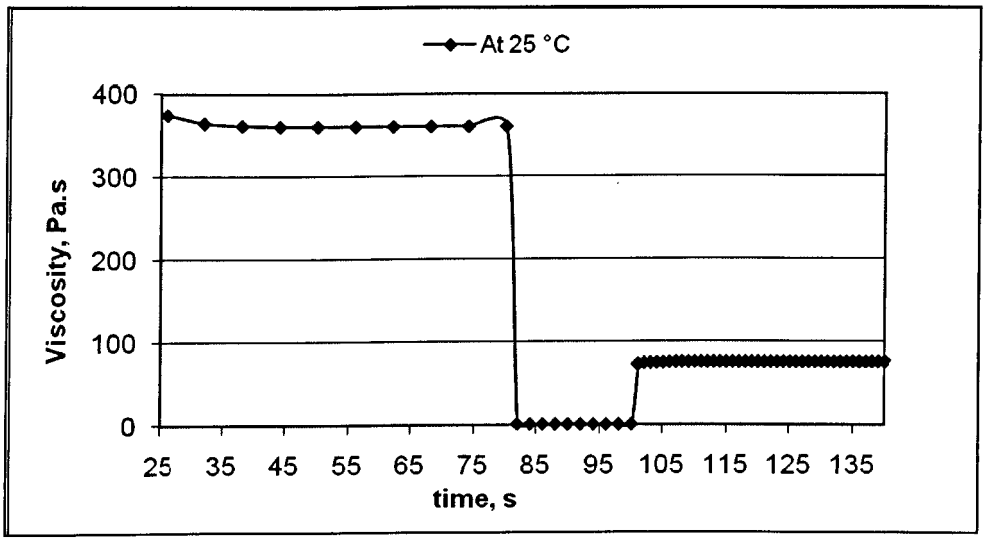

Figure A3.61 Time vs. viscosity: thixotropy phenomena test for Remal oil sample under 0.1, 1000 and 0.1 1/s shear rates at 25 °C

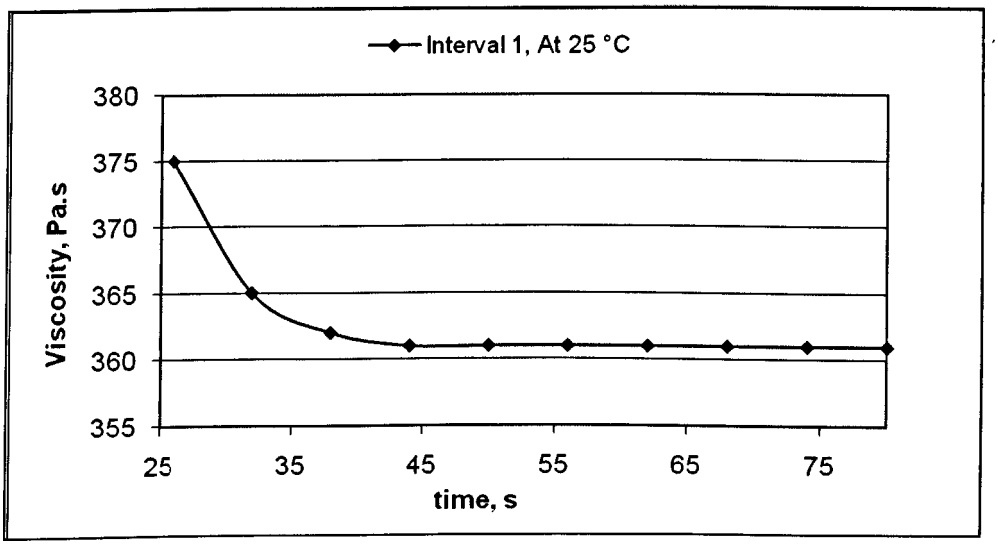

Figure A3.62 Magnification of the data shown in Figure A3.61 from time interval 20 to 80 second

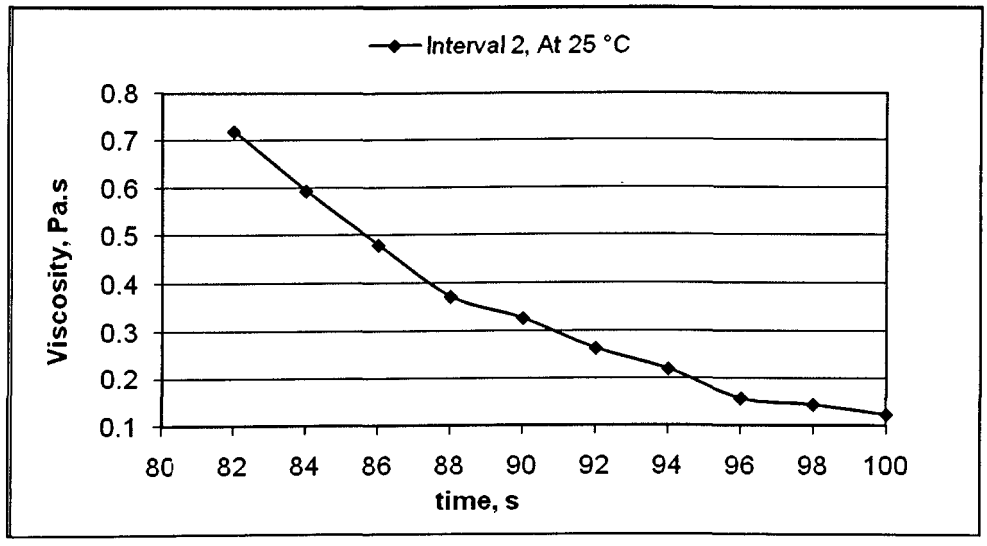

Figure A3.63 Magnification of the data shown in Figure A3.61 from time interval 80 to 100 second

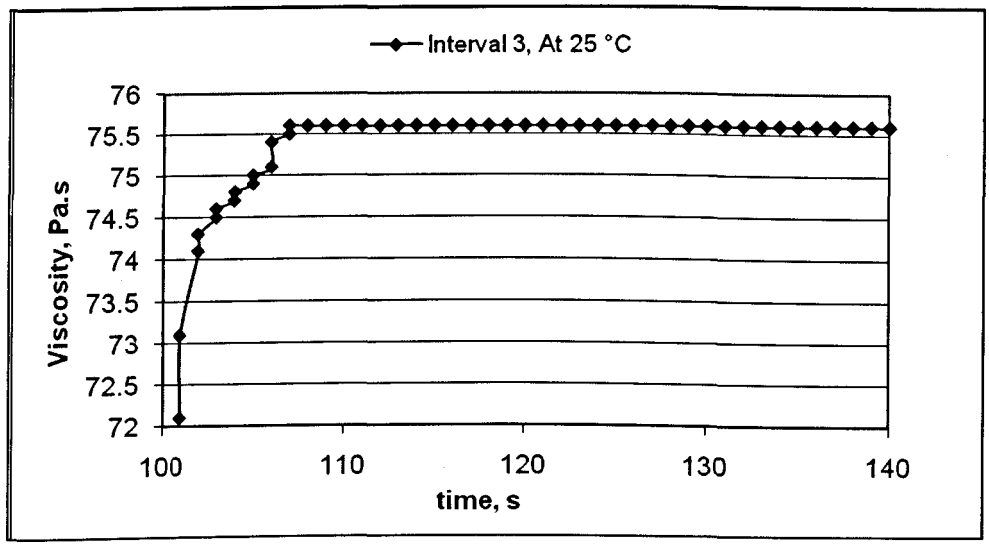

Figure A3.64 Magnification of the data shown in Figure A3.61 from time interval 100 to 140 second

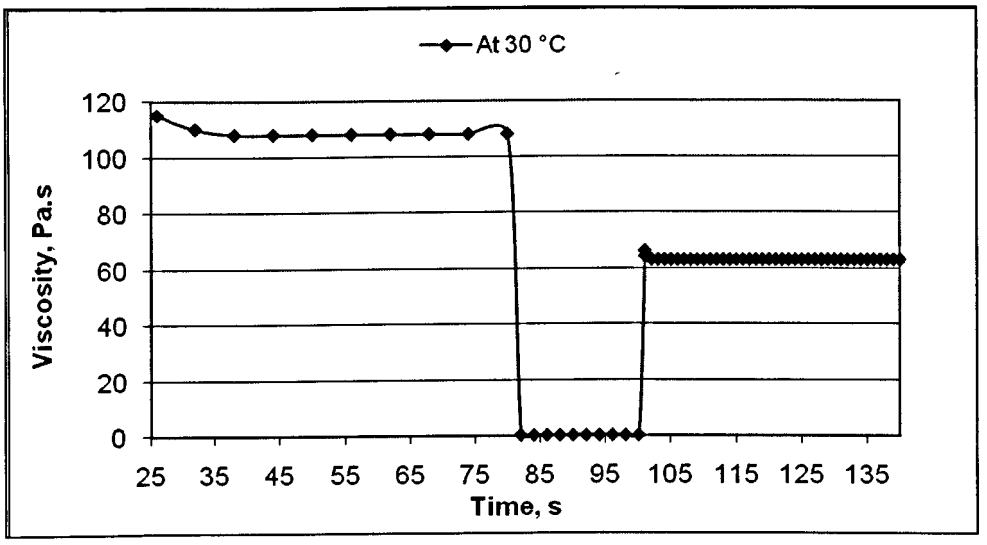

Figure A3.65 Time vs. viscosity: thixotropy phenomena test for Remal oil sample under 0.1, 1000 and 0.1 1/s shear rates at 30 °C

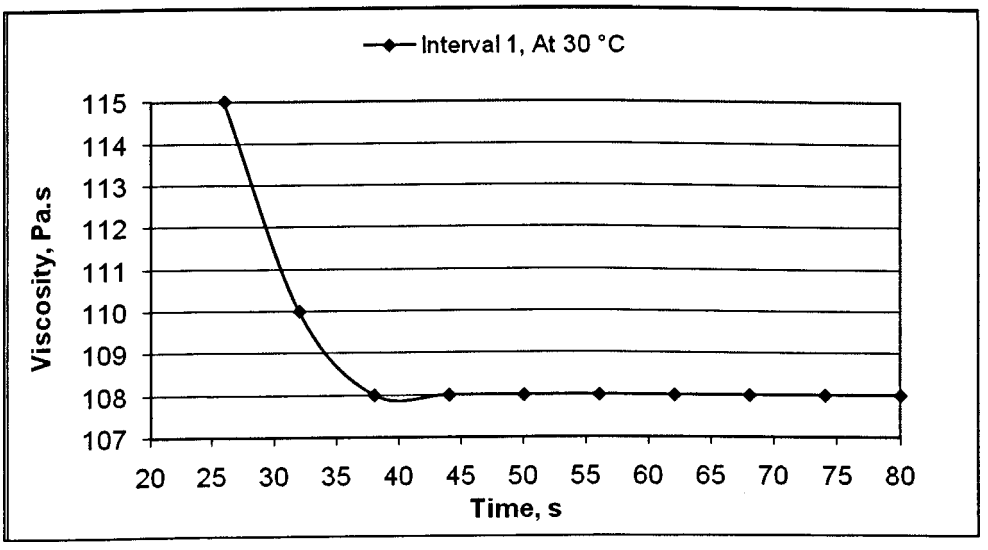

Figure A3.66 Magnification of the data shown in Figure A3.65 from time interval 20 to 80 second

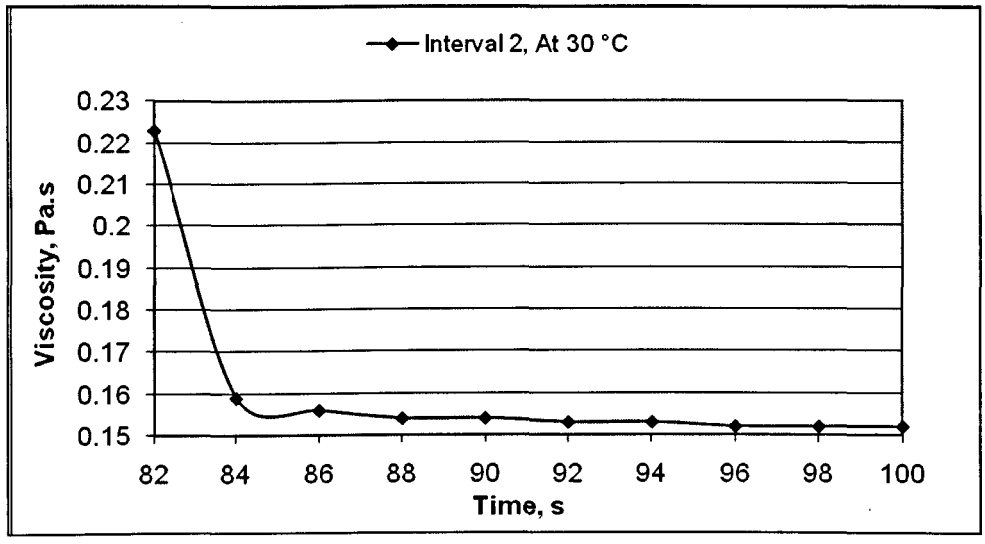

Figure A3.67 Magnification of the data shown in Figure A3.65 from time interval 80 to 100 second

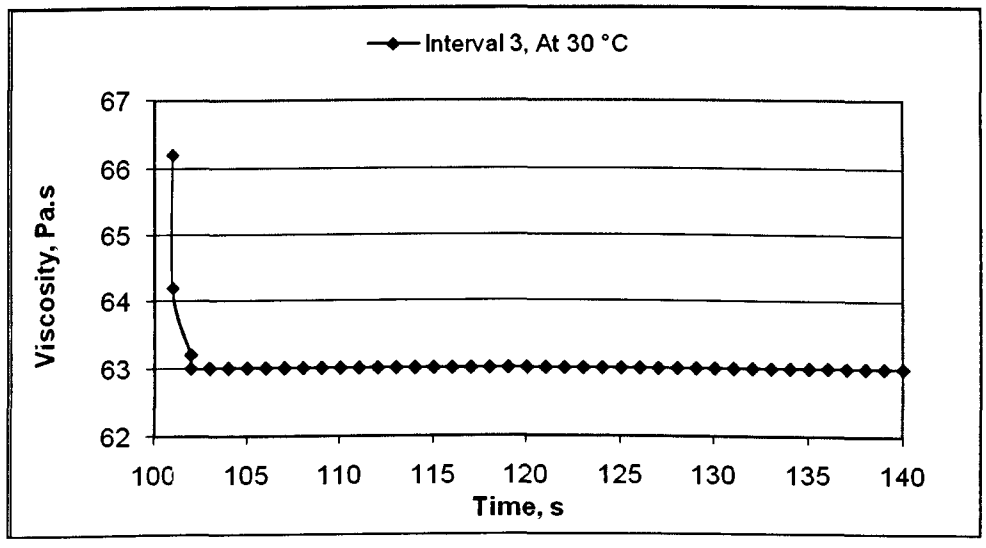

Figure A3.68 Magnification of the data shown in Figure A3.65 from time interval 100 to 140 second

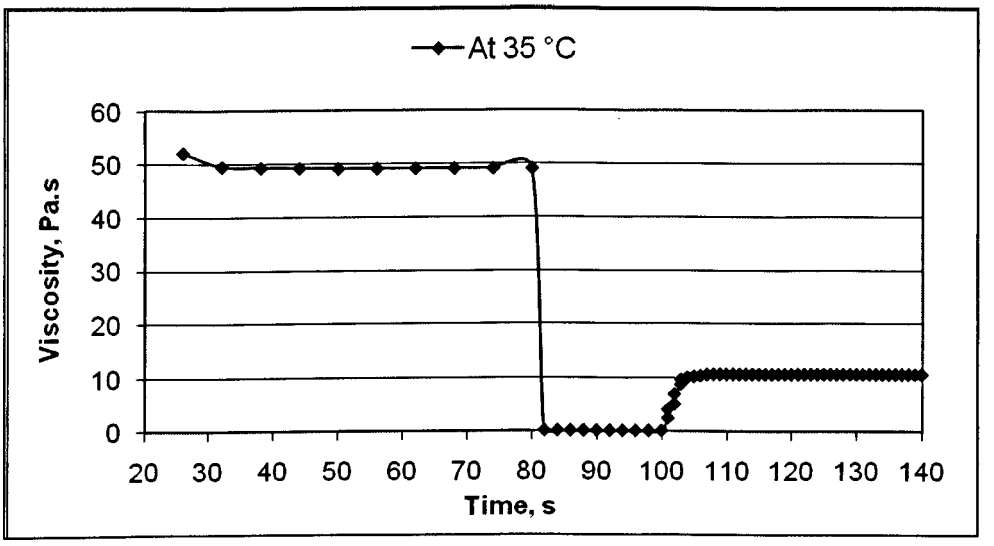

Figure A3.69 Time vs. viscosity: thixotropy phenomena test for Remal oil sample under 0.1, 1000 and 0.1 1/s shear rates at 35 °C

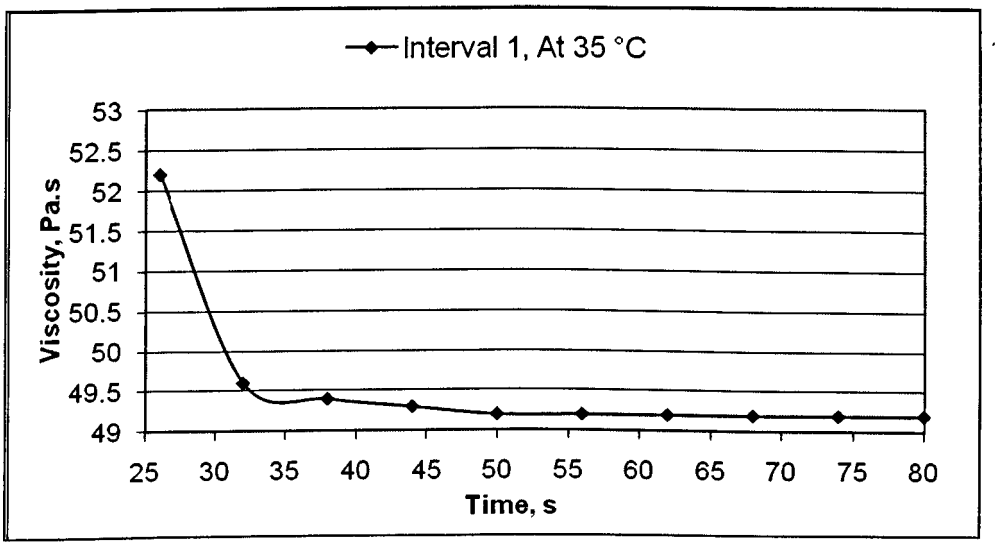

Figure A3.70 Magnification of the data shown in Figure A3.69 from time interval 20 to 80 second

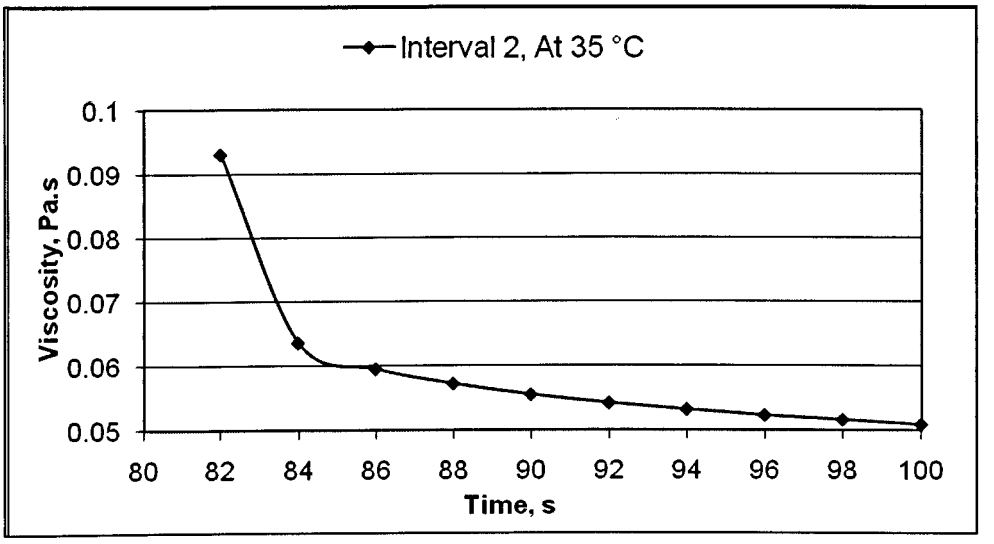

Figure A3.71 Magnification of the data shown in Figure A3.69 from time interval 80 to 100 second

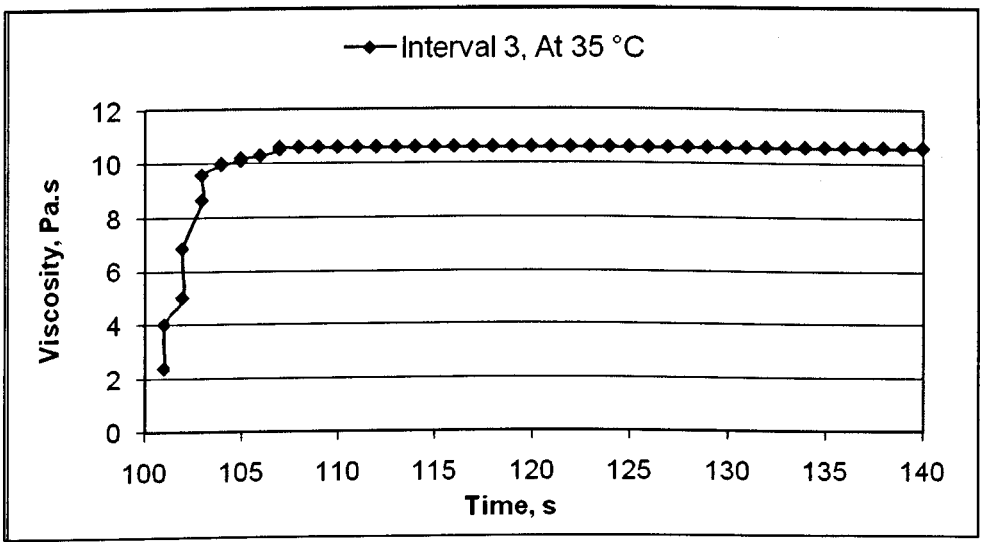

Figure A3.72 Magnification of the data shown in Figure A3.69 from time interval 100 to 140 second

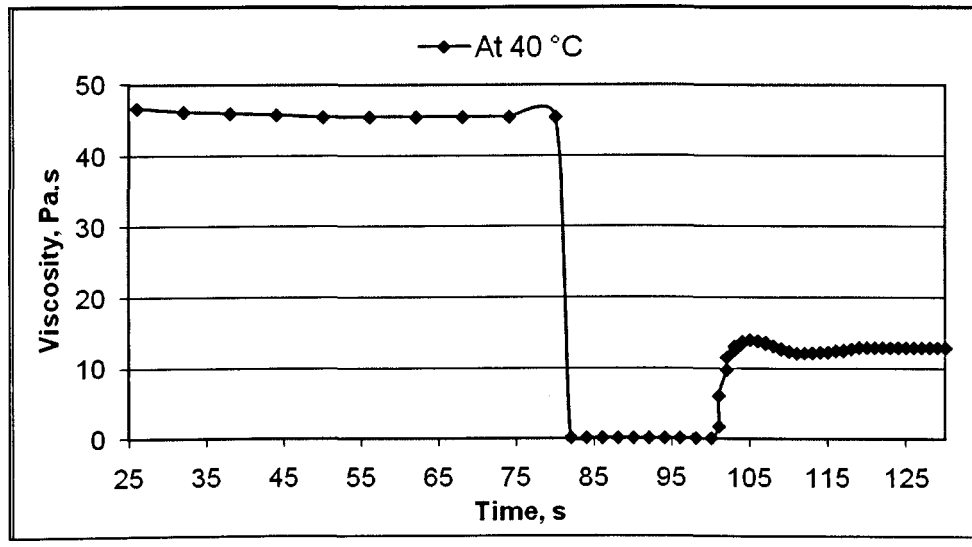

Figure A3.73 Time vs. viscosity: thixotropy phenomena test for Remal oil sample under 0.1, 1000 and 0.1 1/s shear rates at 40 °C

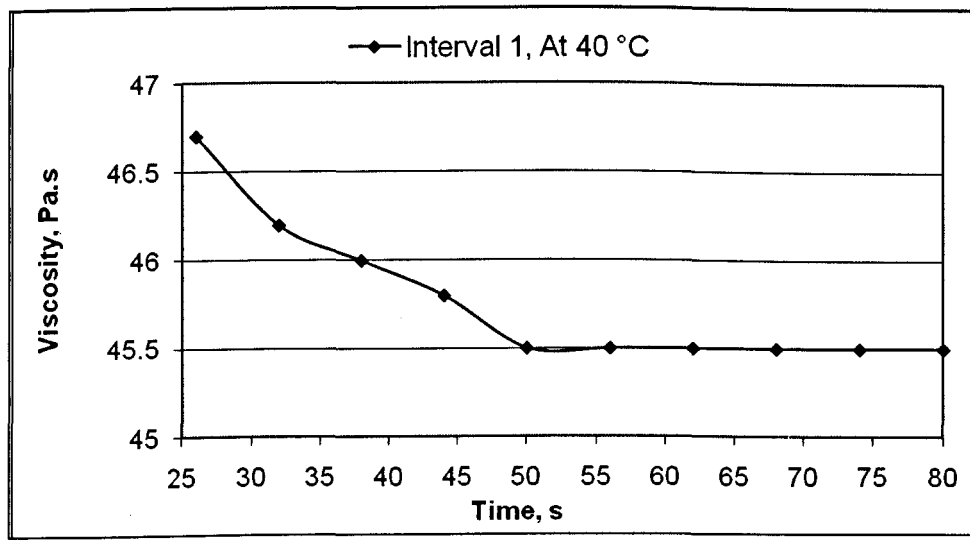

Figure A3.74 Magnification of the data shown in Figure A3.73 from time interval 20 to 80 second

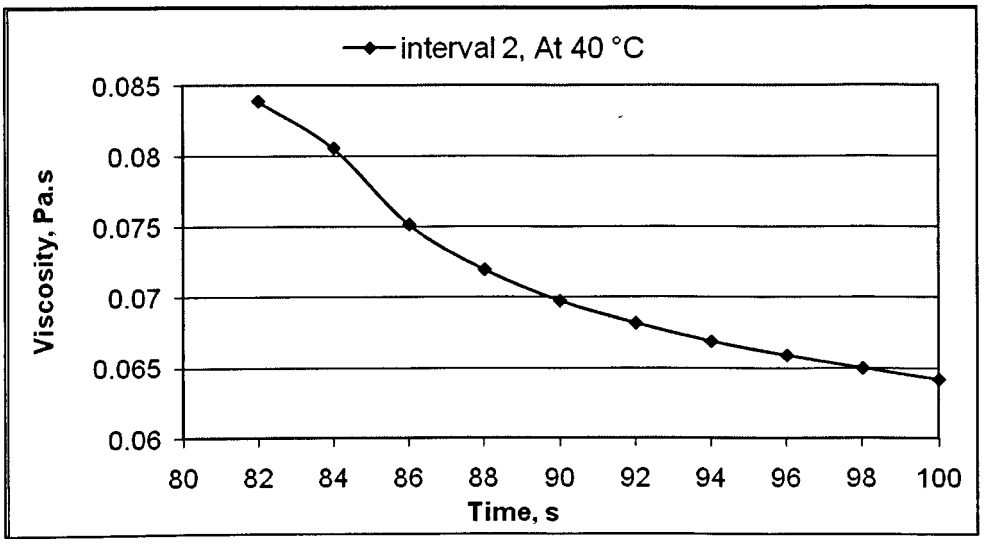

Figure A3.75 Magnification of the data shown in Figure A3.73 from time interval 80 to 100 second

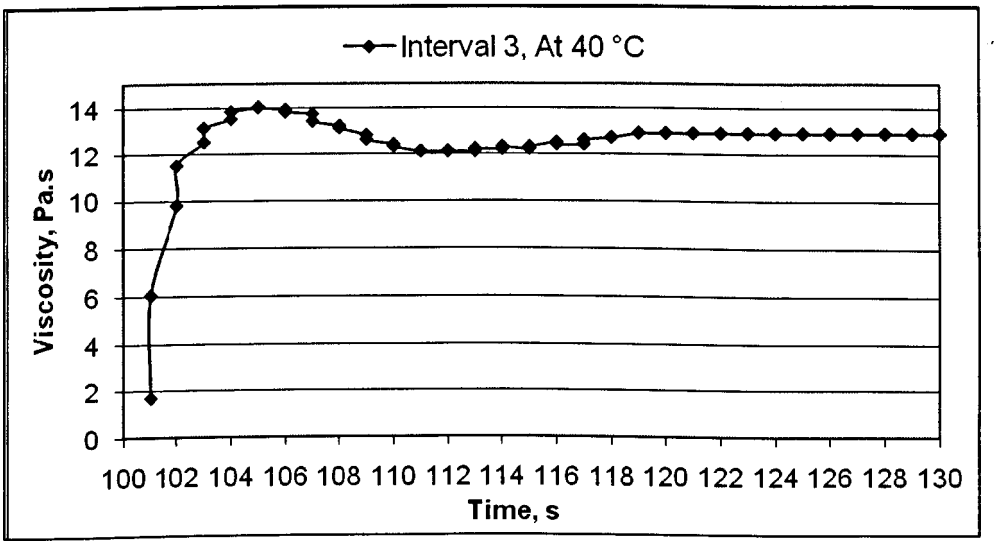

Figure A3.76 Magnification of the data shown in Figure A3.73 from time interval 100 to 130 second

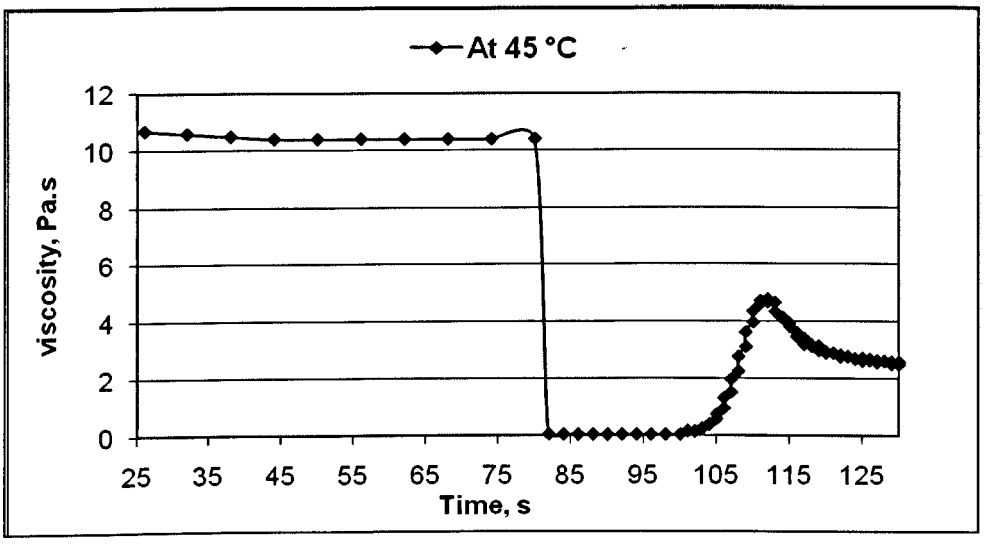

Figure A3.77 Time vs. viscosity: thixotropy phenomena test for Remal oil sample under 0.1, 1000 and 0.1 1/s shear rates at 45 °C

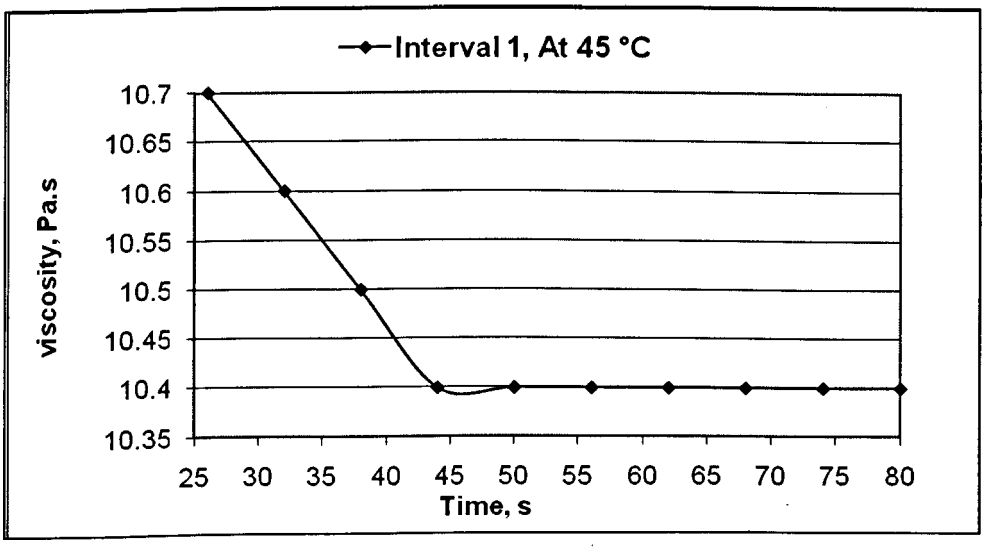

Figure A3.78 Magnification of the data shown in Figure A3.77 from time interval 20 to 80 second

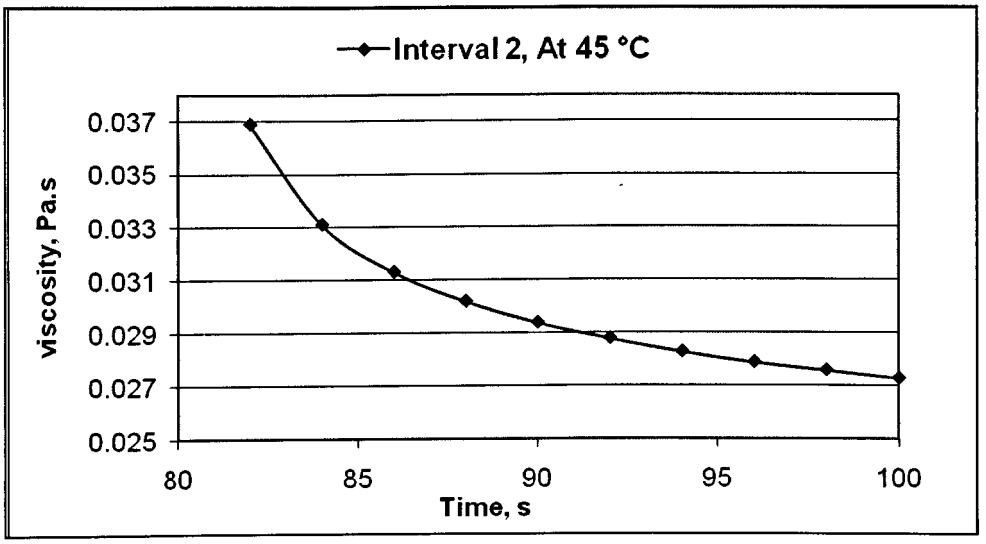

Figure A3.79 Magnification of the data shown in Figure A3.77 from time interval 80 to 100 second

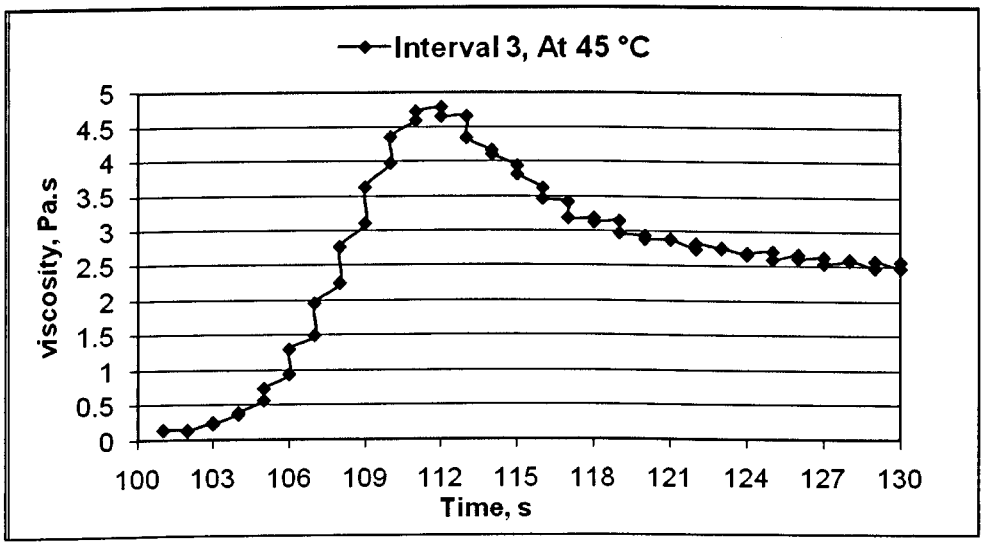

Figure A3.80 Magnification of the data shown in Figure A3.77 from time interval 100 to 130 second

Appendix 4

The behaviour of viscosity at a constant shear rate and a constant temperature

The Measurements were taken every two seconds

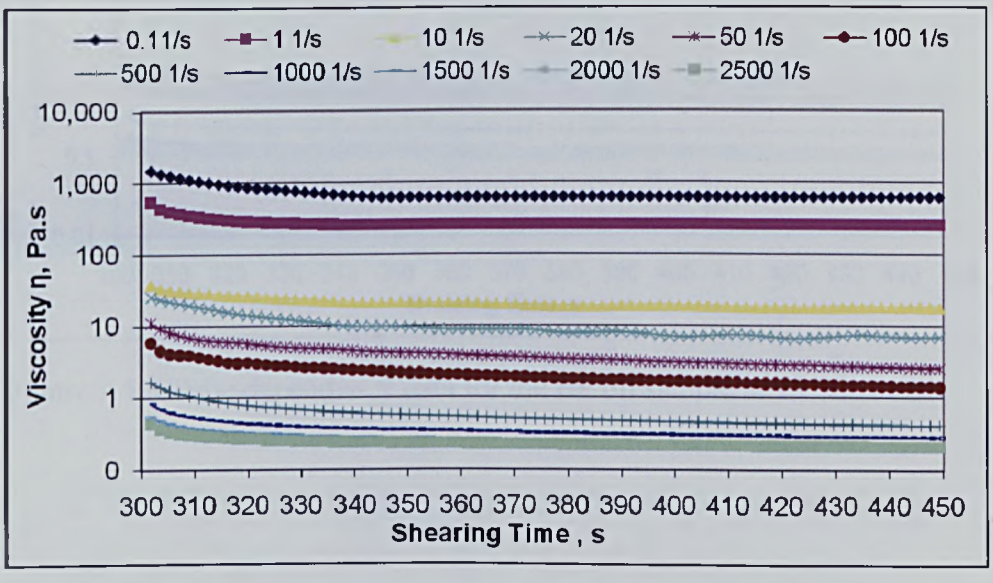

Figure A4.1 Time dependency data for the BP oil sample at 5 °C

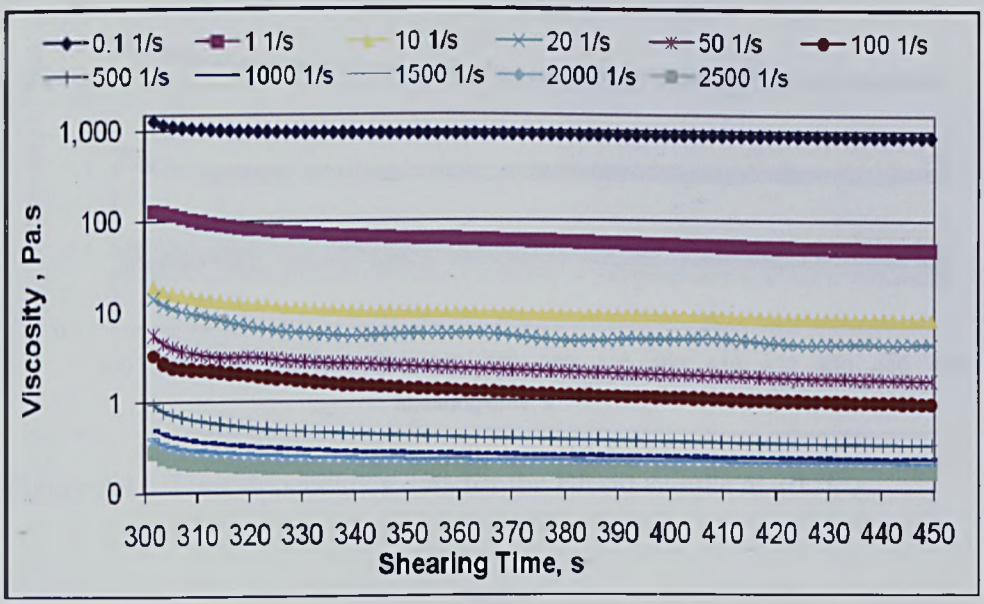

Figure A4.2 Time dependency data for the BP oil sample at 10 °C

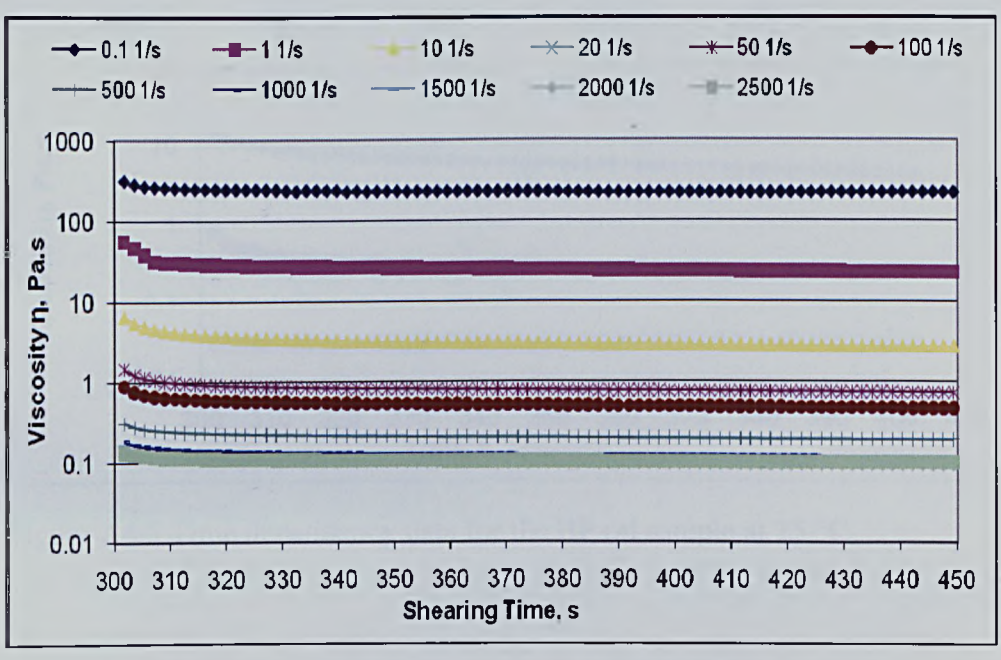

Figure A4.3 Time dependency data for the BP oil sample at 15 °C

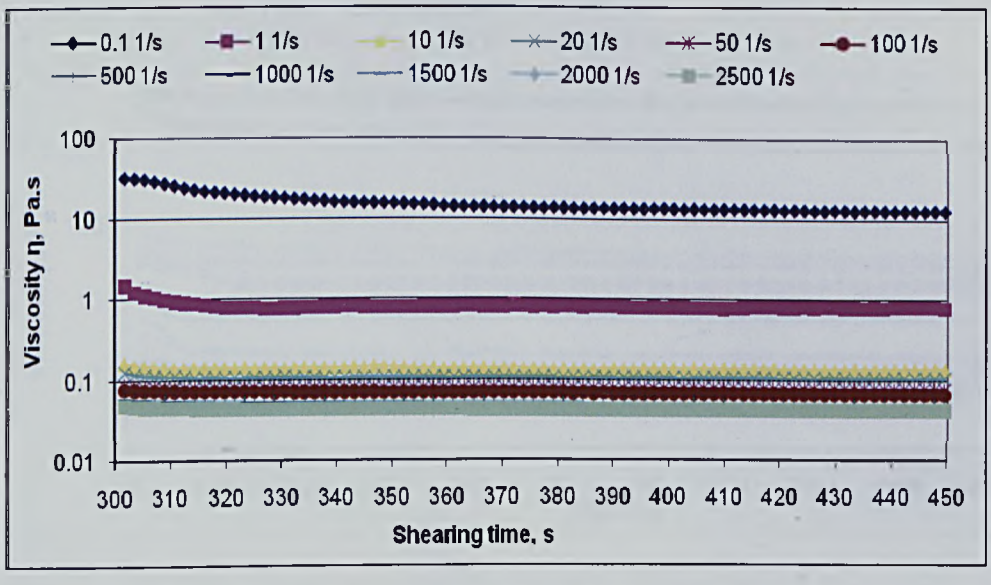

Figure A4.4 Time dependency data for the BP oil sample at 20 °C

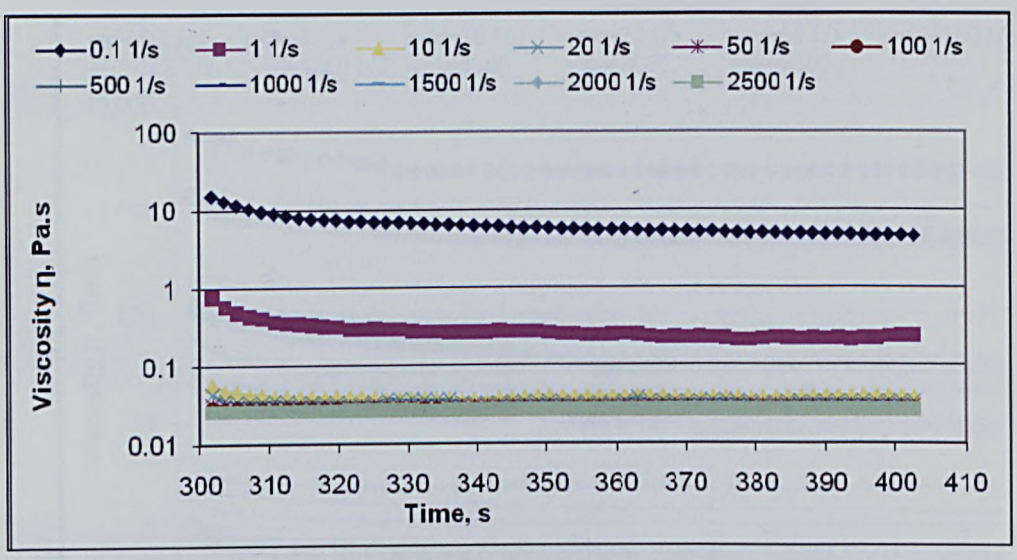

Figure A4.5 Time dependency data for the BP oil sample at 25 °C

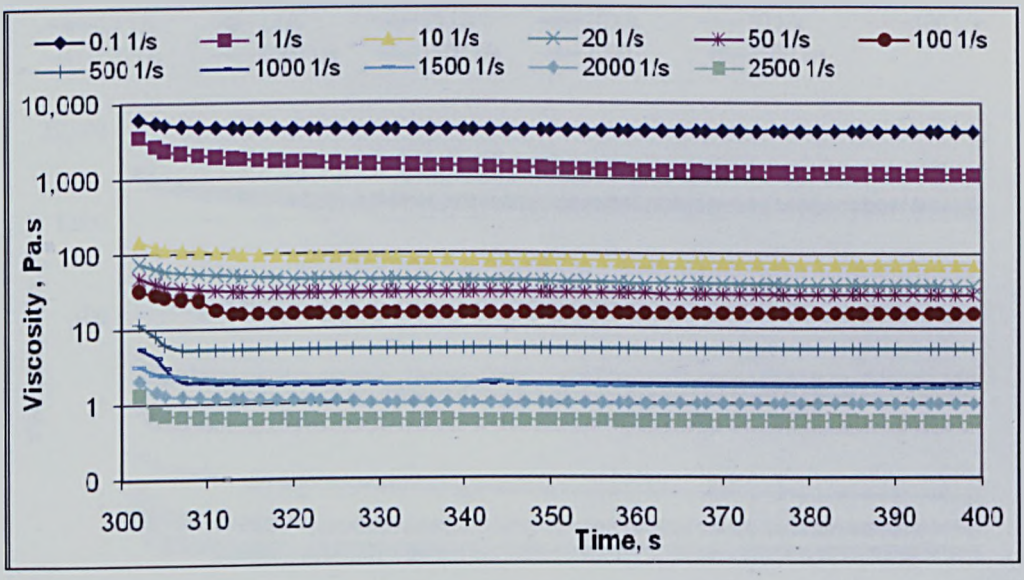

Figure A4.6 Time dependency data for the Mix oil sample at 5 °C

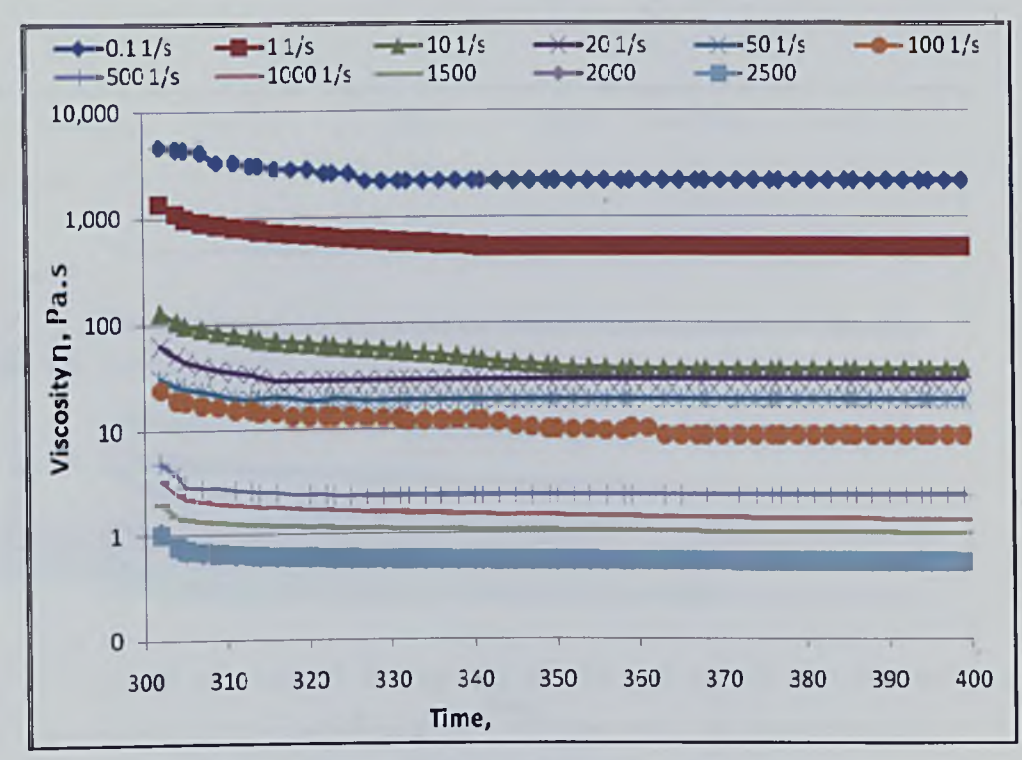

Figure A4.7 Time dependency data for the Mix oil sample at 10 °C

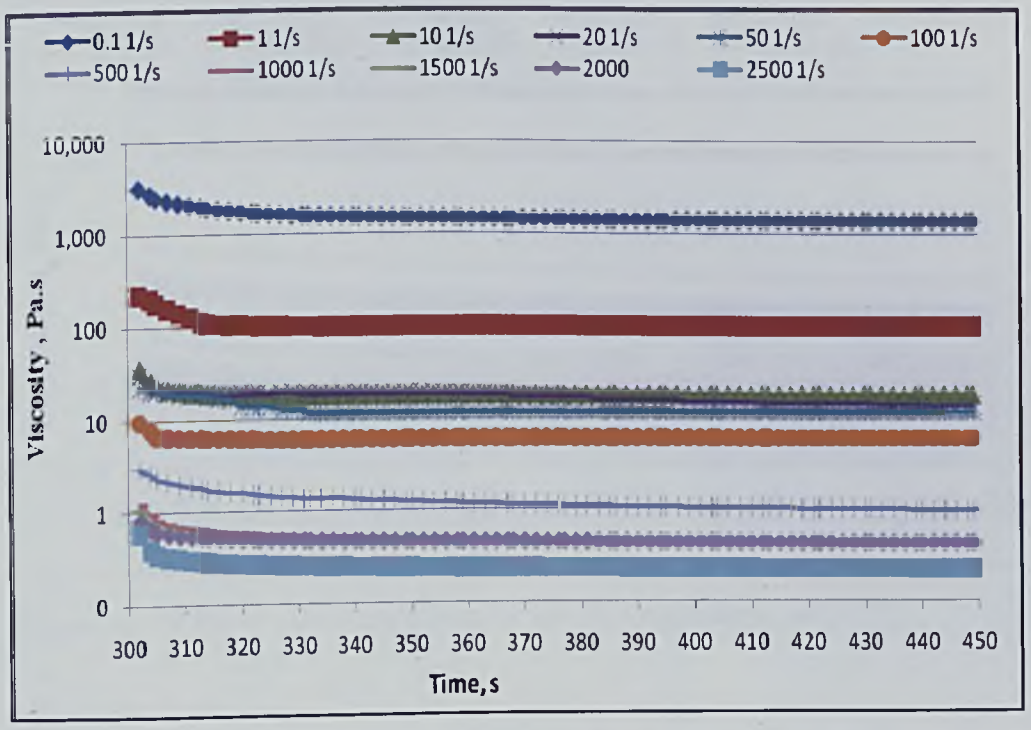

Figure A4.8 Time dependency data for the Mix oil sample at 15 °C

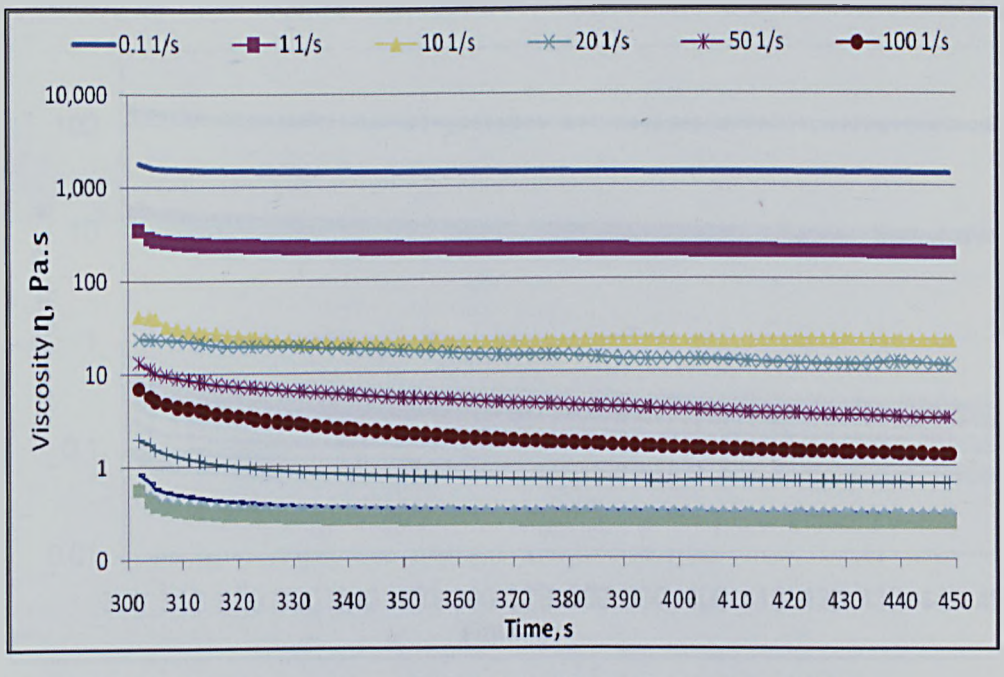

Figure A4.9 Time dependency data for the Mix oil sample at 20 °C

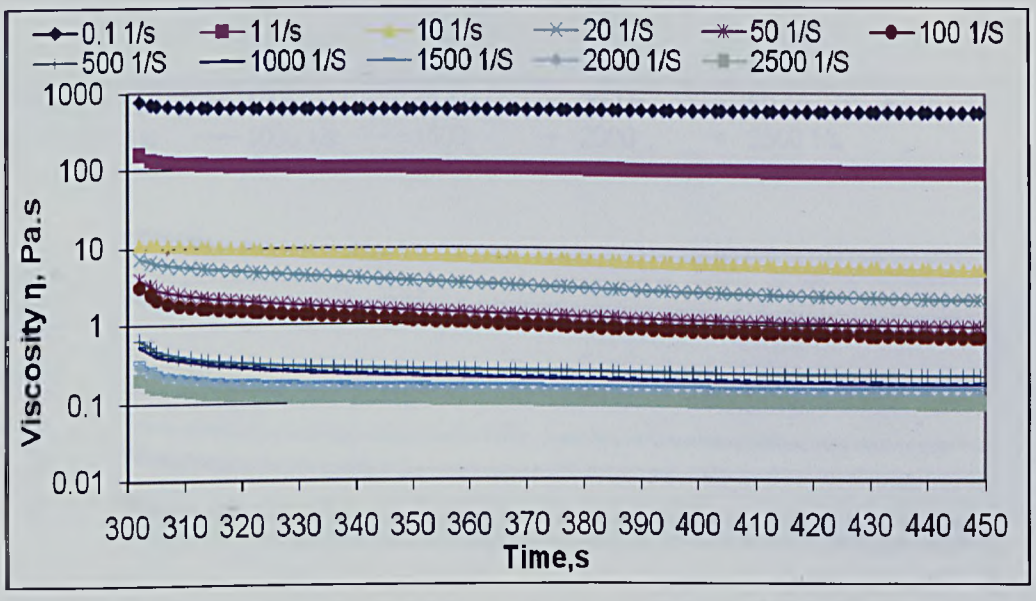

Figure A4.10 Time dependency data for the Mix oil sample at 25 °C

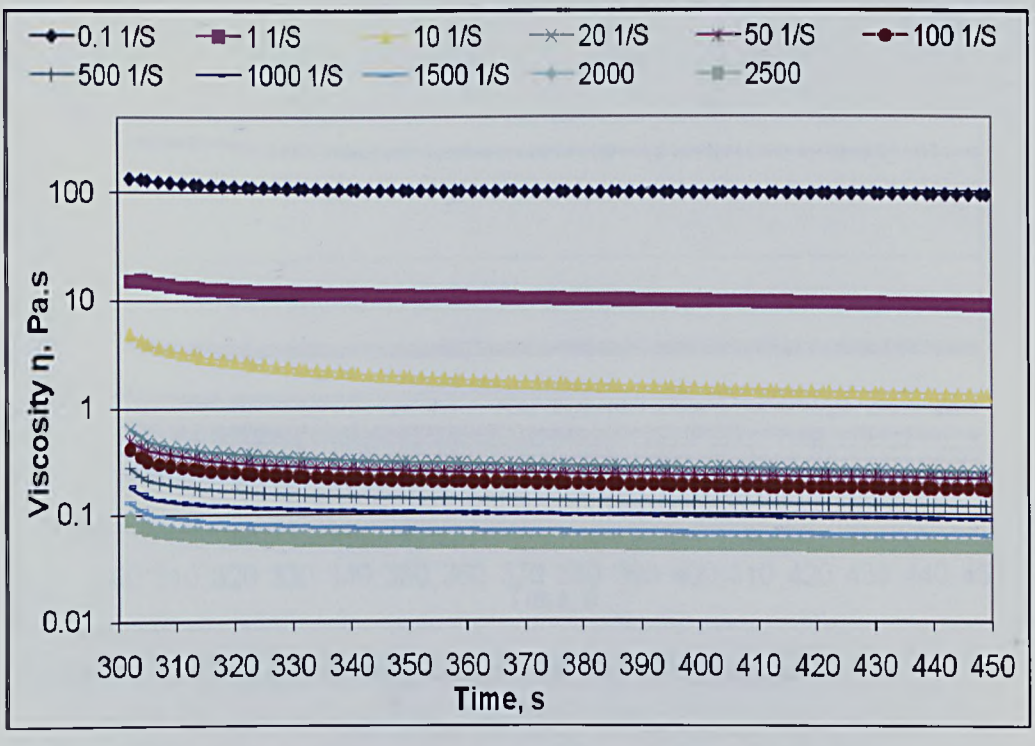

Figure A4.11 Time dependency data for the Mix oil sample at 30 °C

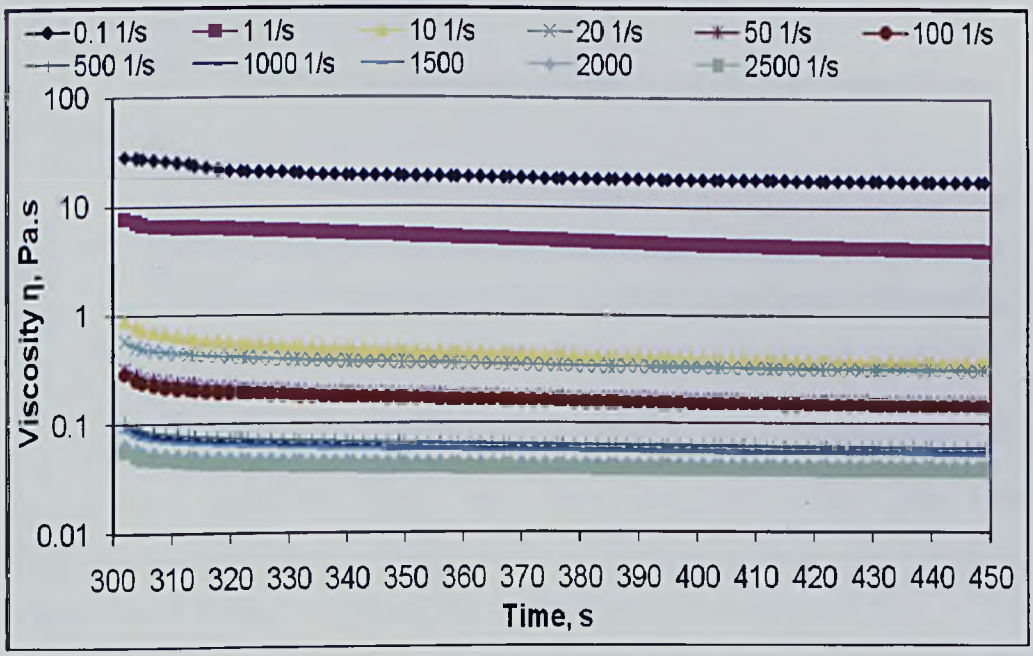

Figure A4.12 Time dependency data for the Mix oil sample at 35 °C

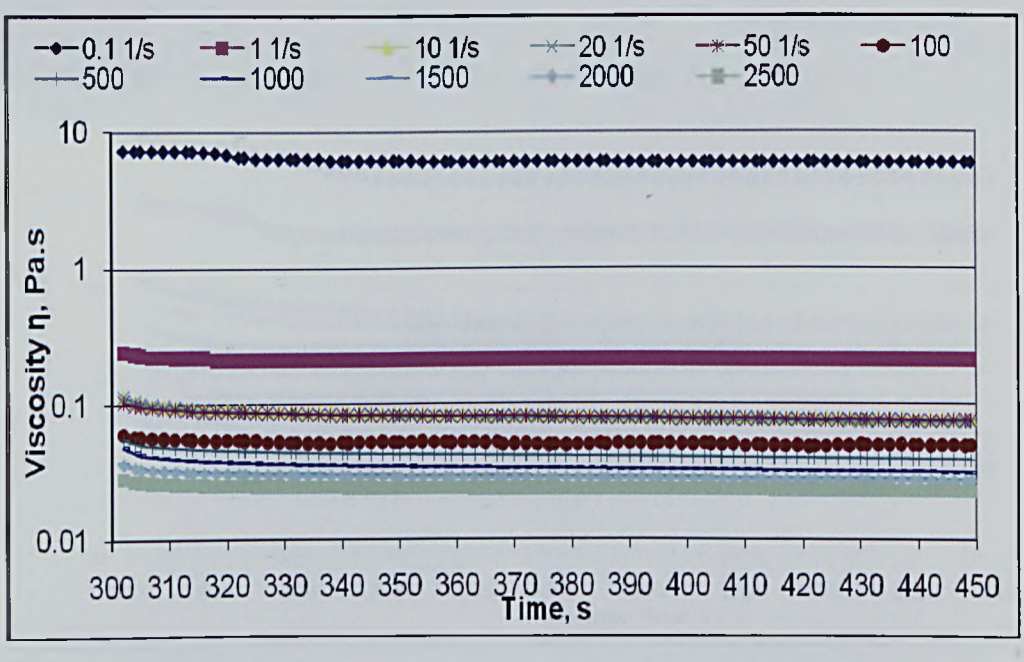

Figure A4.13 Time dependency data for the Mix oil sample at 40 °C

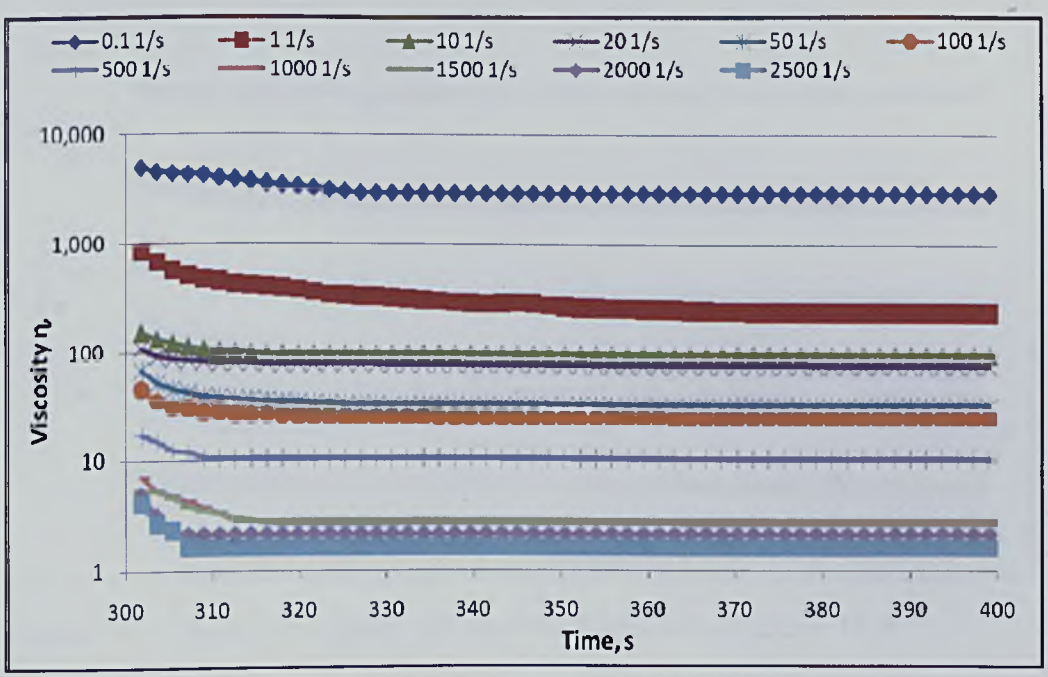

Figure A4.14 Time dependency data for the Remal oil sample at 5 °C

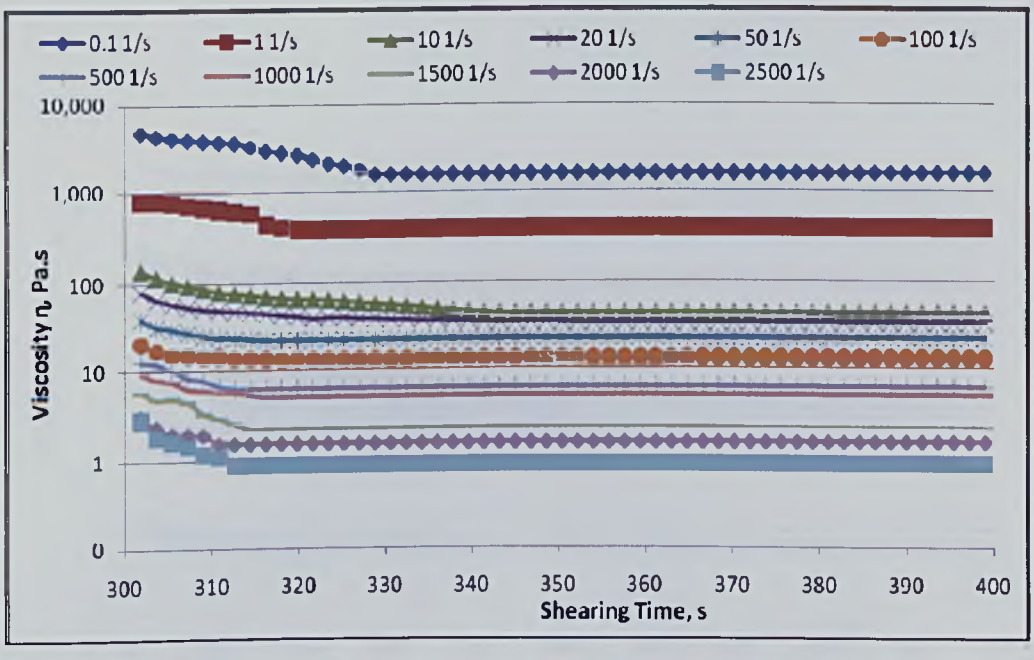

Figure A4.15 Time dependency data for the Remal oil sample at 10 °C

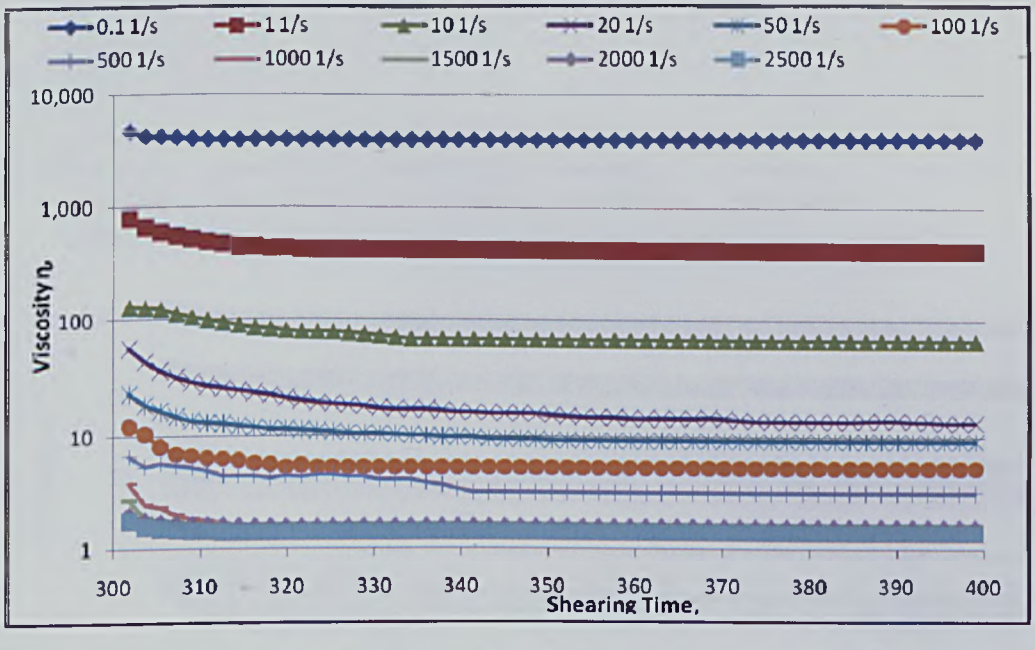

Figure A4.16 Time dependency data for the Remal oil sample at 15 °C

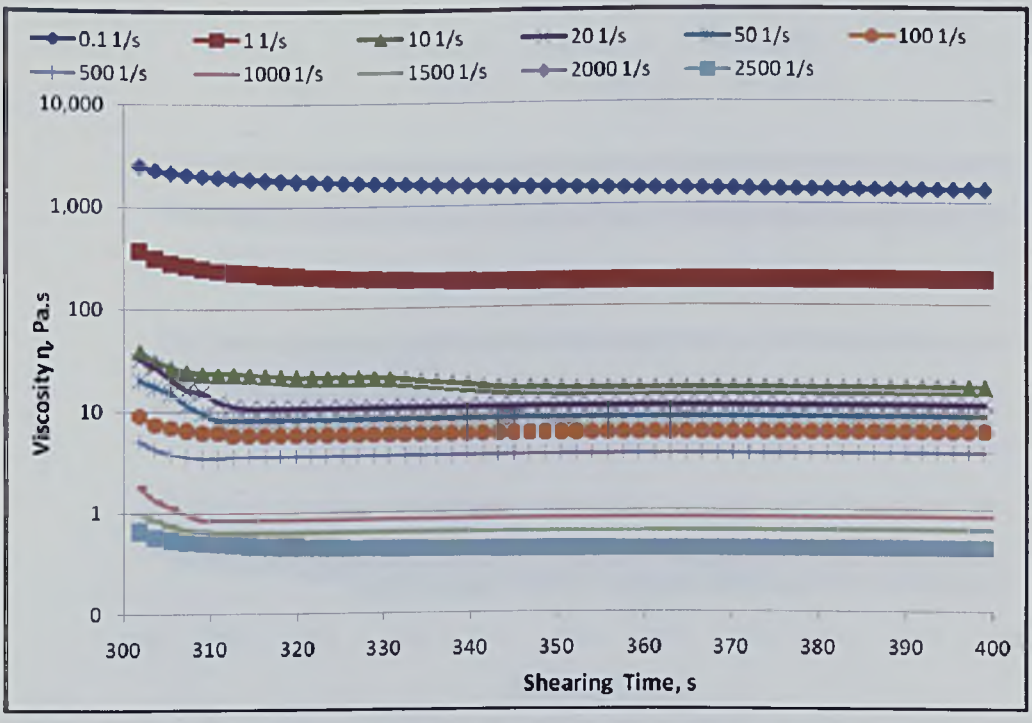

Figure A4.17 Time dependency data for the Remal oil sample at 20 °C

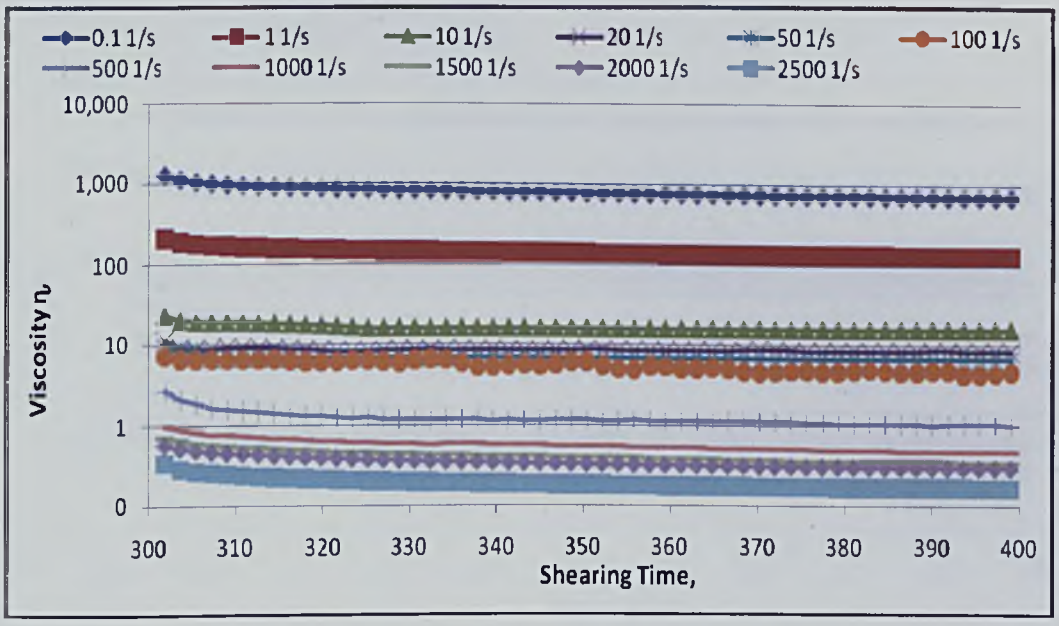

Figure A4.18 Time dependency data for the Remal oil sample at 25 °C

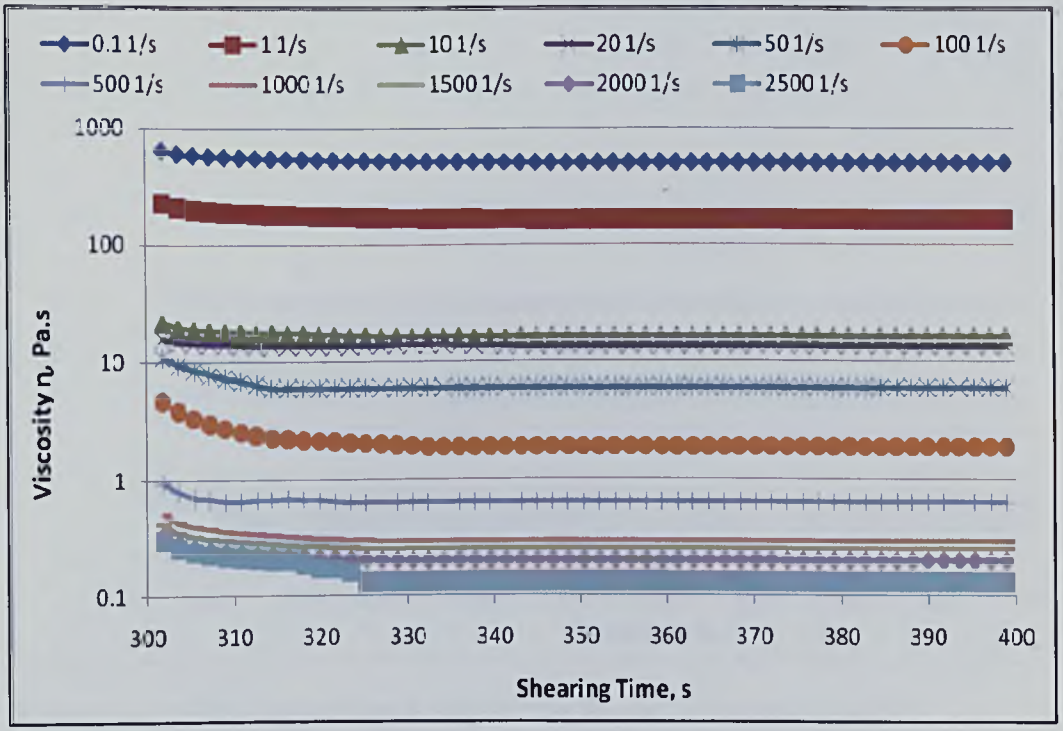

Figure A4.19 Time dependency data for the Remal oil sample at 30 °C

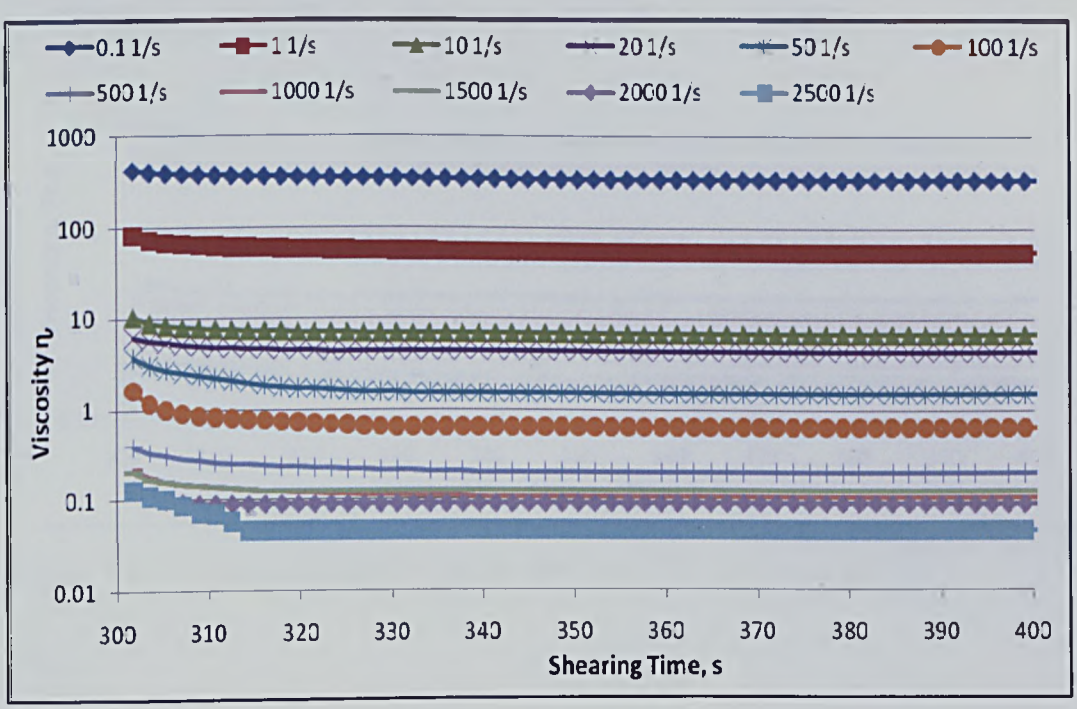

FigureA4.20 Time dependency data for the Remal oil sample at 35 °C

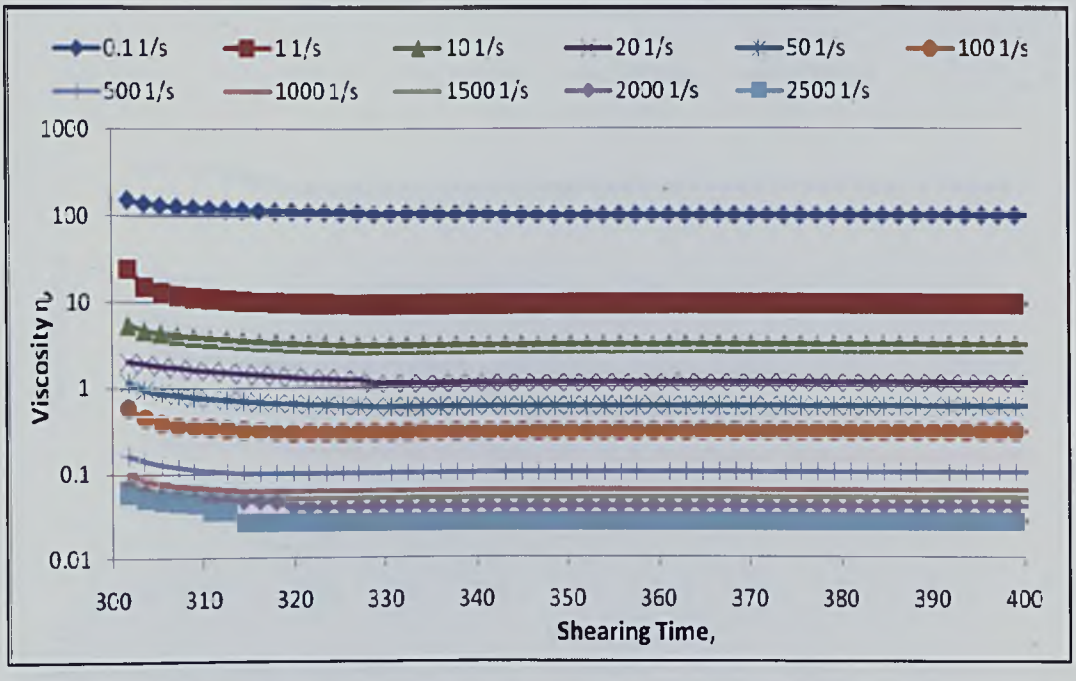

Figure A4.21 Time dependency data for the Remal oil sample at 40 °C

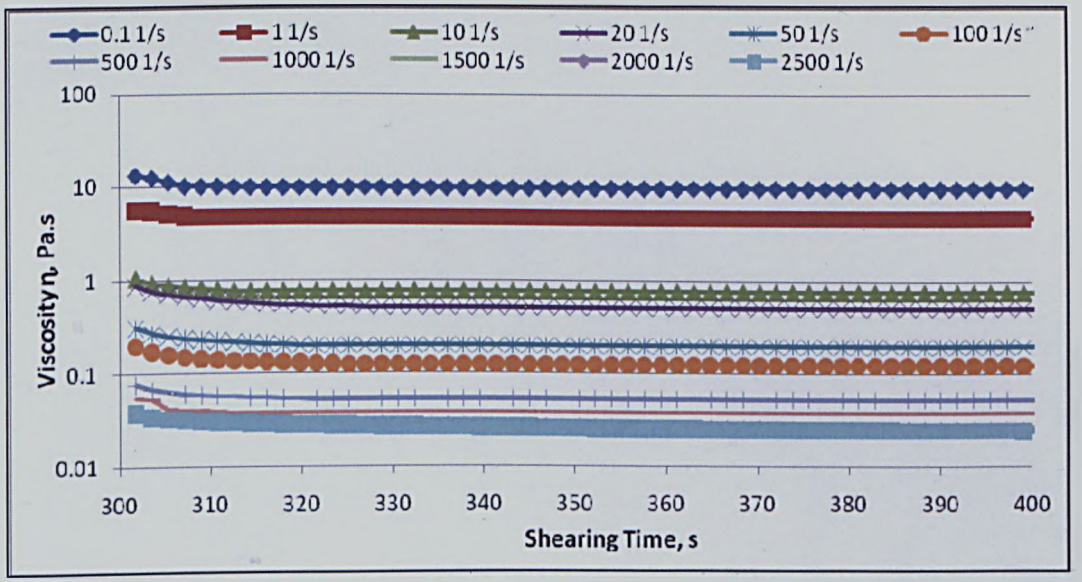

Figure A4.22 Time dependency data for the Remal oil sample at 45 °C

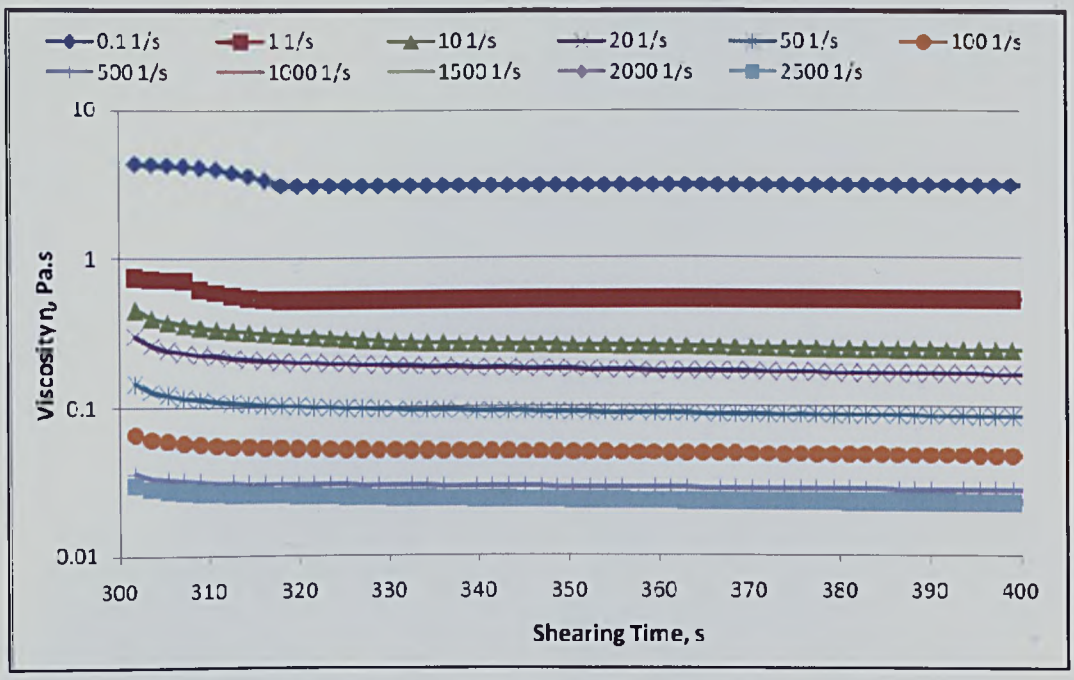

Figure A4.23 Time dependency data for the Remal oil sample at 50 °C